

UNCLASSIFIED

AD NUMBER	
AD108883	
CLASSIFICATION CHANGES	
TO:	UNCLASSIFIED
FROM:	CONFIDENTIAL
LIMITATION CHANGES	
TO: Approved for public release; distribution is unlimited. Document partially illegible.	
FROM: Distribution authorized to DoD only; Test and Evaluation; JUN 1956. Other requests shall be referred to Navy Bureau of Ships, Electronics Division, Washington, DC 20350. Document partially illegible.	
AUTHORITY	
1 May 1959, Tab U-37-9, per document marking; navships 1 apr 1968	

THIS PAGE IS UNCLASSIFIED

UNCLASSIFIED

108883

and Services Technical Information Agency

ARLINGTON HALL STATION

ARLINGTON 22 VIRGINIA

CLASSIFICATION CHANGED FROM  
CONFIDENTIAL TO UNCLASSIFIED  
FOR AGREEMENT LIAISON BY ADIA  
TAB NO. 009-0 1 MAY 80

UNCLASSIFIED



## **DISCLAIMER NOTICE**

**THIS DOCUMENT IS BEST QUALITY  
PRACTICABLE. THE COPY FURNISHED  
TO DTIC CONTAINED A SIGNIFICANT  
NUMBER OF PAGES WHICH DO NOT  
REPRODUCE LEGIBLY.**

**NOTICE: THIS DOCUMENT CONTAINS INFORMATION AFFECTING THE  
NATIONAL DEFENSE OF THE UNITED STATES WITHIN THE MEANING  
OF THE ESPIONAGE LAWS, TITLE 18, U.S.C., SECTIONS 793 and 794.  
THE TRANSMISSION OR THE REVELATION OF ITS CONTENTS IN  
ANY MANNER TO AN UNAUTHORIZED PERSON IS PROHIBITED BY LAW.**



AD No 18883

ASIA FILE COPY



CONFIDENTIAL



SPERRY GYROSCOPE COMPANY  
DIVISION OF SPERRY RAND CORPORATION  
GREAT NECK, NEW YORK

CONFIDENTIAL

CONFIDENTIAL

COPY NO. 15



FC

FURTHER INFORMATION IS AUTHORIZED ONLY TO  
MILITARY PERSONNEL.

FINAL DEVELOPMENT REPORT ON  
STUDY OF TECHNIQUES FOR MEASURING  
MICROWAVE HIGH-POWER BREAKDOWN IN  
WAVEGUIDE TRANSMISSION LINES

THIS REPORT COVERS THE PERIOD 1 MARCH 1951 TO 15 MARCH 1956

MICROWAVE ELECTRONICS DIVISION  
SPERRY GYROSCOPE COMPANY  
DIVISION OF SPERRY RAND CORPORATION  
GREAT NECK, NEW YORK

NAVY DEPARTMENT, BUREAU OF SHIPS, ELECTRONICS DIVISION  
CONTRACT N0bsr-52227, INDEX NO. NE-110607

Prepared by:

ENGINEERING DEPARTMENT

G.K. Hart  
F. Klawnsnik  
F.R. Stevenson  
M.S. Tanenbaum

SPERRY REPORT NO. 7220-13004  
JUNE 1956

PUBLICATIONS DEPARTMENT  
M. Broner

CONFIDENTIAL

OCT 17 1956

56AA-53353  
8240596-56

(19)



CONFIDENTIAL

CLASSIFICATION NOTICE

WARNING: This document contains information affecting the national defense of the United States within the meaning of the Espionage Laws, Title 18, U.S.C., Sections 793 and 794. The transmission or the revelation of its contents in any manner to an unauthorized person is prohibited by law. Reproduction of this document in any form by other than activities of the Department of Defense and the Atomic Energy Commission is not authorized unless specifically approved by the Secretary of the Navy or the Chief of Naval Operations.

CONFIDENTIAL

CONFIDENTIAL

# ABSTRACT

A theoretical and experimental study of microwave breakdown in waveguide was made. A survey was made of the available literature on the subject of high-power breakdown, with particular emphasis upon breakdown in the microwave region. A bibliography of the available literature on the subject of high-power breakdown is given in Appendix A.

The fundamental concepts of direct-current breakdown are discussed and the extension of these ideas to alternating-current breakdown is shown. The prominent theories of microwave breakdown, both for continuous-wave and pulsed power, are presented and the pertinent experimental data are examined for consistency and agreement with theory. It is shown that from a statistical viewpoint the available data on microwave breakdown are consistent.

An experimental approach for determining microwave breakdown, based upon the statistical nature of breakdown, is presented wherein the breakdown power was determined from a plot of sparking probability vs power. A microwave test circuit was designed to experimentally determine the sparking probability. The individual components are discussed both as to purpose and physical form. One unique component is a photocell and electronic counter for detecting and recording the light from the breakdown spark. An evaluation of the

CONFIDENTIAL

CONFIDENTIAL

errors introduced by the test circuit components is also made. The measurement procedure proposed yielded sufficient data to completely describe the power-handling capacity of the test components.

The experimental use of cobalt 60 as a source of electrons to initiate breakdown was investigated and found useful. It permitted the accurate determination of the onset stress and at the same time reduced the time required for the test. The use of various devices, such as microphones, Tempilsq, starch, and photographic paper, for determining the region of breakdown was investigated. The dependence of peak-power capacity on the important microwave design parameters such as pulse width, pulse shape, repetition frequency, gas pressure, nature of the gas, mechanical finish, plating material, and frequency, was theoretically and experimentally investigated.

The peak-power capacity of waveguide and a wide variety of components as a function of gas pressure was studied. The results of the tests are discussed in terms of the statistical theory of breakdown and the similarity in design configuration of the components.

One phase of the program was concerned with investigating the breakdown characteristics of the basic microwave structures or building blocks from which microwave components



CONFIDENTIAL

are synthesized. The microwave structures investigated were probes, bends, posts, slots, irises, and twists. In addition, the proximity effects of the structures and the existence of more than one type of breakdown was studied. Data are presented on building block structures which will be useful to the microwave component development engineer. This approach will reduce the time required to design high-power microwave components. Finally, methods of improving existing components are presented. Recommendations for future work are made.

CONFIDENTIAL



## TABLE OF CONTENTS

<u>Paragraph</u>		<u>Page</u>
	Abstract	i
	List of Illustrations	xii
	PART I	1
	SECTION A - PURPOSE	1
1.	Purpose of Development	1
2.	Study and Work Phases	1
	SECTION B - GENERAL FACTUAL DATA	5
3.	References	5
4.	Formulae	5
4.1	General	5
4.2	Sliding Mismatch Reflectometer Method for VSWR Measurement	5
4.3	Root-Mean-Square Technique For Classifying Surface Roughness	8
4.4	Power Capacity of H-Plane Wave- guide Bend	10
4.5	Power Capacity of E-Plane Wave- guide Bend	11
4.6	Effect of VSWR Upon Peak-Power Capacity	11
4.7	Power Capacity of Rectangular and Ridge Waveguide	18

## TABLE OF CONTENTS (cont)

<u>Paragraph</u>		<u>Page</u>
4.8	Scaling Techniques for the Power Capacity of Waveguides	22
4.9	Voltage Gradient in The Swayback Gap Section	25
4.10	Breakdown Power Accuracy as a Function of Pressure	26
	SECTION C	28
	DETAIL FACTUAL DATA	28
5.	Introduction	28
6.	Theories of Breakdown	30
6.1	Direct-Current Breakdown	30
6.2	Alternating-Current Breakdown	35
6.3	Experimental Data	49
	a. Criterion of Breakdown	49
	b. Presentation of Existing Data	54
	c. Appraisal of Existing Data	60
6.4	Regions of Validity of Theories	65
7.	Experimental Approach	69
7.1	Breakdown Test Circuit	69
7.2	Design Considerations and Performance of Test-Circuit Components	75

CONFIDENTIAL

TABLE OF CONTENTS (cont)

<u>Paragraph</u>		<u>Page</u>
	a. Pressure Window	75
	b. Phase Shifters	76
	c. Thermistor Mount	76
	d. Tchebyscheff Coupler	77
	e. Miscellaneous Components	79
7.3	Experimental Considerations	80
7.4	Analysis of Experimental Errors	96
	a. General	96
	b. Power Measurement	96
	c. Determination of Breakdown	98
	d. Waveguide Losses	98
	e. Waveguide Tolerances	99
	f. Voltage-Standing-Wave Ratio	101
	g. Measurement of Pressure	101
	h. Summary of the Probable Errors	104
8.	Investigation of Methods of Locating the Region of Breakdown	107
9.	Measurement of The Effect On Peak-Power Breakdown of Various Design Parameters	113
9.1	Pressure	113
9.2	Pulse Duration	115
9.3	Repetition Rate	121

CONFIDENTIAL

## TABLE OF CONTENTS (cont)

<u>Paragraph</u>		<u>Page</u>
9.4	Pulse Shape	123
9.5	Mechanical Finish	124
9.6	Nature of The Gas	126
	a. Introduction	126
	b. Variation of Power Capacity With Pressurization Technique	131
	c. Variation of Power Capacity With Different Test Sections	133
9.7	Plating Material	139
9.8	Microwave Frequency	140
9.9	Voltage-Standing-Wave Ratio	142
10.	Measurements of The Power Capacity of Waveguide and Components	153
10.1	Waveguides	153
	a. Breakdown of a 1" x 1/2" Waveguide At Atmospheric Pressure	153
	b. Breakdown Tests on Cover-to-Cover Flange Joints	156
	c. Breakdown Tests on the Misalignment of Cover-to-Cover Flange Joints	157
	d. Breakdown Tests on a Choke-to- Cover Flange Connection	159
	e. Breakdown Tests on a Misaligned Choke-to-Cover Flange Connection	160



## TABLE OF CONTENTS (cont)

<u>Paragraph</u>		<u>Page</u>
	f. Breakdown Tests on the Effect of Separation in a Choke-to-Cover Flange Connection	164
	g. Breakdown Tests on the Effect of Grooves and Gaps in Waveguide Walls	164
	h. Breakdown Tests on Flexible Waveguide	168
	i. Breakdown Tests on USL Cover-to-Cover Flanges for 1.122" x 0.497" I.D. Waveguide	172
10.2	Change of Direction and Polarization Waveguides	176
	a. Breakdown of H-Plane Bends	176
	b. Breakdown of E-Plane Bends	179
	c. Breakdown Tests on a 90-Degree H-Plane Mitered Corner	184
	d. Breakdown Tests on Waveguide Twists	184
10.3	Waveguide Couplers and Tee Junctions	186
	a. Breakdown Tests of a Two-Hole Coupler	186
	b. Breakdown Tests of Crossed-Guide Coupler	186
	c. Breakdown Tests of Schwinger Coupler	188
	d. Breakdown Tests on a Branch-Guide Coupler	189

## TABLE OF CONTENTS (cont)

<u>Paragraph</u>		<u>Page</u>
	e. Breakdown Tests of E-Plane Tee	190
	f. Breakdown Tests of H-Plane Tee	192
	g. Breakdown Tests of Magic Tee	193
	h. Breakdown Tests of an E-Plane Hybrid Ring	194
10.4	Waveguide Rotary Joints	195
	a. Breakdown Tests on a Rectangular-to-Circular Waveguide Rotary Joint	195
	b. Breakdown Tests on a Ridge-Waveguide Coaxial-Line Rotary Joint	196
	c. Breakdown Tests on a Dual-Feed Coaxial-Line Rotary Joint	198
10.5	Miscellaneous Components	199
	a. Breakdown Tests on Sections Containing Hemispherical Bumps	199
	b. Breakdown Tests on a Waveguide Switch	201
	c. Breakdown Tests on an Antenna Assembly	202
	d. Breakdown Tests on a Longitudinal-Serrated Choke	203
	e. Breakdown Tests on a Coaxial-Line-to-Waveguide Adapter	204
	f. Breakdown Tests on High-Power Loads	206

CONFIDENTIAL

# TABLE OF CONTENTS (cont)

<u>Paragraph</u>		<u>Page</u>
	g. Breakdown Tests on a Waveguide Step Transformer	210
	h. Breakdown and High-Power Performance Tests on an Absorption-Type Ferrite Isolator	211
10.6	Comparison of Data Taken in X-, C-, S-, and Large S-Band Components	214
11.	Building Block Structures	217
11.1	Introduction	217
11.2	Breakdown Data on Waveguide Iris	218
	a. General	218
	b. Inductive Irises	219
11.3	Breakdown Data on Waveguide Steps	224
	a. General	224
	b. Inductive Steps	226
	c. Capacitive Steps	229
11.4	Breakdown of a Capacitive Waveguide Post	232
11.5	Breakdown of a Thin Strip In Rectangular Waveguide	237
	a. Inductive Strip	237
	b. Capacitive Strip	238
11.6	Breakdown of Waveguide Capacitive Rod	239
11.7	Breakdown of Waveguide Apertures	241

CONFIDENTIAL

TABLE OF CONTENTS (cont)

<u>Paragraph</u>		<u>Page</u>
11.8	Comparison of the Breakdown Data on The Building Block Structures	246
	a. General	246
	b. Inductive Structures	247
	c. Capacitive Structures	249
	SECTION D	250
	CONCLUSIONS	250
12.	General Conclusions	250
	PART II	264
	RECOMMENDATIONS	264
13.	General Recommendations	264
	Appendix A	A-1
	Bibliography	A-1

CONFIDENTIAL



## LIST OF ILLUSTRATIONS\*

Figure	Title
1.	Setup for Calibration of Sliding-Short Reflectometer
2.	Normalized Plot of Power Capacity of an E-Plane Bend
3.	Pertinent Dimensions of Ridge Waveguide Test Piece
4.	2" x 1" to 1" x 1/2" Taper Waveguide
5.	Circuit for Measurement of High Power Breakdown
6.	Over-all Picture of High-Power Breakdown Breakdown Testing Facilities
7.	Close-up Picture of Test Section
8.	Breakdown Probability for Spark Gap
9.	Histograms for High-Voltage Breakdown (Bridge Reading: 30 Microwaves, Time Interval: 15 Sec.)
10.	Histogram for High-Voltage Breakdown (Bridge Reading: 30 Microwaves, Time Interval: 30 Sec.)
11.	Histogram for High-Voltage Breakdown (Bridge Reading: 30 Microwaves, Time Interval: 1 Min.)
12.	Breakdown Power vs Pressure with Cobalt in Contact with Tapered-Waveguide Breakdown Gap
13.	Breakdown Power vs Pressure with Cobalt 1" Above Tapered-Waveguide Breakdown Gap

\*All illustrations are grouped in numerical order at the rear of the report.

CONFIDENTIAL

LIST OF ILLUSTRATIONS (cont)

<u>Figure</u>	<u>Title</u>
14.	Breakdown Power vs Pressure with Cobalt 2" Above Tapered-Waveguide Breakdown Gap
15.	Breakdown Power vs Pressure For a Pulse Width of 1.2 $\mu$ sec.
16.	Error in Breakdown Power vs Pressure With the Error in Pressure as a Parameter
17.	Photograph of Breakdown Spots
18.	Power vs Pressure for 300-400 Finish (1" x 1/2" x .050" Waveguide)
19.	Variation of Pulse Width at Constant 400 PPS Repetition Rate of 1" x 1/2" x .050" Waveguide Test Section
20.	Variation of Repetition Rate at Constant 0.4-m Sec. Pulse Width of 1" x 1/2" x .050" Waveguide Test Section
21.	Power vs Pulse Width For Constant Repetition Rate of 400 PPS
22.	Pulse-Width Exponent vs Pressure
23.	Power vs Repetition Rate for Constant Pulse Width of 0.4 $\mu$ sec.
24.	Repetition-Rate Exponent vs Pressure
25.	Power vs Pressure for 550-650 PMS Finish (1" x 1/2" x .050" Waveguide)
26.	Power vs Pressure for 650-850 RMS Finish (1" x 1/2" x .050" Waveguide)

## LIST OF ILLUSTRATIONS (cont)

<u>Figure</u>	<u>Title</u>
27.	LN Power vs LN Pressure for Standard 1- x 1/2-inch Waveguide
28.	LN Power vs LN Pressure for 0.150-inch Radius Hemispherical Bump
29.	LN Power vs LN Pressure for Swayback Test Section
30.	Block Diagram of Circuit used to Measure Effect of SF <sub>6</sub> Upon Peak-Power Breakdown by the Balanced Rate Method
31.	LN Power vs LN Pressure for Anodized Waveguide
32.	Block Diagram of Circuit used to Measure Effect of VSWR on Peak-Power Breakdown
33.	Power vs Pressure for Different Values of VSWR (1" x 1/2" x .050" Waveguide)
34.	Calculated Peak-Power Capacity vs VSWR for a Single Mismatch
35.	Calculated Peak-Power Capacity vs VSWR for a Resonant Cavity, Formed from two Properly Spaced Mismatches
36.	Comparison of Calculated Peak-Power, Capacities Shown in Figures 34 and 35
37.	Measured and Calculated Peak-Power Capacities vs VSWR for a Resonant Cavity, Formed by two Properly Spaced Mismatches
38.	Measured and Calculated Peak-Power Capacities vs VSWR for three Most Pertinent Conditions
39.	Breakdown Power vs Pressure with Tapered-Wave- guide Breakdown Gap

## LIST OF ILLUSTRATIONS (cont)

<u>Figure</u>	<u>Title</u>
40.	Power vs Pressure for Specially Aligned Flanges in 1" x 1/2" x .050" Waveguide Test Section
41.	Power vs Pressure for Misalignment Between Cover Flanges in Vertical Plane for 1" x 1/2" x .050" Waveguide Test Section
42.	Power vs Pressure for Misalignment for Cover Flanges in Horizontal Plane for 1" x 1/2" x .050" Waveguide Test Section
43.	Power vs Pressure for Cover Flanges Misaligned .020" in Both Horizontal and Vertical Planes for 1" x 1/2" x .050" Waveguide Test Section
44.	Power vs Pressure for Choke-to-Cover Flange Connection (1" x 1/2" x .050" Waveguide)
45.	Power vs Pressure for Choke-to-Cover Flange Connection Having .040" Vertical Misalignment (1" x 1/2" x .050" Waveguide)
46.	Power vs Pressure for Choke-to-Cover Flange Connection Having a .040" Vertical Misalignment Showing Dual-Slope Curve (1" x 1/2" x .050" Waveguide)
47.	Power vs Pressure for Choke-to-Cover Flange Connection Having a .040" Horizontal Misalignment (1" x 1/2" x .050" Waveguide)
48.	Power vs Pressure for Choke-to-Cover Flange Connection Having a .020" Horizontal Misalignment (1" x 1/2" x .050" Waveguide)
49.	Power vs Pressure for Choke-to-Cover Flange Connection Having a .040" Horizontal Misalignment (1" x 1/2" x .050" Waveguide)

## LIST OF ILLUSTRATIONS (cont)

<u>Figure</u>	<u>Title</u>
50.	Power vs Pressure for Choke-to-Cover Flange Connection Having a .020" Horizontal and Vertical Misalignment (1" x 1/2" x .050" Waveguide)
51.	Power vs Pressure for Choke-to-Cover Flange Connection Having a .040" Horizontal and Vertical Misalignment (1" x 1/2" x .050" Waveguide)
52.	Power vs Pressure for Choke-to-Cover Flange Connection Having a .040" Horizontal and Vertical Misalignment, Showing Dual Slope Curve (1" x 1/2" x .050" Waveguide)
53.	Power vs Pressure for Vertebrae Type Flexible Waveguide (1" x 1/2" x .050" Waveguide)
54.	Power vs Pressure for Typical Welded Butt Joint Having a .005" Groove (1" x 1/2" x .050" Waveguide)
55.	Power vs Pressure for Welded Butt Joint Having a .005" Groove (1" x 1/2" x .050" Waveguide)
56.	Power vs Pressure for Welded Butt Joint Having a .005" Gap
57.	Power vs Pressure for Typical Welded Choke Joint (1" x 1/2" x .050" Waveguide)
58.	Power vs Pressure for Typical Welded Choke Joint Having a .005" Gap (1" x 1/2" x .050" Waveguide)
59.	Power vs Pressure for Titeflex Waveguide No. 40184 and No. 40198 (1" x 1/2" x .050" Waveguide)
60.	Power vs Pressure for Titeflex Waveguide No. 40198 (1" x 1/2" x .050" Waveguide)



## LIST OF ILLUSTRATIONS (cont)

<u>Figure</u>	<u>Title</u>
61.	Power vs Pressure for Flexible Waveguide (1" x 1/2" x .050" Waveguide)
62.	LN Power vs LN Pressure for USL Contact Flange
63.	Power vs Pressure for 90-Degree H-Plane Bend (1" x 1/2" x .050" Waveguide)
64.	Power vs Pressure for 90-Degree H-Plane Bend of Radius 1-1/2 inches (1" x 1/2" x .050" Waveguide)
65.	Power-Pressure Data for E- and H-Plane Bends With Varying Radii, Bend Angle, and Manufactures
66.	Repeat Test Breakdown Data for 90-Degree H- Plane Bend (Ref. to Bend #3, Table 7)
67.	Power vs Pressure for Waveguide Switch and Dummy Load (1-1/4" x 5/8" x .064" Waveguide)
68.	Power vs Pressure for 90-Degree E-Plane Bend of Radius 1.081 inches (1" x 1/2" x .050" Waveguide)
69.	Power vs Pressure for Combination 90-Degree E- and H-Plane Bend (1" x 1/2" x .050" Waveguide)
70.	Power vs Pressure for 90-Degree E-Plane Bend of Radius 0.925 inch (1" x 1/2" x .050" Waveguide)
71.	Power Capacity of E-Plane Bend vs Radius
72.	Power vs Pressure for 90-Degree H-Plane Mitered Corner (1" x 1/2" x .050" Waveguide)
73a.	Power vs Pressure for two 90-Degree Twist Sections (1" x 1/2" x .050" Waveguide)

## LIST OF ILLUSTRATIONS (cont)

<u>Figure</u>	<u>Title</u>
73b.	Breakdown Power vs Pressure for Three-Twist Sections
74.	Breakdown Power vs Pressure for the Two Hole Directional Coupler
75.	Breakdown Power vs Pressure for the Cross-Guide Coupler With Slots Transverse to Primary Waveguide
76.	Breakdown Power vs Pressure for the Cross-Guide Coupler With Slots Parallel to Primary Waveguide
77.	Breakdown Power vs Pressure for the Schwinger Coupler With Slots in the Broad Wall of the Primary Waveguide
78.	Breakdown Power vs Pressure for the Schwinger Coupler With Slots in the Narrow Wall of the Primary Waveguide
79.	Breakdown Power vs Pressure for Branched Guide-Directional Coupler
80.	Breakdown Power vs Pressure for E-Plane Tee
81.	Breakdown Power vs Pressure for H-Plane Tee
82.	Breakdown Power vs Pressure for Magic Tee
83.	Power vs Pressure for Hybrid Ring (1" x 1/2" x .050" Waveguide)
84.	Power vs Pressure for Rectangular to Circular Waveguide Rotary Joint (1" x 1/2" x .050" Waveguide)
85.	Power vs Pressure for Rotary Joint (1-1/4" x 5/8" x .064 Waveguide)

## LIST OF ILLUSTRATIONS (cont)

<u>Figure</u>	<u>Title</u>
86.	LN Power vs LN Pressure for a Dual Feed Coaxial Line Rotary Joint
87.	Power vs Pressure for Section Containing Hemispherical Bumps (1" x 1/2" x .050" Waveguide)
88.	Lossy-Wall Type of High Power Load
89.	Power vs Pressure for Coaxial Line-to-Waveguide Adapter (1" x 1/2" x .050" Waveguide)
90.	Breakdown Power vs Pressure for the 1" x 1/2" Waveguide Dummy Load
91.	Breakdown Power vs Pressure for 1-1/4" x 5/8" Waveguide Dummy Load
92.	Power vs Pressure for Waveguide Dummy Load (1-1/4" x 5/8" x .064" Waveguide)
93.	Power vs Pressure for Steps Transformer from 1" x 1/2" to 1-1/4" x 5/8" Waveguide
94.	Power vs Pressure for Model X20L Ferrite Isolator (1-1/4" x 5/8" x .064" Waveguide)
95.	Power vs Pressure for Model HL86-96 Uniline Isolator (1-1/4" x 5/8" x .064" Waveguide)
96.	Various Types of Waveguide Irises
97.	Power vs Pressure for Various Symmetrical Inductive Irises (d = 1/32 inch)
98.	Power vs Pressure for Various Symmetrical Inductive Irises (d = 1/64 inch)

## LIST OF ILLUSTRATIONS (cont)

<u>Figure</u>	<u>Title</u>
99.	Percentage Waveguide Power vs VSWR for a Symmetrical Inductive Iris
100.	LN Power vs LN Pressure for Various Asymmetrical Inductive Irises ( $d = 1/32"$ )
101.	LN Power vs LN Pressure for Various Symmetrical Capacitive Irises ( $d = 1/32"$ )
102.	LN Power vs LN Pressure for Symmetrical Capacitive Irises with Various Thickness ( $d$ )
103.	LN Power vs LN Pressure for Various Asymmetrical Capacitive Irises ( $d = 1/32"$ )
104.	LN Power vs LN Pressure for Symmetrical Inductive Step
105.	LN Power vs LN Pressure for Symmetrical Capacitive Step
106.	LN Power vs LN Pressure for Asymmetrical Capacitive Step
107.	Power-Pressure Data for Flat-Ended Cylindrical Posts
108.	Power-Pressure Data for Hemispherical Ended Cylindrical Posts
109.	Relative Power Capacity vs Post Length for Flat-Ended Capacitive Waveguide Post (Refer to Table 15)
110.	Relative Power Capacity vs Post Length for Spherical-Ended Capacitive Waveguide Post (Refer to Table 16)



## LIST OF ILLUSTRATIONS (cont)

<u>Figure</u>	<u>Title</u>
111.	Relative Power Capacity vs Post Length for Flat and Spherical-Ended Capacitive Waveguide Posts (Refer to Tables 15 and 16)
112.	LN Power vs LN Pressure for Thin Inductive Strip ( $d = 0.250''$ )
113.	LN Power vs LN Pressure for Thin Capacitive Strip ( $d$ varied)
114.	LN Power vs LN Pressure for Cylindrical Rod ( $d$ varied)
115.	Waveguide Apertures
116.	LN Power vs LN Pressure for Longitudinal Aperture in Broad Wall
117.	LN Power vs Pressure for Round Aperture in Broad Wall
118.	Power Capacity vs Susceptance

CONFIDENTIAL

PART I

SECTION A

PURPOSE

1. PURPOSE OF DEVELOPMENT

This contract is primarily concerned with the development of a measurement technique to determine waveguide peak-power capacity as a function of several electrical and mechanical variables. A secondary purpose involves the determination of the peak-power capacity of specified components in 1-inch x 1/2-inch x .050-inch waveguide. The experimental determination of the peak-power capacity of specified components in the 3-inch x 1-1/2-inch x .080-inch waveguide size was deleted from the contract because of the continued unavailability of an S-band power source. In its place a program to determine the breakdown characteristics of basic microwave structures or "building-blocks" was substituted.

2. STUDY AND WORK PHASES

The program was divided as follows:

- a. study and full appraisal of all available technical information on the subject of breakdown in waveguide transmission lines and components

CONFIDENTIAL

CONFIDENTIAL

b. study and experimental investigation of various means for the positive measurement of peak-power capacity

c. development of the techniques required for the application of the method of measurement chosen from b.

d. investigation into the problem of determining the breakdown region

e. application of the results of the previously described work to an investigation of the dependence of peak-power capacity upon the following design parameters:

- (1) pulse duration
- (2) pulse shape
- (3) pulse repetition frequency
- (4) gas pressure
- (5) nature of the gas
- (6) mechanical finish
- (7) plating material
- (8) microwave frequency

f. testing the following 1-inch x 1/2-inch x .050-inch waveguide components:

- (1) DA-22/U termination
- (2) CU-206/U directional coupler

CONFIDENTIAL

- (3) CU-164/U interlocked flexible waveguide
- (4) CU-168/U convoluted flexible waveguide
- (5) UG-446/U waveguide-to-type N adapter
- (6) UG-456/U series tee
- (7) UG-457/U shunt tee
- (8) UG-40A/U-to-UG-39/U, choke-to-cover flange connection
- (9) UG-39/U-to-UG-39/U, cover-to-cover flange connection
- (10) rotating joint, circular-waveguide type
- (11) rotating joint, rectangular-waveguide type
- (12) directional coupler, branch-guide, 10-db
- (13) directional coupler, two-hole, 20-db
- (14) directional coupler, Bethe-hole, 25-db
- (15) directional coupler, long-slot, 10-db
- (16) directional coupler, Schwinger, 30-db
- (17) waveguide switch, rotating-drive type
- (18) waveguide switch, resonant-ring type
- (19) waveguide switch, rotating-disk type
- (20) hybrid-ring duplexer
- (21) conventional waveguide duplexer

The investigation of the breakdown characteristics of the basic microwave structures or building blocks stressed investigation of the:

- a. performance of the building blocks
- b. proximity effects of the building blocks



CONFIDENTIAL

c. existing components to analyze weak links on the basis of the results of the building-block investigation

d. improvement of existing components based on utilizing optimized building blocks

e. existence of more than one type of breakdown

The following basic microwave structures, or building blocks, received the major emphasis under this program:

a. probes

b. bends

c. posts

d. slots

e. irises

f. twists

CONFIDENTIAL

SECTION B  
GENERAL FACTUAL DATA

3. REFERENCES

All references cited in the text are listed alphabetically according to the authors in Appendix I.

4. FORMULAE

4.1 General

The mathematical considerations concerning certain phases of this program are presented herein. Additional mathematical analyses, whose development is an integral part of the material under discussion, are included in Section C, Detail Factual Data.

4.2 Sliding Mismatch Reflectometer Method for VSWR Measurement (Fifth Quarterly Report)\*

The error analysis made on the sliding mismatch reflectometer method for VSWR was based on the use of the test circuit shown in figure 1.

The following notations were used:

c = difference in coupled power between forward and backward directions in the auxiliary line

d = directivity of the coupler (assumed symmetrical)

\* Refers to the interim report in which the detailed analysis may be found.

CONFIDENTIAL

$\Gamma_1$  = bend voltage reflection coefficient (assumed equal in both directions)

$\Gamma_2$  = pressure-window voltage reflection coefficient (assumed symmetrical)

$\Gamma_3$  = coupling-structure voltage reflection coefficient (assumed symmetrical)

$\Gamma_4$  = detector voltage reflection coefficient

a = voltage reflection coefficient of unknown

b = voltage reflection coefficient of sliding mismatch

Case 1 of the analysis considered that the detector was on the arm of the secondary waveguide which received the incident power, and that the sliding mismatch was on the arm which received the reflected power. For Case 2 of the analysis, it was considered that the detector was on the arm which received the reflected power, and that the sliding mismatch was on the arm which received the incident power.

The maximum relative error for Cases 1 and 2 for several special conditions are the quantities of interest. First when

$$a \ll 1, b \ll 1$$

for Case 1,

$$\text{maximum relative error} = \frac{d + \Gamma_1 + \Gamma_2 + \Gamma_4}{1 + a} \quad (1)$$

for Case 2,

$$\text{maximum relative error} = \frac{d + \Gamma_1}{1 + a} \quad (2)$$

CONFIDENTIAL

Now consider the where

$$a \ll 1, b = 1$$

for Case 1,

$$\text{maximum relative error} = \frac{d + \Gamma_1 + \Gamma_2 + \Gamma_4}{1 + a} \quad (3)$$

for Case 2,

$$\text{maximum relative error} = \frac{\frac{d + \Gamma_1}{1 + \Gamma_1 + \Gamma_2 + \Gamma_3 + \Gamma_4}}{1 + a} \quad (4)$$

When

$$a = 1, b \ll 1$$

for Case 1,

$$\text{maximum relative error} = \frac{\frac{c + \Gamma_2 + \Gamma_4}{1 + \Gamma_1 + d}}{1 + a} \quad (5)$$

for Case 2,

$$\text{maximum relative error} = \frac{\frac{c - \Gamma_2 - \Gamma_4}{1 + d + \Gamma_1 + \Gamma_2 + \Gamma_4}}{1 + a} \quad (6)$$

When

$$a = 1, b = 1$$

for Case 1,

$$\text{maximum relative error} = \frac{\frac{c + \Gamma_1 + 2\Gamma_2 + \Gamma_3 + 2\Gamma_4}{1 + \Gamma_1 + d}}{1 + a} \quad (7)$$

for Case 2,

$$\text{maximum relative error} = \frac{\frac{c - \Gamma_1 - 2\Gamma_2 - \Gamma_3 - 2\Gamma_4}{1 + d + 2\Gamma_1 - 2\Gamma_2 + \Gamma_3 + 2\Gamma_4}}{1 + a} \quad (8)$$



CONFIDENTIAL

A comparison of all four conditions of  $a$  and  $b$  shows that the maximum error is less for Case 2 than for Case 1. In addition, it can easily be shown that the probable error is less for Case 2.

The question arose as to what was the optimum value of  $b$  to minimize the error. When  $a$  is small, the error is smaller for  $b = 1$  than for  $b \ll 1$ ; and where  $a = 1$ , the error is smaller for  $b \ll 1$ . There are several other factors which must be considered. First, for small values of  $b$  the variation of power at the detector is small as the mismatch is moved. This will magnify errors in meter reading and any errors due to noise or other random fluctuations. Second, if the values of  $a$  and  $b$  are of the same order, it is impossible to determine by a single measurement which of these values is the larger. This results in an essential ambiguity in the determination of the unknown VSWR, since the function of VSWR versus meter indication is double-valued. All of the above considerations suggest that a value of  $b = 1$  will yield the most effective results.

#### 4.3 Root-Mean-Square Technique for Classifying Surface Roughness (Twelfth Quarterly Report)

The root-mean-square technique for classifying surface roughness is applicable to machined surfaces only. Surfaces produced by casting, molding, forging, rolling or some

CONFIDENTIAL

similar technique cannot be specified by an RMS value. The term RSM is defined as the square root of the sum of the squares of n measurements of the heights and depths of the surface divided by n. This definition expressed as an equation becomes

$$\text{RMS} = \sqrt{\frac{A^2 + B^2 + C^2 + D^2 + \dots + n^2}{n}} \quad (9)$$

The heights and depths of the surface were measured in microinches from a mean surface, that is, an imaginary surface that would occur if the valleys and peaks were averaged to zero.

The RMS value is truly representative of a machined surface because it gives appropriate emphasis to the peaks and valleys comprising the surface. The actual readings were taken with a profilometer which consisted of a stylus that ran along the machined surface and was connected to an effective-reading voltmeter calibrated to read in microinches.

The waveguide sections actually tested were fabricated by using a milling tool cutter which was preset to a fixed angle. The roughness of the finish was then varied by adjusting the feed rate of the work into the tool. In this manner the depth and spacing of the grooves were varied

CONFIDENTIAL

CONFIDENTIAL

#### 4.4 Power Capacity of H-Plane Waveguide Bend (Thirteenth Quarterly Report)

In order to obtain an expression for the peak-power capacity of an H-plane bend as a function of the radius of curvature, the bend section of the waveguide was visualized as a radial-line structure in which the electric-field distribution was represented by a Bessel function. The particular distribution then could be determined by considering propagation in the transverse direction (along the radius of the radial line) and using standard techniques to find the resonant length. Once the particular half cycle of the particular Bessel function was determined, the power capacity of the bend could be related to the power-carrying capacity of rectangular waveguide. For the particular dimensions chosen, this resulted in a power-carrying capacity of 97 percent of standard waveguide. According to the theory, this is the value of power-carrying capacity that is obtained for the worst case of zero radius, and, as the radius is increased, the peak-power-carrying capacity will approach 100 percent of waveguide power.

The analysis assumed a waveguide of constant cross section and neglected the effect of mismatches due to the ends of the bend.

CONFIDENTIAL

#### 4.5 Power Capacity of E-Plane Waveguide Bend (Thirteenth Quarterly Report)

An approximate expression for the peak-power capacity of E-plane bends as a function of the radius was obtained by comparing the bend to a coaxial waveguide. Figure 2 shows a sketch of the pertinent dimensions for the E-plane bend. The detailed analysis leads to the following expression for the peak-power capacity of an E-plane bend as a function of the radius:

$$\text{Power (E-plane bend)} = \left[ \frac{R_1 \ln \frac{R_2}{R_1}}{R_2 - R_1} \right]^2 \times 100 \quad (10)$$

expressed as a percentage of the waveguide power. A normalized plot of equation 10 is shown in figure 2.

This analysis assumed a constant cross-sectional area in the bend and neglected the effect of the discontinuities at the ends of the bend due to a change of characteristic impedance.

#### 4.6 Effect of VSWR Upon Peak-Power Capacity (Fourteenth Quarterly Report)

##### a. Introduction

The effect of VSWR upon the peak-power capacity of waveguide transmission lines has been theoretically analyzed



CONFIDENTIAL

before\*. The purpose of this paragraph is to reiterate, clarify, and extend the analysis so that the theoretical and experimental results can be compared.

Voltage standing-wave ratio (VSWR) and the reflection coefficient (  $\Gamma$  ) may be defined as:

$$VSWR = \frac{|E_i| + |E_r|}{|E_i| - |E_r|} \quad (11)$$

where

$E_i$  = incident voltage in transmission line

$E_r$  = reflected voltage in transmission line

$$\Gamma = \frac{E_r}{E_i} \quad (12)$$

By combining equations (11) and (12), the following relationships between VSWR and  $\Gamma$  are obtained:

$$|\Gamma| = \frac{VSWR - 1}{VSWR + 1} \quad (13)$$

$$VSWR = \frac{1 + |\Gamma|}{1 - |\Gamma|} \quad (14)$$

b. Lossless, Mismatched Line

The first case considered was that of a single mismatch situated in a transmission line. It was assumed

\*See ref. 1, pp. 169-170 and ref. 81, pp. 30-31

CONFIDENTIAL

that the line was lossless, that the generator was matched to the line, and that the mismatch was a pure shunt reactance. Using these assumptions, the maximum power that may be transmitted was found to be

$$P_{lmax} = \frac{1}{(1 + |\Gamma|)^2} 100 \quad (15)$$

where

$P_{lmax}$  = maximum transmitted power for lossless, mismatched line

Equation (15) is expressed as a percentage of full waveguide power.

#### c. Lossy, Mismatched Line

The equation for a lossy line can be obtained in a similar manner, except that the attenuation of the incident and reflected waves as they travel along the transmission line must be taken into account. The attenuation in the line will increase over that value for a matched line as a result of the presence of the mismatch\*. The assumptions for this analysis were that the mismatch is a pure shunt reactance and that the attenuation is linear with distance. It was found that breakdown will always occur at the point of maximum voltage which is closest to the generator.

\*See ref. 81 pp. 30-31

CONFIDENTIAL

The transmitted power was found to be

$$P_{2max} = \frac{1}{(1 + |\Gamma|^2 x^2)^2} 100 \quad (16)$$

where

$P_{2max}$  = maximum transmitted power for lossy, mismatched line.

$$x = \frac{1}{\log^{-1} \frac{a_{\Gamma} l}{20}}$$

$l$  = distance between generator and mismatch, in feet.

$$a_{\Gamma} = \frac{\text{power lost}}{\text{power incident}} \frac{\text{db}}{\text{ft}}$$

Equation (16) is expressed as a percentage of full waveguide power.

#### d. Lossless, Mismatched Cavity

Two mismatches, properly spaced in a transmission line to form a resonant cavity, were considered next. This analysis was performed assuming that there were no losses, that the mismatch was represented by a pure shunt reactance, and that the input VSWR to the cavity was unity.

The maximum transmitted power for a lossless matched cavity in terms of the VSWR of one of the mismatches was found to be

CONFIDENTIAL

CONFIDENTIAL

$$P_{3\max} = \frac{1}{VSWR} 100 \quad (17)$$

where

$P_{3\max}$  = maximum transmitted power for lossless, matched cavity.

Equation (17) is expressed as a percentage of full waveguide power.

#### e. Lossy, Mismatched Cavity

In order to extend this cavity analysis so that it can have more practical application, the various losses were considered. The two main losses were due to the attenuation in the line and to the mismatch at the input terminals to the cavity. For this case, the attenuation was assumed to be linear with distance and the mismatch was assumed to be a pure shunt reactance.

The maximum transmitted power for a lossy, mismatched cavity was found to be:

$$P_{4\max} = \left[ \frac{1}{(1 + x^2 |\Gamma_2|^2)} \right] \left[ \frac{1 - \Gamma_2^2}{1 - \Gamma_0^2} \right] 100 \quad (18)$$

where:

$\Gamma_0$  = reflection coefficient for total cavity

CONFIDENTIAL



CONFIDENTIAL

$\Gamma_2$  = reflection coefficient of mismatch further from the generator

and

x = maximum value of the incident voltage wave after having been attenuated in traveling along the line a distance L.

If

L = distance between mismatches

then:

$$x = \frac{1}{\log^{-1} \frac{\alpha \Gamma L}{20}}$$

Equation (18) is expressed as a percentage of full waveguide power.

C. G. Montgomery\*\* considered some of the basic properties of resonant cavities that use an inductive iris as the coupling mechanism. The following equation is used in this report, and is derived for the case of lossless, matched, iris-coupled, short-circuited, waveguide, resonant cavity:

$$N^2 = \frac{B_o^2}{2} + B_o \sqrt{\frac{B_o^2}{4} + 1} + 1 \quad (19)$$

where

$B_o$  = normalized susceptance of the mismatch.

For  $B_o \gg 1$ , the voltage increase can be reduced to the following expression:

$$N = B_o \quad (20)$$

\*See ref. 79, pp. 167 and 182-186

CONFIDENTIAL

A. Lawson and R. Fano\* derived the following expression for the loaded Q of a lossless, matched cavity formed by two shunt reactances:

$$Q_L = n \frac{B_o^2 + 1}{4 \left[ 1 - \left( \frac{w_c}{w_o} \right)^2 \right]} \tan^{-1} \frac{2B_o}{B_o^2 - 1} \quad (21)$$

where

n = number of half wavelengths in length of cavity

$$1 - \left( \frac{w_c}{w_o} \right)^2 = \left( \frac{\lambda}{\lambda_g} \right)^2$$

$\lambda$  = free-space wavelength

$\lambda_g$  = waveguide wavelength

When  $B_o \gg 1$ , the Q factor becomes

$$Q_L = \frac{n\pi}{4} B_o \left( \frac{\lambda_g}{\lambda} \right)^2 \quad (22)$$

By combining equations (22) and (20), for the case of  $B_o \gg 1$ , maximum cavity voltage was found to be

$$N = \frac{4}{n\pi} \sqrt{Q_L} \left( \frac{\lambda}{\lambda_g} \right) \quad (23)$$

\*See ref. 58, p. 654 - 657

#### 4.7 Power Capacity of Rectangular and Ridge Waveguide (Fifteenth Quarterly Report)

The transmitted power in a waveguide can be determined from Poynting's equation which is stated as follows:

$$P_T = \int \mathbf{E} \times \mathbf{H} \cdot d\mathbf{A} \quad (24)$$

where

$P_T$  = transmitted power

$E$  = electric field

$H$  = magnetic field

$A$  = cross-sectional area of the waveguide

For the dominant mode in a rectangular waveguide,

$$H = KE \quad (25)$$

and

$$dA = b \, dx \quad (26)$$

where

$K$  = a constant

$b$  = narrow dimension of waveguide

$x$  = distance along broad dimension

The transmitted power for rectangular waveguide ( $P_{T_1}$ ) can therefore be written as:

(27)

CONFIDENTIAL

$$P_{T1} = \int K E^2 b dx \quad (27)$$

If it is assumed that the same voltage gradient causes breakdown for both the ridge and rectangular waveguide, then the ratio of the transmitted power for ridge waveguide to that for rectangular waveguide can be formulated, and the power capacity of ridge waveguide as a function of the known power capacity of rectangular waveguide can be obtained. These operations are performed as follows:

For rectangular waveguide,

$$E_o = E_o \sin \frac{\pi x}{a} \text{ volts per centimeter} \quad (28)$$

where

$E_o$  = peak value of the electric field, in volts per centimeter

$a$  = broad dimension of waveguide

If equation (28) is substituted into equation (27),

$$P_{T1} = \int_0^a K E_o^2 b \sin^2 \frac{\pi x}{a} dx \quad (29)$$

Evaluating this integral over the limits shown results in the following expression for the transmitted power in rectangular waveguide:

CONFIDENTIAL



CONFIDENTIAL

$$P_{T_1} = \frac{K}{2} a b E_0^2 \quad (30)$$

To obtain the field components for ridge waveguide, reference is made to Cohn's<sup>(12)</sup> article on ridge waveguide and to figure 3. The electric field can be divided into two sections as follows:

$$E_1 = E_0 \cos \theta \quad 0 \leq \theta \leq \theta_2 \quad (31)$$

$$E_2 = \frac{b_2 \cos \theta_2}{b_1 \sin \theta_1} E_0 \sin(\theta_1 + \theta_2 - \theta) \quad (32)$$

$$\theta_2 \leq \theta \leq (\theta_1 + \theta_2)$$

All factors described in figure 3 can be stated as follows:

$E_1$  = electric field in region above ridge

$E_2$  = electric field in region between ridge and waveguide side wall

$\theta$  = angular distance along broad dimension

$\theta_2$  = angular distance from centerline of ridge to edge of ridge

$\theta_1$  = angular distance from edge of ridge to waveguide wall

$b_2$  = height of waveguide in section with ridge

$b_1$  = height of waveguide in section without the ridge

CONFIDENTIAL

The transmitted power in ridge waveguide ( $P_{T_2}$ ) is, therefore,

$$P_{T_2} = 2 \int K E_1^2 dA + 2 \int K E_2^2 dA \quad (33)$$

but

$$dA = b dx \quad (34)$$

$$dx = \frac{\lambda_c'}{2\pi} d\theta \quad (35)$$

where

$\lambda_c'$  = wavelength in free space at the ridge waveguide cutoff frequency

Therefore,

$$P_{T_2} = 2 \frac{\lambda_c'}{2\pi} \int_0^{\theta_2} K b_2 E_0^2 \cos^2 \theta d\theta + \frac{\lambda_c'}{2\pi} \left[ \frac{b_2}{b_1} \right]^2 \left[ \frac{\cos \theta_2}{\sin \theta_1} \right]^2 \int_{\theta_2}^{(\theta_1 + \theta_2)} K b_1 E_0^2 \sin^2(\theta_1 + \theta_2 - \theta) d\theta \quad (36)$$

Integration of equation (36) yields the following:

$$P_{T_2} = b_2 \frac{\lambda_c'}{\pi} K E_0^2 \left[ \frac{1}{2} \theta_2 + \frac{1}{4} \sin 2 \theta_2 + \frac{b_2}{b_1} \left[ \frac{\cos \theta_2}{\sin \theta_1} \right] \left[ \frac{1}{2} \theta_1 - \frac{1}{4} \sin 2 \theta_1 \right] \right] \quad (37)$$

Equations (30) and (37) represent the transmitted power for rectangular and ridge waveguide respectively. The power-carrying capacity of the ridge waveguide as a function of the power-carrying of the rectangular waveguide is obtained by dividing equation (37) by equation (30).

#### 4.8 Scaling Techniques for the Power Capacity of Waveguides (Fifteenth Quarterly Report)

Scaling of the power capacity of waveguide from one size to another was performed in the following manner:

The continuous-wave peak-power capacity is\*

$$P_w = k E_o^2 ab \frac{\lambda}{\lambda_g} \text{ watts} \quad (38)$$

where

$k$  = a constant

$E_o$  = peak value of electric field, in volts per centimeter

$ab$  = area of a waveguide having dimensions  $a$  and  $b$

$\lambda$  = free-space wavelength

$\lambda_g$  = waveguide wavelength

Both the voltage gradient and the constant can be eliminated from equation (38), since the continuous-wave

\*See ref. 81, p 124

CONFIDENTIAL

peak-power capacity of 1-inch x 1/2-inch x .050-inch waveguide has been measured (refer to paragraph 10.1g).

Equation (38) then becomes

$$P_w = 4.0 ab \frac{\lambda}{\lambda_g} \text{ megawatts} \quad (39)$$

where

$4.0 = kE_o^2$ , as determined from the data obtained in 1- x 1/2- x 0.050-inch waveguide size using the February 1956 test results (see figure 39)

$ab$  = waveguide area in square inches

Investigation in 1- x 1/2- x 0.050-inch waveguide has shown that the power is proportional to the pulse width raised to the 1/3 power, over the range from 0.4 to 2.35 microseconds (refer to paragraph 9.2). In the region of 2.35 microseconds the 1/3-power curve levels off, and for pulse widths greater than 2.35 microseconds the breakdown characteristics are the same as for continuous-wave power. In order to extrapolate this information to other frequency ranges it was assumed that the ratio of the pulse width to the r-f frequency is the major factor that determines the value at which the pulse width is so large as to appear as a continuous wave. For a discussion of this assumption refer to the fifteenth interim report.



CONFIDENTIAL

On the basis of this assumption

$$g = \frac{9375}{f} \quad 2.35 \text{ microseconds} \quad (40)$$

where

$g$  = threshold pulse width at which the breakdown characteristics for pulsed- and continuous-wave power are the same

$f$  = frequency of operation, in megacycles

Once  $g$  was found, the scaling factor for the desired pulse width was determined by using the 1/3-power law. The equation for the power capacity now is

$$P_w = 4.0 \text{ ab } \frac{\lambda}{\lambda_g} \left[ \frac{g}{\tau} \right]^{\frac{1}{3}} \text{ megawatts} \quad (41)$$

where

$\tau$  = pulse width (in microseconds) for which the power capacity is desired.

$$\left[ \left[ \frac{0.4}{2.35} \right] g \leq \tau \leq g \right]$$

Since very little information was obtained for pulse widths of less than 0.4 microsecond, it was difficult to predict what happens to the breakdown characteristics for short pulse widths. However, since the range covered in this analysis applies to most practical cases the information contained in equation (41) should prove very useful.

CONFIDENTIAL

CONFIDENTIAL

The effect of pulse-repetition rate upon peak-power capacity was investigated (see paragraph 9.2) and it was found that the power capacity was proportional to the repetition rate raised to the  $1/15$  power, in the range from 400 to 2500 pps. It was assumed that the effect of repetition rate is independent of frequency; this is discussed in the fifteenth interim report. When this factor was included in equation (4), the following equation resulted:

$$P_w = 4.0 \text{ ab } \frac{\lambda}{\lambda_g} \left[ \frac{g}{\tau} \right]^{\frac{1}{3}} \left[ \frac{2500}{r} \right]^{1/15} \text{ megawatts} \quad (42)$$

where

$r$  = pulse-repetition rate

No data was obtained for values of repetition rate less than 400 or greater than 2500 pps. It is difficult to predict what happens to the power capacity when the pulse-repetition frequency is reduced to values lower than 400, but it is likely that the effect becomes smaller above 2500 pps. However, the values covered in this report represent those generally encountered in practical applications.

#### 4.9 Voltage Gradient in the Swayback Gap Section (Eighteenth Quarterly Report)

The swayback was experimentally found to consist of two lumped discontinuities,  $\Gamma_1$  and  $\Gamma_2$  of equal magnitude

CONFIDENTIAL

with an overall reflection coefficient  $\Gamma_3$ . The effective breakdown power, in the swayback reduced-height section ( $P_{eff}$ ) between  $\Gamma_1$  and  $\Gamma_2$  due to the cavity effect in terms of the measured power incident on the test section ( $P_o$ ), was calculated to be

$$P_{eff} = \left[ 1 - |\Gamma_3|^2 \right] (VSWR)_2 P_o \quad (43)$$

#### 4.10 Breakdown-Power Accuracy as a Function of Pressure

An expression for the error in breakdown power due to the error in pressure was required. Tests have shown that the breakdown power for standard waveguide is proportional to the square of the absolute pressure. This may be stated mathematically as follows:

$$P = Kp^2 \quad (44)$$

where

$P$  = peak power

$p$  = absolute pressure

$K$  = a proportionality constant

Equation (44) may be differentiated to obtain the incremental change in breakdown power,  $dP$ , due to an incremental change in pressure,  $dp$ . Thus,

$$dP = 2Kpdp$$

CONFIDENTIAL

CONFIDENTIAL

Equation (45) is exactly correct only for infinitesimal changes in power and pressure. However, an approximate expression can be derived in terms of measurable quantities, which will be sufficiently accurate for the present application.

To derive this expression let

$$\Delta P = 2K_p \Delta p \quad (46)$$

where

$\Delta p$  = an increment of pressure corresponding to the error in the pressure measurement

$\Delta P$  = an increment of power corresponding to the resultant error in breakdown power

The relative error in peak-power capacity,  $\Delta P/P$ , as a function of the relative error in pressure,  $\Delta p/p$ , was obtained by dividing equation (46) by equation (44). The result of this operation expressed as a percentage relative error is:

$$\frac{\Delta P}{P} = 2 \frac{\Delta p}{p} \times 100 \text{ percent} \quad (47)$$



SECTION C  
DETAIL FACTUAL DATA

5. INTRODUCTION

During the past decade much scientific endeavor was concentrated upon the production of radar systems to meet specific demands. The consideration of the theoretical and practical limitations of the system and its various components was necessarily set aside because of the urgency of new problems. Today, however, the effective design of a new system demands a greater knowledge of the factors which limit the performance of the system. The range and resolution are two important parameters describing system performance. Both quantities can be increased by employing higher powers. Since the power output of the system is often limited by the power carrying capacity of the various components, it was appropriate that an investigation of high-power breakdown of waveguide components be conducted.

The first experimental investigation of microwave breakdown<sup>(85)</sup> was performed at the Radiation Laboratory at M.I.T. and was reported in 1945. Pulsed power was used, and the purpose of the tests was to determine the variation of breakdown power with such parameters as pressure, gap width,



CONFIDENTIAL

repetition rate, pulse width, and humidity. Radioactive cobalt was employed to produce initial ionization in the breakdown gap, which consisted of a waveguide section of reduced height. This irradiation produced repeatable results as compared to measurements made without irradiation. The process, however, resulted in significantly lower breakdown powers. This difference, coupled with the fact that measurements were made on sections of reduced height, casts considerable doubt upon the results which extrapolate the data to determine the breakdown power of the full waveguide.

Another report (10) from the Radiation Laboratory of M.I.T. in 1946 presented the results of breakdown tests on various waveguide components. The report represents a compilation of individual tests by many different persons over a period of a few years. Since it is unlikely that the various experimenters used a consistent technique and since the data differed in many cases, the results presented in this report cannot be taken as conclusive.

For this reason more intensive investigations, both theoretical and experimental, were initiated by a number of workers. Margenau's studies (70,71,72) are valuable for discharges in the range of gas pressure above 100 mm of mercury, Holstein's theory (42) applies to discharge vessels

CONFIDENTIAL

CONFIDENTIAL

which were large compared to the mean free path of the electron, and Brown's work (38,39,40,67,68) was mainly in the region of pressures between 1 and 100 mm of mercury. In addition to these men, important theoretical work was performed by MacDonald, (6,67,68) Biondi, (4) Hale, (35) Herlin, (38,39,40) and Hartman (72). While these theories were being developed, more carefully controlled experiments were being conducted. These tests, performed by Cooper, (15,89) Gill and VonEngel, (31) Hale, (35) Herline and Brown, (38,39) MacDonald and Brown, (67,68) Pim, (83,84) and Prowse, (89) served to verify many of the theoretical predictions. In this manner a consistent foundation was formed upon which a thorough knowledge of microwave breakdown can be built.

## 6. THEORIES OF BREAKDOWN

### 6.1 Direct-Current Breakdown

All modern theories of breakdown are based upon an approach first formulated by Townsend in 1902. This theory, which describes breakdown under the action of a d-c field, is based upon the physical concept of the breakdown process that a free electron is created at some point in the gap between the anode and cathode. This can occur because of cosmic radiation, external irradiation of the gap with ultraviolet light or a radioactive material, or by photoelectric emission

from the cathode. The electron then proceeds towards the anode under the influence of the electric field. During the course of its flight the electron will collide with a number of neutral gas molecules. In general these collisions are elastic and have little effect upon the electron energy so that the energy continues to increase to such a value that a collision with a neutral gas molecule produces a positive ion and a new free electron. The two electrons then proceed to repeat the process and soon an electron avalanche is formed. The number of new electrons ( $dn$ ) created per unit time in a distance ( $dx$ ) in the field direction is proportional to  $n$ , the number of electrons per unit time crossing a plane parallel to the electrodes and a distance ( $x$ ) from the cathode. That is

$$dn = n \, dx$$

where  $\alpha$  is a proportionality factor called the first Townsend coefficient. If  $n$  and  $dx$  are unity, then  $dn = \alpha$ , and it is seen that  $\alpha$  represents the number of new electrons created by a single electron in traveling a unit distance in the field direction.

Townsend also recognized the necessity of introducing a second constant,  $\beta$ , to explain the available experimental data. This constant is believed <sup>(60)</sup> to represent

CONFIDENTIAL

the number of secondary electrons liberated from the cathode per positive ion incident on the cathode. Integration of equation (48) yields Townsend's equation for the current,  $i$ , across a gap,  $d$ . Given an initial current,  $i_0$

$$i = \frac{i_0 (a - \beta) e^{(a - \beta)d}}{a - \beta e^{(a - \beta)d}} \quad (49)$$

Now if

$$a = \beta e^{(a - \beta)d} \quad (50)$$

the current,  $i$ , becomes infinite. Equation (50) is usually simplified by employing the experimentally determined fact that  $a$  is much greater than  $\beta$ , in which case equation (50) reduces to

$$\frac{\beta}{a} e^{ad} = 1 \quad (51)$$

Townsend interpreted this condition of infinite current as representing the initiation of a spark, and the corresponding voltage between electrodes was taken as the sparking potential.

Today, certain aspects of Townsend's analysis have been abandoned, and others have been modified. Loeb (60) has established the following three criteria for sparking: (a) a conducting path must have formed completely bridging the gap, (b) an efficient source of secondary emission must be provided at the cathode, and (c) under these conditions the

CONFIDENTIAL

conductivity produced must be sufficient to at least discharge the electrodes. On this basis, Loeb stated that Townsend's single sparking criterion was not sufficient to determine the sparking potential in many cases. In addition, data obtained by White (106) and Roether (96) showed that the time required for a spark formation by the Townsend mechanism was much greater than that experimentally observed. This resulted in the development of the streamer theory of sparking by Roether, (96) Meek, (73) and Loeb (64,78). This theory postulates that it is not necessary that any electron cross the entire gap. To explain the observed short time lags, the suggestion was advanced that breakdown occurred due to a succession of electron avalanches along a breakdown path, the distance of travel in each one being short.

To comprehend the physical process, assume the potential to be raised to a value above that necessary to allow a spark to pass, and consider an electron or negative ion to appear near the center of the gap. This electron will start an avalanche as it proceeds toward the anode, leaving in its wake a cloud of slow-moving positive ions. Most of the ions will be bunched in a fairly dense group two or three ionizing paths long. The electrons will be moving towards the anode in a spatially-larger cloud as a result of diffusion. The rear of the electron cloud will be held back

CONFIDENTIAL



CONFIDENTIAL

by the positive-ion space charge while the advance region will be drawn towards the anode. The result is a wedge-shaped positive-ion charge with the axis parallel to the electric field. The charge causes a resultant field which differs from the applied field; therefore, increased potential gradients are created in the region of positive space charge. The increased gradient further accelerates the electrons, and in the ensuing ionizing collisions many photons are created. These are radiated in all directions and some will ionize in the gas. Since the photons travel with the speed of light, electrons are produced almost simultaneously in the gap. Most of these electrons will be located near the axis of the original avalanche, and thus new avalanches are produced in increasing number along the region of axial field distortion. The leading electrons of each avalanche will be drawn towards the positive space charge of the next avalanche, and a continuous stream of electrons will be formed and breakdown is accomplished.

The streamer theory has been partially verified by Roether's <sup>(96)</sup> photographs of developed streamers in a Wilson cloud chamber, as well as by the experiments of Haseltine <sup>(37)</sup>. However, there is no consistent set of data on sparking potentials in mercury-free dry air with varying pressure and

CONFIDENTIAL

constant gap, and vice versa, over a sufficient range of pressure and gap-length values to permit a test of the theory.

## 6.2 Alternating-Current Breakdown

The lack of significant data on breakdown for alternating current is much more acute than for direct current. Since this is so, a number of theories exist, some of which are partially verified by the available data. In addition, because the frequency is variable, a greater number of domains exist wherein the physical representations of breakdown lead to different initial assumptions and hence to different conclusions. For this reason, theories have been developed which apply to such particular conditions of breakdown as, (a) pressure is below 10 mm of mercury (b) gap is long compared with wavelength (c) gap is short compared with wavelength (d) applied frequency is comparable to the collision frequency, and others. These theories are not necessarily mutually exclusive. A consistent presentation of alternating-current breakdown phenomena will be made through a discussion of the more important theories.

Alternating-current breakdown may be considered as representing the general breakdown condition, in which case the previously described theories of direct-current breakdown

CONFIDENTIAL

are particular solutions of the general problem. The unique aspect of direct-current breakdown is that the electrons and ions created in the gap, all eventually reach one of the electrodes due to the steady uni-directional force existing in the gap. For alternating-current, on the other hand, it is possible that the movement of ions and electrons, even in high fields, may be too limited for their removal to the electrodes to constitute an important factor in breakdown. Since the removal is dependent upon the relationship between the applied frequency, the gap length, and the gas pressure, the several transition regions must be discussed in terms of these parameters.

At power frequencies the field strength is such that both the ions and electrons can be removed from the gap within a half-cycle of the applied power. For this reason the breakdown is similar to direct-current breakdown, and each peak may be regarded as an individual test of breakdown. This condition has been experimentally checked by Ekstrand<sup>(22)</sup>. The tests showed that for gap lengths of less than 0.1 inch in air at atmospheric pressure, the spark-over potential was very nearly the same at 700 kc as at 60 cps. In addition, Reukema<sup>(93)</sup> found that for a gap of 2.5 cm the breakdown potential was constant up to 20 kc in air at atmospheric pressure.

CONFIDENTIAL

CONFIDENTIAL

As the frequency is increased, a value is reached at which some of the slow-moving positive ions cannot reach the negative electrode and are forced to oscillate in the gap. Actually, no one positive ion will permanently oscillate in the gap, because all ions will have a resultant drift motion to either one or the other electrode (depending upon the phase of the field when the electron was created). What actually occurs is that the ions are moving more slowly since they are being alternately accelerated and decelerated (and usually reversed in direction during a part of the cycle.) Thus, the ions take a longer time to cross the gap. This fact, coupled with the fact that there are ions moving in both directions, gives the effect of having an ion cloud oscillating in the gap. These ions affect breakdown in two ways: first, they cause a non-uniformity of the field in the gap, which in some regions therefore exceed the nominal value as calculated from the geometry of the electrodes; and second, they are available to stimulate additional production of electrons in the gap; for example, by photo-ionization as a result of recombination processes. Thus, a lowering of breakdown power is predicted in the range of frequencies where the ions cannot be removed from the gap. Reukema found for the gaps used that there was a progressive lowering of the

CONFIDENTIAL

CONFIDENTIAL

sparkling potential with increasing frequency from about 20 kc to 60 kc. Ekstrand's data showed that increasing the gap length lowered the breakdown power at 700 kc as compared with that at 60 cps.

The experiments of Reukema and Ekstrand qualitatively substantiate the theory that the breakdown power is lowered by the inability of positive ions to cross the gap in one-half cycle of applied voltage. This theory is further verified by an approximate quantitative analysis offered by Prowse (87). A comparison of the ionic mobility calculated by Prowse to the breakdown data of Lassen (56) indicates that the calculated value is very nearly equal to the mobility which will just allow the ion to cross the gap in one-half cycle. Lassen's data covers the frequency range from 743 kc to 2.45 mc and gap widths from .05 to 0.5 cm in air at atmospheric pressure so that a good check on the theory is obtained.

Above the critical range of frequencies, where some positive ions cannot cross the gap, the breakdown potential is constant until the next transition region is reached, (87) at which value the electrons cannot all cross the gap. At this frequency the number of electrons in the gap will increase and, since there is a statistical spread of electron velocities,

CONFIDENTIAL



CONFIDENTIAL

the number of electrons of ionizing velocity is increased. On this basis it is predicted that the breakdown potential will decrease when the electrons cannot cross the gap in one-half cycle of applied frequency.

Experiments made by Gill and Donaldson (30) clearly exhibit this effect. In these tests the pressure was varied for several values of frequency and a decrease in breakdown power was noted where the calculated values of electron velocity allowed a travel distance equal to the gap length in one-half cycle. Since the calculated values also agreed with previously known values, the check on theory was complete. Additional verification was supplied by the experimental work of C. and H. Gutton (34) and by Chenot (9).

Above the transition range where some electrons cannot cross the gap, the breakdown potential is again independent of frequency (87). For the range of pressure and gap length found in practice this region includes the microwave frequencies, because at these frequencies the amplitude of electron movement in air just breaking down is probably of the order of  $1.5 \times 10^{-3}$  cm (87) at atmospheric pressure. The various theoretical analyses of microwave breakdown may be differentiated according to the method of removing the electrons from the gap. There are available three possible

CONFIDENTIAL

CONFIDENTIAL

removal mechanisms: (a) diffusion to the walls of the vessel, (b) recombination with positive ions, and (c) attachment to captor molecules. The particular process of electron removal which determines breakdown depends upon the parameters of frequency, gap length, gas pressure, and the structural nature of the gas.

Brown, MacDonald, and Herlin (6,38) have developed a theory which applies when the following conditions exist: (a) the gap length is small compared with the wavelength of the applied oscillations, (b) the mean free path of the electron is not comparable with the dimensions of the vessel, and (c) the oscillation amplitude of the electron is less than the electrode separation. Condition (c) implies the non-removal of electrons from the gap by the applied field, and conditions (a) and (b) make diffusion the dominant removal process. The breakdown criterion established is that the removal of electrons by diffusion must be equal to the release of electrons by collision. Herlin and Brown experimentally verified the theory for parallel-plate electrodes<sup>(38)</sup> containing air at pressures between 0.1 and 10 mm of mercury, and for a coaxial cavity<sup>(39)</sup> containing air at pressures between 1 and 100 mm of mercury, both at 3,000 mc. In addition, MacDonald and Brown<sup>(67)</sup> have shown excellent

CONFIDENTIAL

experimental agreement with the theory for breakdown in a cylindrical cavity containing helium at pressures between 1 and 100 mm of mercury at a frequency of 3,000 mc.

Holstein (42) has proposed a theory for the energy distribution of electrons under the following conditions:

- (a) the electron energy is such that most electron-molecule collisions are elastic;
- (b) the dimensions of discharge region are large compared with the mean free path of the electron;
- (c) the total number of electrons, ions, and excited molecules is small compared with the number of normal molecules; and
- (d) the frequency of the electric field is greater than some minimum value determined by the pressure, type of gas, and dimensions of discharge region.

This theory states that the energy distribution of electrons subject to a high-frequency field is similar to that of electrons in a steady field equal in magnitude to the r.m.s. value of the high-frequency field. The same conclusion reached by Townsend, (101) and Townsend and Gill, (102) states that it is valid for monatomic gases at a pressure of the order of 10 mm and for diatomic gases at about 1.0 mm, both in a tube of 4-cm diameter. On this basis, Holstein formulated a theory for high-frequency breakdown in a non-attaching gas (41). A consideration of the restrictions shows that diffusion is the dominant removal process so that the breakdown criterion is the same as that of Herlin and Brown,

CONFIDENTIAL

the rate of ionization by collision is balanced by the loss due to diffusion. This theory was experimentally checked by Krasik, Alpert, and McCoubrey <sup>(54)</sup> for the breakdown of a cavity containing argon at pressures between 3 and 100 mm, a gap length of 0.223 inch, and at a frequency of 3,000 mc.

Margenau and Hartman have written a series of papers <sup>(72)</sup> wherein the electron distribution functions are calculated and a theory of high-frequency breakdown is proposed. In this development, the assumptions are made that the pressure is low, the frequency of the applied field is of the order of the collision frequency of the electrons, the gas has an infinite volume, and negative ions are not formed. Under these conditions, volume recombination is the only electron removal mechanism. The calculations show that at a certain field strength the density of electrons increases rapidly and this value is taken as the breakdown potential. The theory is applied to breakdown in helium and neon because only these two, among the rare gases, justify the approximation of constant mean free path. For pressures below 1.0 mm, and for an applied field of frequency at 3,000 mc, it was calculated that neon would break down at 5 volts per cm, and that helium would break down at 13 volts per cm. Qualitative verification of these values is supplied by experiments performed at M.I.T. which showed that for discharge in a vessel below a pressure

CONFIDENTIAL

CONFIDENTIAL

of 1.0 mm, the critical field for neon was 9 volts per cm, and for helium was 19 volts per cm. The vessel used in the experiments was small and the condition of infinite volume was not fulfilled. Therefore, the role of diffusion as an electron removal mechanism was not negligible since the effect of the added removal of electrons is to increase the breakdown power so that the observed difference is in the proper direction. The theory was quite well verified.

Hale (35) proposed a theory of high-frequency breakdown which is basically different from those already mentioned. His theory assumes that the electron must reach ionizing energy at the end of one mean free path for breakdown to occur. The theoretical results obtained are in agreement with those of Margenau in the range where the applied frequency is comparable with the collision frequency; however, in contrast to Margenau, Hale did not restrict his analysis to this region. Hale verified his theory by showing that good agreement was obtained with experimental results of breakdown test using argon and xenon at pressures between 20 and 49 microns, gap separations of 5 and 10 cm, and frequencies between 5 and 50 mc. Since these parameters are so related that the applied frequency is between one and ten times the collision frequency, it cannot be said that Hale's theory has been proven valid

CONFIDENTIAL



CONFIDENTIAL

outside the region of applicability of Margenau's theory, and therefore the apparent contradiction may not actually exist.

All of the aforementioned theories apply to discharges wherein the energy is applied in a continuous fashion. In many microwave applications, however, pulsed power is employed because higher levels may be obtained in this manner. Breakdown under pulsed conditions differs from c-w breakdown because of the additional condition that the breakdown must occur within a given amount of time, since the electrons will be accelerated only during the pulse length. An analysis of pulsed-power breakdown was made by Labrum (55) using an approach similar to that used by Townsend for the direct-current discharge. Labrum assumed an exponential increase of ionization with time during the pulse. He writes that if  $N_0$  electrons were present at the beginning of the pulse, the number  $N$ , present at the end of time  $t$ , could be written

$$N = N_0 e^{(G - L)t} \quad (52)$$

where  $G$  = number of ion-pairs produced by one electron in unit time

and  $L$  = fraction of electrons present which disappears in unit time

The requirement for breakdown is that at least  $N_d$  electrons be present in the gap, thus

$$(G - L) > \frac{1}{T} \log \frac{N_d}{N_0} \quad (53)$$

CONFIDENTIAL

where  $T$  = pulse length.

The logarithmic form indicates that, provided  $N_d$  is large, no great precision is needed in its specification. A likely value for  $N_d$  is  $10^{13}$ (87).  $G$  is of the same nature as Townsend's and can be expected to vary in the same manner with the applied field. In a non-attaching gas, where diffusion is the chief agent of electron removal,  $L$  is small and it is assumed that no removal of electrons occurs during the first few microseconds. Thus, for pulse durations less than a few microseconds. Thus, for pulse durations less than a few microseconds the breakdown potential is a function of the pulse length. The breakdown potential is then governed by the relation

$$G = \frac{1}{T} \log \frac{N_d}{N_0} \quad (54)$$

The value of  $G$  is determined from the expression for the average energy gained per mean free path given by Townsend and Gill, (102) and by assuming that the electron gains this energy in equal increments until it is capable of ionization. Using this approach, the breakdown field,  $X_0$ , is given by(87)

$$X_0^2 > \frac{4V_i}{\frac{e}{m}} \frac{W^2 + \frac{1}{3} V^2}{V} \cdot \frac{1}{T} \log \frac{N_d}{N_0} \quad (55)$$

CONFIDENTIAL

where  $V_1$  = ionization potential of the gas

$V$  = collision frequency

$W$  = applied frequency.

Labrum has performed experiments on both air and neon at 10,000 mc and has shown that the breakdown potential decreases for an increase of either pulse duration or repetition rate as predicted by theory. These tests were made at pressures between 1 and 30 mm of mercury, pulse lengths of 1 and 2 microseconds, and repetition rates between 69 and 600 pulses per second. The data also provides qualitative agreement with theory in the respect that a minimum breakdown potential was observed as the pressure was varied.

A different approach to pulsed-power breakdown has been adopted by Lathrop and Brown (57). The analysis proposed that for breakdown to occur, the rate of electron production must be greater than the rate of electron diffusion. Under these conditions, the electron density first will increase slowly (where free diffusion is the controlling factor), and then more rapidly as a positive-ion space charge, which inhibits the diffusion of electrons, is built up. Since the electron density will increase rapidly once the space charge has formed, the formation of an appreciable space charge is taken as the criterion for breakdown. The

CONFIDENTIAL

CONFIDENTIAL

electron density was assumed to increase exponentially with time, in agreement with Labrum's assumption, and the coefficient was taken as the solution of the diffusion equation involving the diffusion coefficient for the gas, the diffusion length, and the average ionization rate. On this basis the breakdown potential was calculated for hydrogen in a cavity of 0.1-cm gap, at pressures between 2 and 32 mm of mercury, and for pulse lengths between 1 and 60 microseconds. The results agree very well with the data obtained for breakdown under these conditions. The experimental results also showed that the breakdown potential was almost independent of the pulse length for values greater than 10 microseconds, which confirms Labrum's assumption.

Lathrop's data also shows a minimum potential at a pressure between 5 and 10 mm of mercury which is close to the value of 4 mm of mercury observed by Labrum for breakdown in air. Lathrop also observed that breakdown during any pulse was unaffected by the other pulses at repetition rates below 80 cps, which is the region wherein the data was taken. At higher repetition rates it is shown theoretically that the electrons cannot all diffuse in the time between pulses so that this theory would have to be modified if higher repetition rates were to be considered.

CONFIDENTIAL

CONFIDENTIAL

Pulsed-power breakdown tests were also made by Posin,<sup>(85,86)</sup> Copper,<sup>(15)</sup> Clarke,<sup>(10)</sup> and Prowse<sup>(89)</sup>. Posin measured breakdown of air at 3,000 mc, 10,000 mc, and 24,000 mc. He found that the breakdown potential was unchanged as the pulse length was increased beyond five microseconds, and that an increase of repetition rate from 200 to 500 pulses per second lowered the breakdown voltage by 15 percent. Posin also found that the breakdown voltage was not proportional to the pressure, and he showed theoretically that at low pressure  $V = f(p^{1/3})$ , at intermediate pressures  $V = f(p^{2/3})$ , and at high pressures  $V = f(p)$ .

Cooper's measurements were made on air at 3,000 mc and 10,000 mc using 1-microsecond pulses applied 400 times per second. These results show that the breakdown voltage is a linear function of pressure times gap length for gap length of 0.144 and 0.32 cm, and over the pressure range of 20 to 760 mm of mercury. Clarke's paper presents the results of breakdown measurements made on a number of waveguide components.

Prowse found that the breakdown voltage for air at 9800 mc is the same for one pulse as for pulses repeated 400 times a second, for a pulse length of 1 microsecond. He also noticed during the 400-cps test that the discharges occurred

CONFIDENTIAL



CONFIDENTIAL

in bursts because a discharge in one pulse often precipitated a discharge in the following pulse.

### 6.3 Experimental Data

#### a. Criterion of Breakdown

To begin with, it is important to have a standard definition or criterion of breakdown. Loeb defined<sup>(60)</sup> a d-c spark as "an unstable and discontinuous occurrence marking the transition from one more or less stable condition of current between electrodes in a gas to another one." He further states that the transition process may start but fall short of achievement because of circuit conditions, in which case only the spark appears. Both this condition and the one wherein glow follows the spark have been experimentally observed in microwave breakdown, and these effects have been used by experimenters as indications of breakdown. The interpretation of the information is by no means standardized. Many workers either do not define breakdown or merely state that a "spark passed." One group<sup>(10)</sup> is more meticulous, however, and considers breakdown to have occurred when the sparks pass more often than once every two minutes. Several experimenters<sup>(15,89,110)</sup> extend this idea to the point of plotting a curve of sparking probability to determine breakdown. The results of these latter tests indicate that

CONFIDENTIAL

single sparks can pass at significantly different potentials; this is substantiated by the contradictory results of many of the experimenters.

In addition to this lack of agreement concerning a criterion of breakdown, the effect that irradiation has on the breakdown gap is also disputed. The use of such irradiators as ultraviolet light, radioactive material, and an auxiliary spark gap have variously been reported as either lowering the breakdown potential or as having no effect. Part of this disagreement is obviously caused by the lack of a standard definition of breakdown, while the rest is due to experimental variations resulting from the experimental apparatus, procedure, and technique. Consequently, in order to appraise the existing experimental information properly, it is first necessary to define breakdown and then to investigate the methods of experimentally determining this quantity.

As previously stated, the accepted concept of high-power breakdown is based upon the bridging of the gap by an electron avalanche initiated by a single electron. The various theories do not consider either the manner in which this electron is liberated or the time required for liberation. The only stipulation made for breakdown is that the electron appear at such a position in the gap and at such a phase of

CONFIDENTIAL

the r-f cycle that it will be accelerated to form an avalanche. Actually, when the electron appears, it will have some initial velocity so that this factor, together with its position and relative phase, determines the minimum potential required for breakdown. Since these factors are all statistical in nature, no absolute minimum can exist. Although, theoretically speaking, a breakdown potential can always be found which is lower than any previous breakdown potential, in practice it is usually unnecessary to wait too long because the high frequency creates many opportunities for breakdown, and because the relative insensitivity of the measurement apparatus makes it impossible to differentiate between many of the breakdown potentials. The actual time required for any measurement is best determined by a direct test.

Since the initial velocity, position, and relative phase of the electron are all statistical quantities, it is natural to adopt an approach to breakdown based upon a probability concept. This approach was used successfully by Wilson<sup>(110)</sup> in 1936 to determine d-c breakdown, and later by Cooper<sup>(15)</sup> as well as Prowse and Cooper,<sup>(89)</sup> to determine microwave breakdown potentials. This procedure involved counting the number of sparks, dividing this value by the number of applied pulses to obtain the sparking probability,

CONFIDENTIAL

and then plotting a curve of sparking probability versus potential. This method was also recommended by Loeb<sup>(60,62,63)</sup> who at one point<sup>(60)</sup> states that the actual value of probability to be used as the criterion of breakdown is arbitrary, and at another point<sup>(62)</sup> suggests that the value of maximum slope be used. The sparking potential chosen by Wilson is the value at which the sparking probability is one-half, while Prowse and Cooper use the value where the probability is virtually zero. Actually, none of these criteria can be used as basically superior to the others since the procedure to be used for any particular test must be determined from a consideration of the purpose of the test. In some cases it may be impossible to allow even one spark to pass, while in other applications the accompanying increase in power may justify the allowance of occasional sparks. In any event, the plotting of a curve of sparking probability will lead to the most complete and most effective presentation of the experimental data.

It is obvious that the waiting period can be reduced and the precision of measurement can be increased, if more electrons are created in the gap. This may be accomplished by irradiating the gap with ultra-violet light or by employing either a radioactive substance or an auxiliary spark. In this manner, a tremendous increase in the number

CONFIDENTIAL

of available electrons can be achieved. One source\* estimates that the irradiation of the gap with 3.2 millicuries of radioactive cobalt produced  $10^7$  ion pairs per second per cubic centimeter, whereas the natural processes of cosmic radiation and normal radioactivity would produce only two pairs per minute per cubic centimeter. In addition, another source<sup>(36)</sup> states that the photo-emission from a surface is proportional to the illumination, and that the value can be increased by properly finishing the surface.

Theoretically, the use of external irradiation should lower the breakdown power because, in addition to allowing a greater number of breakdown trials to be observed, the irradiation causes higher electron velocities which result in a lowering of breakdown potential. The detection of this effect is primarily dependent upon the amount of irradiation employed. In many actual cases the effect may be undetectable with the instruments used. Thus, for a particular set of test conditions and a given radiation intensity, experimental consideration must be given to whether or not the use of external irradiation lowers the breakdown power. For example, experiments were performed during this program on the effect of a 1 millicurie cobalt<sup>(60)</sup> source on the breakdown power. It was found that there was no detectable effect within the measurement accuracy.

\*See ref. 67, page 227.

CONFIDENTIAL



CONFIDENTIAL

b. Presentation of Existing Data

Although a number of experiments have been conducted on high-power breakdown, those involving pulsed microwave power have been relatively few. These, however, are of the greatest interest to this investigation and will be reviewed first.

One of the more significant works on pulsed microwave breakdown was performed by Cooper<sup>(15)</sup>. Tests were conducted in coaxial line at 2800 mc and in waveguide at 9800 mc. In each case the power was applied in 1-microsecond pulses 400 times per second, and breakdown was caused to occur in a section of reduced gap length. The experimental technique involved observing the number of sparks occurring during a 10-minute interval for several different power levels, and the plotting of a sparking probability curve. This was performed both for the condition of no external irradiation and for external irradiation with 0.2 milligrams of radium. As predicted, the effect of the irradiation upon the minimum observable sparking potential was not detectable, although the irradiation greatly increased the sparking probability.

Tests made with different values of standing wave ratios indicated that with other conditions unchanged (maximum gradient constant) an increase of standing wave ratio caused a decrease in sparking probability. In all of the tests, the

CONFIDENTIAL

peak power was determined from measurements of the average power, the pulse repetition frequency, and the pulse width. The sparks were detected by visual observation through a hole placed in a bend of the transmission line, and the standing wave ratio was measured using a specially constructed slotted line. The data showed that the electric-field strength required for breakdown at zero probability (onset stress) was about 28 kv per cm at atmospheric pressure. Additional tests in both waveguide and coaxial line showed that for a single gap length and pressures between 50 mm of mercury and atmospheric, the onset stress was a linear function of the pressure. The use of several different waveguide gaps also showed that the onset stress was a linear function of the product of pressure and gap length, and that these points are co-linear with those for a single gap length with varying pressure, within experimental error. Cooper estimated the probable error in the onset electric field to be  $\pm 5$  percent.

Prowse and Cooper<sup>(89)</sup> made further tests on a cavity resonator at 9800 mc, with the pulse width again 1 microsecond and the repetition frequency 400 times per second. The spark gap in these tests was irradiated with ultraviolet light from an auxiliary spark gap applied immediately before the r-f pulse. The irradiation increased the sparking probability but did not change the onset stress. As an added point of interest, mention is made of the fact that the discharges occurred in bursts.

CONFIDENTIAL

Lathrop and Brown<sup>(57)</sup> performed breakdown experiments at 2800 mc on a cavity containing hydrogen. The pulse width was varied between 1 and 50 microseconds for pressures between 2 and 32 mm of mercury. A radioactive source supplied initial ionization and breakdown was observed as a decrease in transmitted power. The results showed that the breakdown field was relatively constant for pulse widths greater than about 7 microseconds, while for pulse widths below this value the breakdown field rose sharply so that it was about 20 percent higher at 1 microsecond. No mention is made of the repetition rate used, except for the statement that it was observed for repetition rates below 80 cps and that there was no effect between successive pulses. The pulse width was measured on an A/R scope equipped with a crystal-controlled calibration circuit: the estimated error was  $\pm 0.5$  microsecond. The power was measured with a directional coupler and thermistor bridge, and the estimated error was  $\pm 10$  percent.

Breakdown experiments involving variations of the pulse width, repetition rates, pressure, and gap length on a section of reduced height waveguide at 3000, 10,000, and 24,000 mc are reported by Posin<sup>(86)</sup>. A capsule containing radioactive cobalt of 3.2 millicuries intensity was placed on the outside of the waveguide above the breakdown gap to

CONFIDENTIAL

achieve repeatable results, and the breakdown power was taken as that value at which a spark first passed. The results show that irradiation lowered the breakdown power in every instance, the decrease in many cases being 50 percent. An increase in gap length from .006 inch to .059 inch also lowered the breakdown field strength. Tests with the pressure varying between 20 and 760 mm of mercury showed that without irradiation, the variation of breakdown power was linear, while with irradiation, the variation was parabolic. Additional data showed that at atmospheric pressure and at repetition rates between 0 and 2000 pps, the breakdown power increased as the pulse width was made shorter than about 4 microseconds. The effect became more marked as the repetition rate was lowered. An increase of repetition rate from 300 to 2000 pps was found to lower the breakdown power in a fairly uniform manner. In these tests, the spark was usually determined either by sound or by visual observation through a terminating horn. The power was measured using a directional coupler and thermistor bridge calibrated against a water load. The repetition rate was determined by comparing the trigger voltage with a calibrated audio oscillator. The pulse width was found by displaying the current pulse on a synchroscope. The accuracy of the results is not estimated.

CONFIDENTIAL

CONFIDENTIAL

Much of the material presented by Posin was obtained from work performed at M.I.T.<sup>(85)</sup>. In addition to the information already given, this work involved tests with humidity and surface roughness. A series of tests failed to show any significant difference of breakdown power between air at 10 percent relative humidity and air at 80 percent relative humidity. Tests with brass filings between .002 inch and .005 inch diameter, in .040-inch-high waveguide, however, showed that the presence of the filings caused a reduction in breakdown power of 65 percent. Upon the removal of the filings, the breakdown power returned to its original value. In the report the experimental error is estimated to be between -6.5 percent and +10.8 percent in the worst case and between -3.3 percent and +3.6 percent in the best case.

Some excellent work on the breakdown of a parallel-plane gap under the application of c-w power has been performed by Pim<sup>(83,84)</sup>. Tests were conducted in the frequency range from 100 to 300 mc, with the gap length varied between .05 mm and 1.0 mm and the pressure varied between 25 and 1000 mm of mercury. The results show that there was a critical gap width which is dependent primarily on the frequency of the applied electric field, and that a sudden decrease to a constant value in the electric stress produced breakdown. This constant for atmospheric pressure is 29kv per cm. The critical



CONFIDENTIAL

gap width will also decrease slightly with a decrease in pressure. External irradiation in the form of mesothorium was applied and repeatability of  $\pm 1/4$  percent was obtained. Breakdown was determined by visual observation through a hole cut in the test piece. The voltage was measured with a dielectric voltmeter employing a distrene vane calibrated at 50 cps. The estimated accuracy of the observed voltages is  $\pm 3.0$  percent.

Experiments on the c-w breakdown of a cavity containing helium at pressures between 1 and 200 mm of mercury, using a frequency of 3000 mc and the gap length varied between 0.15 and 2.5 cm, were performed by MacDonald and Brown<sup>(67)</sup>. The results show that a minimum exists in the breakdown voltage vs pressure curve, and that this minimum occurs at lower pressures for the longer gaps. In addition, increased gap length for this range of pressure and gap length, decreased the breakdown field strength. Breakdown in these tests was observed as a drop in transmitted power measured with a directional coupler and thermistor bridge. The standing wave ratio was measured with a conventional slotted section. The measurements were reproducible within an experimental error of 5 percent in electric field and less than 1 percent in pressure. Similar results obtained by Herlin and Brown<sup>(38)</sup> were compared to show that for air, the breakdown power is

CONFIDENTIAL

almost 10 times as great as that for helium, and the minimum voltage occurs at a lower pressure. Another series of tests by MacDonald and Brown<sup>(68)</sup> on hydrogen showed that this gas behaves in a similar fashion and the quantitative results were found to be about midway between those of helium and air.

c. Appraisal of Existing Data

A procedure usually adopted to appraise data is as follows: (1) data is examined to determine its self-consistency (2) it is ascertained whether or not the data is in agreement with existing theory, and (3) the data is compared with previously obtained experimental results. A confirmation on all three points indicated that the data was reliable. If any discrepancy arose it was necessary to critically examine the process by which the data was obtained. This involved an investigation of the approach to the problem, the apparatus employed, and the technique used.

The data on high-power microwave breakdown is meager and there is some disagreement between the results of several experimenters. As an example, the work at M.I.T.<sup>(85)</sup> indicates that the use of external irradiation greatly lowers the breakdown power, the reduction factor being as large as 3 in some cases, while Cooper<sup>(15)</sup> presents data which indicates that irradiation has no effect on breakdown. Since both of

CONFIDENTIAL

these experiments refer to pulsed power breakdown of a reduced height section of waveguide at 9800 mc, there appears to exist a direct contradiction. First, an examination of the data for the two sets of tests show that in Cooper's experiments the data is uniform for the conditions of irradiation and no irradiation, whereas the M.I.T. data is markedly erratic without irradiation. Next, a comparison of the two results with theory yields nothing conclusive. One might expect irradiation to lower the breakdown power somewhat, although no quantitative theoretical results are available. Since there is little additional data on the effect of irradiation on pulsed breakdown on waveguides, a more probing form of comparison is required. The approach to the problem adopted by Cooper is preferred.

Cooper used a statistical approach and plotted a probability of sparking curve, whereas the group at M.I.T. considered breakdown to have occurred when the first spark passed. Considering the discussion of the paragraph 6.2a breakdown criteria, it is not surprising that the M.I.T. data for 14 successive runs with no irradiation showed that the lowest breakdown value was about 65 percent of the highest. As a matter of fact, the problem and the solution herein proposed were recognized, as shown by a statement of the effect that averaging sufficient data would probably yield

CONFIDENTIAL

reliable results. It was decided, apparently, that the time required for this procedure was unwarranted and that sufficient information could be obtained with the use of external irradiation which, as mentioned before, is a time-saving device.

It must be mentioned at this point that although the irradiation improved the repeatability and shortened the time of this experiment, some inconsistency still remained. This is shown by the results of the humidity test wherein the breakdown power differed by as much as 25 percent for the same conditions. This too is in agreement with the proposed breakdown mechanism since the use of irradiation is an aid to, but not a substitution for, the statistical approach.

An examination of Cooper's data shows that the use of irradiation increased the breakdown probability, as expected. A closer scrutiny of the curves, however, shows that, although Cooper claims that the irradiation has no effect upon the onset stress, he does not prove it conclusively. Since the onset stress is the zero probability intercept, it must be obtained by an extrapolation of the data and is thus subject to some error. This error may be large inasmuch as the curve represents the integral of a Gaussian type of distribution, and thus is S-shaped. Thus, the intercept is not clearly defined. For the tests with irradiation, the slope

CONFIDENTIAL

CONFIDENTIAL

of the curve is reasonably great so that the extrapolation error is small. For the tests with no irradiation, however, the initial slope is quite small and it is difficult to determine the intercept precisely. Since the curves in the report are drawn to indicate that the intercept is the same for the two cases, Cooper claims that the irradiation has no effect. Actually, a more cautious statement would be that within experimental error, the irradiation appears to have little or no effect upon the breakdown stress. This brings up the points of experimental apparatus and techniques.

Cooper mentions an experimental technique whereby he cleaned the electrodes with metal polish applied with chamois leather, and then washed them with ethyl alcohol. He also states that the air in the spark gap was pumped out and replaced with fresh air between each setting of power level.

The M.I.T. group makes no mention of these aspects of technique, but does discuss in detail several methods of spark detection.

Breakdown was usually detected by the sound of the spark and occasionally by its light, as seen through a terminating horn. The discharge for breakdown under low pressure made little sound so that a stethoscope or contact microphone was used. An alternate method was to detect the

CONFIDENTIAL



CONFIDENTIAL

reflections from the spark by means of a directional coupler. The detection was accomplished with a crystal whose output was amplified and then viewed on an oscilloscope. Occasionally, the occurrence of breakdown was detected by the increase in standing wave ratio in the line between the source and the spark. Cooper detected the sparks visually through an observation hole in an elbow near the spark gap. The power at breakdown was determined in a similar manner in both experiments. The average power was first determined and then the peak power was found from a knowledge of the pulse width and repetition frequency.

Both tests employed a water calorimeter to determine the average power. In the M.I.T. tests, a directional coupler and thermistor mount were used in the actual tests after first being calibrated against the calorimeter. Cooper determined his pulse repetition rate by measuring the speed of the motor-generator set which drove the modulator, while the M.I.T. group determined the repetition rate by comparing it with a calibrated audio signal on an oscilloscope. Both experimenters assumed the r-f pulse shape to be the same as the magnetron current pulse which was viewed on an oscilloscope. Cooper took the pulse width as the area divided by the height. The M.I.T. group defined the pulse width as the distance from the center of the rise to the center of the decay. On the

CONFIDENTIAL

CONFIDENTIAL

question of the accuracy of measurements, the M.I.T. group estimated an error of  $\pm 1.5$  percent in power, while Cooper estimated a corresponding error of  $\pm 3$  percent. M.I.T. further estimated an error of between 2 and 6 percent on pulse width and 0.5 percent on repetition rate, whereas Cooper estimated errors of 2 and 1 percent. M.I.T. lists other errors such as standing-wave effect, waveguide losses and gap height; and estimated an overall error of between -3.3 percent and +10.8 percent in power. Cooper considered a possible error of  $\pm 2$  percent in locating the intercept and estimated an overall error of  $\pm 5$  percent in voltage.

#### 6.4 Regions of Validity of Theories

Considering all factors, it would seem that each set of tests accomplished its prime purpose. Cooper showed that external irradiation does not affect the breakdown power; he also presents quantitative data on breakdown for various conditions of gap height and pressure. The M.I.T. experiments show the qualitative variation of breakdown with the parameters of pressure, gap height, pulse width, repetition rate, humidity, and surface roughness. Quantitatively, the data is fairly accurate, since the use of irradiation greatly reduced the inherent error caused by the lack of use of the statistical approach. It is apparent, however, that

CONFIDENTIAL

errors still exist in the M.I.T. data as shown by the humidity data previously cited, and by repeated tests with different repetition rates, the results of which vary by as much as 25 percent.

The data gathered by Lathrop and Brown<sup>(57)</sup> is self-consistent and shows good agreement with theory, although breakdown was taken as that value at which a spark first passed. There are several possible reasons for the agreement between theory and test. First, the pressures involved, 2 to 32 mm of mercury, are at the lower limit of the pressures used in the tests at M.I.T. A close examination of this latter data shows that the irradiation had little effect below about 30 mm, which indicates that the sparking probability curve rose sharply. This means that for slight over-voltages, the sparking probability was high enough so that the inherent error in the method of measurement was greatly reduced. Another reason for the apparent self-consistency and theoretical verification is that the pulse width was varied over the range from 0.5 to 50 microseconds. Thus, these tests involved pulse widths which were longer than those used in the M.I.T. tests, which were mostly below 0.5 microsecond. Since a longer pulse width affords more opportunity for sparking, it is reasonable to expect the inherent error to be reduced. As a matter of fact, the data of Lathrop and

CONFIDENTIAL

CONFIDENTIAL

Brown show their greatest divergence from theory and their least consistency at the smallest pulse widths, which substantiates this conclusion. Another factor which enhanced the reliability of the data is the use of external irradiation.

The apparatus and technique used by Lathrop and Brown were similar to those used by Cooper and the M.I.T. group, with one exception. The average power was measured using a directional coupler and thermistor bridge which was accurate to about 10 percent. The pulse widths were measured on an oscilloscope to an accuracy of  $\pm 0.5$  microsecond, and the pressure was measured with a mercury manometer to an accuracy of  $\pm 1$  mm of mercury.

The good agreement between the experimental results of Lathrop and Brown and the proposed theory is a verification of the idea that microwave breakdown occurs when the production of electrons by ionization is balanced by their loss through diffusion. This conclusion is of immediate interest to theorists and physicists. From an engineering point of view, however, the experiments are at present of limited usefulness, since the pulse widths and pressures involved are outside the range of normal applications.

CONFIDENTIAL

CONFIDENTIAL

Pim's<sup>(84)</sup> data shows excellent self-consistency and is in good agreement with the theory proposed. As in the experiments of Lathrop and Brown, Pim did not adopt a statistical approach to breakdown, but rather, took that value at which a spark first passed as the breakdown power. The explanation for the good results obtained is simple in this case, inasmuch as c-w microwave power was used. Pim states that the voltage was slowly increased, which means that for the frequencies employed, 100 to 300 mc, a great number of opportunities to breakdown were present at each power level. Thus, the inherent error in the measurement system was greatly reduced. In addition, external irradiation was employed which also tended to decrease the error. As a confirmation of the belief that irradiation had little effect on breakdown power, Pim reports that without irradiation, breakdown always occurred at the same level as it did with irradiation, if sufficient time was allowed.

The equipment used by Pim represents an extension of low-frequency circuitry. The voltage was measured with a voltmeter which utilized a distrene dielectric vane. Since the dielectric constant of distrene does not change over the range from power frequencies to 1000 mc, it was possible to calibrate the voltmeter at 50 cps with the estimated accuracy of the voltage readings being  $\pm 3$  percent.

CONFIDENTIAL



CONFIDENTIAL

The use of c-w power at relatively low microwave frequencies, and the low-frequency circuitry, all combine to significantly reduce the value of Pim's results to an engineer interested in the peak-power-handling capacity of waveguide components.

The data of MacDonald and Brown<sup>(67,68)</sup> and that of Herlin and Brown<sup>(28)</sup> substantiate their proposed theory and are consistent. Although these experimenters did not use the statistical approach to breakdown, they were successful because they used c-w power and low pressures. The results of these experiments are of limited use to engineers.

## 7. EXPERIMENTAL APPROACH

### 7.1 Breakdown Test Circuit

The statistical approach to microwave breakdown was presented as the criterion for breakdown, and was substantiated by the existing data. Accordingly, this approach was adopted for the experiments conducted on this contract.

A diagram of the microwave circuit and auxiliary equipment is shown in figure 4. Stripped to its essentials, this circuit shows that pulsed power from a modulated magnetron was applied to the test unit. Breakdown was observed with a photocell, and recorded on an electronic counter. The average

CONFIDENTIAL

power was measured with a directional coupler and thermistor bridge which was calibrated against a calorimetric load, while the pulse width was determined by viewing the r-f pulse on a synchroscope. Provision was also made for the measurement of frequency, standing wave ratio, and pressure.

A closer examination of the circuit shows that many auxiliary components were included. Starting at the input end, an audio signal generator was necessary as a comparison standard to determine the pulse repetition rate. Initially, a Raytheon type QK 221 magnetron was chosen as the high-power source. This tube combined the advantages of high-power output, dependable performance, and long life. Later in the program, the Litton 4J 50 magnetron was used when it was found to provide comparable performance at less cost. A one-megawatt power supply and pulse modulator unit drove the magnetron. After the magnetron, a waveguide twist is shown. This was included because the magnetron had a waveguide output whose broad side was vertical. Since several crossed-waveguide directional couplers were to be used, and also for reasons of mechanical stability, it was more convenient to operate the system with the broad side horizontal; thus necessitating a twist. Since the magnetron output had a waveguide outside diameter of 1.250 inches x 0.625 inch, an adapter had to be used to reduce the waveguide dimensions to

CONFIDENTIAL

CONFIDENTIAL

to 1.000-inch x 0.500-inch outside diameter as specified by the contract.

Following the adapter in the microwave circuit was a Transvar\* coupler<sup>(24)</sup>. This is a new type of directional coupler which may be varied to transfer any desired amount of the incident power between 0 and 100 percent. An inherent feature of the Transvar coupler eliminates or suppresses even harmonic frequencies. In the present application the coupler was employed to transfer sensibly all the fundamental power while suppressing the harmonics generated by the magnetron. This was important for two reasons; (a) the presence of harmonics could reduce the breakdown power either by creating increased potential gradients or because the breakdown strength may decrease with frequency; and (b) the harmonic content of the electromagnetic wave may lead to spurious power readings. This was probable because the coupling of the directional coupler was different for the fundamental and the harmonics in which case the power in the secondary line was not a true indication of the power in the main line. In addition, the impedance of the thermistor mount was different at the harmonic frequency from that at the fundamental, so that some power was reflected, introducing an error. Associated with the Transvar coupler is a dummy load

- - - - -  
\*Trade mark Sperry Gyroscope Company

CONFIDENTIAL

CONFIDENTIAL

to absorb that portion of the incident power which was not coupled into the secondary line, and a short to terminate the non-directive arm of the secondary line. The short was used mainly for convenience and was permissible inasmuch as the coupler was not used as a calibrated device. The directive arm of the Transvar coupler was connected to a waveguide power-divider network consisting of two hybrids and a phase shifter. This eliminated distortion of the pulse shape that might occur if electronic methods for varying the power were used. The simplest means of varying the power output is to vary the supply voltage since that quantity can be varied continuously while the magnetron is in oscillation. However, rather than attempt to show that this means of varying the power output does not distort the r-f spectrum, the pulse shape was eliminated as a variable by always running the magnetron near full output and varying the power with the waveguide power divider. A ferrite load isolator was inserted after the power divider for the building block tests in order to isolate the magnetron from the mismatch produced by the test piece.

A crossed-guide directional coupler which supplied power to a frequency meter was used next. Since this portion of the circuit was pressurized to insure breakdown in the region of the test unit, it was necessary to insert a

CONFIDENTIAL

CONFIDENTIAL

pressure window between the coupler and the frequency meter. The non-directive arm of the coupler was terminated with a low-power termination. The first crossed-guide coupler was followed by a second crossed-guide coupler which supplied power to the thermistor mount. As in the case of the first coupler, a pressure window and a low-power termination were again employed.

Following this coupler, there was a directional coupler that supplied power to an impedance meter and a sliding short. The impedance meter arm measured the incident power and the short received the reflected power existing in the test unit. The reflected power, incident upon the short, was in turn reflected towards the impedance meter. By moving the short, the phase of the reflected wave was varied relative to the incident wave, and the voltage at the probe of the impedance meter, which was maintained at some fixed position then followed the standing wave pattern. It should be noted that the impedance meter was employed in this application for convenience and because it introduced a very small mismatch. The impedance meter was followed by a low-power termination. Both arms of the coupler were equipped with pressure windows. Following the directional coupler in the main line, was the viewing bend, photocell and counter combination for detecting and recording breakdown. In order to

CONFIDENTIAL



CONFIDENTIAL

count the sparks, a hole was made in an H-plane bend with the center of the hole along the waveguide axis. A circular attenuating tube was soldered over the hole to prevent r-f leakage. An RCA type 1P37 photocell was placed against the attenuating tube and the output was fed to an electronic counter which recorded the spark. Immediately following the viewing bend, was the test piece, which was isolated from the rest of the line by two pressure windows. The microwave system was then terminated in a high-power dummy load.

The other equipment shown on the diagram, are the pressure gauges which measured the pressure in the test section and in the sections before and after. High-vacuum equipment that continuously varied the test-region pressure from atmospheric to as low as 2 mm of mercury was used. Controls were provided to maintain the pressure constant at any given value. Pressures above atmospheric were obtained by using the plant airline which provided a gauge pressure of 60 pounds per square inch. Pressures between this maximum value and atmospheric was obtained by employing an auxiliary tank which was maintained at the desired pressure by the airline. A one millicurie cobalt 60 radioactive source was placed on the broad wall of the test piece near the point of maximum E-field gradient. Figure 6 and 7 show photographs of the experimental layout. Figure 6 shows an overall view

CONFIDENTIAL

CONFIDENTIAL

of the test circuit and most of the auxiliary equipment. Many of the pieces of equipment previously mentioned can be discerned. Figure 7 shows a close-up of the region around the test section.

## 7.2 Design Considerations and Performance of Test Circuit Components

### a. Pressure Window

The pressure window consisted of a thin disk of mica (approximately .005-inch thick) placed in a recess in a standard 2-inch x 1-inch outside diameter waveguide choke flange and supported by a rubber gasket. Because the mica disk was placed in a section of waveguide of increased height, resulting in a lower electric-field gradient, it was able to withstand the maximum power capacity of 1-inch x 1/2-inch waveguide without breakdown. The mica section was then joined to the regular waveguide by means of a low-reflection taper. The input VSWR to the combination of two tapered windows separated by a 1-inch x 1/2-inch straight section was measured to be 1.08. Pressure-test results revealed that the windows would successfully withstand a pressure differential of 40 pounds. Both the step-up and step-down tapers were greater than one and one-half wavelengths, which resulted in an overall window length of 6 inches.

CONFIDENTIAL

CONFIDENTIAL

b. Phase Shifters

The phase shifter used in conjunction with the hybrids divided the power from the magnetron (which was operated near maximum output as previously discussed) between the test piece and an auxiliary dummy load. To obtain a continuous power split from 0 to 100 percent, a total of 90-degrees phase shift was required. The squeeze-section type of phase shifter was chosen as the most satisfactory for this investigation. It could handle high power, was easily pressurized, and presented a reasonably good match. The main disadvantage of this phase shifter was the appreciable length required to obtain the required phase shift. This, however, could be tolerated in the present case.

Accordingly, a squeeze-section phase shifter was designed with a slot 6-wavelengths long and a total waveguide-width variation of .078 inch. Tests showed that a good match was obtained. The highest VSWR being 1.06 as the waveguide was squeezed the maximum amount. The phase-shift measurements showed a maximum variation of 70 degrees, which was sufficient although not optimum.

c. Thermistor Mount

In the present series of experiments the peak power was determined from a knowledge of the average power, the

CONFIDENTIAL

CONFIDENTIAL

pulse duration, and the repetition rate. The value for the average power was obtained using a thermistor mount and bridge to measure a sample of the incident microwave power provided by a directional coupler located in the main line. The bridge readings were calibrated against a water calorimeter. The basic requirement of the thermistor mount, therefore, was that it provide an indication of the power incident upon it. The mount design chosen was a 0-0 double-coaxial-stub type, similar to a design tested by the National Bureau of Standards and found to be at least 96 percent efficient. The only modification made was to optimize the mount performance at the magnetron frequency used in this investigation. Tests indicated that the thermistor mount absorbed more than 99 percent of the power incident upon it, and thus measured the power to good accuracy.

#### d. Tchebyscheff Coupler

As mention in paragraph 7.1, a directional coupler was used to couple power into an auxiliary waveguide to measure the primary line VSWR. It was extremely important that the directivity of this coupler be high because low directivity would introduce an error in the measured VSWR, and such an error would be magnified in the computation of the breakdown power. It also was desirable that the coupler

CONFIDENTIAL

CONFIDENTIAL

be bilaterally symmetrical so that the incident and reflected waves in the primary line would be coupled with equal attenuation into the secondary line. Fortunately this condition was easily fulfilled by careful construction of the instrument, and, in fact, this was the main reason for the choice of an arrangement using one coupler with a sliding short instead of two separate couplers.

A directional coupler employing multiple-hole elements could be designed for high directivity if the sizes and spacing of the apertures are properly chosen. It can be shown that the optimum response is obtained by spacing the holes a quarter-wavelength apart and varying the coupling according to the coefficients of the Tchebyscheff polynomial. In accordance with this approach, a coupler employing seven holes in the common narrow wall between the two waveguides was designed and constructed. The coupling of this unit was measured to be 33 db. and was essentially equal to both directions within experimental error. In addition, the directivity was sufficiently high so that the probable error in maximum voltage was less than one percent. These characteristics constitute an assurance of good accuracy when the instrument was used in conjunction with well-matched pressure windows and a well-designed sliding short.

CONFIDENTIAL



CONFIDENTIAL

e. Miscellaneous Components

In addition to the microwave components already discussed, many other units were required to complete the test circuit. Foremost among these is the Transvar coupler which suppressed the propagation of higher-order modes in the unit under test. Tests showed that for the normal magnetron frequency, between 9230 and 9404 mc, the minimum coupled power was 98 percent of the incident power, which was satisfactory.

The test circuit employed two other directional couplers in addition to the Tchebyscheff and Transvar couplers. These were used to provide power for the frequency meter and thermistor mount. The main requirements of the frequency-meter coupler were that it provide sufficient power and that it be physically compatible with the rest of the system. These conditions were most easily met with a 30 db cross-guide directional coupler.

Since the thermistor-mount coupler had essentially the same requirements as those for the frequency-meter coupler, a 40 db cross-guide coupler was used for this unit.

Both high-power dummy loads and low-power terminations were included in the test circuit. The required loads

CONFIDENTIAL

had to be capable of dissipating a maximum of 300-watts average power and had to have a reasonably low VSWR. The loads chosen, the carbon-cement type, were able to handle this amount of power adequately. They had a VSWR less than 1.05. Three low-power terminations were also required. It was necessary that two of them, those for the thermistor mount and VSWR functions, be well matched. The terminations were constructed using a tapered resistance card of 400 ohms per square, and the maximum measured VSWR was 1.01.

### 7.3 Experimental Considerations

Experimenters in the past had encountered difficulties. Therefore, it was extremely important that breakdown tests be controlled as much as possible. Control not only served to improve the repeatability of a set of tests, but will also allow direct comparison of tests made at various times by different experimenters employing different test circuits and equipment. It was important that both the pulse shape and harmonic content of the signal source be controlled. The Transvar coupler and waveguide power-dividing network provide the solution to this problem. The Transvar coupler suppressed the even harmonics, thus reducing the possibility of higher-order modes. The waveguide power divider permitted a continuous variation of the power, without pulse distortion

CONFIDENTIAL

CONFIDENTIAL

as might occur if electronic methods for varying the signal output were employed. However, since the magnetron could not always be operated at the same supply voltage, a set of photographs of the rectified r-f pulse were taken while the signal output was varied by adjusting the power-supply voltage. The results show that for the tests, both with and without the Transvar coupler the pulse was normal, reasonably square-shaped, and uniform from full power down to about 60 watts average power. This means that reasonable variations in power due to changes in supply voltage can be tolerated with little error if care is taken to avoid large changes.

Another important point considered, while striving for reproducible data, was the manner in which the magnetron was loaded. It is well known<sup>(14)</sup> that the output of a magnetron is dependent upon both the magnitude and phase of the load impedance. To determine the exact effect on the particular magnetron used in this series of measurements, tests were made on the variation of power output with impedance. The results showed that the maximum delivered power, which is the significant quantity, was about 10 percent greater for a VSWR of 1.8 than that delivered to a matched load. This raised the question as to whether it was desirable to take advantage of this additional available power. The

CONFIDENTIAL

CONFIDENTIAL

arguments in favor of operating the magnetron with a matched load far outweighed the advantage of this additional power (see fourth interim report) and thus the former course of action was adopted.

The manner in which breakdown was detected was another important problem that had to be solved before reliable breakdown measurements could be made. It was possible to obtain an indication of sparking using a viewing bend and photocell combination. The output of the photocell was displayed on an oscilloscope or an electronic counter by carefully shielding all leads and reducing the ambient light. In these tests, both the 931A and 1P21 photocells responded to the light accompanying breakdown in the waveguide. Several other methods for detecting breakdown were tried unsuccessfully. A type 1N77 photocell was placed within a hole located in the dummy load at a spacing of about 24 inches from the spark but gave no response. The 1N77 cell was moved closer to the spark by placing it at the eyepiece of the viewing bend but still no response was obtained.

A simultaneous investigation into the use of contact microphones was tried with no visible response on the oscilloscope after 40 db of amplification. This insensitivity

CONFIDENTIAL

CONFIDENTIAL

may be due to the relatively large mass of the portion in contact with the waveguide, so that the use of a needle-type pickup may have proved satisfactory.

Two other systems of spark detection were considered; one was dependent upon the assumption that the occurrence of a spark caused a change in the pulse shape. If this were so, then an electronic circuit which measured the pulse width could possibly serve to detect a spark. The second method was based upon the fact that the spark would introduce a standing wave into the line. Thus, a device which responded to a sudden increase in standing wave ratio could be used to count the sparks. However, these systems were not investigated because the viewing-bend-photocell combination proved satisfactory.

At this stage of the program most of the test procedures were crystallized, so that it was possible to start breakdown tests immediately. It was decided that the first tests should use the minimum number of auxiliary components and the simplest technique so that the general approach could be verified with the least possible interference from extraneous factors such as pressure, VSWR, and breakdown of auxiliary components. For this reason, a breakdown section was constructed featuring a capacitive window of small



CONFIDENTIAL

separation. The initial runs proved to be disappointing inasmuch as the breakdown did not appear to be random, nor was the onset stress reproducible. An investigation of the setup revealed that breakdown was occurring at the waveguide end of the attenuating tube used for spark viewing. This construction was corrected by pressure-sealing a mica sheet across the open end of the tube and then pressurizing the bend. Subsequent tests showed that the bend no longer broke down. However at this point, breakdown occurred at a pressurizing window. An examination of the window showed that the mica had broken down internally between layers. To remedy this condition more uniform sheets of mica were used.

As these conditions were corrected the input power was successively increased. The next increase in power (after the window breakdown problem was solved) resulted in breakdown across the flanges. This new development focused attention on a problem which existed when the choice of flanges was made. Since the field of waveguide component breakdown is so new, there was insufficient data to determine which flange arrangement would carry the most power.

Before going into the problem of determining the breakdown power of flanges at great length (as was done later in the program), it was decided to employ plain flanges.

CONFIDENTIAL

CONFIDENTIAL

By employing the information provided by an observation of the breakdown, techniques were developed which lead to an improvement of the power-handling capacity as the need arose. An examination of the flanges showed that breakdown occurred in the section of the flange next to the center of the broad wall of the waveguide. This was not unexpected since any space existing between the flanges is transverse to the current flow in the broad walls, and parallel to the current flow in the side walls. The sections of the flange near the broad walls act as a capacitor, and it was the capacitor that broke down. This was corrected by insuring good contact between the flanges in the vicinity of the broad walls of the waveguide. This could be accomplished by extending the flanges near the broad walls to obtain a butt-type joint, by beveling the sides of the flanges so that the center protruded in a convex fashion, or by inserting some malleable metallic substance between the flanges to insure electrical continuity along the broad walls. The second method, that of beveling the flanges near the side walls, was adopted. This scheme improved the power-handling capacity of the flanges so that breakdown was caused to occur in the test gap as desired.

Two sets of tests were made on the test gap. One set consisted of periodically observing the number of breakdowns at a constant power level. A test of this sort can be

CONFIDENTIAL

CONFIDENTIAL

used to analyze the break-down process and to determine to what extent the process can be considered a random one, subject to the laws of statistics. The second set consisted of observing the number of breakdowns occurring in an interval of time for a series of different power levels. The information derived from this latter test also was an indication of the degree of randomness of the break-down process.

To justify the use of a statistical approach to the problem of breakdown, it was necessary to show that such a method possesses some advantage. The experiments of Cooper<sup>(15)</sup> indicated that a plot of sparking probability versus power results in a reproducible value of onset stress, the knowledge of which represents a considerable advantage. Hence, the first experiments made during this program were an attempt to corroborate this conclusion. Figure 8 shows the results of this test; the similarity of the curve to those obtained by Cooper indicates that the conclusion was justified.

In addition to providing an excellent means for data presentation, the statistical approach also can provide information about the process of breakdown. A set of data was taken wherein the amount of breakdown was observed for a number of successive 15-second intervals. This data was plotted in the form of a histogram, with the number of breakdowns in a 15-second interval as the variable. The curve is

CONFIDENTIAL

CONFIDENTIAL

shown in figure 9. Similar curves plotted from the same data, but with 30- and 60-second intervals as the variable, are shown plotted in figures 10 and 11 respectively. Although the data is obviously meagre, it is apparent that all three curves strongly resemble a slightly skewed normal distribution curve. To be more specific, it can be easily shown that in all three cases the mean is larger than the median and the median is larger than the mode, which is characteristic of this type of distribution.

At this point some mention should be made of the manner of plotting the breakdown probability curve shown in figure 8. For this test the power level was held constant and the total number of breakdowns in a 10-minute interval was observed. The probability of breakdown for one pulse was determined by dividing the number of breakdowns by the total number of pulses. This method was employed by Cooper and is the obvious one to use since it follows directly from the definition of probability. For the sake of completeness, however, some consideration had to be given to this use of the mean as an average. The criteria used in the choice of an average was, that the average be reasonably accurate so that a smooth curve would be obtained, that the computation be simple, and that the necessary data be held to a minimum. In addition, for the purpose of this program it was important

CONFIDENTIAL

CONFIDENTIAL

that the portion of the curve where the average was small be well defined so that the onset stress could be determined with reasonable accuracy.

To obtain the best average, the data of figures 9, 10, and 11 were divided in the following fashion. For each time interval, the mean, median, and mode were computed for the entire set of data as well as for the data considered in groups of ten and twenty readings. A tabulation of the computations may be found in the fourth interim report.

A consideration of the data shows that for each group of tests the mean had the least standard deviation and the least maximum deviation. From the standpoint of simplicity of computation, the mean again was superior since only one reading was required at the end of the total time interval. The mean also gave the greatest precision in the region where the probability was very small since both the mode and the median were not well defined.

For these reasons the arithmetic mean was used in the computation of the probability of breakdown in figure 8. The choice was justified because the curve was smooth and well defined.

CONFIDENTIAL



CONFIDENTIAL

Additional tests, made on a section of 1-inch x 1/2-inch x .050-inch waveguide (figure 4) using the test circuit shown in figure 5, indicated that the pressure window near the generator broke down because the straight section broke down first (see fifth interim report).

It was decided that it would be significant to determine the effect of external irradiation upon the breakdown of waveguide. This would provide a check against the results of previous experiments. In addition, if the effect could be determined, it would greatly simplify future testing. The source chosen for this work was an irradiated cobalt-60 wire which was hermetically sealed in a steel rod. The source strength was approximately one millicurie. The radiation consisted of equivalent amounts of two gamma rays of 1.1 and 1.3 MEV. This source was chosen because it was easily obtained, easily handled, required few safety precautions, and was adequate for the job.

In the tests that followed, the value given for the breakdown power was that which corresponded to the minimum sparking probability. This value was referred to as the onset stress. A complete probability curve was not taken for two reasons. First, breakdown in the test section traveled back to the pressure window and caused continuous

CONFIDENTIAL

breakdown at this point. This made it impossible to count the number of breakdowns in the test section. Second, a complete probability run at each point would considerably lengthen the test time and thus would limit the useful data.

The effect of external irradiation on the breakdown section at the breakdown power was determined from a series of tests employing varying amounts of irradiation. This was accomplished by setting the cobalt at several fixed distances from the waveguide and measuring the breakdown power as a function of the gas pressure. The tapered waveguide section in 1-inch by 1/2-inch waveguide was the test piece (figure 4). For consistency this same test piece was used throughout the program for all tests to determine the peak-power capacity of this size waveguide.

The procedure adopted was to set the magnetron output at a value near its rated maximum. The phase shifter (figure 5) was then adjusted to produce a convenient power level in the test section. The pressure in the test section was reduced in small increments until breakdown occurred, as noted by the photocell and electronic counter. This reading was then checked and the process was repeated for other power levels.

CONFIDENTIAL

CONFIDENTIAL

This procedure was repeated with the cobalt in contact with the waveguide and also at one- and two-inch intervals from the waveguide wall. The complete test results are shown in figures 12, 13, and 14. It should be noted that the average power is used as the abscissa. Since the magnetron was operated at the same power level in all the tests, the curves are self-consistent and errors due to pulse shape and repetition-rate measurements are eliminated.

A comparison of figures 12, 13, and 14 shows that for power levels above 80 watts the curves are approximately co-linear. This indicates that for powers between 80 and 200 watts, and pressures between 7 and 13 inches of mercury, a variation in intensity of irradiation produced no change in breakdown power. The magnitude of this variation could be approximated since the geometry of the cobalt was known and the intensity varied inversely as the square of the distance from the source. This was not necessary, however, since another test was run using no external irradiation. This data is shown in figure 15 wherein the indicated points refer to breakdown with irradiation and the solid curve represents breakdown with the cobalt in contact with the waveguide. In this connection it should be noted that the solid curve is not a reproduction of the data of figure 12. The difference

CONFIDENTIAL

CONFIDENTIAL

between the two curves is that the data was taken with two different magnetrons.

As shown in figure 15, the breakdown power without irradiation was never lower than that obtained at the same pressure with irradiation. This was consistent with normal expectation. In general, without irradiation the breakdown power was about 20 percent higher than that under the same conditions with irradiation. However, it should be noted that there were three points which coincide with the line. This indicated that the irradiation did not lower the breakdown power. These points were obtained by waiting for a period of one hour before breakdown occurred without irradiation, whereas most of the other points were obtained using a 10-minute interval. The normal waiting period with irradiation was 5 minutes and breakdown usually occurred after several minutes. Since the number of available electrons with the cobalt source was of the order of  $10^6$  times that otherwise present, it can be seen that the probability of breakdown in one hour without cobalt is considerably less than the probability in 5 minutes with cobalt. This would explain the fact that the breakdown power without cobalt was generally higher.

CONFIDENTIAL

CONFIDENTIAL

It must be mentioned at this point that several other runs were made wherein the power was held constant for one hour with no external irradiation. After no breakdown was observed the cobalt was introduced and breakdown resulted. This is not surprising in view of the number of electrons available.

Considering figures 12, 13, 14, and 15 it may be said with a good degree of certainty that external irradiation does not lower the breakdown power. The results were not conclusive for several reasons. First, it was impossible to achieve the same probability of breakdown with no external irradiation because a waiting period of about  $10^6 \times 5$  minutes, or about 10 years would be required. Second, figures 13, 14, and 15 are not uniform over the entire range. Since figure 12 is linear over the entire range, this casts some doubt as to the accuracy of the measurements at lower power and pressure. Fortunately, there was good agreement at the high-pressure end which was closest to the normal operating range of atmospheric and higher pressures.

As a consequence of the theoretical result, (described in paragraph 5.2 of the error in the high-power reflectometer method of measuring VSWR), the reflectometer was set up as shown in figure 5. A combination of sampling probe

CONFIDENTIAL



CONFIDENTIAL

and termination was used to pick up power because of the good match so obtained. Several elements, including a barretter, 1N23B crystal, and several values of Littelfuses were employed as detecting elements. The best results were obtained with a 1/200 ampere Littelfuse housed in a tuned-probe assembly.

The VSWR of several mismatches was measured using both the reflectometer arrangement and a standard impedance meter. In the impedance-meter measurement, the detecting element was the same 1/200 ampere Littelfuse. The results of the test are listed in table 1.

TABLE 1

CALIBRATION OF SLIDING-SHORT REFLECTOMETER

Low-Power VSWR Using Standard Impedance-Meter Setup	High-Power VSWR Using Sliding- Short Reflectometer
1.02	1.03
1.07	1.06
1.11	1.11
1.19	1.19
1.43	1.48
2.0	2.1
5.0	4.8

From the data it is seen that the maximum error occurred at a VSWR of 2.0. The error is given by

CONFIDENTIAL

CONFIDENTIAL

$$\begin{aligned}\text{relative error} &= \frac{\left[1 + \frac{2.1 - 1}{2.1 + 1}\right] - \left[1 + \frac{2.0 - 1}{2.0 + 1}\right]}{\left[1 + \frac{2.0 - 1}{2.0 + 1}\right]} \\ &= .014 = 1.4 \text{ percent}\end{aligned}$$

The value of  $a$ , the reflection coefficient, was 0.33; so that this case is closest to the condition  $a \ll 1$  and  $b = 1$ , for which the theoretical result from equation 4 is

$$\text{maximum relative error} = \frac{d + \Gamma_1}{1 + \Gamma_1 + \Gamma_2 + \Gamma_3 + \Gamma_4}$$

For the equipment used in the test,

$$d = .01$$

$$\Gamma_1 = .01$$

$$\Gamma_2 = .02$$

$$\Gamma_3 = .02$$

$$\Gamma_4 = .02$$

$$c = .01$$

so that

CONFIDENTIAL

CONFIDENTIAL

$$\begin{aligned}\text{maximum error} &= \frac{\frac{.02}{1.07}}{1.33} \\ &= .014 = 1.4 \text{ percent}\end{aligned}$$

This is seen to compare exactly with the experimentally-determined maximum error. Thus, the results obtained by using a high-power sliding-short reflectometer compared to the conventional impedance meter method agreed within the theoretically predicted error.

#### 7.4 Analysis of Experimental Errors

##### a. General

The following factors must be considered in estimating the accuracy of the data.

##### b. Power Measurement

The primary standard of power measurement was the water load. This consisted of a glass tube inserted in a waveguide and tapered to minimize reflections. Water was circulated through this glass tube and the difference between input and output temperatures was indicated by thermocouples. The power calibration was made by equating the heating effect of the microwaves to the heating of the water by 60 cps a-c

CONFIDENTIAL

CONFIDENTIAL

power which can be measured quite accurately. Because of possible errors in measuring the 60 cps power due to instability of the power meter or the water flow, and the assumption of equal heating effects between the 60 cps and microwave power, the probable error in this measurement was estimated to be 3 percent. This substitution method eliminated unknown heat losses and inaccuracies in measuring the absolute flow rate.

Although the water load was an accurate, absolute power measuring device, it was undesirable for breakdown tests because of its slow response time and bulk. Therefore, it was found convenient to use a Sperry Microline\* Model 84C thermistor bridge coupled to the line by a directional coupler, and calibrated against the water load. The probable error of this power monitoring device was estimated to be about 2 percent of the calibrated reading.

Since power measurements using thermal devices measure average power, it was necessary to compute peak power from the repetition rate and duty cycle. The repetition rate was determined by using the Berkley counter. The probable error in this measurement was estimated to be 0.25 percent.

- - - - -  
\*Trade Mark, Registered, Sperry Gyroscope Company

CONFIDENTIAL

CONFIDENTIAL

The pulse width was measured as the time from the center of the rise of the current pulse to the center of the fall of the pulse as viewed on an oscilloscope. The probable error of the measurement was estimated to be about 7 percent for the 1.2-microsecond pulse.

c. Determination of Breakdown

Because of the statistical nature of breakdown, the point of onset stress, or power level at which breakdown first occurred, was obtained by extrapolating the breakdown probability versus power level data to the point of zero probability. Since the interval between breakdown sparks sometimes became long, the onset stress power level was difficult to determine. The error in determining the point of onset stress was estimated to be 1 percent.

d. Waveguide Losses

In X-band, the waveguide losses were about .07 db per foot. As may be seen from figure 5, the power level at the coupler exceeded the power level at the test piece. The distance from the coupler to the test piece was about 2 feet (an attenuation of about 0.14 db). In addition, because this length of waveguide contained 7 choke-to-cover flange connections, the total attenuation, including the waveguide, was

CONFIDENTIAL



CONFIDENTIAL

estimated to be 0.3 db. Since the calibration was made with the water load connected directly to the directional coupler, the power level at the thermistor had to exceed the power at the test piece by a non-negligible amount. Hence, the estimate in breakdown power was in error by about +6 percent.

e. Waveguide Tolerances

In determining the accuracy of the breakdown power as a function of the tolerances of the waveguide dimensions, it was convenient to start with the general equation for the power capacity for the  $TE_{10}$  mode\*

$$P = K ab \frac{\lambda}{\lambda_g} \quad (56)$$

Substituting the general wavelength equation\*\* for the  $TE_{10}$  mode

$$\frac{\lambda}{\lambda_g} = \sqrt{1 - \left(\frac{\lambda}{2a}\right)^2} \quad (57)$$

Therefore

$$P = K ab \sqrt{1 - \left(\frac{\lambda}{2a}\right)^2} \quad (58)$$

\*See ref. 81, page 124.

\*\*See ref. 69, page 62.

CONFIDENTIAL

CONFIDENTIAL

After taking natural logarithms

$$\ln P = \ln K + \ln a + \ln b + \frac{1}{2} \ln \left[ 1 - \left( \frac{\lambda}{2a} \right)^2 \right] \quad (59)$$

and then taking its derivative, the following equation results

$$\frac{dP}{P} = \frac{da}{a} \left[ 1 + \left[ \frac{\lambda^2}{4a^2} \right] \frac{1}{1 - \left[ \frac{\lambda}{2a} \right]^2} \right] + \frac{db}{b} \quad (60)$$

The tolerance of commercial X-band waveguide is about .003 inch  
Thus,

$$\frac{\Delta a}{a} = \frac{1}{300} \quad (61)$$

$$\frac{\Delta b}{b} = \frac{1}{133}$$

and

$$\frac{\Delta P}{P} = \frac{1}{300} [1 + 0.954] + \frac{1}{133} \quad (62)$$

$$= \frac{1.954}{300} + \frac{1}{133} = .0065 + .0075$$

$$\frac{\Delta P}{P} = .0115 \pm 1 \text{ percent}$$

The error in power due to changes in microwave frequency calculated by an extension of this analysis was found to be negligible.

## f. Voltage Standing Wave Ratio

In the breakdown tests, the test piece was followed by a pressure window and a dummy load. The VSWR of the window and dummy-load combination was measured to be 1.07. This lead to breakdown in the test section at a computed power 7 percent lower than with no standing wave. Hence, the estimate of breakdown power was in error by -7 percent because of the standing wave.

## g. Measurement of Pressure

The error in breakdown power depended upon the relative error in pressure and the absolute pressure in the manner shown in equation 47:

$$\frac{\Delta p}{p} = 2 \frac{\Delta p}{p} \text{ 100 percent}$$

Thus, it can be seen that the error in breakdown power increases as the absolute pressure decreases for a constant error in pressure,  $\Delta p$ . A quantitative estimate of how this error will vary with pressure can be calculated from equation 47 by substituting typical values of the parameters. The results of such a series of calculations are plotted in figure 16. It is seen that at low pressures, the error in power can become quite large unless care is taken in the pressure measurements.

CONFIDENTIAL

In general, the error in the pressure measurement,  $p$ , came from two sources; the accuracy of the instrument and the accuracy in reading the instrument. These two sources of error were independent of each other. Two pressure meters were used during the course of the program.

The relative pressure gauge had another source of error in addition to the two already mentioned. An error due to parallelax in reading the gauge was estimated to be 0.1 inch of mercury. Also, the gauge was calibrated against a manometer in order to check the linearity of the readings. It sometimes happens that a spring loaded gauge does not give a true reading due to failure of the mechanism. From the calibration, it was estimated that the gauge read to within 0.2 inch of mercury of the true reading. Finally, the most significant source of error in the gauge was probably fluctuation of the atmospheric pressure. The U.S. Weather Bureau Reports for this area indicated that the mean daily barometric pressure may change by 0.5 inch of mercury in the course of a week and that fluctuations of one inch are not uncommon. Since the breakdown data was uncompensated for changes in atmospheric pressure, 30 inches of mercury, absolute pressure, was taken as standard atmospheric pressure for converting the gauge readings to absolute pressure.

CONFIDENTIAL

CONFIDENTIAL

Therefore, the error in the measurements made at low pressures could be large. In addition, the error would probably remain constant in the course of testing of components (the barometric pressure is relatively constant for a period of several hours) and therefore would not show up as internal inconsistency in the breakdown data. Because of the fluctuations in barometric pressure, the most probable error in pressures was estimated to be 0.3 inches of mercury.

A pressure meter used in the latter part of the building block phase of the program to perform some of the low-pressure tests was an absolute pressure manometer purchased from the Emil Greiner Company (Model 10709). This instrument can be read to the nearest 0.01 centimeter of mercury and provided extreme accuracy even at very low pressures.

Since the relative pressure gauge was used for most of the breakdown tests, the errors were estimated on the basis of its accuracy.

The best case refers to tests in which the pressure was 15 inches of mercury or above and the worst case is for pressure of 5 inches or above. See table 2.

CONFIDENTIAL



TABLE 2  
PRESSURE VS POWER ERRORS

Source of error	Estimated Pressure Errors ( $\Delta p$ )	Calculated Power Errors ( $\frac{\Delta P}{P}$ )	
		Worst case	Best case
reading instrument	0.1	4%	1.3%
accuracy of instrument	0.2	8%	2.6%
barometric fluctuations	0.3	12%	3.9%
	overall rms error	15%	4.9%

In most of the tests, some or all of the data was obtained above 15 inches of mercury, absolute pressure. Therefore, the most probable error for the tests was taken as the best of the two cases (table 2) resulting in an overall error due to pressure measurements of 4.9 percent. However, it should be noted that it was possible for these factors to add in phase for a particular test, subsequently resulting in a much larger error than estimated.

#### h. Summary of the Probable Errors

##### Parameter errors

water load	3 percent
thermistor bridge	2 percent
repetition rate	0.25 percent
pulse width (for 1.2-microsecond pulse)	7 percent

CONFIDENTIAL

onset stress	1 percent
standing wave (VSWR)	-7 percent
attenuation	+6 percent
Pressure measurement errors	
reading instrument	1.3 percent
accuracy of instrument	2.6 percent
barometric fluctuations	3.9 percent
Overall probable error	9.4 percent

The probable errors were estimated on the basis that there was 50 percent probability that the measurement would be within the stated limits. The error due to pulse width could approach 21 percent for the shortest pulse width (0.4 microsecond). The overall probable error was taken as the square root of the sum of the squares of the individual probable errors. Note that there are two constant errors in the power carrying capacity; a -7 percent error due to the VSWR and a +6 percent error due to attenuation. For very precise work, a -1 percent adjustment should be made in the reported values of power carrying capacity. The combined results of these effects have a negligible effect on the overall probable error in the breakdown measurements.

Since the peak power is an important measured quantity in breakdown tests, an attempt was made to measure

CONFIDENTIAL

it by two independent means. As noted elsewhere, the method adopted for measuring peak power for test purposes was to measure the average power and divide by the duty cycle to obtain peak power. This method assumes that the pulse is rectangular in shape and neglects the fact that even in the best actual pulse, ripple and overshoot are present. In order to check the validity of this assumption the results obtained by the average power method were compared with measurements made with the Sperry Model 630A Peak Power meter.

This instrument employs a baratter detecting in conjunction with differentiating and integrating circuits to measure peak power. Thus it provides an independent method for measuring peak power. The results of the tests are not conclusive because the background ringing in the area where the tests were made could not be easily eliminated. However, the tests indicate that for ring levels less than 25 percent of the peak power meter reading, the difference between the measured values obtained by the two methods was less than 6 percent. This result was obtained by subtracting the ringing algebraically from the meter reading.

This agreement is only an indication of the accuracy of the measured peak power level because the peak

CONFIDENTIAL

power meter is not an absolute reading device since it is calibrated using a low power pulse. However, the results do indicate that there is close agreement between the shapes of the high power pulse and the low power calibration pulse, which has a good rectangular shape. Since this is so, it is safe to conclude that the average power method of measuring peak power, which is based upon the assumption of a rectangular pulse shape, is valid for the equipment used in these tests.

#### 8. Investigation of Methods of Locating the Region of Breakdown

Several attempts were made to locate the region of breakdown by using an Amperite contact microphone and a set of throat microphones. There was no visible response on the oscilloscope after 40 db attenuation. As stated previously, this insensitivity might be due to the relatively large mass of the portion in contact with the waveguide. Therefore, it was thought that the use of a needle type pickup might work. A crystal pickup device was tested with negative results. In an effort to find a substance which was physically affected by exposure to breakdown, pressure sensitive masking tape, wax paper, Tempilaq and several organic starches, including potato starch were tried. (Tempilaq is a wax-like substance

CONFIDENTIAL

CONFIDENTIAL

which melts at a specific temperature and changes its appearance upon solidifying.) However, none of these substances gave a satisfactory indication of breakdown.

Defender Brand velour black enlarging paper was used but gave no indication of breakdown. Success was finally achieved using Contura Brand contact orthochromatic reflex paper. The paper was placed sensitive side facing the air gap, along the walls of the test section. This operation, as well as placing of the test section in the circuit, was carried out in subdued light. The microwave energy was then applied until breakdown was noted, both by the sound and by the photocell and counter combination. At this point the power was turned off and the paper removed and developed.

The picture shown in figure 17a, reveals several interesting and important features. First, the marks are on those portions of the paper which were adjacent to the broad walls of the waveguide. This is as expected inasmuch as the breakdown was parallel to the electric field. The next feature to observe is that marks occur in pairs, one on each wall. This indicated that every spark traveled the full distance between the walls. Another important feature is the axial spacing between the spots. Although this was

CONFIDENTIAL



CONFIDENTIAL

difficult to measure because several of the breakdowns show up as small clusters, the spacings were measured to be approximately  $24/64$ ,  $30/64$ , and  $30/64$ , measuring to the center of the cluster. At 9375 mc, the operating frequency, one quarter waveguide wavelength was approximately  $28/64$ . This value was exactly equal to the average of the three measured values. This indicated that in the plane of the spark, the admittance is that of a short circuit which creates a voltage maximum one-quarter wavelength towards the generator. This point then breaks down, shifting the voltage maximum another quarter wavelength towards the generator, and so on. The chain was broken when the voltage maximum fell on the generator side of the pressure window, at which point the pressure was sufficiently great to inhibit breakdown.

Several other pictures were taken following the same procedure, and one of these is shown in figure 17b. This shows the same characteristics as does figure 17a except there is one spot which has no mate on the opposite wall. This indicates that the spark did not traverse the full gap width but occurred as a point-to-plane discharge. Another interesting feature of this picture is the apparent gap of about one-half wavelength between one set of spots. This

CONFIDENTIAL

CONFIDENTIAL

would imply that either the breakdown occurred at a low-voltage point, which is hardly likely, or that the spark did not touch either wall but was point-to-point in nature. Whether this is true or the print is merely misleading, is difficult to say on the insufficient evidence available at this time. The spacing of the spots in figure 17b are very close to one-quarter wavelength or multiples thereof.

Some comments of a more general nature are in order at this point. The record of a spark breakdown within a waveguide is an innovation in the field. Previously, photographs had been obtained of low frequency and cavity discharges, but the photographs presented here are unique. The great amount of detail shown on these pictures reveals a significant amount of information concerning the breakdown process. It indicates that breakdown is often initiated by more than a single electron. This is shown first, by the cluster of marks in a single area, which indicates that several sparks crossed the gap independently. The premise is also substantiated by the forked nature of the other spots. This indicates that several electrons initiated sparks which were originally independent, but were sufficiently close to be joined in a common path. This is as one

CONFIDENTIAL

CONFIDENTIAL

might expect, inasmuch as a single electron, which creates an avalanche, leaves in its wake a cloud of positive ions which then attract any other electrons.

Another significant feature of breakdown is revealed by figure 17b. Here it can be seen that the spark does not always cross the entire gap. This is not surprising, if one considers that the spark is the result of an avalanche initiated by a single electron. Since this electron is created at some internal point, it is plausible that the sparkover should occur between this point and that wall which is instantaneously at a positive potential with respect to ground. Such a sparkover will distort the field, so that an increased gradient is created between the wall at negative potential and the internal point where the spark originated. This will serve to promote another spark in the region, and by a chain reaction the entire space between the walls may be covered. However, it is possible that the initial point was sufficiently close to the wall, at positive potential, that the initial spark did not distort the field significantly. Or else the time involved for the entire process to occur, and the voltage phase at the time of initiation, might be such that the entire gap was not traversed. It should be noted here, that there was no assurance that the spark

CONFIDENTIAL

CONFIDENTIAL

crossed the entire gap, even in those cases where spots appeared on both walls. This uncertainty is due to the fact that the photographic paper will pick up the light from a short distance away. However, the nature of the paired spots, and the fact that the spots do not always occur in pairs, is a good indication that the entire gap was actually traversed in those instances.

Further information about the spark itself is revealed by the spacing of the spots. These spaces are nearly one-quarter waveguide wavelength in every case. This indicates that the spark represents a very high admittance which approximates a short circuit.

As has been stated before, the means of location of the region of breakdown, and the results obtained, are a distinct contribution to the study of microwave breakdown. However, it should be recognized that the method has several limitations. First, in order to use the photographic paper the breakdown section must consist of flat surfaces which are accessible from the outside. This is necessary in order to satisfy the assumption that the paper does not change the field configuration thus affecting the voltage gradient and the region where breakdown occurs. Second, there is the necessity of loading the paper in subdued light, and then

CONFIDENTIAL

CONFIDENTIAL

developing the paper after the tests are completed. The first objection can be a very severe limitation in the study of the breakdown of the complicated waveguide components. Therefore, more work should be done to improve the general technique and thereby overcome this limitation. One such attempt might involve an investigation into the use of some light sensitive liquid, which can be applied directly to the walls of the test piece.

## 9. Measurement of The Effect on Peak-Power Breakdown of Various Design Parameters

### 9.1 Pressure

Pressurization of waveguide components with air or some other insulating gas is a widely used technique for increasing the power carrying capacity of a radar system. On the other hand, this program used evacuation of the test piece as a technique for inducing breakdown with the limited amount of available power. Therefore, the range in which the extrapolation of breakdown power vs pressure data above and below atmospheric pressure is valid, had to be determined.

As shown by the data, figure 12 is linear over its entire range and figures 13, 14, and 15 are linear for higher power and pressure. If it is assumed that the linear region is more reliable, then it is established that the natural



CONFIDENTIAL

logarithm of power versus the natural logarithm of pressure curve is a straight line. This means that the breakdown power is a function of the pressure raised to some power.

First, assume

power = constant x pressure<sup>exponent</sup>

$$\text{or, } P = K_p^n$$

$$\text{Then, } \ln P = \ln K + n \ln p$$

$$\text{Slope of } \ln P \text{ vs. } \ln p = \frac{\ln P_1 - \ln P_2}{\ln p_1 - \ln p_2}$$

$$\text{Slope} = \frac{\ln K + n \ln p_1 - \ln K - n \ln p_2}{\ln p_1 - \ln p_2}$$

$$\text{slope} = n$$

Therefore, if the curve of  $\ln$  power vs.  $\ln$  pressure is linear, then the slope of the curve is the exponent to which the pressure must be raised. This exponent varied from a maximum of 2.08 in figure 12 to a minimum of 1.84 in figure 13; the mean was 1.95. For breakdown under low-frequency conditions, the corresponding value was 12, which was arrived at by a consideration of Paschen's Law. This Law states that the breakdown voltage is a unique function of pressure times the gap width. Since the voltage was approximately proportional to the gap width, this means that the breakdown voltage was very nearly directly proportional to the pressure. As a consequence, the breakdown power is proportional to the square of the pressure and the exponent is 2.

CONFIDENTIAL

CONFIDENTIAL

The close agreement between the mean value of 1.95 and the low-frequency value of 2 was gratifying. This provided a check on the accuracy of the measurements, and it justified the extrapolation of the data to higher values of pressure.

Additional breakdown power vs pressure data to be presented later in this report indicates that a linear relationship between  $\ln$  power and  $\ln$  pressure existed from at least 5 inches to 40 inches of mercury (absolute pressure).

#### 9.2 Pulse Duration

To investigate the variation of pulse width and repetition rate on peak-power breakdown, the standard tapered waveguide section of 1-inch x 1/2-inch x .050-inch waveguide was used (see figure 4).

A chart showing the different pulse widths and repetition rates tested is shown in table 3. Included in this chart are the slopes of the  $\ln$  power vs  $\ln$  pressure curves obtained from the data.

CONFIDENTIAL

CONFIDENTIAL

TABLE 3  
PULSE WIDTHS AND REPETITION RATES  
USED IN BREAKDOWN TESTS

Pulse Width (microseconds)	Repetition Rate pulses per second			
	300	400	800	2500
0.4	-	2.36	2.35	2.5
0.8	-	2.13	2.14	-
1.2	-	2.17	2.2	-
2.35	-	2.3	-	-
3.55	2.8	2.4	-	-

The number of variations of pulse widths and repetition rates was limited by the equipment available. Since the values used encompass most of the useful radar range, this data is considered sufficient. Only one point was taken at 300 pps. Since this point was so close to 400 pps it was felt that the data would be inconclusive, and further testing at this repetition rate was discontinued. Some of the data that was obtained is plotted in figures 19 and 20 in the form of  $\ln$  breakdown power vs  $\ln$  pressure for different pulse widths and repetition rates (see tenth interim report for complete presentation of the data). Figure 19 contains the data on the variation of pulse width as the repetition rate was held constant at 400 pps. In figure 20 the pulse width was held constant at 0.4 microsecond and the

CONFIDENTIAL

CONFIDENTIAL

repetition rate was varied. All the curves are straight lines with approximately the same slope which varies from 2.1 to 2.5 as compared with data in the seventh report. This indicates a slope of 2.08 for the same test section.

Since the relationship between power and pressure is

$$\text{power} = (\text{constant}) \times (\text{function of repetition rate}) \times (\text{function of pulse width}) \times (\text{pressure})^{\text{exponent}} \times (\text{function of other parameters}),$$

it was decided to plot a family of curves of power vs pulse width at a constant repetition rate, with pressure as the parameter. By this method, the effect of the known parameters of repetition rate and pressure were eliminated and the effect of pulse width could be determined.

This was done on a logarithmic scale since it was expected that the function would be exponential. This data is shown in figure 21. It can be seen from this graph that all of the curves are straight lines, which indicates that the exponential assumption was correct.

The data taken at a 3.55 microsecond pulse width was not plotted since at this point the curve tended to flatten and the data was almost identical with the 2.35-microsecond pulse. The data for a constant repetition rate

CONFIDENTIAL

of 800 pps and varying pulse widths yielded curves similar to the curves shown in figure 21. In figure 22, the slopes of the various curves of figure 21 are plotted as a function of pressure. It can be seen from this curve that the slope variation with pressure was very small, which means that the effect of pulse width is independent of pressure. The average value of the slope was 0.36 which is very close to the decimal equivalent of the fraction  $1/3$ . Therefore, for convenience, the peak-power, to close approximation, is inversely proportional to the pulse width raised to the  $1/3$  power in the range from 0.4 to 2.35 microseconds.

The data obtained on pulse width and repetition rate can be compared with information contained in several references<sup>57,85,87</sup>. In the M.I.T. report on microwave breakdown,<sup>85</sup> data on the effect of pulse width upon breakdown is analyzed and a relationship between power and pulse width is established. Tests were made using pulse widths between 0.2 and 5 microseconds at a repetition rate of 500 pps in the 1-inch x 1/2-inch x .050-inch waveguide. It was concluded that the peak-power carrying capacity varied inversely as the square root of the pulse width for pulse widths less than 2 microseconds. Above 2.5 microseconds the pulse width has no effect.



CONFIDENTIAL

The M.I.T. data compares favorably with the data contained in this report, where power varies inversely with the pulse width to the  $1/3$  power. Also, the data presented in this report shows that the power-handling capacity is essentially the same for 2.35- and 3.55-microsecond pulses. This agreement was expected, since beyond a certain value of pulse width there is sufficient time for the formation of a spark, so that increasing the pulse width should have little effect.

There are two reasons for the discrepancy between the values of  $1/2$  and  $1/3$  for the exponent: first, the test piece used by M.I.T. was a reduced-height section of waveguide, which means that an extrapolation of the data was necessary to obtain the final values; and second, the M.I.T. data was not consistent. An examination of several of the curves presented indicated that a value of  $1/3$  for the exponent is more in agreement with the data than a value of  $1/2$ .

The effect of pulse width on breakdown power in hydrogen gas is discussed by Lathrop and Brown<sup>(57)</sup>. This work was done with a resonant cavity in the 10.7-cm range (2800 mc), with pulse widths varying from 1 to 60 microseconds at a repetition rate of 80 pps. Two curves of breakdown

CONFIDENTIAL

CONFIDENTIAL

field vs pulse width were plotted with pressure as a parameter, one containing pressures to the right of the knee of the Paschen curve for hydrogen and the other to the left of the knee.

Several things are apparent from these curves. First, as the pulse width was increased from 10 to 50 microseconds, the breakdown field remained approximately the same. On a qualitative basis, this agrees quite well with the data in this report. Exact quantitative results were difficult to obtain, since the curves are not too well defined at low pulse widths, and the data was taken in hydrogen which might exhibit different breakdown characteristics than air. Secondly, in the region from 1 to 10 microseconds the breakdown-field vs pulse-width curve appears to be exponential; but again, no quantitative results can be obtained. Thirdly, it is to be noted that Lathrop and Brown<sup>57</sup>, together with Prowse<sup>67</sup>, plotted their data with pressure as a parameter, indicating that the relationship between peak-power capacity and pulse width might be a function of pressure.

An examination of the curves by Lathrop and Brown indicates that from pressures of 2 to 32 mm of mercury the relationship remains essentially the same. To substantiate these views at the higher pressures used on this project

CONFIDENTIAL

CONFIDENTIAL

(5 to 10 inches of mercury), figure 22 contains a curve showing the variation of the pulse-width exponent as a function of pressure. The almost constant slope of the curve indicates that pressure is not a factor in determining the pulse-width vs peak-power carrying capacity relationship.

### 9.3 Repetition Rate

The data on the effect of repetition rate upon peak-power breakdown was presented in conjunction with the pulse-duration data in paragraph 9.2.

In considering the effect of repetition rate on peak-power breakdown, a family of curves was plotted of power vs repetition rate at a constant pulse width of 0.4 microsecond, with pressure as the parameter. The relationship between power and repetition rate was assumed to be exponential and a log-log graph was utilized. This is shown in figure 23.

An examination of these curves shows that they are straight lines with approximately the same slope. In order to illustrate the independence of the power-repetition-rate relationship upon pressure and to obtain the exponent, the slopes of the curves of figure 23 were plotted as a function of pressure. This is shown in figure 24. The slope is

CONFIDENTIAL

CONFIDENTIAL

essentially constant with pressure and has an average value of .067. Further examination of the data indicates that the repetition-rate exponent remained essentially constant as the pulse width was varied up to 3.55 microseconds. Therefore, to a close approximation the power is inversely proportional to the repetition rate raised to the  $1/15$  power in the region from 400 to 2500 pps.

Prowse<sup>87</sup> discusses the breakdown fields in waveguides at 9375 mc (3.2 cm) using air and neon at pressures from 2 to 30 mm of mercury. The pulse width was varied from 1 to 2 microseconds and the repetition rate from 200 to 600 pulses per second. No quantitative analysis can be performed since the pressures are very close to the knee of the Paschen curve and the data is not too well defined. However, it is apparent that the pulse width and repetition rate influence the power-handling capacity of waveguides in a fashion similar to that indicated by the results in this report.

The M.I.I. report<sup>57</sup> also discusses the effect of repetition rate on peak-power-handling capacity at 9375 mc, and is concerned with the range of 500 to 2000 pulses per second and a pulse width of 1 microsecond. An expression is arrived at, that

$$\text{Peak power} = (8000 - \text{RR})$$

CONFIDENTIAL

CONFIDENTIAL

Comparing this result to the relationship obtained from the data in this report, it can be concluded that because the M.I.T. data is not too consistent, the M.I.T. expression may be accurate over a small range, but that the exponential relationship where the peak-power capacity varies inversely with the repetition rate to the  $1/15$  power is more nearly correct. (See tenth interim report for further discussions.)

#### 9.4 Pulse Shape

The most common way of measuring pulsed peak power is to measure the average power and convert to peak power by dividing by the duty cycle. (This method was adopted for these tests.) It assumes an ideal rectangular pulse shape. However, actual pulses have finite rise and decay times and uneven tops. Therefore, the calculated peak power did not correspond to the actual peak power to which the test piece was subjected and this lead to errors. In addition, the top of the pulse shape may suffer from overshoot on the leading edge and ripple or fluctuation of the top of the pulse. The ripple and overshoot voltages definitely had an effect on the peak-power breakdown for which it was difficult to compensate. These effects could be remedied in two ways. First the pulsing network could be designed so effects were held to a minimum. Second, the magnetron could be operated at the same drive

CONFIDENTIAL



CONFIDENTIAL

voltage for all tests so that whatever portion of these effects could not be eliminated, could be held constant. This approach was implemented by utilizing a waveguide power-divider network to obtain changes in power level to the test piece. In addition, pictures of the r-f pulse indicated that the pulse shape was reasonably good.

#### 9.5 Mechanical Finish

Three pieces of waveguide were fabricated with different values of roughness on all four walls in order to investigate the effect of surface roughness on peak-power capacity. (The definition and measurement of an RMS finish is contained in paragraph 4.3. After the completion of the tests the RMS values of the pieces were measured and found to be as follows:

- a. piece number one varied from 300 to 400 RMS
- b. piece number two varied from 550 to 650 RMS
- c. piece number three varied from 650 to 850 RMS

Since these values are higher than those normally encountered, they represented an extreme condition of surface roughness and as such formed an upper limit, above which no practical application exists. For example, drawn brass waveguide is generally better than 64 RMS. These tests were valuable

CONFIDENTIAL

CONFIDENTIAL

since the data indicated breakdown values which are considerably better than those of most waveguide components.

The data on the three test pieces are plotted in figures 18, 25, and 26. As shown in the figures, the slope of the  $\ln$  power vs  $\ln$  pressure curves remains essentially constant at 2.0, which is the same as the slope for a standard waveguide section. By extrapolation of the curves, the peak-power capacity at atmospheric pressure was found to be:

- a. piece number one (300-400 RMS) - 89 percent of the full waveguide power carrying capacity, or 1.23 megawatt.
- b. piece number two (550-650 RMS) - 82 percent of the full waveguide power carrying capacity, or 1.14 megawatt.
- c. piece number three (650-850 RMS) - 74 percent of the full waveguide power carrying capacity or 1.03 megawatt.

Thus, it is seen that the 300-400 RMS finish, which was worse than that generally encountered in practice, could carry 91 percent of the full waveguide power carrying capacity. This is considerably more power than most waveguide components will carry and enables a relaxation of surface finish specifications on many components.

CONFIDENTIAL

## 9.6 Nature of the Gas

### a. Introduction

A complete investigation of the nature of the gas upon peak-power breakdown was obviously beyond the scope of this program. However, it has been suggested in the literature<sup>(98)</sup> that other gases would be preferred to air in applications where high-voltage gradients are encountered because of their superior insulating properties. One such gas is sulphur hexafluoride ( $\text{SF}_6$ ). This gas has several desirable features. It is colorless, odorless and non-toxic. For these reasons, sulphur hexafluoride may be useful in high-power radar systems and therefore its peak-power breakdown characteristics were investigated.

Three different test pieces were used in measuring the effect of the gas upon peak-power breakdown. The first test piece was the standard tapered section (see figure 27) used to find the peak-power capacity of 1-inch x 1/2-inch x .050-inch waveguide. The second test piece was a section of standard 1-inch x 1/2-inch x .050-inch waveguide containing two hemispherical bumps as shown in figure 28. The bump section was suggested by Wheeler Laboratories<sup>(20)</sup> for the purpose of standardizing the breakdown tests made in various laboratories throughout the country. It also has the

CONFIDENTIAL

added advantages of breakdown at considerably lower power than the waveguide and of being easily matched. The particular unit used had 0.150-inch radius bumps and a VSWR of 1.09 at 9375 mc. Wheeler Laboratories claim that the hemispherical bump or spark gap section will breakdown at one-ninth of standard waveguide power. The third test piece, similar to the one used by Posin, Mansur and Clarke<sup>(85)</sup>, was a swayback test section in which the inner dimensions of standard 1-inch x 1/2-inch waveguide was gradually tapered from 0.900-inch x 0.400-inch to a 0.900-inch x 0.012-inch cross section as shown in figure 29. In this manner the VSWR was kept low. The swayback was computed to carry 1/33 of standard 1-inch x 1/2-inch waveguide power capacity on the assumption that the field gradient required for breakdown was constant. A swayback section 2.5 feet long was selected as a compromise between match and length. It had a VSWR of 1.6 at 9375 mc which did not adversely affect the oscillations of the magnetron. As the frequency was varied the VSWR did not exceed the value at 9375 mc. At frequencies above and below this value, such that the gap length was an odd multiple of quarter wavelengths, the swayback approached a matched condition. This indicated that the swayback could be considered as a mismatched cavity formed by two lumped

CONFIDENTIAL

CONFIDENTIAL

susceptances. In computing the field gradient in the gap at breakdown, the effect of the standing wave in the cavity was included.

Three methods of pressurization were employed in the  $\text{SF}_6$  tests. The first one utilized basically the same test circuit that was used for previous tests with the addition of an adapter to inject the gas into the test piece. In order to obtain the data, the test section was evacuated with the gas tank closed from the rest of the system. The best vacuum obtainable from this arrangement was 1.8 inches of mercury, absolute pressure. When this vacuum was achieved, the  $\text{SF}_6$  gas was fed into the test piece until the desired pressure was obtained. The power was then varied until breakdown occurred. The gas mixture in the test section was estimated to be more than 60 percent  $\text{SF}_6$ . This method of obtaining the data will be referred to as the single evacuation method.

The second method of pressurizing the test section was similar to the single evacuation method. The test section was evacuated to 2 inches of mercury while it was isolated from the  $\text{SF}_6$  supply. When this vacuum was achieved, the gas was fed into the test piece until the pressure reached one atmosphere absolute. Then the gas tank was closed off from

CONFIDENTIAL



CONFIDENTIAL

the system, and the test piece was again evacuated to 2 inches of mercury. The gas was again fed into the test piece until the desired pressure was obtained. Assuming a perfect mixture of air and gas when the test section was raised to atmospheric pressure, a simple calculation indicated that the residual air in the test section was reduced from 2 inches to 0.07 inch of mercury. The power was then increased in small increments until breakdown occurred. The amount of gas in the test piece during the tests was estimated to vary between 93 and 98 percent. This method of obtaining the data was referred to as the double evacuation method.

The third method of pressurization used to investigate the breakdown of sulphur hexafluoride gas was referred to as the balanced rate method. The test circuit is shown in figure 30. In the balanced-rate method, the test section was evacuated to two inches of mercury absolute pressure and filled with sulphur hexafluoride gas to one atmosphere absolute. Then the pressure desired in the test piece was attained by adjusting the input and output valves until the amount of gas removed from the system by the pump, which was left on during the tests, was balanced by the amount of gas injected plus whatever air leaked through the waveguide pressure seals. This method assured a constant gas pressure of essentially

CONFIDENTIAL

CONFIDENTIAL

uniform composition throughout the duration of the test. The effect of gas turbulence in this method was kept to a minimum by maintaining a slow gas flow rate through the test piece.

The data obtained on the breakdown of sulphur hexafluoride gas is shown in figures 27, 28, and 29 in the form of  $\ln$  power vs  $\ln$  pressure. Figure 27 shows the data for the standard 1-inch x 1/2-inch x .050-inch waveguide test section obtained by the three pressurization methods. Figures 28 and 29 show similar data obtained for the hemispherical bump and the swayback test pieces respectively. All the curves are straight lines with approximately square-law slopes. The displacement between the curves obtained on each test piece by the various pressurization techniques indicates differences in power capacity.

The results of the tests are presented in table 4 as a ratio of measured power carrying capacity of the component, when filled with sulphur hexafluoride gas by a particular pressurization method, to the power capacity when filled with air. It can be seen from table 4 that the slopes of the  $\ln$  power vs  $\ln$  pressure curves for all test sections and methods conformed approximately to a square-law relationship. This square-law relationship has been observed many times before for the breakdown of components in which

CONFIDENTIAL

CONFIDENTIAL

there were at least an approximately uniform E-field. It indicates, although not conclusively, that the power carrying capacity of the three test sections differed because of the size of the breakdown gap and the composition of the gas rather than because of a non-uniform field in the breakdown region.

TABLE 4  
SUMMARY OF BREAKDOWN TESTS FOR SF<sub>6</sub> GAS

Pressur- ization Technique	Test Section					
	Standard Waveguide		Hemispher- ical Bump		Swayback	
	Power Ratio SF <sub>6</sub> air	Slope	Power Ratio SF <sub>6</sub> air	Slope	Power Ratio SF <sub>6</sub> air	Slope
Single- Evacuation	1:1	2.0	1.3:1 to 2.8:1	2.0 1.9	No test	
Double- Evacuation	1.2:1	2.0	No test		4:1	Insuf- ficient Data
Balanced- Rate	6:1	1.8	6:1	1.9	13:1	2.1

b. Variation of Power Carrying Capacity with Pressurization Technique

For the standard waveguide test section, the data indicates that the relative power carrying capacities for

CONFIDENTIAL

sulphur hexafluoride ( $\text{SF}_6$ ), injected by the single-evacuation, double-evacuation and balanced-rate methods, were in the ratio 1.1:1.2:6. Similar results, indicating that the greatest relative power carrying capacity for a component occurred for the balanced-rate method, were observed for the hemispherical bump and swayback sections. The results of the balanced-rate method were probably higher than either the single- or double-evacuation methods because it provides the greatest purity of  $\text{SF}_6$  gas. The superior breakdown characteristics of this gas as compared to air have been attributed by Schumb, Trump, and Priest<sup>98</sup> to the relatively large collision cross section of the gas molecule and the affinity of it and its dissociation products for the attachment of electrons. For uniform-field breakdown, it was expected that the dielectric strength of 100-percent  $\text{SF}_6$  gas would be reduced by mixing it with a gas of lower dielectric strength such as air. Thus, the breakdown of a gas mixture composed of varying percentages of  $\text{SF}_6$  and air would vary from a maximum for 100 percent  $\text{SF}_6$  to a minimum for 100 percent air. In using the available equipment, the balanced-rate method came closer to attaining 100 percent  $\text{SF}_6$  than either the single- or double-evacuation methods. The inherent weaknesses in the ability of the single- and double-evacuation methods to provide high gas purity was attributable to two conditions. First, the pumping

CONFIDENTIAL

equipment did not remove the residual air from the test piece. (The lowest attainable vacuum was two inches of mercury.) Initially, therefore, a comparatively large amount of air was left in the test section, which contaminated the  $\text{SF}_6$ . Secondly, additional contaminating air entered from the outside through the waveguide pressure seals because of the pressure differentials existing during the tests. This leakage further reduced the  $\text{SF}_6$  gas purity. If these limitations could be removed by application of high-vacuum techniques, it is expected that the single-evacuation method (double evacuation would then be no longer necessary) would provide the same results as the balanced-rate method and would have the further benefit of not consuming  $\text{SF}_6$  gas so extravagantly. Since high-vacuum techniques are beyond the scope of this program, the balanced-rate technique was found to be the superior method of pressurization.

c. Variation of Power Carrying Capacity with Different Test Sections

As previously stated, the data on the standard waveguide utilizing the balanced-rate method indicated a power carrying capacity ratio for  $\text{SF}_6$  to air of 6:1; for the single- and double-evacuation methods it was only 1.1: and 1.2:1, respectively. In most applications,  $\text{SF}_6$  gas was used to increase the power carrying capacity of waveguide components.

CONFIDENTIAL

CONFIDENTIAL

If the purity of the gas could be kept high, an increase in power carrying capacity of 6:1 could be expected for these components.

The data on the hemispherical bump section was obtained by the single-evacuation and balanced-rate methods and resulted in power carrying capacities of 1.3:1 to 2.8:1 for single evacuation, and 6:1 for balanced rate. With the single-evacuation method, as can be seen in figure 28, the power carrying capacity of the bump section changed abruptly at 15.6 inches of mercury, absolute pressure, from 1.3:1 below to 2.8:1 above the bend in the curve. An abrupt change was not observed for the balanced-rate method. Therefore, a change in the breakdown mechanism for the bump structure as was suggested in the fifteenth report is highly unlikely. The probable explanation is that the gas purity increased at pressures above 15.6 inches and resulted in an increase in power capacity, as previously commented upon.

The data on the swayback with a .012-inch gap indicates a 13:1 ratio in power carrying capacity for  $\text{SF}_6$  to air for the balanced-rate method, and a 4:1 ratio for the double-evacuation method. The major portion of this difference can probably be attributed to variation in gas purity for the two methods. The 11:1 power ratio reported in the sixteenth



CONFIDENTIAL

report for this swayback is an average value obtained for several different pulse widths and repetition rates, whereas the 13:1 value of this report pertains to a 1.2-microsecond pulse width and an 800-pps repetition rate.

In addition to variations in the results on the various test pieces due to gas purity, it was indicated in the sixteenth report that a change in the breakdown mechanism could also cause variations. Paschen's law states that the voltage gradient required for breakdown is a function of pressure and gap width. For the range of pressures used in the tests, the gradient increased slightly as the gap width was reduced. The magnitude of this phenomenon was obtained by comparing the breakdown voltage gradient for air in the standard waveguide and the swayback test sections. For this purpose, the ratio of the effective power (effective power is the power causing the swayback section to breakdown taking into account the presence of standing waves) to the measured power of the generator was determined to be 1.23 utilizing equation (43).

The peak-power carrying capacity of the air-filled swayback at atmospheric pressure was measured to be 53 kw, and thus the effective power was 65 kw. The power carrying capacity of 0.900-inch x 0.400-inch rectangular waveguide was

CONFIDENTIAL

CONFIDENTIAL

scaled to 0.900-inch x .012-inch waveguide on the assumption that the field gradient required for breakdown is relatively constant. (Refer to equation (42.)) This calculation indicated that the power carrying capacity of the swayback is  $1/33$  of standard 0.900-inch x 0.400-inch waveguide, or 44 kw. Thus, the ratio of the measured to the scaled value for the breakdown gradient was 1.5 in power or 1.23 in voltage. The enormous change in the gap height required to produce a 23-percent increase in the breakdown voltage gradient demonstrated why this phenomenon can be neglected for most radar applications. Independent experimental results verifying the experiments conducted under this contract have been obtained by Herlin and Brown<sup>40</sup>. They measured the breakdown gradient of air for various pressures and gap heights in a cylindrical cavity at 2800 mc. Figure 5 of their paper contains a curve of pressure times wavelength ( $p\lambda$ ) vs voltage breakdown gradient per unit pressure ( $E/P$ ) for a number of cavity heights ( $L$ ). Data was taken for values of  $p\lambda$  up to 300 mm of mercury per cm and for values of  $L$  ranging from .0635 to 7.62 cm. The results indicate that variations of as much as 4:1 in voltage breakdown gradient can occur for the range of gaps measured. The appropriate value for  $p\lambda$  in the present experiments was 2280 mm of mercury per cm which is outside

CONFIDENTIAL

CONFIDENTIAL

the range of Herlin and Brown's data. Extrapolation of their data to this value is of doubtful accuracy since the curves are not linear. However, qualitative estimates based on the Herlin and Brown data of the difference in voltage gradient between the two gap heights, corresponding to the standard waveguide and swayback test sections, indicated the same effect and order of magnitude as were observed in the data reported here.

A similar analysis of the data for the  $\text{SF}_6$ -filled swayback and standard waveguide test sections was made. The ratio of the measured value of the breakdown gradient of  $\text{SF}_6$  for the swayback (compensated for the standing wave by equation (43)) to the value scaled down from the measured value for standard waveguide was 3.2 in power or 1.8 in voltage. It is very likely that the same gas purity was attained by the balanced-rate method for both test sections. Therefore, the major reason for the difference in breakdown power was probably the size of the breakdown gaps. It is seen that the change in gap produced an 80-percent increase in breakdown voltage gradient for  $\text{SF}_6$  and only a 25-percent increase for air. Unfortunately, the literature does not reveal any information on the breakdown of  $\text{SF}_6$  as a function

CONFIDENTIAL

CONFIDENTIAL

of gap size which might support this result. However, the heavier  $\text{SF}_6$  molecule can certainly be expected to have different physical properties than air.

From this discussion it can be concluded that the balanced-rate method is the superior pressurization technique. Increases in power capacity of the order of 6:1 for waveguide and waveguide components and 11:1 for gap widths in the order of .012 inch are to be expected with the use of  $\text{SF}_6$  gas. It should be pointed out that the increase in power capacity of  $\text{SF}_6$  to air of 10.5:1, as reported by Kaplan<sup>49</sup> and Sutherland<sup>100</sup> was obtained from data taken on swaybacks with gap widths that correspond to the swayback gap size reported here. The two sets of data agree very well. However, their reports claim that the value of 10.5:1 will hold for waveguide and waveguide components. This extrapolation of their data to larger gap widths is incorrect because, as pointed out in this report and in the work by Herlin and Brown, the voltage gradient required for breakdown varies with gap width. Therefore, the factor of 6:1 for waveguide and waveguide components appears to be the more correct figure.

Data is presented in the sixteenth interim report in which the balanced-rate method was used to investigate the effect of variation of the pulse width and repetition

CONFIDENTIAL

rate on the peak-power breakdown of the  $\text{SF}_6$ -filled swayback section. The results indicated that the breakdown power of  $\text{SF}_6$ -filled waveguide is inversely proportional to the pulse width raised to the 0.22 power in the range from 0.4 to 1.2 microseconds and inversely proportional to the repetition rate raised to the 0.12 power in the region from 400 to 2500 pulses per second.

#### 9.7 Plating Material

The most common radar application of plating materials is undoubtedly the anodization of aluminum waveguide. Since it would be beyond the scope of this program to intensively investigate plating finishes, it was decided to make a high-power test of a typical anodized waveguide.

Aluminum waveguide is used in many radar applications where weight is a consideration. Prolonged exposure to the atmosphere causes the surface of the aluminum to oxidize, thereby increasing its attenuation. To prevent this, a protective anodize finish is usually applied to aluminum waveguide. Since this protective film is non-conductive, the current flows only in the aluminum and the amount of attenuation is not increased.

CONFIDENTIAL

CONFIDENTIAL

The anodizing process may, however, affect the power carrying capacity of the waveguide. Therefore an investigation of the effect was made. The test piece used was a 3-inch length of standard 1-inch x 1/2-inch anodized aluminum waveguide (see figure 31).

Since waveguides used in radar applications are sometimes too long to fit entirely into the anodizing bath, they must be placed in the bath first from one end and then the other. Two layers of anodizing film are deposited at the center of the waveguide. This "double dipped" condition was reproduced in the waveguide tested. In addition, the test section consisted of two lengths instead of a single length of anodized waveguide, so that an anodized choke-to-cover flange connection would also be included. The test-result points are plotted in figure 31. For comparison, the curve for the standard waveguide has been included in the figure, and it can be seen that the test data agrees quite well with it, indicating that the anodizing has an insignificant effect on the power carrying capacity of a waveguide.

#### 9.8 Microwave Frequency

The effect of microwave frequency on peak-power breakdown was not experimentally investigated because a variable frequency high-power source was not available.



CONFIDENTIAL

However, the theoretical power carrying capacity of rectangular waveguide is given by equation 38.

$$P_T = \frac{k}{2} a b E_o^2 \frac{\lambda}{\lambda_g}$$

As the microwave frequency varies, the quantities  $K$ ,  $a$ , and  $b$  (which refer to a constant of the medium, and the narrow and broad walls of the waveguide respectively) remain fixed.  $E_o$  is the breakdown field gradient for the medium. With reference to paragraph 6.1b, it was found that breakdown at microwave frequencies was characterized by the fact that some electrons and positive ions cannot cross the gap within a half cycle of the applied power, and therefore the breakdown potential is independent of frequency. Thus, the quantity  $E_o$  should not change over the operating frequency band of the waveguide. This leads to the conclusion that the power carrying capacity of rectangular waveguide as a function of frequency will vary with the quantity  $\lambda/\lambda_g$ , the ratio of free space to waveguide wavelength. In the recommended operating frequency range of standard 1-inch x .050-inch waveguide (8.2 kmc to 1.24 kmc)  $\lambda/\lambda_g$  will vary from 0.60 to 0.84 which may be considered typical for all waveguide sizes. This means that the power carrying capacity of

CONFIDENTIAL

CONFIDENTIAL

waveguide varies by the ratio 1.4:1 over the normal operating frequency range. Breakdown in other frequency ranges is discussed in a later paragraph.

#### 9.9 Voltage Standing Wave Ratio

The power carrying capacity of a mismatched transmission line and a resonant cavity will be considered in this paragraph. If a transmission line is mismatched, a standing wave will be set up. The effect of a standing wave is to increase the voltage gradient at points along the line towards the generator separated by half wavelengths. The circuit used to investigate this effect of a standing wave upon peak-power breakdown is shown in figure 32. Inductive iris No. 1 was used to introduce a reflection in the line; different irises were used to obtain the desired VSWR's. Since the operating characteristics of a magnetron are such that load changes affect the power output, and also because the increase in the standing wave ratio may cause some of the auxiliary components in the test system to break down, it was decided to limit the standing wave to the region of the test section. To accomplish this a second inductive iris, No. 2, and a phase shifter were used to cancel the reflections from the first mismatch. The reactances of the two irises were made equal and the phase shifter was adjusted

CONFIDENTIAL

CONFIDENTIAL

until a minimum VSWR was obtained. A perfect match was not obtained in all cases because of the attenuation in the line between the first and second irises, extraneous reflections from other components, and a slight inequality between the two reactances. However, the input VSWR was less than 1.5 for all tests and was generally less than 1.2. This value was sufficiently low to assure an accurate test.

It should be noted that because of the structure of the circuit a resonant cavity existed between the two inductive irises. This caused increased voltages and losses which were considered in the formulae section, paragraph 5.

Tests were conducted for voltage standing wave ratios of 1.19, 1.39, 2.0, 5.1, and 10.0. The results of these tests are shown in figure 33. For VSWR's up to 2, the slopes of the curves of  $\ln$  power vs  $\ln$  pressure were identical to that for standard matched waveguide; for VSWR's of 2, 5.1, and 10, the slopes were just slightly below that for matched waveguide. The peak-power capacities as extrapolated to atmospheric pressure are given in table 5. It should be noted that this data is not to be used to determine the peak-power capacity as a function of VSWR, since the test conditions were different from actual operation conditions, as will be shown later.

CONFIDENTIAL

TABLE 5  
PEAK-POWER CAPACITY FOR VARIOUS VSWR'S

VSWR of Inductive Iris No. 1	Percent of Full Waveguide Power
1.2	95
1.4	82
2.0	60
5.0	30
10.0	13

The results shown in figure 33 were expected, since the type of breakdown should remain the same as the VSWR was varied, thus assuring a constant slope for the power-pressure curves. As the VSWR was increased, the maximum voltage present in the waveguide increased and hence the peak-power capacity had to decrease. The data on the effect of VSWR upon peak-power capacity was obtained by the use of a resonant cavity since this was the best way to avoid loading the magnetron and introducing further errors. This necessarily complicates the interpretation of the data and requires a more complete analysis before the information can be utilized. However, since in actual practice several mismatches are generally present at some random spacing which may approach a resonant condition, this data is very pertinent. The

CONFIDENTIAL

breakdown characteristics of a single mismatch and of a cavity formed by two mismatches are discussed in the formulae section, paragraph 4.5, and will now be compared with the experimental data.

Figure 34 shows the percentage of waveguide power vs VSWR for the case of a single mismatch. The graph was drawn for lossless and lossy transmission lines, as described by equations (15) and (16). The curve for the lossy line was drawn assuming 10 feet of brass waveguide (.054 db per foot) between the generator and mismatch. In both cases the mismatch was assumed to be a pure shunt reactance. Figure 35 shows the percent of full waveguide power vs VSWR of one mismatch for the case of a resonant cavity formed by two properly spaced mismatches in a waveguide. There are two conditions shown in this graph: one for the lossless case with a cavity input VSWR of unity (equation (17)) and one for the case of a lossy cavity, 3-1/2 feet long (.054 db per foot), with an input VSWR of 2 (equation (18)). Here again, the mismatches were assumed to be pure shunt reactances. The curve for the lossy line, input VSWR of 2, was not extended for VSWR values lower than 2 since these values are not realizable and have no meaning.

CONFIDENTIAL



CONFIDENTIAL

For comparison purposes, figure 36 contains curves of the various conditions described in equations (15), (16), (17), and (18). These curves indicate that for low values of VSWR (under 2.0) and for the conditions shown, the difference in peak-power capacity is 10 percent or less. This was expected because, for low values of reactance for the mismatch, the cavity Q will remain relatively low and will not give rise to a large increase in the maximum voltage present in the cavity. As the reactance of the mismatch was increased and approached a short circuit, the difference between the power capacity for the lossy, single-mismatch line and the lossy-cavity arrangement increased until it approached 28 percent of full power carrying capacity of the waveguide.

In applying these equations it should be mentioned that most applications will lie between the two extreme conditions of a single mismatch and a cavity. This is true because a transmission line generally contains several mismatches arbitrarily spaced along the line, with insertion losses that will vary from one component to another. This type of problem is a statistical one and will not be dealt with here.

Before explaining the practical effect of VSWR upon peak-power capacity in microwave systems, it will be well to

CONFIDENTIAL



CONFIDENTIAL

compare the experimental data with information that can be obtained from a knowledge of the insertion losses, Q factors, and reactances of the mismatches. This will help to clarify the breakdown phenomena and will present a firm basis for the interpretation of the data. To simplify this comparison, the data was replotted (figure 37) in the form of percent of full power carrying capacity of the waveguide vs VSWR of mismatch, along with the values obtained from the measurement of the insertion losses, Q factors, and reactances of the mismatches.

To calculate the power carrying capacity using measurements of the insertion loss of the cavity, an analysis similar to that used to obtain equation (18) was employed. The only difference is that in the experimental circuit the general position of breakdown was known; this is the position where the maximum voltage was determined. The attenuation was considered to be linear with distance and the cavity input VSWR, to be 1.25. These calculations are plotted in figure 37 and are shown in table 6.

CONFIDENTIAL

CONFIDENTIAL

TABLE 6  
MEASURED AND CALCULATED DATA

Measured Percent of Power Carrying Waveguide at Atmospheric Pressure	Calculated Percent of Power Carrying Capacity of Waveguide			VSWR of One Mismatch
	Using Insertion-Loss Measurements	Using Reactance of Mismatch	Using Q Measurements	
89.0	90.5	89.0	-	1.2
77.0	79.0	78.0	-	1.4
56.0	55.0	59.0	-	2.0
28.1	25.3	27.8	-	5.0
12.2	13.5	15.5	12.5	10.0

To determine the peak power carrying capacity using the reactance of the mismatch, an understanding of the basic properties of an iris when considered as a transformer must be utilized. This is considered in detail by Montgomery\* and the necessary equations are presented in the formulae section, paragraph 4.5. Since the condition required for this report was different from that for which the equation was derived, the analysis must be extended to meet the present case. The particular arrangement used for the breakdown tests

\*See ref. 79, p. 167 and 182-186

CONFIDENTIAL

consisted of two irises so spaced as to form a cavity. The cavity input VSWR was always less than 1.50. However, since the voltage buildup in the cavity was a function only of the iris, provided that the cavity was matched and lossless conditions prevailed, equation (19) could be used as an approximation for the present case. These values are shown in table 6 and are plotted in figure 37.

Lawson and Fano\* present an analysis of a lossless, resonant cavity formed by two shunt reactances and derive an expression for the loaded  $Q$  of such a cavity. This expression is presented in the formulae section, (equation (21)) and determines  $Q$  as a function of the reactance of the iris ( $B_0$ ). Since an expression for the maximum voltage ( $N$ ) inside a cavity formed by two shunt reactances in terms of the reactance of the iris has already been determined (equation (19)) it is possible to substitute one into the other to obtain an expression for  $N$  in terms of  $B_0$ . However, because of the complex structure of equations (19) and (21), this solution is a very lengthy one. If it is assumed that  $B_0 \gg 1$ , then the solution can be reduced to that shown in equation (23).

\*See ref. 58, p. 654-657

CONFIDENTIAL

CONFIDENTIAL

For a VSWR of 10, the normalized susceptance was found to be equal to 2.13. The  $Q$  for this case was measured and substituted into equation (23). It was found that the power carrying capacity was equal to 12.5 percent of the power carrying capacity of waveguide. This is plotted in figure 36 and shown in table 6. No other points were determined using  $Q$  measurements because of the difficulty of the experimental procedure and the good correlation obtained from the other calculations.

The information contained in table 6 shows an excellent correspondance between the measured high-power data and the calculated values using low-power measurements. It must be pointed out that, the correlation obtained was much better than that which should normally be expected since the experimental and approximation errors were of the order of 10 percent. Nevertheless, it placed the experimental data on a firm basis and enabled the power carrying capacity of resonant cavities to be calculated with a good degree of accuracy.

The overall practical effect of VSWR upon power carrying capacity could then be determined. Figure 38 shows a plot of percent of waveguide power carrying capacity (full waveguide power) vs VSWR for three of the most pertinent

CONFIDENTIAL

CONFIDENTIAL

conditions that were previously discussed. One curve is for a single mismatch at the end of 10 feed of brass waveguide. Although no experimental data was taken for this condition, the theory is well known and reliable, and should be correct to within a few percent.

The other two curves represent the case of a resonant cavity formed by two properly spaced mismatches. The first of these is a theoretical curve for a lossy cavity and the second is an experimental curve taken on an actual lossy cavity. The theoretical curve was plotted assuming the following conditions: that the input VSWR to the cavity was equal to 1.25, that the mismatches were pure shunt reactances, and that the exact position of breakdown was known to be 2.35 feet from the input mismatch and 0.72 feet from the output mismatch (line attenuation = 0.054 db/per foot). These conditions are the same as those used in the experimental setup and were chosen to indicate the degree of accuracy that can be achieved by using the theoretical calculations. Figure 38 indicates a maximum error of 6 percent between the theoretical and experimental curves; this is well within the experimental and approximation errors involved for this case.

CONFIDENTIAL

CONFIDENTIAL

Between these three curves all conditions of VSWR present in a transmission line are considered. For example, the practical case of the VSWR present in a radar system can be discussed. In this case the individual mismatches are usually small and regardless of their spacing, the overall VSWR of the system is generally less than 2. Using this information, the graph indicates that regardless of which curve is chosen the difference between the power carrying capacities in the two extreme conditions is less than 10 percent. However, if greater accuracy is desired, it can be determined whether a resonant cavity exists, and, if it does, what the power carrying capacity will be in this portion of the system. In this manner the curves of figure 38 can be used to solve any problem arising out of mismatches present in a transmission line.

R. Cooper<sup>15</sup> gives information on the effect of VSWR upon peak-power breakdown. He presents data taken for three different gap sizes as the VSWR is varied from 1.7 to 5.9. Over this range of VSWR the voltage gradient necessary for breakdown remained essentially constant, which is in agreement with the data in this report. As was stated previously, the constant slope of the power-pressure curves indicated that the type of breakdown remained constant as the VSWR was varied. The fact that the voltage gradient remained

CONFIDENTIAL



CONFIDENTIAL

constant as the VSWR was varied is essentially the same thing, since if the gradient did not change, the type of breakdown remained the same.

There is another point worth mentioning with regard to the experimental data. It can be seen from figure 38 that the power capacity of a resonant cavity can be reduced to as low as 5 to 10 percent of full waveguide power by increasing the Q factor. Because of the shortage of high-power sources, this can be a very useful property. By means of a controlled test, the breakdown characteristics of components can be studied utilizing power sources with  $1/5$  to  $1/10$  the power output that would normally be required. This suggests an alternate to the necessity of using evacuating equipment to reduce the power carrying capacity and is another means of checking data obtained by means of conventional techniques.

## 10. MEASUREMENT OF THE POWER CAPACITY OF WAVEGUIDE AND COMPONENTS

### 10.1 Waveguides

#### a. Breakdown of a 1-inch x $1/2$ -inch Waveguide at Atmospheric Pressure

The standard 1-inch x  $1/2$ -inch tapered waveguide section (figure 4) was tested at various times in the course

CONFIDENTIAL

of the program to check the accuracy of the measurements. Since it was decided to classify the breakdown of components and structures by their percentage of power carrying capacity of the waveguide, it was important to establish the power carrying capacity of the waveguide and periodically check the result. The data of the tests are plotted in figure 39 in the form of  $\ln$  power vs  $\ln$  pressure curves. The fact that the data appears linear when presented in this manner indicates the breakdown power is an exponent function of pressure. The exponent for the tests varied between 2.0 and 2.1. This result agrees very well with theoretical square-law relationship between power and pressure based upon an extension of Paschen's Law that was discussed in paragraph 9.1.

The data in figure 39 is sufficiently uniform and consistent to permit an extrapolation to values of higher pressure. Thus, the lines in figure 39 have been extended to atmospheric pressure. This permits the value of the average power at breakdown for the three tests to be read directly from the curve. The peak power carrying capacity of a 1-inch x 1/2-inch waveguide at atmospheric pressure and with a matched termination is:

$$\text{peak power carrying capacity} = (\text{average power}) \times \frac{k^2}{(\text{repetition rate} \times \text{pulse width})}$$

CONFIDENTIAL

CONFIDENTIAL

when  $K = \frac{\text{peak voltage under test conditions}}{\text{peak voltage for matched conditions}}$

$$P = (\text{average power}) \times \frac{(1.035)^2}{800 \times 1.2 \times 10^{-6}}$$

The results of this calculation for the three tests are tabulated in table 7.

TABLE 7

POWER CAPACITY OF 1-INCH x 1/2-INCH WAVEGUIDE

Test date	Power capacity at atmospheric pressure (Megawatts)
October, 1952	1.43
March, 1954	1.56
February, 1956	1.39
Test conditions: 1.2 microsecond pulse width 800 pps repetition rate.	

It can be seen from table 7 that the March 1954 test results differed from the February 1956 test by 12 percent. This difference was attributed to experimental accuracy. However, since the February 1956 data was obtained using a manometer for the pressure readings whereas the other data was obtained using a relative pressure gauge, there is good reason to favor the February 1956 data. This conclusion is bolstered by the fact that this data appears to be more

CONFIDENTIAL

CONFIDENTIAL

self-consistent than either of the two remaining sets of data. For this reason the final test on 1-inch x 1/2-inch waveguide made in February of 1956 near the end of the program will be used as the standard for waveguide power carrying capacity. It should be noted that whereas the standard curve drawn on the component breakdown data curves that will be presented in the following paragraphs of this report may be either the April 1954 or the October 1952 data, depending upon when the component was tested, the percentage of waveguide power carrying capacity reported in the test for these components has been adjusted to the new standard.

b. Breakdown Tests on Cover-to-Cover Flange Joints

A test was next performed on two sections of 1-inch x 1/2-inch x .050-inch waveguide coupled together by means of a cover-to-cover flange joint. The two waveguides were aligned at the flange joint by pinning the two flanges and by taking a milling cut on the faces of the flanges to assure that they would mate flush to one another. A plot of the data obtained is given in figure 40. It was found by extrapolation of the data that the power-handling capacity was 1.35 megawatts at atmospheric pressure. This is essentially the

CONFIDENTIAL

CONFIDENTIAL

the same value as that for standard 1-inch x 1/2-inch x .050-inch waveguide. The slope of the  $\ln$  power vs  $\ln$  pressure was 2.04 which is essentially the same as for standard waveguide.

c. Breakdown Tests on the Misalignment of Cover-to-Cover Flange Joints

Since the cover-to-cover flange joint carried full waveguide power when properly aligned, it was decided to investigate the effect of flange misalignment on standard 1-inch x 1/2-inch x .050-inch waveguide with a cover-to-cover flange joint. The flanges were removed and markings placed on the edges, so that they could be misaligned set amounts in the vertical and horizontal planes.

Data for the vertical misalignment of the cover-to-cover flange joint is shown in figure 41. It can be seen that as the misalignment was increased, the slope of the curves decreased as well as the absolute power handling capacity. For a .040-inch displacement (10 percent of the waveguide height) the slope was 1.6. By extrapolation of the data to atmospheric pressure, the peak power handling capacity is reduced to 30 percent of the power carried by a properly aligned cover-to-cover flange joint.

CONFIDENTIAL

A five percent misalignment of waveguide height yielded a curve whose slope is 1.76. At one atmosphere the power handling ability was reduced to 45 percent of a properly aligned cover-to-cover flange.

The data for the misalignment of the cover flange joint in the horizontal plane is shown in figure 42. It can be seen that the slope as well as the absolute power level decreased as the misalignment was increased, but not so markedly as for the vertical plane. For a separation of .040-inch (4.5 percent of the waveguide width) the slope of the  $\ln$  power vs  $\ln$  pressure curve is 1.91. The peak power carrying capacity at atmospheric pressure was found by extrapolation of the data to be 70 percent of the power carried by a properly aligned cover flange joint.

The data on the misalignment of the cover-to-cover flange joint in both the horizontal and vertical planes is presented in figure 43. The slope of the curve is 1.67. The power handling capacity was 47 percent of a properly aligned joint's power handling capacity. This is reasonable since it would be expected that the power handling ability as well as the slope would be less than the corresponding vertical misalignment case. As is shown on the graph, the power handling capacity is the same, while the slope is less



CONFIDENTIAL

less (1.67 as compared to 1.76). Since the results of the two cases were expected to be approximately similar, the error was probably an experimental one.

d. Breakdown Tests on a Choke-to-Cover Flange Connection

Tests were conducted in the 1-inch x 1/2-inch x .050-inch waveguide size using a UG-39/U cover flange and a UG-40A/U choke flange. The dimensions of the choke flange are shown in figure 1 of the eleventh interim report. The primary function of the choke flange was to present an electrical short circuit at the broad waveguide wall over the operating range of the waveguide. A representative choke flange was chosen, and no special precaution was taken to insure the alignment of the internal dimensions of the waveguides when mating with the cover flange.

It is seen that the data curve of ln pressure vs ln power is linear and has a slope of 2.07 (figure 44). The peak power handling capacity was 1.35 megawatts at atmospheric pressure. Both the slope and the peak power handling capacity was the same as that of regular waveguide. This was expected since both depend upon the electrical continuity, which is a property of the choke-to-cover flange connection.

CONFIDENTIAL

CONFIDENTIAL

e. Breakdown Tests on a Misaligned Choke-to-Cover Flange Connection

The standard 1-inch x 1/2-inch x .050-inch waveguide with choke and cover flanges was used. Markings were placed on the edges of the flanges so that they could be misaligned predetermined amounts in the vertical and horizontal planes.

The data taken when the displacement was .020-inch in the vertical plane is shown in figure 45. The slope of the curve of  $\ln$  power vs  $\ln$  pressure is 1.96, which is essentially the same as that for a properly aligned choke-to-cover flange connection. However, the peak power handling capacity was reduced. By extrapolating the data to atmospheric pressure, it was found that this joint could carry 1.12 megawatts or 81 percent of the full waveguide power.

The data taken when the vertical displacement was .040 inch is shown in figure 46. Note that the points do not seem to indicate a linear relationship for  $\ln$  power vs  $\ln$  pressure. This was unexpected since all previous data had indicated that the peak power handling capacity and the pressure were related by an exponential function, which would produce a linear log-log plot. Because of this fact, it was decided to average the array of points so that a linear curve

CONFIDENTIAL

CONFIDENTIAL

would be obtained (figure 46). This curve indicates a slope of 1.86. By extrapolation, the power capacity was found to be 0.94 megawatt at atmospheric pressure or 68 percent of waveguide power handling capacity. As an added step, the points were replotted in figure 47. This indicated two different slopes as the pressure was varied. It was thought that this effect may be due to two different types of breakdown; that is, one due to current and one due to voltage (see figure 47). However, very little is known about the existence of this effect.

The data taken when the choke-to-cover flange connection was misaligned in the horizontal direction is shown in figures 48 and 49. From figure 48, the slope of the curve of  $\ln$  power vs  $\ln$  pressure for a horizontal displacement of .020-inch is 2.06. This value is the same as that for the aligned choke-to-cover flange connection. By extrapolation, a peak power handling capacity of 1.25 megawatts at atmospheric pressure was found. This is 90 percent of full waveguide power. The data for horizontal displacement of .040 inch is shown in figure 49. The slope of the curve of  $\ln$  power vs  $\ln$  pressure was found to be 1.93. This again is essentially the same as that for the properly

CONFIDENTIAL

CONFIDENTIAL

aligned choke-to-cover flange connection. Extrapolation to atmospheric pressure indicated a peak-power capacity of 1.06 megawatts, or 76 percent of full waveguide power.

The data gathered on the combined vertical and horizontal displacement of the choke-to-cover flange connection is presented in figures 50, 51, and 52. Figure 50 contains the results of a vertical and horizontal displacement of .020-inch. The slope of the curve of  $\ln$  power vs  $\ln$  pressure is 2.06. By extrapolation, a peak power handling capacity of 1.25 megawatts at atmospheric pressure was found. This is 90 percent of the full waveguide power. In figure 51, the data taken when vertical and horizontal displacement was .040 inch is presented. Here again the same condition was encountered as in the case of the 0.040-inch vertical displacement. This was expected, since whatever conditions existed in the vertical case alone should exist in the combined horizontal and vertical case. The data was plotted in the same manner as before. The average slope of the array of points is 1.95. The peak power handling capacity at atmospheric pressure was found by extrapolation to be 1.04 megawatts or 75 percent of full waveguide power. In figure 52, the data is shown replotted on a dual-slope basis. A comparison between figure 52 and figure 47 shows a good

CONFIDENTIAL

CONFIDENTIAL

correlation, which was expected. Here again two different types of breakdown are suggested.

Table 8 gives a comparison between the data on the vertical and horizontal misalignment for the choke-to-cover flange connection and the cover-to-cover section.

TABLE 8  
COMPARISON BETWEEN VERTICAL AND HORIZONTAL  
MISALIGNMENT

MISALIGNMENT		PERCENT OF WAVEGUIDE POWER AT ATMOSPHERIC PRESSURE	
Type	Extent	Cover-to-Cover Flange Connection	Choke-to-Cover Flange Connection
Vertical	5% b .020 inch	45%	81%
	10% b .040 inch	29%	68%
Horizontal	2.2% a .020 inch	89%	90%
	4.5% a .040 inch	70%	76%
Combined Horizontal and Vertical	5%b 2.2% a .020 inch	46%	90%
	10% b 2.2% a .040 inch	no test	75%

CONFIDENTIAL

f. Breakdown Tests on the Effect of Separation in a Choke-to-Cover Flange Connection

Tests were conducted to determine the effect of separation in a choke-to-cover flange connection because there are several microwave applications where a flange connection will have to be separated, and also to complete the overall investigation of flange connections. These tests were conducted in the 1-inch x 1/2-inch x .050-inch waveguide size. The test piece consisted of a UG-40A/U choke flange separated from a UG-39/U cover flange. Precautions were taken to line up the inside dimensions of the waveguide in order to avoid the effects due to misalignment.

Since the unit tested could not be pressurized, no curve was plotted. Up to a gap of .011 inch no breakdown occurred at a peak power of 230 kw, the maximum output from the magnetron. For spacings of 0.011 inch or larger, arcing occurred between the flanges along the outer surfaces.

g. Breakdown Tests on the Effect of Grooves and Gaps in Waveguide Walls

This investigation was significant because several high-power radar systems are now using heliarc-welded junctions, which often leave small grooves and spaces in the



CONFIDENTIAL

waveguide wall. The heliarc-welding techniques are used to save money and time when assembling complicated microwave components.

Five different heliarc-welded test sections in 1-inch x 1/2-inch x .050-inch waveguide were selected for test (see figures 54 to 58). Those illustrated represent some of the conditions that would probably occur on a production basis. These conditions were the goal, but not necessarily those which were obtained. Therefore, as a check, all test sections were cut in cross section to determine what actually existed. The curve of  $\ln$  power vs  $\ln$  pressure for a typical welded butt joint is shown in figure 54. As expected, the curve was a straight line with a slope of 1.90. The peak power carrying capacity at atmospheric pressure, as determined by extrapolation, was 0.98 megawatt or 71 percent of full waveguide power. Figure 55 shows the results for the welded butt joint having a .005 inch groove. The slope of the curve of  $\ln$  power vs  $\ln$  pressure is 1.85. The unit can carry 0.88 megawatt or 63 percent of full waveguide power at atmospheric pressure, as determined by extrapolation. The data for the welded butt joint having a .005-inch gap is shown in figure 56. The slope of the curve of  $\ln$  power vs  $\ln$  pressure is 2.09, and the peak power handling capacity is

CONFIDENTIAL

1.1 megawatts or 79 percent of full waveguide power at atmospheric pressure. A plot of the data obtained for the typical welded choke flange is shown in figure 57. The slope of the curve of  $\ln$  power vs  $\ln$  pressure is 1.90. This curve indicates that the power handling capacity is 66 percent of waveguide power. Extrapolated to atmospheric pressure, this means that the welded choke flange can carry 0.92 megawatt.

The data for the welded choke flange having a .005-inch gap is plotted in figure 58. Here again note the same type dual-slope curve as reported in paragraph 10.1e. The same technique in handling this data was used again; that is, plotting the dual-slope curve as well as an averaged single-slope curve. It is interesting to note that the slopes encountered here, 1.3 and 2.03, are essentially the same as in figure 47 (1.5 and 2.1). The average slope of the curve of  $\ln$  power vs  $\ln$  pressure is 1.80. Extrapolation to atmospheric pressure indicated a peak-power capacity of 0.78 megawatt, or 56 percent of waveguide power.

A special test section, shown in figure 1 of the twelfth interim report, was constructed to complete the tests on the effects of grooves and gaps in waveguide walls. A section of the broad waveguide wall was removed and a plate was heliarc welded in its place. No special gap was intended.

CONFIDENTIAL

CONFIDENTIAL

The gap that occurred was the normal result of this welding process. The dimensions of the removed section were made to correspond to that of standard 1-inch x 1/2-inch x .050-inch waveguide. In this manner the data could be compared directly with other test results. The peak power handling capacity at atmospheric pressure was found by extrapolation to be 1.25 megawatts or 90 percent of the full waveguide power and the slope was 2.1. This data agrees with the results presented in the eleventh interim report on the specially constructed section used to simulate gaps and grooves in waveguide walls.

In order to clarify the data on heliarc-welded test sections, the test pieces were dissected to see how well the desired dimensions were maintained during manufacture.

Figures 4, 5, 6 and 7 of the twelfth interim report show photographs of the cross section of the heliarc-welded test pieces which tend to justify the results on the basis of mechanical deficiencies such as rough surface, gaps at the juncture of the waveguides or excess drops of solder.

The information on the effects of gaps and grooves in waveguide walls, on peak power handling capacity, indicates that heliarc-welding techniques are feasible for fabrication of waveguide components. It has been shown (with the exception

CONFIDENTIAL

CONFIDENTIAL

of the choke weld having a .005-inch gap) that power handling capacities of 70 percent of the full waveguide power and higher can be realized in heliarc-welded components without resorting to special manufacturing precautions. Power-handling abilities of the order of 90 percent of the full waveguide power can be realized if special steps are taken to ensure proper alignment of mating surfaces and a reasonably smooth surface finish is maintained. Since practically all microwave components have peak power handling capacities less than 70 percent of the full waveguide power, the use of this heliarc-welding technique is permissible and will not lower the peak power handling capacity of any component. With the trend toward making radar systems lighter by using aluminum in the construction of waveguide components, the use of heliarc welding will greatly reduce the cost of such systems.

#### h. Breakdown Tests on Flexible Waveguide

Two units were tested, both 12 inches long; one with choke and cover flanges (Titeflex part No. 40198), and one with two cover flanges (Titeflex part No. 40184). These units are of the so-called convoluted and interlocking type.

Figure 59 shows the results for the two units tested. The unit with two cover flanges (No. 40184) carried slightly more power than the unit with choke and cover flanges

(No. 40198). In both instances the slope was essentially the same; that is, 1.70 for the choke-cover unit and 1.60 for the cover-cover unit. By extrapolation, it was noted that the choke-cover unit would be able to carry 42 percent of full waveguide power at atmospheric pressure or 0.58 megawatt, while the cover-cover unit had a peak power handling capacity of 0.48 megawatt or 35 percent of full waveguide power.

Figure 60 shows the results for the choke-cover unit when it was subjected to a 90- and a 180-degree twist. The slope of the two curves of  $\ln$  power vs  $\ln$  pressure is 1.7, which is the same as that for the untwisted case. The peak power handling capacity at atmospheric pressure, as determined by extrapolation, was 0.55 megawatt or 40 percent of full waveguide power for the 180-degree twist, and 0.51 megawatt or 37 percent of full waveguide power for the 90-degree twist.

Two samples of Flexaguide, 6 and 12 inches long, were obtained from Airtron for test purposes. The data is presented in figure 61. It can be seen that the slopes of the curves of  $\ln$  power vs  $\ln$  pressure are both 1.7. This is identical to the slope obtained for a similar piece of Titeflex flexible waveguide as shown in figure 59. The peak power handling capacity at atmospheric pressure was found by extrapolation to be 0.60 megawatt or 43 percent of full



CONFIDENTIAL

waveguide power for the 12-inch piece and 0.47 megawatt or 34 percent of full waveguide power for the 6-inch section. The data was essentially the same as that for the Titeflex flexible waveguide where the power handling capacity varied from 42 percent to 35 percent for the two units tested. This 10 percent difference in the two units was due essentially to the normal manufacturing tolerances. Because Airtron claimed a power handling capacity equal to that of rigid waveguide, representatives of that company were consulted to determine how they obtained their results. It was explained that Flexaguide could carry the peak power as was listed on the standard waveguide charts, which includes a safety factor of four. In addition, if higher peak power handling capacities were desired, they could be obtained by increasing the area of the waveguide and utilizing auxiliary matching structures.

Tests were made on a Technicraft Laboratories flexible waveguide assembly No. U64-65B vertebrae in standard 1-inch x 1/2-inch x .050-inch waveguide. The construction features of this type of flexible waveguide are shown in figure 9 of the twelfth interim report. This unit consisted of a series of quarter-wavelength sections separated by choke-to-cover flange joints housed in a rubber jacket. Electrical

CONFIDENTIAL



CONFIDENTIAL

continuity was maintained by means of the choke-to-cover connection even though the unit was flexed. The gaps allowed relative motion of the sections.

The results of the tests, shown in figure 53, consist of a curve with two slopes, 2.0 and 1.5. The two slopes were averaged to give a slope of 1.72 which is also shown in figure 53. The peak power handling capacity at atmospheric pressure was found, by extrapolation of the average slope curve, to be 53 percent of the full waveguide power. The appearance of the dual-slope curve was not too unexpected since the construction of the vertebrae produced choke-to-cover connection misalignments of a type that have previously resulted in a dual-slope curve.

The amount and type of misalignment varied from one quarter-wave section to the next as did the gap between them, since the sections were not held together very rigidly. Measurement of the gap indicated an average value of .022 inch. Comparison of the data on the vertebrae section with the data on the .040-inch vertical and horizontal misalignment of the choke-to-cover flange connection indicated the following.

CONFIDENTIAL

CONFIDENTIAL

for the vertebrae section - slopes of ln power vs ln pressure curve were 1.97 and 1.45

power capacity at atmospheric pressure was found to be 53 percent of waveguide power

for the .040-inch vertical and horizontal misalignment of the choke-to-cover flange connection - slopes of ln power vs ln pressure curve were 2.30 and 1.50

power capacity at atmospheric pressure was found to be 75 percent of waveguide power

It can be seen that the slopes compare very favorably while the power handling capacity differed by 22 percent. The difference in power handling capacity was reasonable since the vertebrae sections have, by virtue of their construction, gaps between mating sections.

1. Breakdown Tests on USL Cover-to-Cover Flanges for 1.122-inch x 0.497-inch Inside Diameter Waveguide

At the request of the Bureau of Ships, a flange designed and developed by the U.S. Navy Underwater Sound Laboratory, (USL) New London, Connecticut for use with RG-163/U waveguide was tested. Further information may be obtained from USL (part Nos. 38894-B and 38895-C).

CONFIDENTIAL

The RG-163/U waveguide was required to operate over the frequency range of 6275 mc to 8890 and carry very high power. It had internal dimensions identical with RG-51/U waveguide (1.122 inches x 0.497 inch) but a considerably greater wall thickness. (The outside dimensions of RG-163/U waveguide are 1.342 inches x 0.717 inch.) The use of a contact type flange was used in preference to a choke-type joint in the design because of the wide frequency band and the inherent frequency sensitivity of chokes. In addition, there was a socket-type connection between the waveguide and the flange. This design reduced the maximum amount of misalignment possible within tolerances at the face between the two flanges, as compared with the use of two UG-51/U's in a contact flange coupling since the effect of tolerances in the waveguide and hole were removed from this face. In addition, the socket type connection removed the possibility that the flange surface and waveguide were not exactly flush as might occur in the standard push-through type flange unless the completed assembly was faced off and polished.

To test the flange, two sections of RG-163/U waveguide were fabricated as shown in figure 62. At one end of the waveguide the thickness of the waveguide was reduced so that a typical push-through contact-type flange could be

CONFIDENTIAL

mounted. These sections were assembled and the VSWR of the entire assembly was carefully measured and found to be under 1.04 over the band both when aligned properly and when misaligned by .020 inch in both the E and H planes. Figure 62 also shows the complete test section assembly. The data were obtained using the standard test circuit shown in figure 5. The results of the tests are shown in figure 62, by plotting a  $\ln$  power vs  $\ln$  pressure curve. It can be seen that the piece carried considerably more power than the standard 1-inch x 1/2-inch waveguide. In addition, the slope of the curve agreed very well with the square-law relationship of 1-inch x 1/2-inch waveguide. These observations suggest that breakdown was due to the waveguide and not the flanges. This observation was further strengthened when examination of the flanges showed no signs of breakdown pitting and burning. Thus, it was decided to determine the power handling capacity of the 1.122 inch x 0.497 inch inside-diameter test piece from the data, and compare it to the calculated power handling capacity scaled from the measurement of 1-inch x 1/2-inch waveguide (refer to equation 42). The results calculated for atmospheric pressure and matched lines, are:

from measurements of 1.122-inch x 0.497-inch inside-diameter waveguide

$$P_{\text{atmospheric pressure}} = 3.2 \text{ megawatts.}$$

CONFIDENTIAL

CONFIDENTIAL

From calculations based upon 1-inch x 1/2-inch waveguide measurements:

$$P_{\text{atmospheric}} = 2.5 \text{ megawatts.}$$

These values show fair agreement. It can be seen that the measured power carrying capacity of 1.122-inch x 0.497-inch waveguide was 28 percent higher than the calculated value. This difference can be almost accounted for by the experimental error of  $\pm 9.4$  percent as analyzed in paragraph 7.4. There are two additional sources of error for this test which was not taken into account in that analysis. First, extrapolation of the power-pressure data over approximately 3:1 range of pressure from 9 inches to 30 inches of mercury will lead to significantly large errors unless the slope is very accurately determined. In addition, there is some doubt as to the exact VSWR in the test section. The results were computed on the basis of a 1.3 VSWR; if the VSWR was actually 1.15, the test results would be 2.85 megawatts at atmospheric pressure. While these arguments are not conclusive, they serve to indicate that the experimental results are not in disagreement with the predicted power carrying capacity of the 1.122-inch x 0.497-inch inside diameter waveguide. Thus, it was concluded that the USL flanges are able to carry the full power handling capacity

CONFIDENTIAL

CONFIDENTIAL

of RG-168/U waveguide but that the power handling capacity of this size waveguide is somewhat less precisely determined than would ordinarily be expected due to conflicting results.

## 10.2 Change of Direction and Polarization of Waveguides

### a. Breakdown of H-plane bends.

An analysis was made of the H-plane bend (see paragraph 4.3) which indicated a peak-power capacity of 97 percent of waveguide power with very little dependence on the radius of the bend. In order to verify this theory, a number of bends with different radius bend-angles and different methods of manufacture were tested, covering the conditions most likely to be encountered in radar applications. The results of the tests are plotted in figures 63, 64, 65a, and 65b in the usual form of ln-power vs ln-pressure curves. In order to test as many bends as possible, a limited amount of data was obtained for each test piece. The slopes of the ln-power vs ln-pressure curve were not accurately determined. However, this was not a serious handicap since there was sufficient theoretical and experimental evidence that the slope of an H-plane bend power-pressure curve similar to waveguide, follows a square law junction. A comparison of the theoretical calculations with the experimental data is

CONFIDENTIAL



CONFIDENTIAL

presented in table 9. Also included is a physical description of the H-plane bends that were tested, and the slopes of the ln-power vs ln-pressure curves. The power handling capacity of each bend relative to standard waveguide was computed for a power-pressure point at the center of the range of data.

The theoretical analysis predicted that the H-plane bend would carry 97 percent of waveguide power, regardless of the radius, while the results indicated that the bends carried from 87 to 124 percent. Although the discrepancy was somewhat large, the difference between the two results was probably due to experimental error as discussed in paragraph 7.4. It was found that the accuracy of the breakdown power measurements became very dependent on the accuracy of the pressure measurement at low pressure. Since the tests on the bends were performed at pressures between 5 and 15 inches of mercury (absolute), it can be seen by referring to figure 16 that the error due to pressure alone could approach 40 percent under extremely adverse conditions. The theory and experiment were not in disagreement within experimental accuracy. Since the bends have considerably more power handling capacity than other components in a radar system, no practical benefit could be gained by repeating the tests using the more accurate manometer as the pressure meter.

CONFIDENTIAL

CONFIDENTIAL

TABLE 9

## SUMMARY OF BREAKDOWN DATA ON H-PLANE BENDS

Description	For Data See Fig- ure	Radius (inch)	Slope	VSWR	Peak-power Capacity	
					Meas- ured	Theo- retical
1. Machined 90° H- Plane Bend	65(a)	0.125	2.4	1.03	99%	97%
2. Machined 90° H- Plane Bend	65(a)	0.250	2.2	1.03	116%	97%
3. Machined 90° H- Plane Bend	65(a)	0.375	2.2	1.09	124%	97%
4. Fabricated 45° H- Plane Bend	65(b)	0.625	1.9	1.05	98%	97%
5. Fabricated 90° H- Plane Bend	65(b)	0.625	1.7	1.04	110%	97%
6. Fabricated 180° H- Plane Bend	65(b)	0.625	1.9	1.07	90%	97%
7. Fabricated 90° H- Plane	64	1.5	2.0	-	87%	97%
8. Fabricated 90° H- Plane	63	0.3	2.0	-	94%	97%

CONFIDENTIAL

CONFIDENTIAL

However, in order to verify the conclusions of this discussion and to establish the accuracy of the manometer, one of the bends which appeared to carry more power than waveguide was retested. The particular H-plane bend chosen for retest was bend No. 3 (table 9). It was previously found that this bend carried 124 percent. The results of the tests are shown in figure 66. Note that the results are nearly equal to that expected; the bend carried about 86 percent of waveguide power. In addition, the slope of the  $\ln$ -power vs  $\ln$ -pressure curve was found to be 1.9 which agrees closely with the previous contention that the bends follow the square-law relationship between power and pressure.

b. Breakdown of E-Plane Bends

An approximate equation was obtained for the power (see equation 10, para. 4.4) capacity of an E-plane bend expressed as a percentage of waveguide power. In order to verify the validity of this result a number of E-plane bends representing the values most likely to be encountered in radar applications were tested. The results of breakdown tests on E-plane bends reported in the thirteenth and nineteenth interim reports are plotted in figures 65c, 65d, 65e, 67, 68, 69, 70 in the usual form of  $\ln$  power vs  $\ln$  pressure. An outline drawing of the waveguide switch which contains a 90-degree

CONFIDENTIAL

CONFIDENTIAL

E-plane bend is shown in figure 8 of the thirteenth interim report. The results of the test are summarized in table 10. In order to compare the results of the tests with the predicted values of peak-power capacity the information in table 10 has been plotted in figure 71 together with the theoretical curve (equation 10).

The correlation between the predicted values and the actual values are within experimental error in most cases. The other cases, in which the agreement is not so good, are attributed to mechanical defects in the test piece and limitations due to the approximate analysis.

On the basis of these tests, the universal curve in figure 71 should prove very useful in predicting the performance of E-plane bends. A deviation because of a non-coaxial voltage distribution would tend to increase the actual power capacity above the predicted value. Thus, in applying this curve to the power-handling requirements of a radar system, any deviation would be in the form of an additional safety factor.

CONFIDENTIAL

TABLE 10

## SUMMARY OF BREAKDOWN TESTS ON E-PLANE BENDS

Description	For Breakdown Data See Figure	E-Plane Bend Radius, $R_1$ (inch)	Peak-Power Capacity				Mean Circumferential Length Divided By Waveguide Wavelength
			VSWR	Meas.	Theor.	Slope	
1. Fabricated 90° E-plane Bend	65(c)	1.581	1.04	75	80	1.9	1-1/2
2. Fabricated 90° E-plane Bend	65(c)	0.784	1.04	72	64	1.8	3/4
3. Fabricated 90° E-plane Bend	65(c)	0.519	1.08	63	53	1.8	2/3
4. Machined 90° E-plane Bend	65(d)	0.125	1.05	60	20	1.9	1/4
5. Machined 90° E-plane Bend	65(d)	0.250	1.2	56	36	1.9	1/3

CONFIDENTIAL

TABLE 10 (cont)

## SUMMARY OF BREAKDOWN TESTS ON E-PLANE BENDS

Description	For Break-down Data See Figure	E-Plane Bend Radius, $R_1$ (inch)	VSWR	Peak-Power Capacity			Mean Cir- cumferen- tial Length Divided By Waveguide Wavelength
				Meas.	Theor.	Slope	
6. Machined 90° E- plane Bend	65(d)	0.375	1.11	63	46	1.9	1 1/2
7. Machined 45° E- plane Bend	65(e)	0.625	1.02	87	60	1.7	1/3
8. Machined 90° E- plane Bend	65(e)	0.625	1.02	76	60	1.7	3/4
9. Machined 180° E- plane Bend	65(e)	0.625	1.02	73	60	1.7	1-1/2
10. Wave- guide Switch 1-1/4 x 5/8 O.D. Wave- guide	67	0.490	-	41	46	2.0	3/4



CONFIDENTIAL

TABLE 10 (cont)

## SUMMARY OF BREAKDOWN TESTS ON E-PLANE BENDS

Description	For Break-down Data See Figure	E-Plane Bend Radius, $R_1$ (inch)	VSWR	Peak-Power Capacity			Mean Cir- cumferen- tial Length Divided By Waveguide Wavelength
				Meas.	Theor.	Slope	
11. Fabri- cated 90° E- plane Bend	68	1.081	-	73	74	2.0	1
12. Fabri- cated Comb. E- and H-plane Bends	69	1.050	-	70	72	2.0	1
13. 90° Cast Aluminum E-plane Bend	70	0.925	-	74	70.5	2.1	1

CONFIDENTIAL

CONFIDENTIAL

c. Breakdown Tests on a 90-Degree H-Plane Mitered Corner

A 90-degree H-plane mitered corner as shown in figure 72 was next tested. The results of the tests are plotted in the same figure. The slope of the ln-power vs ln-pressure curve is 2.1. This is identical to that for standard waveguide. The peak power handling capacity was found by extrapolation to be 84 percent of full waveguide power at atmospheric pressure. These were approximately the same breakdown characteristics as those obtained for the 90-degree H-plane bend. This was expected from the similarity of the two components. The value of 2.1 for the slope of the power-pressure curve was expected, since once again the type of breakdown was expected to remain the same as that for standard waveguide.

d. Breakdown Tests on Waveguide Twists

Several waveguide twist sections were tested. The type of twist tested (shown in figure 73a) had a twist angle of 90 degrees. However, the angle of the twist can vary for a particular application. The twist is made either by casting the waveguide or by twisting a drawn waveguide along its control axis. All the units tested were made in the latter manner. The design of the twist allowed for a smooth

CONFIDENTIAL

CONFIDENTIAL

transition in the plane of the E-field while the cross-sectional dimensions in any plane of the waveguide, were the same as those of a straight waveguide. Because of this, the VSWR's of the twists were under 1.1 in all cases.

The data on the waveguide twist sections are shown in figures 73a and 73b. The results for the twists, obtained by extrapolation to atmospheric pressure, are given in table 11.

TABLE 11

WAVEGUIDE TWIST DATA

<u>Description</u>	<u>Power Handling Capacity (megawatts)</u>	<u>Percent Waveguide Power Capacity</u>	<u>Slope</u>
90° - 7-5/8"	1.06	76%	1.3
90° - 3-1/8"	1.15	83%	2.0
90° - 2"	1.25	90%	1.6
45° - 2"	1.11	80%	1.8
90° - 2-1/2"	0.75	54%	1.7

All of the twists, except one, carried more than 80 percent of waveguide power. The exception was an indication of the reduction in power handling capacity that can be expected for a distorted test piece.

CONFIDENTIAL

### 10.3 Waveguide Couplers and Tee Junctions

#### a. Breakdown Tests of a Two-Hole Coupler

A Microline Model 136, 20 db directional coupler shown in figure 74 was selected for test. This unit employs two round holes in the common narrow wall between two parallel 1-inch x 1/2-inch waveguides.

The circuit used to measure the breakdown power of the two-hole coupler was similar to that shown in figure 5, except that an additional pressure window was placed between the test piece and the load. A plot of the data is shown in figure 74.

The two-hole coupler carried about 6 percent less power than the standard 1-inch x 1/2-inch waveguide. This difference was so small that it could be partially due to experimental error and partially due to the variation between two pieces of waveguide. In any case, it was apparent that the presence of the two holes had only a slight effect upon the power carrying capacity of the waveguide.

#### b. Breakdown Tests of Crossed-Guide Coupler

The next unit tested was a laboratory model crossed-guide directional coupler, similar to Sperry Microline Model

CONFIDENTIAL

234 directional coupler. This piece had two long, narrow slots in the common broad wall between two crossed waveguides. The coupling between the two waveguides was 31 db. A sketch of the coupler layout is shown in figure 7 of the eighth interim report.

A plot of the data for the coupler oriented with the slots transverse to the primary waveguide is shown in figure 75. The power handling capacity of this coupler was considerably less than that of the standard waveguide. Extrapolation to atmospheric pressure indicated a peak-power handling capacity of 290 kw or 21 percent of waveguide power capacity. In addition, the slope of the curve was 1.49 as compared to the value of 2.0 for the standard waveguide.

Before commenting on these results, the data obtained with the slots oriented parallel to the primary waveguide will be considered. A plot of this data is shown in figure 76. Here again the data is linear and the slope is 1.37. An extrapolation to atmospheric pressure indicated a power handling capacity of 310 kw or 22 percent of waveguide power capacity. A comparison of figures 75 and 76 shows the two curves representing the different orientations are nearly parallel. The coupler can carry about 10 percent more

CONFIDENTIAL

CONFIDENTIAL

power with the slots parallel to the primary waveguide. This was not unexpected, since the current transverse to the slot is less when the slot is parallel to the axis of the primary waveguide.

c. Breakdown Tests of Schwinger Coupler

A Schwinger coupler, tested to determine its power handling capacity, was a laboratory model in 1-1/4 inch x 5/8 inch waveguide. The Schwinger coupler features two parallel waveguides with the broad wall of one in contact with the narrow wall of the other. This arrangement and the pertinent dimensions are shown in figure 10 of the eighth interim report. Coupling is obtained using two long, narrow slots in the common wall, cut parallel to the axes of the waveguides.

A plot of the data for the coupler oriented with the slots in the broad wall of the primary waveguide is shown in figure 77. It can be seen that the slope is essentially constant at a value of 1.42, and an extrapolation to atmospheric pressure indicated a peak-power handling capacity of 430 kw or 21 percent of standard waveguide power. The power handling capacity of this size waveguide under these conditions was calculated from equation 41 to be 2.1 megawatts.

CONFIDENTIAL



CONFIDENTIAL

Also plotted on the same graph is a theoretical curve for the breakdown power of a 1-1/4 inch x 5/8 inch waveguide. This curve was obtained by extrapolating the data for a 1 inch x 1/2 inch waveguide on the basis of the ratio between waveguide wavelength and internal dimensions.

A plot of the data for the coupler oriented with the slots in the narrow wall of the primary waveguide is shown in figure 78. This curve has a constant slope of 2.05 over most of the range. This is very nearly the same as that of the standard waveguide. Extrapolation of the data to atmospheric pressure indicated a peak power handling capacity of 1.2 megawatts or 57 percent of waveguide power capacity.

#### d. Breakdown Tests on a Branch-Guide Coupler

A branch-guide coupler was chosen as the next unit in the series of breakdown tests of directional couplers. The particular model used was a laboratory model having 1-inch x 1/2-inch x .050-inch waveguide and having a coupling of 13 db. A sketch of the coupler showing the significant electrical dimensions is given in figure 1 of the ninth interim report.

A plot of the data is given in figure 79. The data indicated a power handling capacity of 400 kw at

CONFIDENTIAL

CONFIDENTIAL

atmospheric pressure or 29 percent of standard waveguide power handling capacity. It is seen that the  $\ln$ -power vs  $\ln$  pressure curve is linear and has a slope of 1.7. This behavior is different from couplers employing slots in the broad or narrow wall. Since the branch-guide structure is similar to a set of E-plane junctions, the behavior of E-plane tee-junctions will be considered before this data is analyzed.

e. Breakdown Tests of E-Plane Tee

An E-plane tee composed of 1 inch x 1/2 inch waveguide was the next component tested for breakdown. A sketch of the unit employed, Sperry Microline Model 165A, is shown in figure 4 of the ninth interim report. The broad wall of the waveguide has an opening to provide for the E-plane arm of the tee.

In operation, the tee is analogous to a series circuit. The power splits between the E arm and the side arm in proportion to the impedances of the two arms, neglecting the junction reactance. For the unit tested the impedances were equal, and so the power division was approximately equal.

CONFIDENTIAL

CONFIDENTIAL

Power is applied to one side arm while the other arms are terminated in matched impedances. A plot of the data obtained is given in figure 80. Although the curve was linear, considerable difficulty was encountered in obtaining the data because breakdown occurred at a value much below the power handling capacity of the waveguide. This means that the increased voltage due to the power reflected from the spark was not sufficient to cause the pressure window to break down. Thus, the data represents a true probability run which required care and time for both test and analysis in order to determine the true breakdown point. The method used is described in the seventh interim report. The intercept of zero probability on a plot of breakdown probability vs power was determined. The almost perfect linearity of the curve in figure 80 justified this approach.

The data for the E-plane tee indicated a power handling capacity of 85 kw or 6 percent of waveguide power carrying capacity at atmospheric pressure. The curve for breakdown of the branch-guide coupler shown in figure 79 is seen to be midway between those for standard waveguide and for the E-plane tee. This is reasonable since the branch-guide structure is basically a combination of two E-plane junctions, each of which represents a smaller discontinuity than the E-plane tee.

CONFIDENTIAL

CONFIDENTIAL

f. Breakdown Tests of H-Plane Tee

An H-plane tee fabricated from 1-inch x 1/2-inch waveguide was the next component tested for breakdown. A sketch of the unit, Sperry Microline Model 166A, is shown in figure 6 of the ninth interim report. The narrow wall of the waveguide had an opening to provide for the H-plane arm of the tee, thereby introducing a discontinuity. There were no other discontinuities in the waveguide.

In operation, this tee is analogous to a shunt circuit. The power division between the H arm and the side arm is inversely proportional to the two impedances, neglecting the junction reactance. For the unit tested the impedances were equal, so that there was an equal power division.

The circuit used in the breakdown tests is given in figure 5. Power was applied on one side arm, with the other arms terminated in matched impedances. A plot of the data is given in figure 81. Note that the power handling capacity was close to that of standard 1-inch x 1/2-inch waveguide and that the slope of the  $\ln$ -power vs  $\ln$ -pressure curve is very nearly 2. The data indicated that the shunt tee could carry 80 percent of the waveguide power. Extrapolated to atmospheric pressure, this means that the tee is capable of transmitting one megawatt.

CONFIDENTIAL

## g. Breakdown Tests of Magic Tee

A magic tee composed of 1-inch x 1/2-inch waveguide was tested for breakdown. A sketch of the unit employed, Sperry Microline Model 406, is shown in figure 8 of the ninth interim report. A matching structure was introduced at the center of the junction serving to reduce the waveguide inner dimensions as well as to distort the electromagnetic field pattern. Otherwise the magic tee was a combination of the E- and H-plane tees.

In operation this tee is analogous to a series branch and a shunt branch located at the same point on the line. For the case of the matched tee, the power applied to either side arm is evenly divided between the E and H arms, with no power reaching the other side arm. In addition, power applied to either the E or H arms is evenly divided between the two side arms with no power reaching the opposite arm. The unit tested was matched so that these conditions were obtained.

Power was applied to one side arm, with the other arms terminated in matched impedances. The data plotted in figure 82 indicates a power handling capacity similar to that of the E-plane tee. This is reasonable, inasmuch as the



CONFIDENTIAL

construction of this tee was similar to a combination of the E- and H-plane tees. Since the E-plane tee carries considerably less power than the H-plane tee, one would expect a combination of the two to behave like the E-plane tee. Extrapolation of the data to atmospheric pressure indicated that the magic tee breakdown occurred at 110-kw peak power, which is about eight percent of the waveguide power carrying capacity.

h. Breakdown Test on an E-Plane Hybrid Ring

A 1-inch x 1/2-inch x .050-inch E-plane hybrid ring, is shown in figure 14 of the twelfth interim report, was tested. The operation of the hybrid ring is similar to that of a magic tee. From the data plotted in figure 83, the slope of the ln-power vs ln-pressure curve is 1.6. By extrapolation, the peak power handling capacity at atmospheric pressure was found to be 0.25 megawatt or 19 percent of the full waveguide power carrying capacity.

Since the hybrid ring used for the tests was essentially a set of E-plane tees, a comparison with the results for the E-plane tee, which carried 7 percent of waveguide power, is pertinent. The difference in the VSWR between the two units accounted for the 12 percent difference in peak-power handling capacity.

CONFIDENTIAL



#### 10.4 Waveguide Rotary Joints

##### a. Breakdown Tests on a Rectangular-to-Circular Waveguide Rotary Joint

The test piece was a  $TM_{01}$  mode rectangular-to-circular waveguide rotary joint. Figure 19 and 20 of the twelfth interim report shows a sketch of the pertinent dimensions of the joint and a curve of VSWR vs frequency. At the test frequency, the VSWR was 1.09.

The joint consisted of two individual half sections, each containing a rectangular-to-circular waveguide transition ( $TE_{10}$  to  $TM_{01}$ ). Each half section also contained a filter ring and absorbing slots to eliminate any  $TE_{11}$  mode which might be generated by the transition. The  $TE_{11}$  wave had to be eliminated because it was capable of propagating in the circular waveguide and impairing the performance of the joint. Due to the addition of the filter ring, an inductive iris had to be added to provide a match at the transition and thereby keep the VSWR relatively low. Because of the geometry of the rotary joint, the use of the photocell to indicate breakdown was greatly limited and much time and care had to be used in obtaining the data. Each point had to be checked several times to make sure of its reliability.

CONFIDENTIAL

As shown in figure 84, a plot of the data obtained, an entirely different type of phenomena was observed. On plotting the ln-power vs ln-pressure relationship, two distinct constant-slope curves resulted. Each curve had the same slope, which is essentially that of standard waveguide, but the curves were displaced from one another. Since these points cannot be averaged to give a single curve, as done previously, the performance at atmospheric pressure was obtained by extending the upper, or high-power, portion of the data. Thus, the peak power handling capacity at atmospheric pressure was found to be 14 percent of the full waveguide power or 0.193 megawatt.

b. Breakdown Tests on a Ridge-Waveguide Coaxial-Line Rotary Joint

A 1-1/4-inch x 5/8-inch x .064-inch ridge-waveguide coaxial-line rotary joint (see figure 2 of the fifteenth interim report) was tested to obtain some comparative data on rotary joints. Basically, the joint consisted of a taper from rectangular to ridge waveguide and a doorknob transition from the ridge to the coaxial line. Because this joint used ridge waveguide, it had an inherent bandwidth of the order of 15 percent, with a VSWR of less than 1.1 over the band.

CONFIDENTIAL

CONFIDENTIAL

The data are plotted in figure 85 in the form of a curve of  $\ln$ -power vs  $\ln$ -pressure. The slope of this curve was 2.0, which is essentially the same as that for standard waveguide. The peak power handling capacity at atmospheric pressure was 15 percent of full waveguide power. The power handling capacity of 1-1/4-inch x 5/8-inch x .064-inch waveguide, computed by using standard scaling techniques for the frequency, cross-sectional area, and pulse width was found to be 2.5 megawatts. (See paragraph 4.7.)

The peak power handling capacity of the ridge waveguide used was determined to be approximately 39 percent of the peak power handling capacity of rectangular waveguide by using the equations derived in paragraph 4.6. Since the rotary joint carried only 15 percent of waveguide power, or 380-kw peak power, the ridge-waveguide portion did not cause the breakdown. A calculation of the power carrying capacity of the coaxial portion of the rotary joint showed it to be approximately 490 kw. Since this was not much greater than the breakdown power of the joint, some consideration was given to the fact that a standing wave may have existed in the coaxial region between the two doorknobs, even though the input VSWR to the rotary joint was less than 1.1. This was possible because the tests were conducted at the high-frequency end of the bandwidth and the two doorknob sections

CONFIDENTIAL

CONFIDENTIAL

of the joint may have been so spaced as to cause a slight mismatch in the coaxial line. If a VSWR of 1.25 did exist in the coaxial region, the breakdown power of this region would be reduced to 380 kw which was the measured power. Thus, it is quite possible that breakdown occurred in the coaxial-line section. On the other hand, it is also possible that breakdown occurred in the region of the doorknob since this was a region of increased field gradients and is often the weak link in a rotary joint.

c. Breakdown Tests on a Dual-Feed Coaxial-Line Rotary Joint

A dual-feed coaxial-line rotary joint for 1-1/4-inch x 5/8-inch x .064-inch waveguide was tested. It was designed for operation over a 20-percent bandwidth with a VSWR less than 1.15. The joint was composed of several basic structures. At the inputs of the joint, the main waveguide was divided into a pair of reduced-height waveguides by a septated series junction. The septated waveguide sections contained a pair of double quarter-wave step transformers for matching the coaxial-line and waveguide impedances. A pair of reduced-height waveguides were used in parallel to feed opposite sides of the coaxial line. The transition from the coaxial to the waveguide mode was accomplished by a cone-shaped doorknob

CONFIDENTIAL

CONFIDENTIAL

transition, and in addition there was a non-contact choke joint for the inner and outer conductors of the coaxial line. The references<sup>25,99</sup> contain pictures and a detailed account of the electrical structure of the joint. The data shown in figure 86 is a ln-power vs ln-pressure curve. The slope of the curve is 1.8 which is approximately the same as that for waveguide. The peak power handling capacity at atmospheric pressure was found to be 17 percent of full waveguide power or 0.42 megawatt. From a consideration of the basic structures of the joint it appears that breakdown occurred in the coaxial line or the transition.

#### 10.5 Miscellaneous Components

##### a. Breakdown Tests on Sections Containing Hemispherical Bumps

The hemispherical bump section was suggested by Wheeler Laboratories<sup>(20)</sup> for the purpose of standardizing the breakdown tests made in various laboratories throughout the country. Wheeler Laboratories claim that the bump section will breakdown at one-ninth of standard waveguide power and that the dimension of the hemisphere is not critical. The hemispherical bump or spark gap was tested to investigate the effect of the bump radius on breakdown and the linearity of the power-

CONFIDENTIAL

CONFIDENTIAL

pressure relationship over a different and larger range of pressures than was previously encountered.

The test piece was a standard 1-inch x 1/2-inch x .050-inch waveguide with the hemispherical bumps inserted as shown in figure 87. The results of the tests on a .050-inch, a 0.100-inch and a 0.150-inch bump are shown in figure 87. It can be seen that the slopes of the three curves are essentially constant at approximately 1.7 and the power carrying ability decreased as the bump radius was increased. By extrapolation to atmospheric pressure, the results for the bumps are as follows:

<u>Bump Radius</u>	<u>Power Carrying Capacity</u>	<u>Waveguide Power</u>
.050 inch	0.20 MW	14.4%
0.100 inch	0.18 MW	13%
0.150 inch	0.135 MW	9.7%

Thus, the information reported by Wheeler Laboratories, that a section containing a 0.100-inch radius bump will carry one-ninth or 11 percent of the full waveguide power, has been reasonably verified.

Wheeler Laboratories' statement that this type of bump section would make an excellent spark gap to use as a standard for comparing data taken by various individuals



CONFIDENTIAL

throughout the country, seems plausible. As they reported, the spark-gap breakdown is at a comparatively low power level. It is easily matched and small variations in the dimensions of the bump do not have a pronounced effect upon the peak power carrying capacity of the unit.

b. Breakdown Tests on a Waveguide Switch

Tests were performed on the mechanically rotated waveguide switch shown in figure 12 of the twelfth interim report. As shown in the drawing, the switch consisted of a rotor and contained a 90-degree E-plane bend which was separated from the stator by a nominal .003-inch gap. A set of choke slots were machined into the stator to increase the peak power carrying capacity of decreasing the effect of the gap. The switch used standard 1-1/4-inch x 5/8-inch x .064-inch waveguide. The temperature of the switch was held constant and independent of the load temperature because trial runs indicated that switch heating affected results. This effect was probably caused by changes in the width of the gap between the stator and rotor resulting from unequal heating of the two parts. The data is plotted in figure 67 as a ln-power vs ln-pressure curve. The slope of the curve is 1.93 and the peak power handling capacity was found by extrapolation to be 1.05 megawatts or 42 percent of full waveguide

CONFIDENTIAL

CONFIDENTIAL

power at atmospheric pressure. By examining the construction of the waveguide switch and taking into account the discussion of the effect of gaps in paragraph 10.1, the breakdown of the switch was attributed to the E-plane bend.

c. Breakdown Tests on an Antenna Assembly

The antenna assembly shown in figure 22 of the twelfth interim report was selected for breakdown power tests. Basically the unit consisted of a waveguide section twisted 90 degrees, a matching screw and iris, and a transition from rectangular-to-circular waveguide. A solid Teflon cylinder was mounted in the circular waveguide to enable the waveguide to be pressurized and also to protect the waveguide from the elements. The antenna itself consisted of a parabolic reflector, to ensure a good match at the input to the antenna assembly (since this was how the antenna assembly was originally matched). The VSWR at the test frequency (9375 mc) was 1.10.

A ln-power vs ln-pressure curve was not plotted for this component since the unit could not be evacuated because it was an experimental model and had several air holes in the solder joints. Here again the point of onset stress was difficult to obtain for the geometry of the unit made it

CONFIDENTIAL

difficult to detect breakdown with the photocell. The test data indicated that the antenna assembly would carry 0.224 megawatt at atmospheric pressure or 16 percent of standard waveguide power carrying capacity.

The construction of the antenna assembly (figure 22 of the twelfth interim report) indicated that the weakest point, insofar as peak power carrying capacity is concerned, was the matching screw. Comparing the data on the screw, (inserted .060 inch into the waveguide) with that for a .050-inch bump radius the following was obtained:

1/4-40 screw inserted  
.060 inch

the power carrying capacity  
was 0.224 megawatt at  
atmospheric pressure

.050-inch radius  
hemisphere

had a power carrying capacity  
of 0.20 megawatt at atmos-  
pheric pressure

It is seen that the data compares favorably.

#### a: Breakdown Tests on a Longitudinal Serrated Choke

Since it was necessary to use a longitudinal choke in the construction of certain microwave components (such as Transvar rotational joints and Foster-Scanner phase shifters), measurements were made on a serrated longitudinal choke. Figure 24 of the twelfth interim report is a sketch of the unit tested together with the dimensional variations used.

CONFIDENTIAL

A ln-power vs ln-pressure relationship was not plotted because the test unit could not be pressurized. Therefore, the tests were performed at atmospheric pressure. The data showed that the serrated choke test unit had a power handling ability greater than 0.230 megawatt which remained unchanged for all the dimensional variations listed in figure 24 of the twelfth interim report.

e. Breakdown Tests on a Coaxial-Line-to-Waveguide Adapter

The next unit tested was a 1-inch x 1/2-inch x .050-inch coaxial-line to waveguide adapter (figure 6 of the fifteenth interim report). The diameter of the ball probe, its position with respect to the bottom wall of the waveguide, and the spacing of the shorting plate with respect to the centerline of the coaxial line determined the VSWR and the bandwidth of the unit. The three dimensions shown in the figure are those which have been found to give optimum bandwidth and VSWR. The VSWR of this adapter, when terminated with the load used during the test was 1.15.

The test circuit used to measure breakdown was basically the same as that used in previous tests and is shown in figure 5. The one difference in the circuit for this test was that the dummy load was in the coaxial line and was not isolated from the test piece because of the

CONFIDENTIAL

CONFIDENTIAL

difficulty involved in designing a coaxial pressure window. However, the peak power rating of the RG-18/U cable was sufficiently high to insure that breakdown did not occur in this unit. It is interesting to note that because the adapter carried very little power a general breakdown did not occur. Instead, the arc-over was intermittent and a statistical approach has been used to determine the point of onset stress or zero probability of breakdown.

The data are plotted in figure 89 in the form of a curve of  $\ln$ -power vs  $\ln$ -pressure whose slope is 1.5. The power carrying capacity at atmospheric pressure was 4.3 percent of full waveguide power.

The data obtained on the coaxial-line to waveguide adapter indicated a peak power carrying capacity of 60 kw at atmospheric pressure. The peak power carrying capacity of the coaxial section of the adapter, calculated by using the standard equation for coaxial lines, was found to be 160 kw. The RG-18/U cable used for the termination had a peak power carrying capacity of at least 450 kw. Measurements were made on the VSWR. They indicated that the maximum reduction in power carrying capacity of the coaxial portion of the adapter or of the cable due to the VSWR was approximately

CONFIDENTIAL



CONFIDENTIAL

25 percent. Thus, it is reasonable to assume that the breakdown occurred because of the presence of the ball probe in the waveguide.

#### f. Breakdown Tests of High-Power Loads

The high-power dummy load, tested was a Sperry Microline product (Model 400), having a 1-inch x 1/2-inch waveguide load. This employed a lossy-wall composed of a mixture of carbon and cement to absorb the microwave energy. The currents which normally flow in the walls cause a heat loss in the carbon and the incident power is thus dissipated.

As shown in figure 88, the inner dimensions of the waveguide were essentially unaltered in the high-power region of the load. There was a slight disturbance of the cross-section because the porous nature of the lossy material resulted in a non-uniform wall surface. However, breakdown still occurred in a section which did not differ significantly from the 0.900-inch x 0.400-inch inner dimension (I.D.) of the normal waveguide.

The test circuit was as shown in figure 5 except that the dummy load was now the test piece. The data was plotted (figure 90). The slope of the curve varied between a value of 2.0 at pressures of the order of 1/5 atmosphere

CONFIDENTIAL



CONFIDENTIAL

and 1.0 in the region of  $1/2$  atmosphere. This result differed considerably from the earlier constant slope curves obtained using a standard waveguide as the test piece. In those tests the slope was essentially constant at a value of 2.0 for the same pressure range. Before discussing the reason for this difference, the results of additional tests on high-power loads will be reported.

A  $1-1/4$ -inch x  $5/8$ -inch waveguide dummy load, Sperry Microline Model 242, was tested. This unit is the same as the Model 400 except that the waveguide size is larger. The test circuit was the same as above except that a tapered section was introduced between the load and the evacuating adapter. Tests were made using photographic paper to establish conclusively that breakdown occurred at the load rather than the taper.

The initial breakdown power vs pressure data for the  $1-1/4$ -inch x  $5/8$ -inch dummy load was very erratic. However, by meticulous care and great attention to experimental technique consistent data was finally obtained. The results are shown in figure 91.

A comparison of figures 90 and 91 shows that at the higher values of pressure the power handling capacity of the  $1-1/4$ -inch x  $5/8$ -inch load was the same as for the 1-inch

CONFIDENTIAL

CONFIDENTIAL

x 1/2-inch load. In addition, the slope of the two curves was essentially the same so that an extrapolation to higher values of pressure would indicate the same power handling capacity for both loads. In particular, an extrapolation to atmospheric pressure indicated that the loads would carry 340 kw at a pulse width of 2.35 microseconds and a repetition rate of 400 pulses per second or the value for the 1-inch x 1/2-inch waveguide under these conditions was 1.1 megawatt. This indicated that the load could carry 31 percent of the full waveguide power under these conditions of operation.

A 1-1/4-inch x 5/8-inch x .064-inch waveguide dummy load was tested to provide more information on existing dummy loads. A load of a new design was utilized (figure 92). Basically, it consisted of several slots milled into the two broad walls of the waveguide and filled with a lossy material. The milled slots were tapered to improve the match, and a VSWR under 1.1 over a 12 percent frequency range was achieved. It was found that the performance was a function of the temperature of the load; therefore, data was taken for both cooled and uncooled conditions. The data on the uncooled load was taken in conjunction with a waveguide switch. However, since other tests on the switch alone had indicated that it would carry twice as much power as the load, it has

CONFIDENTIAL

CONFIDENTIAL

been reasoned that the load must have been the unit that caused the breakdown. A curve of  $\ln$ -power vs  $\ln$ -pressure (figure 92) shows that the curve for the cooled load had a slope of 2.0, which is essentially the same as that for standard waveguide, while the uncooled load had a slope of 1.4. The power handling capacity at atmospheric pressure was found by extrapolation to be 50 percent of full waveguide power for the cooled dummy load and 23 percent of waveguide power for the uncooled load. As before, the power capacity of standard 1-1/4-inch x 5/8-inch x .064-inch waveguide was scaled from the X-band data and found to be 2.5 megawatts.

Some comments are now in order regarding the shape of the  $\ln$  power vs  $\ln$  pressure curves for the high-power loads. As previously noted, the slope of these curves fell off from a value of 2 to a value of 1 as the power was increased. This probably occurred because the temperature of the air within the load was raised by the heat developed in the lossy material. Since the pressure within the load was kept constant by the evacuation system, this means that the gas density was reduced. This reduction lowered the power handling capacity by increasing the mean-free path of the electron, an effect similar to that caused by a reduction of pressure. One would expect this effect to be more pronounced at the higher power levels where more heat is generated. The curves show this to be true.

CONFIDENTIAL

This analysis also explains the erratic data which was originally obtained with the 1-1/4-inch x 5/8-inch load. In the initial tests, breakdown occurred under transient conditions before the temperature and pressure were stabilized. The later, and more consistent, tests involved a more painstaking approach so that there was sufficient time for equilibrium to be obtained.

g. Breakdown Tests on a Waveguide Step Transformer

A 1-1/4-inch x 5/8-inch-to-1-inch x 1/2-inch waveguide step transformer (figure 93) was tested to provide information on step discontinuities in waveguide. The transformer consisted of a set of four steps, spaced a quarter wavelength apart. This transformed the 1-1/4-inch x 5/8-inch waveguide cross section to a 1-inch x 1/2-inch waveguide cross section. Since each step presented only a small discontinuity and since the steps were spaced so that the multiple reflections cancelled each other, the transformer had a VSWR under 1.05 over the frequency range from 8400 mc to 11,000 mc.

The data was plotted (figure 93) and the curve of ln-power vs ln-pressure had a slope of 2.1, which is the same as for standard waveguide. The peak power handling capacity

at atmospheric pressure, referred to 1-inch x 1/2-inch waveguide, was 1.15 megawatts or 83 percent of full waveguide power.

h. Breakdown and High Power Performance Tests on an Absorption-Type Ferrite Isolator

An absorption-type ferrite isolator used in the building-block phase of the contract to isolate the magnetron from large mismatches was tested to evaluate its performance. The isolator is a device that transmits energy from a generator to a load with little attenuation and attenuates rapidly the energy reflected from the load towards the generator. Thus, large mismatches on the load side of the isolator do not affect the operation of the generator. The particular unit tested was the Litton Industries Model X20L for 1-inch x 1/2-inch waveguide as shown in figure 94. This model utilizes a transverse permanent magnetic field that is applied to a ferrite strip cemented to the waveguide wall; it operates on the basis of the resonant absorption principle of ferrite materials at microwave frequencies. The low power VSWR of the unit at 9375 mc was 1.10 in both the forward and reverse directions and high-power isolation measurements indicated that the unit would provide more than 17 db isolation at all power levels.

CONFIDENTIAL

The breakdown data are plotted as a ln-power vs ln-pressure curve (figure 94). Note that the slope of the breakdown power vs pressure curve varied from a value of 1.4 at pressures of the order of  $1/3$  atmosphere (ln pressure = 2.3) to 0.4 in the region of 1 atmosphere (ln pressure = 3.4). This result differs considerably from the constant slope curves obtained for most of the components tested previously. The change in the slope of the power-pressure curve was attributed to the temperature rise in the component at high-power levels similar to the effect noted for the dummy loads (see paragraph 10.5f). Refer to sixteenth and seventeenth interim reports. The data indicates that the isolator carried 170 kilowatts (peak power) at atmospheric pressure for a pulse width of 1.2 microseconds and a repetition rate of 800 pulses per second, or 12 percent of full waveguide power.

Since this was not sufficient, a large (1-1/4-inch x 5/8-inch) X-band isolator was used for increased power handling capacity.

The unit tested is (see figure 95) a product of the Cascade Research Corporation and is designated as Uniline Model HL86-96. It is similar in design and operates on the same principle as the Litton Industries Model X20L unit.

CONFIDENTIAL



CONFIDENTIAL

The manufacturer claims that it can carry more power because of the larger waveguide size. At a frequency of 9375 mc, the VSWR of the HL86-96 unit was measured and found to be 1.03 in the forward direction and 1.09 in the reverse direction. From information reported by the manufacturer, the forward attenuation is 0.5 db and the reverse attenuation is more than 9 db.

The data, shown plotted in figure 95, is a  $\ln$ -power vs  $\ln$ -pressure curve whose slope varies from a value of 2.1 at pressures in the order of  $1/4$  atmosphere ( $\ln$  pressure = 2.0) to 1 in the region of  $4/10$  atmosphere ( $\ln$  pressure = 2.5). A similar variation in slope was observed in the tests on the Litton Industries Model X20L isolator (see figure 94). The slopes of the curves for both components differ considerably from the constant-slope curves obtained for most components tested. The dotted line in figure 95 represents a reasonable extrapolation of the data (under the circumstances) to atmospheric pressure and indicates that the HL86-96 isolator is capable of carrying 310 kw or 12 percent of waveguide power for a 1.2-microsecond pulse width and an 800-pulse-per-second repetition rate.

CONFIDENTIAL

CONFIDENTIAL

#### 10.6 Comparison of Data Taken in X-, C-, S-, and Large S-Band Components

In order to meet the specifications of C- and S-band radar systems, high-power breakdown measurements were made on several components in these waveguide sizes. This system testing was done under other contracts. However, since the information obtained from these tests presented an opportunity to check some of the data obtained under this contract and, also, since it helped to justify the use of scaling techniques, the data obtained in the four waveguide sizes are compared in this report.

Basically, the same test circuit and measurement techniques employed in X band were also used for the C- and the S-band tests (figure 11 of the fifteenth interim report). The C-band circuit consisted of a power source to supply the pulsed r-f power, a set of pressure windows to enable the pressure in the test section to be varied independently of the rest of the system, a viewing bend, a photocell and electronic counter to detect breakdown, and a water load and thermocouple to measure power. The S-band circuit was the same except that a directional coupler and power bridge calibrated against a water load was used to measure the power. The r-f power level was varied at the source since tests

CONFIDENTIAL

CONFIDENTIAL

indicated only a minor deterioration of the pulse width and shape as the power level was varied. Since the equipment and test conditions were not as refined as the X-band tests, the probable error in the tests was estimated to be 15 percent.

Radioactive cobalt was used in all tests to reduce the waiting time and improve the accuracy. The test data were taken by keeping the power constant and varying the pressure until breakdown occurred. This information was plotted as  $\ln$ -power vs  $\ln$ -pressure, and in all cases a straight line resulted. This indicated that the power-pressure relationship is a power function, which checks with the X-band information and provides a firm basis for the interpretation of the data.

In table 12, the data on the components are compared on the basis of both percentage of full waveguide power at atmospheric pressure and the slope of the curve of  $\ln$ -power vs  $\ln$ -pressure. The slope of the power-pressure curve is given in table 12 since it presents a means of double-checking the data. An analysis of the method used to scale the power carrying capacity of waveguide is presented in paragraph 4.7. A discussion of the assumptions used in determining the pulse-width and repetition-rate scale factors is given in the fifteenth interim report.

CONFIDENTIAL

CONFIDENTIAL

TABLE 1.2

COMPARISON OF BREAKDOWN DATA IN VARIOUS FREQUENCY BANDS

Component	X BAND (1" x $\frac{1}{2}$ " x .050")	C BAND (2" x 1" x .064")	S BAND (3" x 1- $\frac{1}{2}$ " x .080")	LARGE S BAND (3.560" x 1.860" x .080")
Doorknob type coaxial- line rotary joint	15 percent of swp* 2.0 slope (ridge waveguide)	6 percent of swp* 1.6 slope (rectangu- lar wave- guide)		6 percent of swp* 1.7 slope (rectangular waveguide)
Vertabrae type flexible waveguide	54 percent of swp* dual-slope curve resulted in aver- age slope of 1.8 (twelfth interim rpt.)	18 percent of swp* 1.1 slope	20 percent of swp* 1.3 slope	
E-Plane- junction hybrid ring	19 percent of swp* 1.6 slope (twelfth interim rpt.)	17 percent of swp* 1.8 slope		
Moreno type direc- tional coupler	(31 db) 25 percent of swp* 1.4 slope (eighth interim rpt.)	(40 db) 23 percent of swp* 1.6 slope		
Dielectric type phase shifter		12 percent of swp* no curve obtained	14 percent of swp* 1.6 slope	

\*Standard waveguide power

CONFIDENTIAL

CONFIDENTIAL

The information in table 12 represents a practical engineering comparison and should not be considered as a controlled laboratory experiment. When viewed in this light the information is most encouraging. A detailed analysis of the corresponding components in the various size waveguides is given in the fifteenth interim report.

## 11. BUILDING BLOCK INVESTIGATION

### 11.1 Introduction

The investigation of the breakdown of the microwave components reported in the previous section has suggested an interesting fact. Components of widely varying functions but with similarities in physical structures showed close agreement in their high-power breakdown behavior. This fact suggested that an investigation of the basic microwave structures from which components are synthesized might be useful to microwave engineers for optimizing the high-power performance of existing components and designing new components. The data on several basic microwave structures will now be presented.

The same test techniques used in the components test were again utilized. The test circuit is shown in figure 5. It is basically the same as that used for most of

CONFIDENTIAL

CONFIDENTIAL

the previous component testing except that the HL86-96 ferrite isolator was inserted in the pressurized portion of the circuit in order to isolate the magnetron from excessive mismatches developed by the test piece.

## 11.2 Breakdown Data on Waveguide Iris

### a. General

The first structure investigated was the waveguide iris. This structure is often used on waveguide transmission lines for matching purposes.

The effect of an iris in waveguide has been discussed by several authors\* in terms of an equivalent circuit consisting of lumped constant parameters. If the iris is thin, the equivalent circuit will consist of a susceptance shunted across the waveguide at the point of the discontinuity. The magnitude of the susceptance will change with frequency, so that the analysis will be rigorously correct for a single frequency, or approximately correct for a small frequency band.

The iris plate is usually placed perpendicular to the axis of the waveguide. If the edges of the iris opening are parallel to the electric field of the dominant mode, the

\*See ref. 69, p. 217 et. seq. and ref. 81, p. 142 et. seq.



equivalent circuit is an inductive reactance shunted across the waveguide. If the edges are perpendicular, the equivalent circuit is a capacitive shunt reactance. The irises thus described are referred to as inductive and capacitive irises respectively.

Several possible iris designs are shown in figure 96. Note that the aperture can take several geometric shapes, depending upon the portion of the cross-sectional area occupied by the iris. The symmetrical inductive and capacitive irises reduce the waveguide opening in the a and b dimensions to a' and b' respectively (figures 96a and 96b). The asymmetrical inductive and capacitive irises do likewise, but extend into the waveguide from only one side (figures 96c and 96d).

#### b. Inductive Irises

Data on the symmetrical inductive iris are shown in figures 97 and 98.

The range of discontinuities tested encompasses the range normally encountered in radar design problems. All of the curves are straight lines with slopes varying between 2.1 and 2.4. Figure 97 contains data on variation of breakdown power with iris opening (a') for a series of 1/32-inch

CONFIDENTIAL

thick symmetrical inductive irises. Figure 98 also contains data on iris opening, but in this case the thickness is  $1/64$  inch.

Table 13 shows the results of the tests on breakdown power vs iris opening. The first column lists the iris dimensions; the second column the measured VSWR of the iris at low power; the third column the power handling capacity of the iris referred to standard waveguide at atmospheric pressure, obtained by extrapolating the data; and the last two columns list the predicted power handling capacity. The first prediction was based on the VSWR present on a lossless mismatched transmission line due to the iris reflection coefficient calculated from equation (15). The second prediction was based on the reduction in cross-sectional area calculated from equation (30). In the calculation based on equation (15) it was assumed that the energy reflected from the iris was absorbed without reflection by the Uniline isolator, or in other words that there was no resonant cavity effect. This assumption was reasonable since the 1.09 reverse VSWR of the Uniline indicated that the power reflected from it was 27 db down from the incident power.

TABLE 13

## SUMMARY OF BREAKDOWN TESTS ON INDUCTIVE IRISES

Iris Dimensions a' (inch)	t (inch)	Measured VSWR	Measured Power Handling Capacity	Predicted Power Handling Capacity	
				VSWR (Eq. 15)	Area (Eq. 30)
0.760	1/32	1.22:1	80%	84%	84%
0.694	1/64	1.37:1	72%	75%	77%
0.695	1/32	1.45:1	64%	71%	77%
0.615	1/32	2.1:1	57%	55%	68%
0.550	1/32	3.1:1	43%	44%	61%
0.490	1/64	4.4:1	35%	38%	54%
0.490	1/32	5.2:1	35%	36%	55%
0.420	1/32	11:1	28%	30%	47%

Figure 99 shows a curve of percentage of waveguide power vs VSWR for symmetrical inductive irises. As the VSWR was increased, the maximum voltage present in the waveguide was increased and hence the peak power handling capacity decreased. The theoretical curve is for a single mismatch on a lossless transmission line, as calculated from equation (15). The experimental points show excellent agreement with the theoretical curve. At no place do the curves differ by more than 8 percent which is within experimental error.

CONFIDENTIAL

Tests were performed on a series of asymmetrical inductive irises shown in figure 100. The VSWR's of the irises were varied from 1.32 to 5.6; these values are representative of the irises encountered in practice. The data are presented in figure 100 as ln-power vs ln-pressure curves which are straight lines with slopes varying from 2.0 to 2.2. The results of the tests on asymmetrical inductive irises are presented in table 14 in columnar form. The first column lists the iris opening, the next measured VSWR, the third measured power capacity, and the last column lists the power handling capacity predicted by equation (15).

TABLE 14  
SUMMARY OF BREAKDOWN TESTS ON  
ASYMMETRICAL INDUCTIVE IRISES

Window Opening a' (inches)	VSWR	Power Handling Capacity	Predicted Power Handling Capacity (equation 15)
0.760	1.32	75%	77%
0.711	1.63	75%	65%
0.630	2.70	53%	47%
0.603	3.50	46%	41%
0.544	5.60	37%	35%

It can be seen from table 14 that the breakdown of asymmetrical inductive irises follows the relationships obtained for the breakdown of a waveguide transmission line due to a standing wave, as predicted by equation (15).

The next tests were performed on three types of capacitive irises: (1) a symmetrical iris with various window openings, (2) a symmetrical iris with various window thicknesses, and (3) an asymmetrical iris with various window openings. The data have been plotted in figures 101, 102 and 103 as  $\ln$ -power vs  $\ln$ -pressure curves. Each graph contains a diagram showing the pertinent dimensions of the appropriate iris. All the curves are straight lines whose slopes vary from 1.2 to 1.5. These slopes are significantly less than the approximately square-law relationship between power and pressure which was obtained for standard waveguide.

A chart showing the different irises and their measured peak power handling capacity at atmospheric pressure as a percentage of the power handling capacity of standard 1-inch x 1/2-inch waveguide is presented in table 15. The slopes of the  $\ln$ -power vs  $\ln$ -pressure curves are also included.

The data obtained on the inductive and capacitive irises have indicated a marked difference in power carrying

capacity between the two units. (Inductive-iris power carrying capacity was approximately 10 times that of a capacitive iris with the same reflection coefficient.) This factor can be utilized in the design of matching structures for microwave components since the choice of an inductive or capacitive reactance is determined by the physical position at which the reactance is inserted. By selecting the position for an inductive reactance the power carrying capacity will be increased ten fold. It should be mentioned, however, that this technique will slightly reduce the bandwidth of the component if more length is required between the matching structure and the component.

### 11.3 Breakdown Data on Waveguide Steps

#### a. General

The waveguide step was next investigated. This structure is widely used in microwaves as an impedance transformer for different size waveguides. Basically, the waveguide step is an abrupt change in either the dimension of the broad wall, the narrow wall, or both. Broad wall and narrow wall waveguide steps have been discussed in terms of equivalent circuits by Marcuvitz and Moreno\*. If the step is lossless,

\*See ref. 69, p. 296-302, 307-310



TABLE 15

## SUMMARY OF BREAKDOWN DATA FOR CAPACITIVE IRISES

Type	Window Opening b' (inch)	Thickness d (inch)	VSWR	Power capacity Relative to Standard Waveguide at Atmospheric Pressure
Symmetrical capacitive (capacitance varied)	0.236	1/32	1.40	9.8%
	0.188	1/32	1.75	6.6%
	0.126	1/32	2.60	4.5%
	0.078	1/32	4.40	3.6%
	0.060	1/32	5.80	2.7%
Symmetrical capacitive (thickness varied)	0.188	1/64	1.63	6.6%
	0.188*	1/32	1.75	6.6%
	0.188	1/16	2.10	7.9%
	0.060	1/64	4.70	2.6%
	0.060*	1/32	5.80	2.7%
	0.060	1/16	9.30	3.4%
Asymmetrical capacitive (capacitance varied)	0.286	1/32	1.32	7.6%
	0.238	1/32	1.60	6.6%
	0.200	1/32	2.30	4.9%
	0.152	1/32	3.50	3.7%
	0.136	1/32	4.20	2.9%

\*reproduced from above for convenient comparison

CONFIDENTIAL

the effect of the discontinuity can be represented by a shunt susceptance on the transmission line. The waveguide steps tested are shown in figures 104, 105, 106. The equivalent circuits for the steps (with the assumption that the losses are negligible) are also included. As was the case for the iris, it is seen that a broad-wall step is represented by a capacitive susceptance and the narrow-wall step by an inductive susceptance. Since it was desirable from the viewpoint of practicability to retain the 1-inch x 1/2-inch waveguide in the test circuit, it was necessary to utilize two steps in the test piece. This allowed an additional parameter, the length of the step, to be varied and thereby yielded information on the proximity effect between two steps.

#### b. Inductive Steps

Breakdown data on the symmetrical inductive step is shown in figure 104. The slopes of the  $\ln$ -power vs  $\ln$ -pressure curves are 1.9 for both test pieces which is essentially the same as for standard waveguide. The power handling capacity of a transmission with a single mismatch was calculated from equation 15 utilizing the measured VSWR's of the steps. The results are summarized in table 16.

CONFIDENTIAL

TABLE 16

## SUMMARY OF BREAKDOWN DATA ON INDUCTIVE STEPS

a'	VSWR	(at atmospheric pressure)	
		P calculated	P measured
0.800	1.47	71%	78%
0.700	3.0	45%	62%

It can be seen that the measured values were larger than the calculated values. In the worst case ( $a' = 0.700$  inch) the two values differed by 17 percent. Since the calculated values represent the maximum power the transmission line can carry, the difference between the theoretical and experimental results must be attributed to experimental error. For the smaller step ( $a' = 0.800$  inch) the difference is 7 percent and for the larger step ( $a' = 0.700$  inch) the difference is 17 percent. Since the calculated values represent the maximum power carrying capacity of the transmission line, the difference between the measured and calculated results must be due to experimental errors. The experimental error associated with the test circuit has been estimated to be plus or minus 9.4 percent (see paragraph 7.4). In order to account for the 17 percent difference, the waveguide and step data would have to be in error by almost the maximum amount, and of opposite signs. Since this is very unlikely, the

CONFIDENTIAL

difference is probably not due to the test circuit accuracy but rather some hitherto neglected source of error. One very likely source of error lies in the measurement of the VSWR of the step. The measurement was made on a standard impedance-meter setup utilizing a crystal rather than a Littlefuse for the detecting element. Since the crystal does not maintain a square law response over a wide range, it may have led to an error in the measurement of the VSWR of the  $a = 0.700$  inch step. Measurements taken at this laboratory on a sampling of crystals indicate that the error can be as high as 25 percent for a 3:1 voltage ratio. This would lead to a VSWR of 2.25 and a calculated power carrying capacity of 52 percent. This is in closer agreement with the breakdown data and is the most probable explanation of the results.

Once it was established that the breakdown of the symmetrical inductive step was due to the standing wave created on the transmission line by the mismatch, as was also found for the inductive iris, the tests were terminated without investigating the effect of varying the step length, or use of asymmetrical steps since this could not be expected to yield any new information.

## c. Capacitive Steps

The results of the breakdown tests on capacitive steps are shown in figures 105 and 106. Figure 105 contains the results on five quarter-wavelength-long, symmetrical, capacitive steps and one-half wavelength step. Figure 106 contains data on five quarter-wavelength asymmetrical steps. The slopes of the  $\ln$ -power vs  $\ln$ -pressure curve are significantly different from square-law relationship for linear-field breakdown in standard waveguide. This indicated that the step was causing E-field distortion which resulted in non-uniform field breakdown. This type of breakdown is characterized by a lowering of the slope of the power-pressure curve. The slope of the curves are predominantly 1.5 which indicates that the field configuration for the step remained relatively insensitive to large changes in the step dimension. This result agreed with the data on the hemispherical bump section (see paragraph 10.5a) where it was found that the slope was again fairly independent of bump radius.

The results of the tests on the capacitive steps are summarized in table 17. By referring to table 16, it can be readily seen that the capacitive steps can carry considerably less power than the inductive steps for a given

CONFIDENTIAL

waveguide opening. This result will be discussed more fully in paragraph 11.8 as a characteristic of capacitive structures.

TABLE 17  
SUMMARY OF BREAKDOWN DATA ON CAPACITIVE STEPS

<u>b'</u>	<u>b'/b(%)</u>		<u>VSWR</u>	<u>Power Handling Capacity of Test Piece at Atmos- pheric Pressure Relative to Standard Waveguide</u>
Symmetrical:				
0.380	95%	$\lambda_g/4$	1.10	60%
0.360	90%	$\lambda_g/4$	1.20	38%
0.340	85%	$\lambda_g/4$	1.38	27%
0.320	80%	$\lambda_g/4$	1.56	20%
0.200	50%	$\lambda_g/4$	3.80	13%
0.360	90%	$\lambda_g/2$	1.06	24%
Asymmetrical:				
0.390	97.5%	$\lambda_g/4$	1.08	81%
0.380	95%	$\lambda_g/4$	1.13	39%
0.370	92.5%	$\lambda_g/4$	1.20	30%
0.360	90%	$\lambda_g/4$	1.24	24%
0.300	75%	$\lambda_g/4$	1.73	14%

By comparing the information in table 17 for the capacitive step with the results for the symmetrical capacitive iris in table 15, it can be seen that for a given waveguide opening ( $b'/b$ ), the performance of these two structures



CONFIDENTIAL

are nearly in agreement. Thus, just as the performance of the inductive step and iris were found to be similar, an analogous relationship holds between the capacitive step and iris.

Several interesting results may be obtained from table 17. First, the symmetrical capacitive step carried about 50 percent more power when the step was a quarter-wavelength long than when it was a half-wavelength long. This can be explained by the fact that the two equal shunt susceptances comprising the equivalent circuit of the step add in phase for a half wavelength and are out of phase for a quarter wavelength. Thus, when the quarter wavelength step was used, the reactances tended to cancel and minimize the field distortion. When the half-wavelength step was used, the reactances added in phase, tending to increase the distortion.

Table 17 also indicates that the symmetrical capacitive step carried somewhat more power than the asymmetrical one for a given value of  $b'/b$ . This amount varied from 50 percent to about 30 percent as  $b'/b$  was decreased.

#### 11.4 Breakdown of a Capacitive Waveguide Post

A metallic post extending part way across a waveguide parallel to the electric field is used quite often for such applications as a launching probe, a detecting probe, or a matching structure. For these reasons an investigation of the breakdown of this type of post was considered important. Figure 4 of the nineteenth interim report shows a typical test fixture that was used in the breakdown test. It may be seen that the length  $l$ , the diameter  $d$ , and the shape of the end of the post may be varied.

This structure, treated theoretically and experimentally by Moreno\* and Marcuvitz\*\*, was found to exhibit resonance phenomena similar to a shunting series-resonant circuit for a particular value of post diameter and length. However, for most applications the resonating property of the post is not utilized. Therefore, it has been called a capacitive post to take cognizance of the fact that its reactance is capacitive in most applications. The equivalent circuit for a centrally located metallic cylindrical post of variable height, as given by Marcuvitz, is shown in figure 107.

---  
\*see ref. 81, pp. 152-153  
\*\*see ref. 69, pp. 271-273

CONFIDENTIAL

Experimental data is presented by Marcuvitz which indicates that the reactance  $X_b$  is negligible for most post lengths and diameters.

Tests were made on the breakdown of posts of various lengths for two different conditions. First, the posts were located centrally in the waveguide ( $x$  equal to 0.450) and second, at a point one quarter of the distance from wall to wall ( $x$  equal to 0.225). At each position, breakdown data was obtained for 0.125-inch and 0.250-inch posts with both hemispherical and flat ends. The results of the tests for the flat-ended posts are plotted in figure 107 and those for the hemispherical-ended posts are plotted in figure 108. It is seen that the slopes of the majority of the  $\ln$ -power vs  $\ln$ -pressure curves fall between 1.4 and 1.7. Those cases where the slopes were 1.8 or 1.9 were attributed to the limited amount of data taken, from which it was impossible to accurately determine the slope. The power handling capacities determined in the tests on the flat-ended and hemispherical-ended posts are summarized in tables 18 and 19 respectively, as percentages of standard waveguide power at atmospheric pressure. The VSWR of the post and the slope of the  $\ln$ -power vs  $\ln$  pressure curve are included in these tables.

CONFIDENTIAL

TABLE 18

## SUMMARY OF BREAKDOWN TESTS ON FLAT-ENDED CYLINDRICAL POSTS

x (inch)	l (inch)	d (inch)	VSWR	Power Handling Capacity (% of Standard Wave- guide Power at Atmospheric Pressure)	Slope
0.450	0.041	0.125	1.10	10.6	1.5
0.450	0.090	0.125	1.34	5.3	1.6
0.450	0.148	0.125	2.5	2.3	1.7
0.450	0.204	0.125	5.4	1.9	1.7
0.225	0.050	0.125	1.04	18.4	1.4
0.225	0.097	0.125	1.16	7.9	1.5
0.225	0.150	0.125	1.5	3.5	1.5
0.225	0.200	0.125	2.8	1.7	1.4
0.225	0.050	0.250	1.06	17.2	1.5
0.225	0.150	0.250	2.0	4.9	1.5
0.450	0.050	0.250	1.16	14.8	1.5
0.450	0.100	0.250	1.9	7.4	1.4
0.450	0.150	0.250	3.8	5.1	1.5
0.450	0.205	0.250	6.4	6.4	1.4

CONFIDENTIAL

TABLE 19  
SUMMARY OF BREAKDOWN TESTS ON  
HEMISPHERICAL-ENDED CYLINDRICAL POSTS

x (inch)	l (inch)	d (inch)	VSWR	Power Handling Capacity (% of Standard Wave- guide Power at Atmospheric Pressure)	Slope
0.450	0.050	0.125	1.04	12.9	1.5
0.450	0.100	0.125	1.26	7.2	1.6
0.450	0.150	0.125	1.75	5.1	1.6
0.450	0.200	0.125	4.1	4.9	1.6
0.225	0.045	0.125	1.01	34.3	1.7
0.225	0.095	0.125	1.09	16.7	1.6
0.225	0.150	0.125	1.41	6.6	1.6
0.225	0.200	0.125	2.2	3.6	1.8
0.225	0.050	0.250	1.04	45.	1.9
0.225	0.150	0.250	1.43	12.4	1.9
0.450	0.050	0.250	1.06	26.5	1.7
0.450	0.150	0.250	2.2	11.4	1.6

In order to observe how the power carrying capacity of the post varied with diameter, position and shape, the information in tables 18 and 19 was replotted as shown in figures 109, 110, and 111. Figure 109 contains graphs of power handling capacity vs post length as a function of position and diameter for the flat-ended post. Figure 110



CONFIDENTIAL

contains similar graphs for the hemispherical-ended posts. In figure 111, the power handling capacity for the flat-ended and hemispherical-ended posts are compared as a function of length, position, and diameter.

Correlation of this information leads to several general conclusions about the performance of the cylindrical waveguide post. It was found that the power handling capacity of a given post can be increased as much as three times by rounding the end. This was accomplished by a slight lowering of the reactance of the post.

The results that the power carrying capacity of waveguide components could usually be improved by removing sharp edges agreed with the practical experiences gained in the component testing phase of the program. It was also concluded that the power carrying capacity of the post increased as the diameter increased. The effect was accompanied by an increase in VSWR. This fact would be an advantage if the post were to be used as a matching structure. The required VSWR can be obtained with less sacrifice in power handling capacity with a large diameter post than with a small diameter post. Although the resonant post is extremely flexible as a matching structure, it has little other use in high-power applications, since other structures, such as the

CONFIDENTIAL



inductive iris, have a far greater power carrying capacity. It was found that there is a tendency for the power carrying capacity to increase as the position of the post was changed from the center of the waveguide to the side. This result was expected since the electric gradient reached maximum in the center of the waveguide.

#### 11.5 Breakdown of a Thin Strip in Rectangular Waveguide

##### a. Inductive Strip

A thin strip of metal of width  $d$ , centrally located in the broad dimension and extending across the waveguide with its edges parallel to the electric field as shown in figure 112, is called an inductive obstacle. This structure was selected for tests both because of its application as a matching device and for comparison with other types of matching structures.

The equivalent circuit\* of this structure is an inductive susceptance shunted across the line. As  $d$  was increased, the admittance also increased until the waveguide was completely closed off by the metal strip and the waveguide was terminated in a short circuit. If the thickness of the post is not neglected, the equivalent circuit of the

\*see ref. 81, p. 145 and ref. 69, p. 227

CONFIDENTIAL

inductive obstacle can be considered a tee network as shown by Marcuvitz\*. However, for most cases, the magnitude of the reflections from such a structure can be computed by considering only the shunt arm of the network. The series arms have an appreciable effect only on the phase of the reflection.

The results of the tests on an inductive strip with a thickness,  $d$  equal to 0.250 and a VSWR of 8.9 are plotted in figure 112 in the form of a  $\ln$ -power vs  $\ln$ -pressure curve. The power carrying capacity of the strip relative to standard waveguide at atmospheric pressure was 12 percent and the slope was 1.4. This is considerably less power than a mismatched transmission line with a VSWR of 8.9, calculated to carry from equation 15. Thus, it can be concluded that the disturbance of the field, due to the inductive obstacle, caused gradients to be set up in the neighborhood of the structure which were greater than the gradient produced on the transmission line because of the mismatch.

#### b. Capacitive Strip

A thin metallic strip of width  $d$ , centrally located in the narrow dimension and with edges perpendicular to the

---  
\*see ref. 69, p. 263

electric field as shown in figure 113, has for its equivalent circuit a capacitive susceptance\*. The results of tests made on this type of structure as the width of the strip was varied are shown in figure 113. The power carrying capacity of this structure relative to standard waveguide at atmospheric pressure, for d equal to 0.100 and 0.200 inches, was 14 and 7 percent respectively. The slope of the ln-power vs ln-pressure curve was 1.4 in both cases.

#### 11.6 Breakdown of Waveguide Capacitive Rod

A waveguide rod is a metal cylindrical which extends across the walls of the waveguide perpendicular to the direction of energy propagation. If the axis of the rod is perpendicular to the broad wall of the waveguide, it may be represented by a shunt inductance\*\*. Physically, the inductive rod is an extension of the capacitive post discussed in paragraph 11.4. The post was capacitive for the initial penetration, then resonant, and then inductive for penetrations up to and including the opposite wall. Because of the extensive data obtained on the capacitive post and the inductive strip, both of which can be expected to perform similar to the inductive rod, it was decided not to perform

---  
\*see ref. 69, p. 221 and ref. 81, p. 146

\*\*see ref. 69, p. 257

CONFIDENTIAL

tests on the rod. On the other hand, if the axis of the rod is perpendicular to the narrow wall it may be represented by a tee network of three capacitive susceptances provided the losses are negligible\*.

The breakdown of this structure was investigated for three values of rod diameter  $d$  and the results are plotted in figure 114. The data for these tests are summarized in table 20.

TABLE 20  
SUMMARY OF BREAKDOWN DATA ON THE  
CYLINDRICAL CAPACITIVE ROD

<u>Rod Diameter (d inches)</u>	<u>VSWR</u>	<u>Power Handling Capacity</u> <u>at Atmospheric Pressure</u>	<u>Slope</u>
0.050	1.04	24.7%	1.6
0.100	1.26	19.7%	1.5
0.150	2.6	14.3%	1.6

Note that as the diameter of the cylindrical rod was increased, the power handling capacity decreased and the VSWR increased, as was expected.

\*see ref. 69, p. 268

### 11.7 Breakdown of Waveguide Apertures

Sampling of the microwave energy in a waveguide is accomplished by placing small apertures in the wall of the waveguide at a suitable position. In small aperture couplers, energy is usually abstracted by interrupting the current flowing in the walls of the waveguide. This represents a radiating source for the secondary waveguide, and electromagnetic energy can be propagated.

Directional couplers are obtained by combining two or more slots in such a manner that the waves generated in one direction add in phase.

The current flowing in the walls of a rectangular waveguide propagating the dominant  $TE_{10}$  mode in the  $z$  direction are shown in figure 115. Two examples of non-radiating apertures are, a long thin slot in the center of the broad wall of the waveguide parallel to the  $z$  direction (as is used in the slotted-line impedance meter), and a thin slot in the narrow wall parallel to the  $y$  direction. This is so because these slots cause only a slight disturbance in the current density distribution. Radiating slots, which are of more interest to the present discussion, occur whenever either the



CONFIDENTIAL

x component ( $J_x$ ) or the z component ( $J_z$ ) of current density is interrupted. The amount of radiation from the slot depends upon its size, shape and position.

Quantitative information on the effect of these parameters applied to directional couplers may be found in a report furnished to the Department of the Army\*. The size, shape, and position of the slot also affects the breakdown of the slot. However, the relationship is complicated by the interplay of several effects. For example, breakdown may occur across the slot due to current arcing. This in turn may produce a space charge which distorts the electric field and causes voltage breakdown. Another example, the normal current distribution is disturbed by the slot, and causes a perturbation of the propagating mode. This results in electric field distortion and increased gradients leading to breakdown. This effect can be contributed to the bunching of the electric field caused by the sharp edges of the slot. For a particular coupling slot geometry, any one of these effects may predominate. Therefore, no general theory for the breakdown of coupling slots can be given at present.

- - - - -  
\*Final Report for unidirectional Couplers Research and Development Program furnished by the Sperry Gyroscope Company to the Army Squier. Signal Corp Engineering Laboratory on Contract No. DA-36-039-sc-5486

CONFIDENTIAL



CONFIDENTIAL

The test piece used to investigate the breakdown of apertures is shown in figure 115. A primary waveguide was made with the various slots to be investigated. Omni-directional radiating apertures were tested since the insertion of one or more additional slots for directional coupling purposes does not affect the breakdown. The secondary arm was machined to fit all the primary arms and was soft soldered to each one in turn for test purposes. The secondary arm of the test piece was necessary mainly for pressurization purposes. This test piece eliminated duplication of many parts and at the same time removed extraneous variables such as solder joints from the primary arm.

The results of the tests on a series of thin slots in the broad wall parallel to the direction of propagation are shown in figure 116. Figure 117 shows the data for a round hole in the broad wall. All machining burrs were removed from the test pieces to insure a good test. The power handling capacity of the apertures relative to standard waveguide at atmospheric pressure is summarized in table 21. The results of attenuation measurements between the primary and secondary lines are also included.

CONFIDENTIAL

TABLE 21  
SUMMARY OF BREAKDOWN TESTS ON APERTURES

Transverse Slot in Broad Wall of Test Piece	Position (P) (inch)	Length (L) (inch)	Width (W) (inch)	Power Handling Capacity	Slope	Att. (db)
1	0.150	0.400	0.063	82%	1.9	35
2	0.225	0.200	0.063	82%	1.9	53
3	0.300	0.400	0.063	38%	1.7	31
4	0.225	0.500	0.100	27%	1.5	53
round hole						
5	0.225	0.094 (diameter)		94%	2.0	60

In general, note that when the aperture did not appreciably affect breakdown, the test piece carried nearly full waveguide power and the slope of the ln-power vs ln-pressure curve followed approximately a square law function. As the aperture appreciably affected the power handling capacity, the slope dropped to about 1.5 indicating a change in the breakdown mechanism as when bunching of the E-field takes place. The broad wall couplers explained in paragraph 10.2 had similar slots and were also characterized by slopes of approximately 1.5.

CONFIDENTIAL

Examination of the data in table 21 more closely reveals several interesting facts. First, for test pieces 1 and 3, which differed only in the position of the slot, it was seen that the slot placed 0.300-inch, or 67 percent of the distance from the center line to the outside wall, carried nearly half the power of the slot displayed 33 percent of the distance, while the attenuation of both slots was the same. This indicated that current breakdown was the controlling mechanism since the electric field was larger in the center of the waveguide and the current was a maximum at the side wall. Since the coupling from both slots was the same, this result may be useful in the design of directional couplers provided bandwidth and directional properties can still be retained.

It can be seen that test piece 2 in which the position and length of the slots were changed carried 82 percent of total waveguide power. Although the position of the slot was shifted to 50 percent of the distance from the center line, the reduction in the length of the slot reduced the amount of current lines interrupted and thereby diminished the likelihood of current arcing. This observation was supported by the fact that very little power (53 db attenuation) was radiated from the slot. In test piece 4, the

CONFIDENTIAL

slot was placed in the same position as in the second test piece, but it was lengthened and widened. It is difficult to say which one, or to what degree these parameters reduced the power handling capacity from 82 to 27 percent.

The results, using testpiece 5 with the round hole, indicated that it could carry essentially full waveguide power. However, because the coupling was more than 60 db down, the use of this type of aperture may be limited to the very high-power systems in which the measurement of one one-millionth of the main-line power (60 db) is feasible.

The use of multiple holes will reduce this objectional feature if directional characteristics and bandwidth requirements can be met this design shows promise.

#### 11.8 Comparison of the Breakdown Data on The Building Block Structures

##### a. General

Several of the building-block structures investigated, namely, the iris, the rod, and the strip may be represented as a equivalent circuit having pure shunt susceptances. Since they often find application as an impedance

matching device, this information should be useful for determining the best structure for obtaining a desired reactance at a given point in a high-power transmission line.

The data on these structures have been previously presented in paragraphs 11.2, 11.5, 11.6. The results will be repeated in this new form of presentation with the susceptances calculated from the measured VSWR's or curves given by Marcuvitz\*. For brevity, only the symmetric structures will be considered. However, the results may be readily extended to the asymmetric structures from the information presented in this report.

#### b. Inductive Structures

The physical geometries and equivalent circuits for the symmetrical inductive iris and strip are shown in figures 96 and 112. Figure 118a shows the power handling capacity of the iris and the strip as a function of the equivalent inductive susceptance. The susceptances of the structures were calculated from the measured VSWR's with the assumption that the structures were lossless, pure-shunt reactances. This assumption is applicable for thin structures, and since the thickness of the iris and the strip was only

-----  
\*see ref. 69, p. 268



0.031 inch, or 2 percent of the guide wavelength, it was considered a valid assumption. It can be seen from figure 118a that the iris carried approximately 2-1/2 times more power than the strip for the same value of inductive susceptances. This indicated that the breakdown mechanism for the two structures was different. For example, it was concluded in paragraph 11.2, that for the iris, the breakdown was actually due to the standing wave setup on the transmission line which caused the line to breakdown. For the strip, breakdown probably occurred in the region of the structure due to increased gradients caused by the electric field distortion. Therefore, there is an important distinction that can be made between the breakdown of waveguide structures. Breakdown will either occur on the transmission line at some point towards the generator due to the VSWR, or it will occur at the structure due to the electric field distortion. The first case, represented by the iris, permits transmission of the maximum power that the mismatched line will carry, whereas, the second case, represented by the strip, limits the power handling capacity of the line. All waveguide structures may be divided into these two categories. Where a choice can be made, it is preferable to use the first type.



## c. Capacitive Structures

The equivalent circuit breakdown characteristics of several symmetrical capacitive structures such as the iris, the rod, and the strip can now be considered. The physical geometries and equivalent circuits for these structures are shown in figures 96, 113, and 114. The results of the tests are shown in figure 118b, as a percentage of standard waveguide power carrying capacity at atmospheric pressure vs the susceptance of the equivalent circuit. The susceptance of the iris and the strip were calculated from the measured VSWR's with the assumption that the structure could be represented by thin lossless, capacitive-shunt susceptances. The susceptance of the rod was calculated using the information given by Marcuvitz\*. It can be noticed (by comparing figure 118a and 118b) that the capacitive structures are capable of carrying considerably less power than the inductive structures. This result is understandable since capacitive structures launch E-type modes (TM) which create greater E-field gradients in the region of the structure. From figure 118b it can be seen that the capacitive iris and strip carry approximately the same power for a given susceptance. This was not unexpected since the structures have identical equivalent circuit parameters, and somewhat similar geometries.

-----  
\*see ref. 69, p. 268

CONFIDENTIAL

The data obtained for the rod indicated a power handling capacity two to three times greater than the iris and strip for a given susceptance. A complete analysis of these results was not attempted due to the complexity of the field structure in the region of these structures. However, the results can be analyzed qualitatively.

The rod presented a rounded surface to the electric field. This tended to reduce the intensity of the electric-field lines terminating on the rod as compared to the increased electric-field gradients caused by the bunching of the electric field on the sharp edges of the strip and iris. As with the capacitive posts discussed in paragraph 11.4, empirical evidence indicated that an increase in power handling capacity from two to three times is not unusual when sharp edges are rounded.

#### SECTION D

#### CONCLUSIONS

##### 12. GENERAL CONCLUSIONS

A survey of the available literature on the subject of high-power breakdown has shown that a number of different theories exist regarding the field of high-power breakdown. Each of these theories describe breakdown as an increase in

CONFIDENTIAL

current across the breakdown gap due to electrons being created in the gap at a rate greater than the removal rate. Breakdown is caused by an electron avalanche, wherein an initial electron, accelerated by the applied field, creates new electrons by collisions with neutral molecules.

The existing data on microwave breakdown was discussed and appraised. It was first shown that in the case of Cooper's work, the statistical approach led to consistent results which agree with theory. The work performed at M.I.T. was then discussed and the discrepancies observed in these experiments were traced to the fact that a statistical approach to breakdown was not adopted. The work of Lathrop and Brown, MacDonald and Brown, and Herlin and Brown was also discussed. It was shown that in each of these experiments, special conditions existed which reduced the inherent error because the statistical approach was not used.

An experimental approach to the problem of microwave breakdown was presented. This approach was based upon the concept that the breakdown process is a statistical one, wherein the probability is a function of the initial velocity of the electron, its phase relative to that of the r-f field, and its position in the gap. On this basis, there can be no absolute minimum breakdown power, nor will any one criterion

CONFIDENTIAL

CONFIDENTIAL

of breakdown be suitable for every application. Thus, a curve of sparking probability vs power was plotted and the breakdown power for a particular application was determined by a judicious use of the resulting curve.

The initial breakdown tests indicated that the statistical approach yielded valid and reproducible information. Tests were made to determine the breakdown power of a straight section of 1-inch x 1/2-inch waveguide using a 1-inch x 1/2-inch tapered waveguide section. This test piece was used as the standard for 1-inch x 1/2-inch waveguide and was retested at various times during the course of the program with good consistency.

The maximum power-handling capacity of a 1-inch x 1/2-inch waveguide was computed to be 1.4 megawatts. This value applies for the following conditions:

pressure	atmospheric
pulse width	1.2 microseconds
repetition rate	800 pps
VSWR	1.00
frequency	9375 mc

CONFIDENTIAL

After several unsuccessful attempts, a method was devised to locate the region of breakdown on the interior of the 1-inch x 1/2-inch waveguide section. A contact-type photographic printing paper was placed against the inner walls of the waveguide and the light from the spark on the sensitized paper was thus recorded. It was shown that the sparks traveled back towards the generator and occurred at intervals which were very nearly one quarter of the waveguide wavelength.

Tests were conducted to determine the effect of external irradiation upon the power-carrying capacity of waveguide. It was shown that the use of one millicurie of radioactive cobalt increased the probability of breakdown, but did not lower the minimum power required for breakdown.

Additional measurements were made of the variation of breakdown power with pressure. In these tests the pressure was varied between 5 inches and 40 inches of mercury (absolute pressure) and radioactive cobalt was employed. The data indicated that for this range of pressure the breakdown power was proportional to the pressure raised to an exponent. For waveguide, the exponent has a value of 2.

CONFIDENTIAL



CONFIDENTIAL

It was also found that the peak power handling capacity varied inversely with the pulse width raised to the  $1/3$  power. This expression is justified only up to pulse widths smaller than 2.35 microseconds since above this value the power capacity will remain essentially constant. These results were obtained using pulse widths between 0.4 and 3.55 microseconds and repetition rates of 400 and 800 pps.

The peak power handling capacity varied inversely with the repetition rate raised to the  $1/15$  power. This relationship was obtained using repetition rates from 400 to 2500 pps and at a constant pulse width of 0.4 microseconds.

Tests on the effect of mechanical surface finishes (on all four waveguide walls) on peak power handling capacity indicated that an RMS 300-400 finish carried 89 percent of the full waveguide power with essentially the same slope for the  $\ln$ -power vs  $\ln$ -pressure curve as that of standard waveguide. A finish as rough as RMS 650-850 carried 74 percent of the full waveguide power with the same slope for the  $\ln$ -power vs  $\ln$ -pressure curve as standard waveguide.

Tests were made to investigate the effect of sulphur hexafluoride gas ( $\text{SF}_6$ ) upon peak power breakdown. It was found that the power carrying capacity of waveguide and

CONFIDENTIAL



CONFIDENTIAL

waveguide components increased as the ratio of  $\text{SF}_6$  to air increased. For high  $\text{SF}_6$  gas purity, an increase in power-carrying capacity by a factor of approximately 6:1 can be expected for most waveguide components.

For a 0.012-inch swayback section filled with air, the power handling capacity varied inversely with the pulse width raised to the  $1/3$  power and inversely with the repetition rate raised to the  $1/15$  power over the range from 0.4 to 2.35 microseconds and 400 to 2500 pulses per second.

For a 0.012-inch swayback section filled with  $\text{SF}_6$  gas, the power handling capacity varied inversely with the pulse width raised to the 0.22 power and inversely with the repetition rate raised to the 0.12 power over the range from 0.4 to 2.35 microseconds and 400 to 2500 pulses per second.

The increase in power handling capacity for a  $\text{SF}_6$  filled, 0.012-inch swayback section over that for an air-filled 0.012-inch swayback section was in the ratio of approximately 11:1. This agreed with information reported in the literature.

The data on anodized waveguide indicated that the anodization process had a negligible effect on the power-carrying capacity of waveguide.

CONFIDENTIAL

A theoretical analysis indicated that the power-carrying capacity of waveguide will vary nearly as the ratio 1.4:1 over the normal operating frequency range.

The effect of VSWR upon peak power handling capacity was theoretically and experimentally investigated for the following cases:

a. a single mismatch present in a lossless transmission line, b. a lossless, matched, resonant cavity formed by two mismatches properly spaced in a waveguide, and c. a lossy mismatched resonant cavity. The experimental results were in agreement with the theoretical analysis.

Tests on properly aligned choke-to-cover and cover-to-cover flange connections indicated a power handling ability which is the same as that for standard 1-inch x 1/2-inch x .050-inch waveguide. Test data has been presented which indicate the manner in which the power handling capacity of these connections were reduced by misalignment.

Tests on heliarc-welded sections showed that the peak power handling capacity was reduced to as low as 60 percent of waveguide power. The test pieces were cut through the cross-section and examined to determine what conditions

CONFIDENTIAL

CONFIDENTIAL

actually existed. It was found that the pieces that carried less power had mechanical deficiencies.

The power handling capacity of a number of waveguide components was determined. The breakdown tests on interlocked and convoluted types of flexible waveguides indicated a peak power handling capacity of 40 percent of full waveguide power at atmospheric pressure. The breakdown characteristics were the same whether the unit was straight or, twisted 90 or 180 degrees.

Tests on the peak power handling capacity of a vertebrae section resulted in a dual-slope curve and the power handling capacity at atmospheric pressure was 54 percent of the full waveguide power or 0.73 megawatt.

Tests were made on a contact flange for RG-163/U waveguide developed by U.S. Navy Underwater Sound Laboratory. The results indicated that the flanges could carry as much power as the waveguide.

The data on H- and E-plane bends are presented in tables 9 and 10 respectively. A theoretical analysis indicated that the power handling capacity of the H-plane bend was 97 percent of standard waveguide with very little dependence on the bend radius. The actual values agreed with

CONFIDENTIAL

CONFIDENTIAL

this result within experimental error. The actual and predicted values of power handling capacity for E-plane bends compared quite favorably. The 90-degree H-plane mitred corner carried 84 percent of standard waveguide power. This resulted in an agreement with the test on the H-plane bends.

Tests were made on four 90-degree waveguide twist sections from 1-1/4-wavelengths to 4-1/3-wavelengths long and one 45-degree twist 1-1/4-wavelengths long. Most of the twists carried close to full waveguide power. However, a short length twist appeared to be more sensitive to mechanical defects which tend to reduce the power capacity.

The breakdown powers of 1-inch x 1/2-inch crossed-guide and two-hole couplers, and a 1-1/4-inch x 5/8-inch Schwinger coupler were experimentally determined. The results indicated that the power handling capacity of couplers varied from about 20 percent to essentially full waveguide power.

The H-plane tee carried about 80 percent of the standard waveguide power. Extrapolated to atmospheric pressure, this indicated a power carrying capacity of one megawatt. The power varied as the square of the pressure for this unit.

CONFIDENTIAL

CONFIDENTIAL

The E-plane tee broke down at 85 kw at atmospheric pressure. This was six percent of the standard waveguide power. For this unit the power varied as the pressure raised to the 1.3 power.

The magic tee behaved like the E-plane tee. Extrapolation of the data to atmospheric pressure indicated a power handling capacity of 110 kw, which is 8 percent of the standard waveguide power. For this unit the power varied as the pressure raised to the 1.4 power.

The branch-guide coupler exhibited the characteristics of the E-plane tee in a less marked fashion. The data indicated a power handling capacity of 400 kw at atmospheric pressure. The power varied as the pressure raised to the 1.7 power.

The breakdown tests on the E-plane hybrid ring indicated a slope of 1.6 for the ln-power vs ln-pressure curve with a peak power handling capacity at atmospheric pressure of 19 percent of the full waveguide power, or 0.256 megawatt.

The breakdown tests on the  $TM_{01}$  rotary joint produced a result which had not been encountered previously in this program. The ln-power vs ln-pressure curve consisted



of two regions of constant slope separated by a range of pressure wherein the power was independent of the pressure. The slope of both curves of ln-power vs ln-pressure was 2.0 and the peak power handling capacity at atmospheric pressure was 0.193 megawatt, or 14 percent of the full waveguide power.

The breakdown tests on the ridge-waveguide coaxial-line rotary joint indicated a peak power handling capacity of 15 percent of waveguide power at atmospheric pressure.

The breakdown tests on the dual-feed coaxial-line rotary joint indicated a peak power handling capacity of 17 percent of standard waveguide power.

The data obtained on the hemispherical bump section agreed reasonably well with that reported by Wheeler Laboratories. The unit was capable of carrying 10 and 15 percent of waveguide power for bump radii of 0.150 inch and 0.050 inch respectively.

Tests on the mechanical waveguide switch and dummy load indicated a peak power handling capacity at atmospheric pressure of 1.05 megawatt, or 42 percent of the full waveguide power, with a slope of 1.9 for the ln-power vs ln-pressure curve.



CONFIDENTIAL

Tests on the antenna assembly indicated a peak power handling capacity of 0.224 megawatt at atmospheric pressure.

The longitudinal serrated chokes had a peak power handling capacity at atmospheric pressure of greater than 0.230 megawatt.

The data on the coaxial-line-to-waveguide adapter indicated a power handling capacity at atmospheric pressure of 4.3 percent of full waveguide power.

Breakdown tests were made on 1-inch x 1/2-inch x .050-inch and 1-1/4-inch x 5/8-inch x .064-inch waveguide dummy loads. The results indicated that at low power levels the load can carry essentially the full waveguide power. At high power levels, the heat developed changed either the pressure or the density of the gas. This made the peak power handling capacity of the load dependent upon its particular application.

The breakdown tests on a new design dummy load for the cooled and uncooled conditions indicated a power handling capacity at atmospheric pressure of 50 and 23 percent of full waveguide power, respectively.

CONFIDENTIAL

CONFIDENTIAL

The data taken on the Model X20L isolator (for 1-inch x 1/2-inch waveguide) and the Model HL86-96 Uniline isolator (for 1-1/4-inch x 5/8-inch waveguide) indicated a peak power handling capacity of 12 percent of standard waveguide power.

Comparison of data taken in X, C, and S bands indicated an encouraging correlation between similar components in the various bands.

The waveguide structures tested were the iris, the step, the post, the strip, and the aperture. The breakdown tests on symmetrical and asymmetrical inductive irises agreed, within experimental error, with the theoretical analysis performed for a single mismatch on a lossless transmission line. This analysis indicated that breakdown occurred on the transmission line because of standing waves, and that the power handling capacity varied inversely with the factor  $(1 + |\Gamma|)^2$ .

The breakdown tests on symmetrical and asymmetrical capacitive irises indicated that their power handling capacity was about 10 percent of that of an inductive iris with the same VSWR. The asymmetrical iris carried about 30 percent less power than the symmetrical iris for a given window

CONFIDENTIAL

opening. As the thickness of the iris was increased from  $1/64$  to  $1/16$  inch the power handling capacity was increased by 25 percent.

The data on the symmetrical inductive step agreed with the results for the inductive iris. The breakdown was due to the standing wave setup in the waveguide.

The high-power performance of the capacitive step was found to have the same relationship to the inductive step as existed between the inductive and capacitive iris.

The data on the cylindrical capacitive post are summarized in tables 18 and 19. It was found that the power handling capacity depended on the end shape, the diameter, the length, and the position of the post in the waveguide.

It was found that an inductive strip with an 8.9 VSWR carried 12 percent of waveguide power. The data on the thin capacitive strip indicated that the power-carrying capacity decreased as the width of the strip was increased.

The data on the cylindrical capacitive rod are summarized in table 20 and indicates that the power handling capacity decreased with rod diameter.

CONFIDENTIAL

The data in waveguide apertures indicated that the power handling capacity of an aperture depends upon its shape and position. The power handling capacity of a broad wall aperture was found to depend on the current density in the wall of the waveguide at the aperture. Apertures which do not disturb the normal mode current distribution can carry more power.

The breakdown of the structures that can be represented by a simple equivalent shunt susceptance were compared as a function of susceptance. It was found that the inductive structures carried considerably more power than capacitive structure for the same magnitude of susceptance.

## PART II

### RECOMMENDATIONS

#### 13. GENERAL RECOMMENDATIONS

A large amount of information was obtained on the breakdown of microwave components. Included are the important design parameters which affect breakdown, and the techniques for making accurate and reliable breakdown measurements. This information should be widely publicized in order to guide microwave engineers in the development of high-power radar systems. In particular, much of the previous work in

CONFIDENTIAL

the field had limited value because of unsatisfactory test techniques. It should be emphasized that only by proper care can experimental data yield significant information for the complete classification of the power handling capacity of microwave components.

Because of the excessive outlay in time and money required to set up and maintain a high-power testing facility at individual companies working in the field, it is recommended that high-power test facilities in all major frequency bands be set up at convenient locations throughout the country. In this manner the high-power facilities may be used by all the services and civilian establishments on a cooperative basis thereby permitting the interested personnel to directly share the expenses and information of such a venture.

Studies of the breakdown behavior of microwave structures should be extended to other structures such as dielectric loaded waveguides including both the ordinary dielectrics and ferrites. Subsequently, using this information as a guide, experimental and development work should be performed to obtain components of optimum design for microwave applications.

CONFIDENTIAL



CONFIDENTIAL

Studies of breakdown properties and the subsequent development of high-power components should be extended to both the lower and higher microwave frequencies where new radar systems are being suggested or developed.

CONFIDENTIAL



APPENDIX A  
BIBLIOGRAPHY

The following references, listed alphabetically according to the authors, represent a bibliography of the pertinent literature on the subjects of microwave breakdown and transmission-line theory. In addition, a number of articles on direct-current and low-frequency breakdown are included in order to present more completely the phenomena involved in breakdown. The articles containing information on breakdown at frequencies above one megacycle per second are marked with an asterisk.

1. Barlow, H.M. and Cullen, A.L., Microwave Measurements, London, Constable and Co., 1950, pp. 169-170.

\*2. Bevan, A.R., "High-Frequency Discharges Localized Along Tracks of Ionizing Particles", Nature, p. 454, September 10, 1949.

\*3. Biondi, M.A. and Brown, S.C., "Measurements of Ambipolar Diffusion in Helium", Technical Report No. 96, Research Laboratory for Electronics, M.I.T., 1949.

\*4. Biondi, M.A., "Microwave Gas Discharges", Electrical Engineering, vol. 69, p. 806, 1950.

\*5. Brown, S.C., "High Frequency Gas Discharge Breakdown", Proc. I.R.E. 39, 1493 - 501, December 1951.

\*6. Brown, S.C. and MacDonald, A.D., "Limits for the Diffusion Theory of High Frequency Gas Discharge Breakdown", Physical Review, vol. 76, p. 1629, 1949.

\*7. Brown, S.C. et al, "Methods of Measuring the Properties of Ionized Gases at Microwave Frequencies", M.I.T. Research Laboratory for Electronics, Technical Report No. 66, May 17, 1948.

\*8. Cahn, J.H., "Electronic Interaction in Electrical Discharges in Gases", Physical Review, vol. 75, p. 293, 1941.

\*9. Chenot, 1<sup>re</sup> These, Paris, 1947.

\*10. Clarke, H.F., Ragan, G.L., Walker, R.M., and Mansur, I., "Summary of High-Power Breakdown Tests on Microwave Components", M.I.T. Radiation Laboratory, Report No. 1071, Jan. 10, 1946.

11. Cobine, J.D., "Gaseous-Conduction Phenomena and their Application in Electrical Engineering", Electrical Engineering, vol. 69, p. 499, 1950.

CONFIDENTIAL

12. Cohn, S.B., "Properties of Ridge Waveguides", Proc. I.R.E., Vol. 35, pp. 783-788, August 1947.

\*13. Collard, J., "The Measurement of Voltage at Centimetre Wavelengths", Journal of the Institution of Electrical Engineers, vol. 93, Part IIIA, p. 1393, 1946.

14. G.B. Collins, Microwave Magnetrons, M.I.T. Radiation Laboratory Series, Vol. 6, McGraw-Hill Book Co. 1948.

\*15. Cooper, R., "Experiments on the Electric Strength of Air at Centimetre Wavelengths", Journal of the Institution of Electrical Engineers, vol. 94, Part III, p. 315, 1947.

16. Cooper, R., "A Note on the Measurement of Short-Duration Recurrent Voltage Impulses by Means of Spark-Gaps", Journal of the Institution of Electrical Engineers, vol. 95, Part II, p. 370, 1948.

\*17. Cooper, R., "The Mechanism of Breakdown of Air at Ultra High Frequencies", Rep. Brit. Elect. Res. Ass., Ref. L/T 189, 1948.

18. Craggs, J.D. and Meek, J.M., "The Initiation of Low-Pressure Glow Discharges", Proceedings of the Physical Society, vol. 61, p. 327, 1948.

CONFIDENTIAL

\*19. Craggs, J.D. and Meek, J.M., "Recent Research on Spark Discharges in Gases", Research Lond, 4, 4-10, January 1950.

\*20. D. Dettinger and R. Wengenroth (Wheeler Laboratories) "A Standard Waveguide Spark Gap", Transaction of I.R.E. Professional Group on Microwave Theory and Techniques, Vol. M.T.T. -1, pp. 39-48, March, 1953.

21. Druyvestyn, M.J. and Penning, F.M., "The Mechanism of Electrical Discharges in Gases of Low Pressure", Reviews of Modern Physics, vol. 12, p. 87.

\*22. Ekstrand, P.A., "Radio-Frequency Sparkover in Air", Proc. I.R.E., vol. 28, p. 262, 1940.

\*23. Everhart, E. and Brown, S.C., "The Admittance of High Frequency Gas Discharges", Physical Review, vol. 76, p. 839, 1949.

24. Final Report on L-Band Triple Rotating Joint, furnished by Sperry Gyroscope Company to Bureau of Ships under Contract No. NObSr-42419, June 30, 1951.

25. Final Report on Rotary Joints, furnished by Wheeler Laboratories to the Signal Corps Engineering Laboratories, Fort Monmouth, New Jersey, under Contract DA-36-039-sc-5575.

CONFIDENTIAL

26. Fisher, L.H., "An Attempt to Verify the Theory of the Long Spark of Loeb and Meek", Physical Review, vol. 76, p. 423, 1942.

27. Fisher, L.H., "Mechanism of the Spark Breakdown, Electrical Engineering, vol. 69, p. 613, 1950.

28. Fisher, L.H. and Bederson, B., N.Y.U. "Formative Time Lags of Spark Breakdown in Air in Uniform Fields at Low Overvoltages", Physical Review, p. 109, Jan. 1951.

\*29. Francis, G. and Von Engel, A., "Development of the Low-Pressure Electrodeless Discharge in a High-Frequency Electric Field", Letter in Proceedings of the Physical Society B, vol. 63, p. 823, 1950.

\*30. Gill, E.W.B. and Donaldson, R.H., "The Sparking Potential of Air for High-Frequency Discharges", Philosophical Magazine, vol. 12, p. 719, 1931.

\*31. Gill, E.W.B. and Von Engel, A., "Starting Potentials of High-Frequency Gas Discharges at Low Pressure", Proceedings of the Royal Society A, vol. 192, p. 446, 1948.

\*32. Githens, S., "The Influence of Discharge-Chamber Structure Upon the Initiating Mechanism of the High-Frequency Discharge", Physical Review, vol. 57, p. 822, 1940.



\*33. Gould L., and Brown, S.C., "Microwave Determination of the Probability of Collision of Electrons in Helium", Physical Review, vol. 95, pp. 897-903, August 15, 1954.

\*34. Gutton, C. and Gutton, H., Comptes Rendus, vol. 186, p. 303, 1928.

\*35. Hale, D.H., "The Breakdown of Gases in High-Frequency Electrical Fields", Physical Review, vol. 73, p. 1046, 1948.

36. Hardy, D.R. and Craggs, J.D., "The Irradiation of Spark Gaps for Voltage Measurement", Transactions of the American Institute of Electrical Engineers, vol. 69, Part I, p. 584, 1950.

37. Haseltine, W.R., "The Sparking Threshold in Air", Physical Review, vol. 58, p. 188, 1940.

\*38. Herlin, M.A. and Brown, S.C., "Breakdown of a Gas at Microwave Frequencies", Physical Review, vol. 74, p. 291, 1948.

\*39. Herlin, M.A. and Brown, S.C., "Electrical Breakdown of a Gas Between Coaxial Cylinders at Microwave Frequencies", Physical Review, vol. 74, p. 910, 1948.



CONFIDENTIAL

\*40. Herlin, M.A. and Brown, S.C., "Microwave Breakdown of a Gas in a Cylindrical Cavity of Arbitrary Length", Physical Review, vol. 74, p. 1650, 1948.

\*41. Holstein, T., Physical Review, vol. 69, p. 50(A), 1946.

\*42. Holstein, T., "Energy Distribution of Electrons in High-Frequency Gas Discharges", Physical Review, vol. 70, p. 367, 1946.

\*43. Honda, K., "On the Sparking Criterion of High Frequency Breakdown", Japan Sc. Rev., vol. 1, pp. 64-8, March 1949.

44. Jahnke and Emde, "Tables of Functions with Formulae and Curves", Fourth Edition 1945.

\*45. Jones, F.L., "Electrical Discharges", Rep. Prog. Phys., vol. 16, pp. 216-65, 1953.

46. Jones, F.L. and Parker, A.B., "Mechanism of the Electric Spark", Nature, vol. 165, p. 960, 1950.

\*47. Jones, F.L., Morgan, G.D., "High Frequency Discharges - I. Breakdown Mechanism and Similarity Relationships", Proc. Phy. Soc., Lond B 64, pp. 560-73, July 1951.

CONFIDENTIAL

\*48. Jones, F.L., Morgan, G.D., "High Frequency Discharges - II Similarity Relationship for Minimum Maintenance Potentials", Proc. Phy. Soc., Lond B 64, pp. 574-8, July, 1951.

49. M. Kaplan, Report No. RR-605, "Engineering Report on the Measurement of the Effect of Sulphur Hexafluoride SF<sub>6</sub> on the Power Carrying Capacity of Waveguide, Airtron, Inc. October 16, 1953.

50. Kennard, E.H., Kinetic Theory of Gases, pp. 271, 286, McGraw-Hill, New York, 1942.

51. Kihaka, Taro, "The Mathematical Theory of Electrical Discharges", Rev. Mod. Phys., 24, pp. 43-61, January 1952

52. Kirchner, F., "The Effect of a Direct-Current Potential on the Initiation of Radio-Frequency Discharge", Letter in Physical Review, vol. 72, p. 348, 1947.

\*53. Kojima, S. and Takayama, K., "Probe Measurements for High-Frequency Discharge", Journal of the Physical Society of Japan, vol. 4, p. 349, 1949.

\*54. Krasik, S., Alpert, D. and McCoubrey, A.O., "Break-down and Maintenance of Microwave Discharges in Argon", Physical Review, vol. 76, p. 722, 1949.

\*55. Labrum, C.S., I. R. Australia, RPR. 85, December, 1947.

\*56. Lassen, arch. f. Elek. vol. 25, p. 322, 1931.

\*57. Lathrop, J.W. and Brown, S.C., "The Relationship of Pulsed to C-W Breakdown of a Gas at Microwave Frequencies", M.I.T. Research Laboratory for Electronics, Technical Report No. 146, December 1, 1949.

58. Lawson, A. and Fano, R., "The Design of Microwave Filters", Microwave Transmission Circuits, ed. G. Ragan, Radiation Laboratory Series, Vol. 9, New York, McGraw-Hill, 1948, pp. 654-657.

\*59. Lax, B., et al, "The Effect of a Magnetic Field on the Breakdown of Gases at Microwave Frequencies", M.I.T. Research Laboratory for Electronics, Technical Report No. 165, June 30, 1950.

60. Loeb, L.B., Fundamental Processes of Electrical Discharge Through Gases, John Wiley and Sons, Inc., New York, 1939.

61. Loeb, L.B., "Electrical Discharge Through Gases", Journal of the Institution of Electrical Engineers, vol. 94, Part I, p. 349, 1947.

62. Loeb, L.B., "Statistical Factors in Spark Discharge Mechanisms", Review of Modern Physics, vol. 20, p. 151, 1948.

63. Loeb, L.B., "Certain Aspects of Mechanism of Spark Discharge", Proceedings of the Physical Society, vol. 60, p. 561, 1948.

64. Loeb, L.B., "The Threshold for Spark Development by Streamer Mechanism in Uniform Fields", Physical Review, vol. 74, p. 210, 1948.

65. Loeb, L.B., "Some Aspects of Breakdown Streamers", Physical Review, vol. 94, p. 227-32, April 15, 1954

\*66. McDonald, A.D. and Betts, D.D., "High Frequency Gas Discharge Breakdown in Neon", Canad. J. Phys. 30, pp. 565-76, September, 1952.

\*67. MacDonald, A.D. and Brown, S.C., "High-Frequency Gas Discharge Breakdown in Helium", Physical Review, vol. 75, p. 411, 1949.

\*68. MacDonald, A.D. and Brown, S.C., "High-Frequency Gas Discharge Breakdown in Hydrogen", Physical Review, vol. 76, p. 1634, 1949.

69. Marcuvitz, N., Waveguide Handbook, Radiation Laboratory Series, vol. 10, New York, McGraw-Hill, 1951.

\*70. Margenau, H., "Conduction and Dispersion of Ionized Gases at High Frequencies", Physical Review, vol. 69, p. 508, 1946.

\*71. Margenau, H., McMillan, F.L., Dearnley, I.H., Pearsall, C.S. and Montgomery, C.G., "Physical Processes in the Recovery of T-R Tubes", Physical Review, vol. 70, p. 349, 1946.

\*72. Margenau, H. and Hartman, L.M., "Theory of High-Frequency Gas Discharges", Physical Review, vol. 73, Parts I-IV, p. 297, 1948.

73. Meek, J.M., "A Theory of Spark Discharge", Physical Review, vol. 57, p. 722, 1940.

74. Meek, J.M., "The Electric Spark in Air", Journal of the Institution of Electrical Engineers, vol. 89, p. 335, 1942.

75. Meek, J.M., "The Influence of Irradiation on the Measurement of Impulse Voltages with Sphere Gaps", Journal of the Institution of Electrical Engineers, vol. 93, Part II, p. 97, 1946.

\*76. Meek, J.M. and Craggs, J.D., Electrical Breakdown of Gases, Oxford, Caredon Press, p. 507, 1953.



\*77. Mehta, G.K., "Phenomena of High-Frequency Discharge", Journal of the University of Bombay, vol. 16, p. 63, 1948.

78. Miller, C.G. and Loeb, L.B., "Spark Breakdown at Atmospheric Pressure and Above in Relation to Paschen's Law", Physical Review, vol. 73, p. 84, 1948.

79. Montgomery, Dicke, Parcell, Principles of Microwave Circuits, M.I.T. Radiation Laboratory Series, vol. 8, McGraw-Hill, First Edition, 1948.

\*80. Moore, K.R. and Miley, H.A., "Magnetron Starting Time", M.I.T. Radiation Laboratory, Technical Report No. 509, March 1944.

81. Moreno, T., Microwave Transmission Design Data, New York, McGraw-Hill, 1948.

\*82. Morgan, G.D., "High Frequency Discharges In Gases", Sci. Prog., vol. 41, pp. 22-41, January 1953.

\*83. Pim, J.A., "Electrical Breakdown Strength of Air at Ultra-High Frequencies", Nature, vol. 161, p. 683, 1948.

\*84. Pim, J.A., "The Electrical Breakdown Strength of Air at Ultra-High Frequencies", Proceedings of the Institute of Electrical Engineers, vol. 96, Part III, p. 117, 1949.



\*85. Posin, D.Q., Mansur, I. and Clarke, H., "Experiments in Microwave Breakdown", M.I.T. Radiation Laboratory, Technical Report No. 731, Nov. 28, 1945.

\*86. Posin, D.Q., "The Microwave Spark", Physical Review, vol. 73, p. 496, 1948.

\*87. Prowse, W.A., "The Initiation of Breakdown in Gases Subject to High-Frequency Electric Fields", Journal of the British Institution of Radio Engineers, vol. 10, p. 333, 1950.

\*88. Prowse, W.A., "A Note on Ultra-High-Frequency Gas Breakdown", Proceedings of the Institution of Electrical Engineering, vol. 97, Part III, p. 253, 1950.

\*89. Prowse, W.A. and Cooper, R., "Gas Discharges at Centimetre Wavelengths", Nature, vol. 161, p. 310-11, 1948.

\*90. Prowse, W.A. and Jasinski, W., "Oscillographic Observations on Ultra-High-Frequency Sparks", Letter in Nature, vol. 163, p. 103, 1949.

\*91. Prowse, W.A., Jasinski, W., "Observations on The Electrical Breakdown of Gases at 2800 Mc", Inst. Elec. Eng. Monogra. No. 10, October 1951, (to be published - Proc. Inst. Elec. Engrs. Pt. IV, 98, pp. 101-11, October 1951.

\*92. Ragan, G.L., Microwave Transmission Circuits, Radiation Laboratory Series, vol. 9, McCraw-Hill, New York, 1948.

93. Reukema, L.E., Transactions of American Institute of Electrical Engineers, vol. 47, p. 38, 1928.

\*94. Robertson, J.K., Kenney, J.R. and Nixon, W.C., "Discharges Excited by Microwaves", Letter in Nature, vol. 164, p. 100, 1949.

\*95. Robinson, C.F., "Observations on Some Properties of Ultra-High Frequency Gas Discharges", Review of Scientific-Instruments, vol. 21, p. 617, 1950.

96. Roether, H., Z. Physik, vol. 97, p. 758, 1935.

\*97. Rose, D.J. and Brown, S.C., "High Frequency Gas Discharge Plasma in Hydrogen", Phys. Rev., vol. 96, No. 2, pp. 310-16, April 15, 1955.

98. Schumb, W.D., J.G. Trump, and G.L. Priest, "Effect of High Voltage Electrical Discharge on Sulphur Hexafluoride", Industrial and Engineering Chemistry, vol. 41, pp. 1348-1351, July 1949.

99. Schwiebert, H., "Wideband Waveguide Rotary Joint", IRE Convention Record: Part 8 - Communications and Microwave, 1955.

100. J.W. Sutherland, "Electrical Breakdown in Waveguides at 3000 Mc/s," Electrical Engineering, vol. XXVI, pp. 538-540, December 1954.

\*101. Townsend, J.S., Philosophical Magazine, vol. 7, p. 745, 1932.

\*102. Townsend, J.S. and Gill, E.W.B., "Generalization of the Theory of Electrical Discharges", Philosophical Magazine, vol. 26, p. 290, 1938.

103. Trump, J.D., Cloud, R.W., Mann, J.G. and Hanson, E.P., "Influence of Electrodes on D-C Breakdown in Gases at High Pressure", Electrical Engineering, vol. 69, p. 961, 1950.

\*104. Varela, A.A., "Effect of Direct-Current Potential on Initiation of Radio-Frequency Discharge", Letter in Physical Review, vol. 71, p. 124, 1947.

\*105. Walker, R., "K-Band High Power Water Load", M.I.T. Radiation Laboratory, Technical Report No. 723.

106. White, H.J., Physical Review, vol. 46, p. 99, 1934.

107. White, H.J., "Variation of Sparking Potential with Intense Ultra-Violet Illumination", Physical Review, vol. 48, p. 113, 1935.

108. White, H.J., "Effect of Intense Illumination on Time Lag in Static Spark Breakdown", Physical Review, vol. 49, p. 507, 1936.

109. Wijsman, R.A., "Breakdown Probability of a Low-Pressure Gas Discharge", Physical Review, vol. 75, p. 833, 1949.

110. Wilson, R.R., "Very Short Time Lag of Sparking", Physical Review, vol. 50, p. 1082, 1936.



CONFIDENTIAL

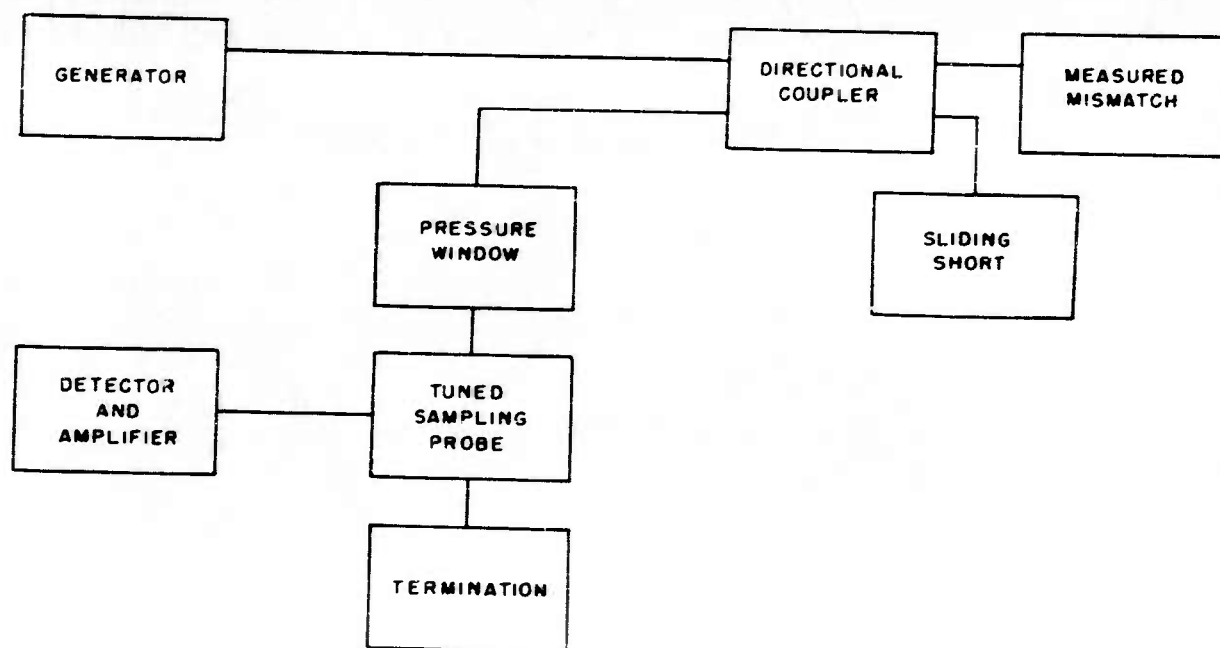


FIGURE 1  
SETUP FOR CALIBRATION  
OF SLIDING-SHORT REFLECTOMETER

CONFIDENTIAL





CONFIDENTIAL

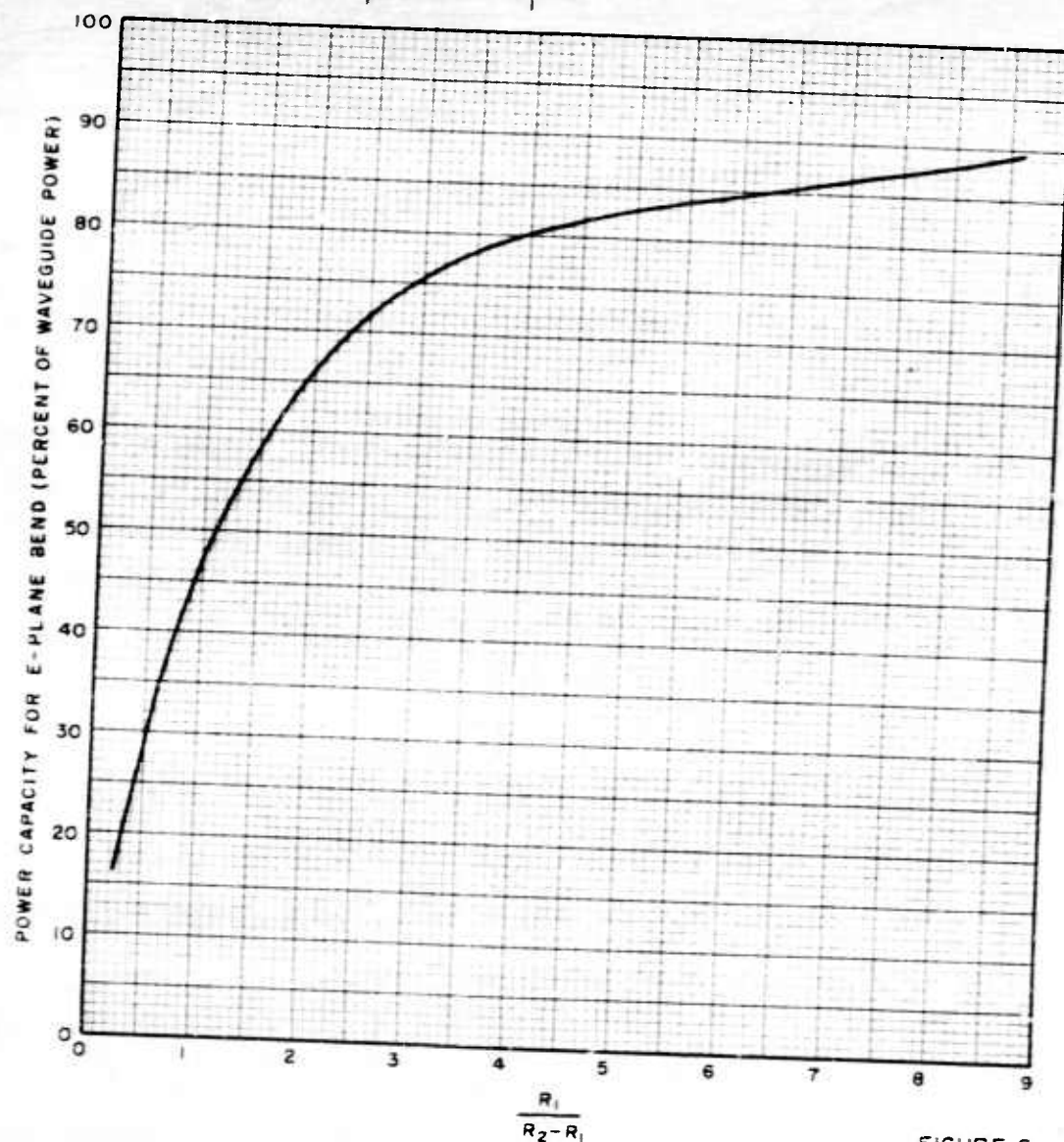
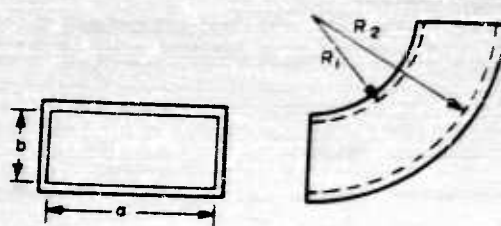


FIGURE 2  
NORMALIZED PLOT OF  
POWER CAPACITY OF AN  
E-PLANE BEND

CONFIDENTIAL





CONFIDENTIAL

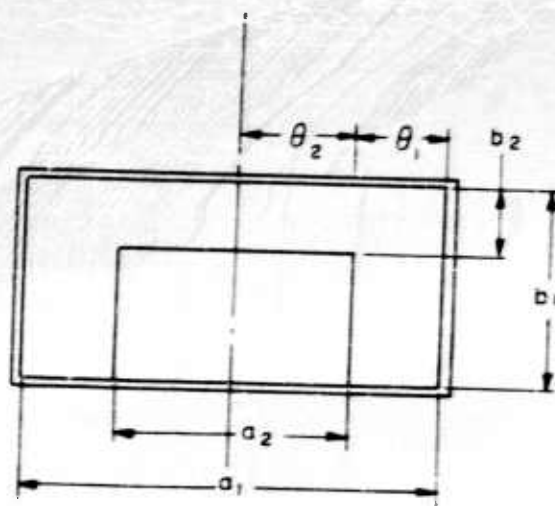


FIGURE 3  
PERTINENT DIMENSIONS  
OF RIDGE WAVEGUIDE

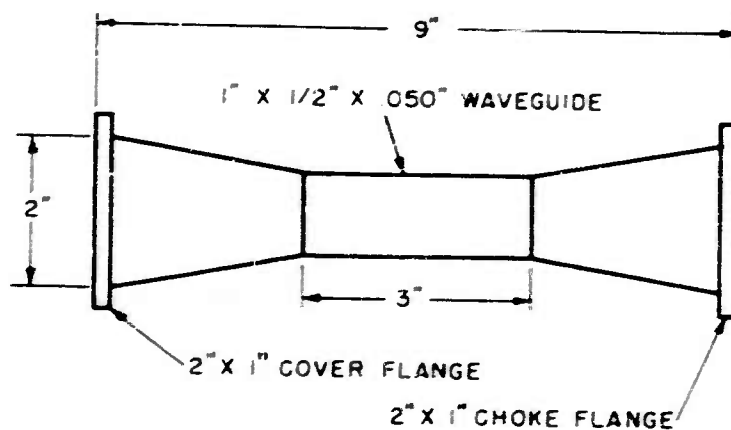


FIGURE 4  
TEST PIECE  
2" X 1" TO 1" X 1/2" TAPER WAVEGUIDE

CONFIDENTIAL

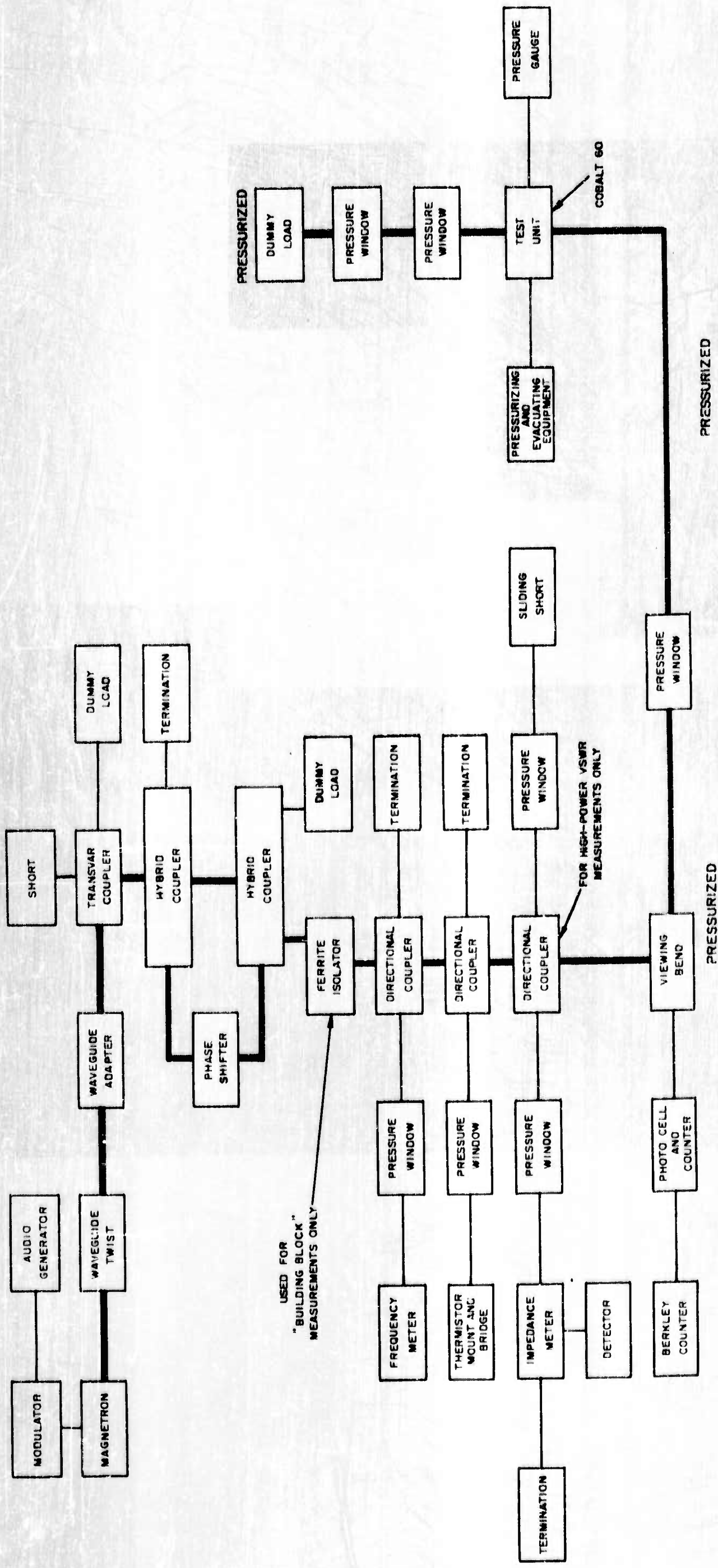


FIGURE 5  
CIRCUIT FOR MEASUREMENT OF  
HIGH-POWER BREAKDOWN



CONFIDENTIAL

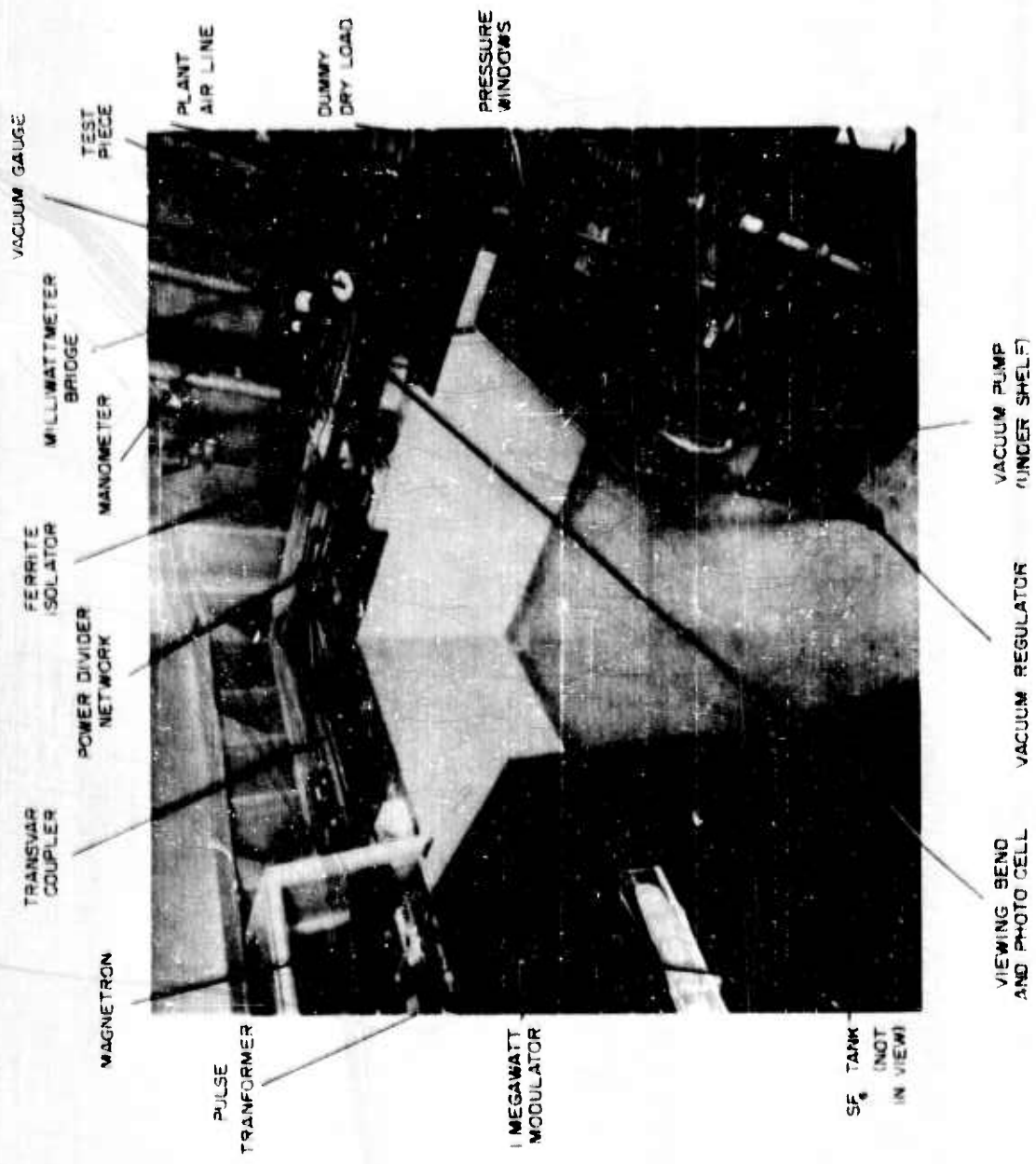


FIGURE 6  
OVER-ALL PICTURE OF HIGH-POWER  
BREAKDOWN TESTING FACILITIES

CONFIDENTIAL





CONFIDENTIAL

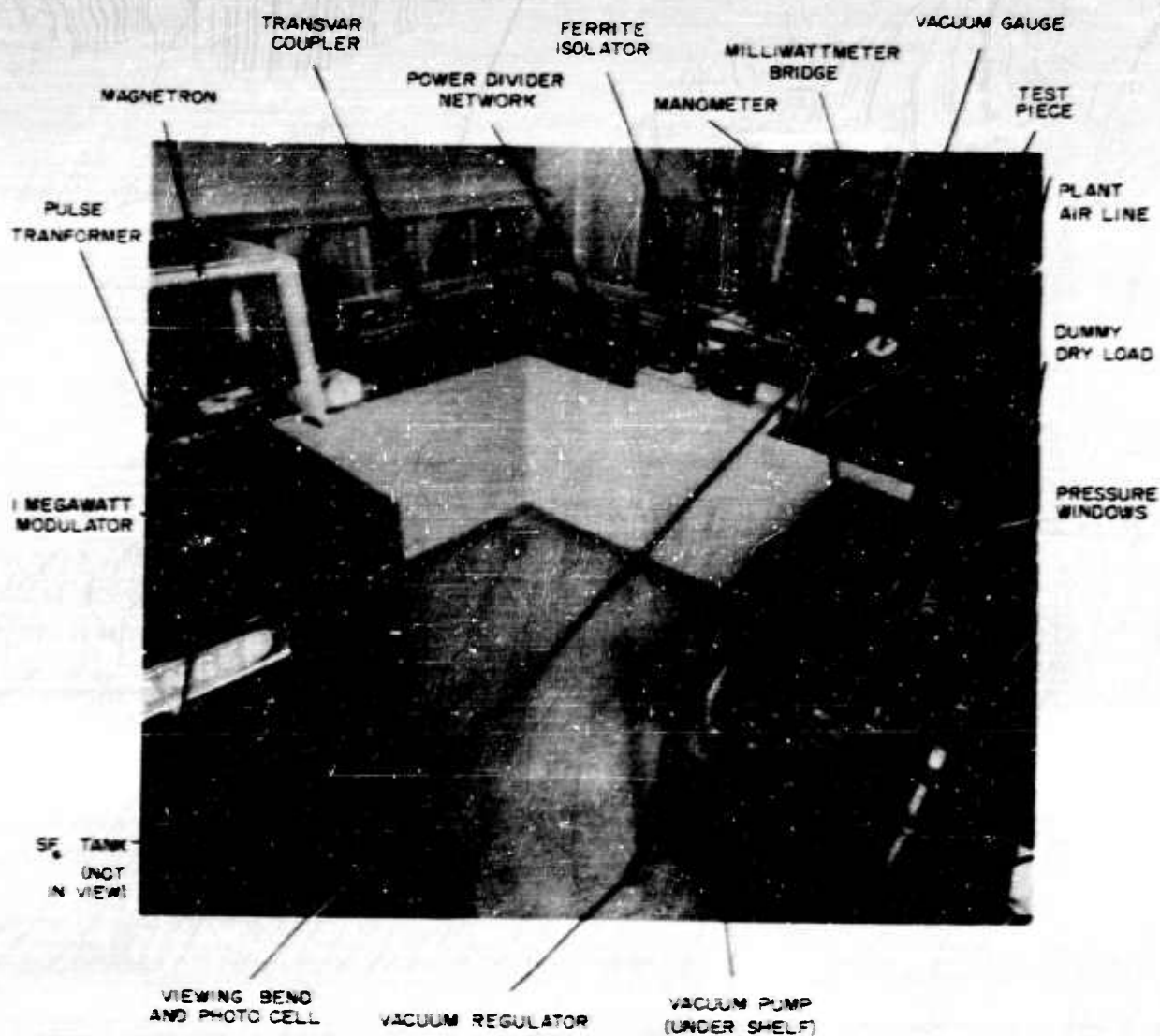


FIGURE 6  
OVER-ALL PICTURE OF HIGH-POWER  
BREAKDOWN TESTING FACILITIES

CONFIDENTIAL



CONFIDENTIAL

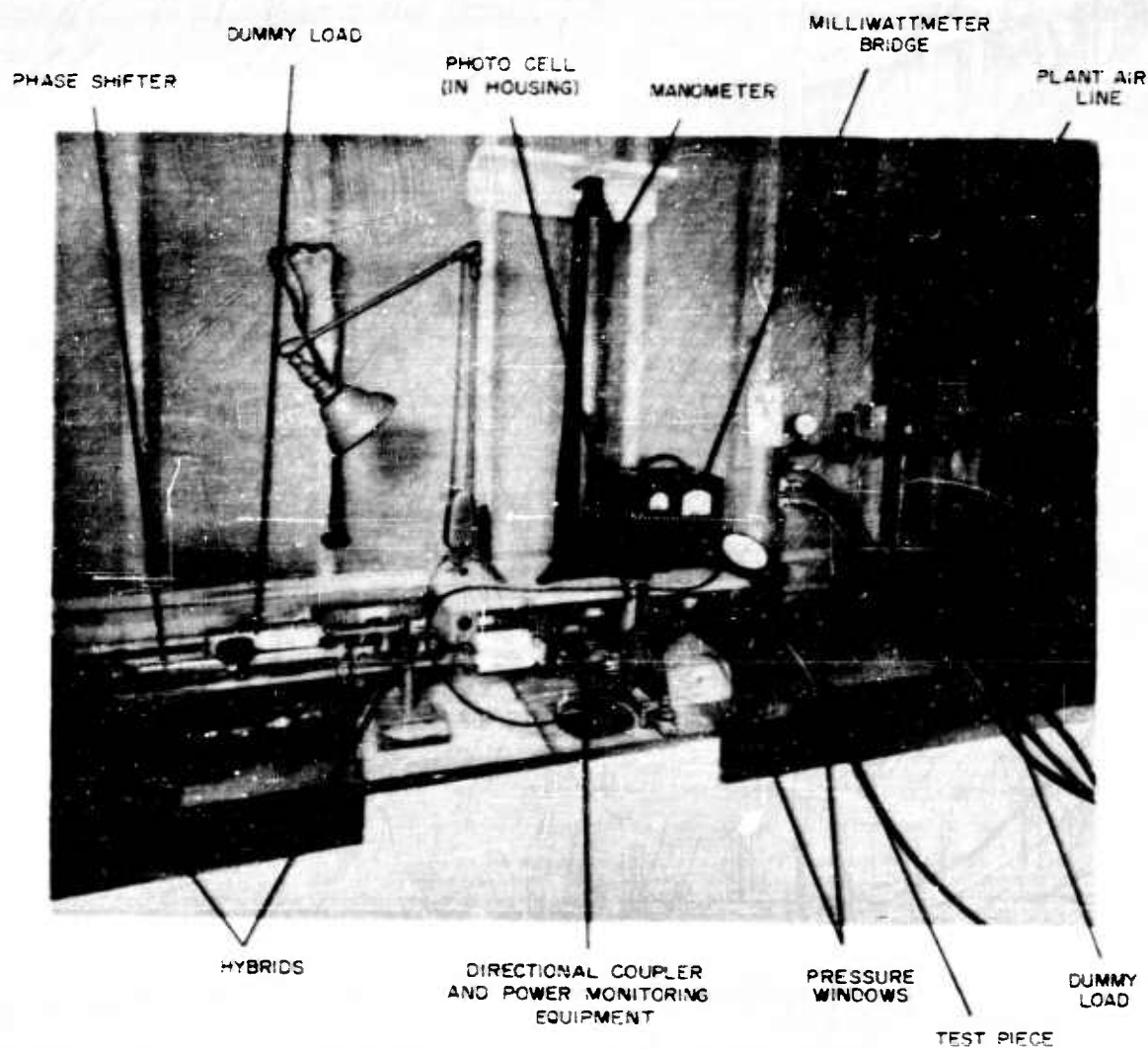


FIGURE 7  
CLOSE-UP PICTURE OF TEST SECTION

CONFIDENTIAL



CONFIDENTIAL

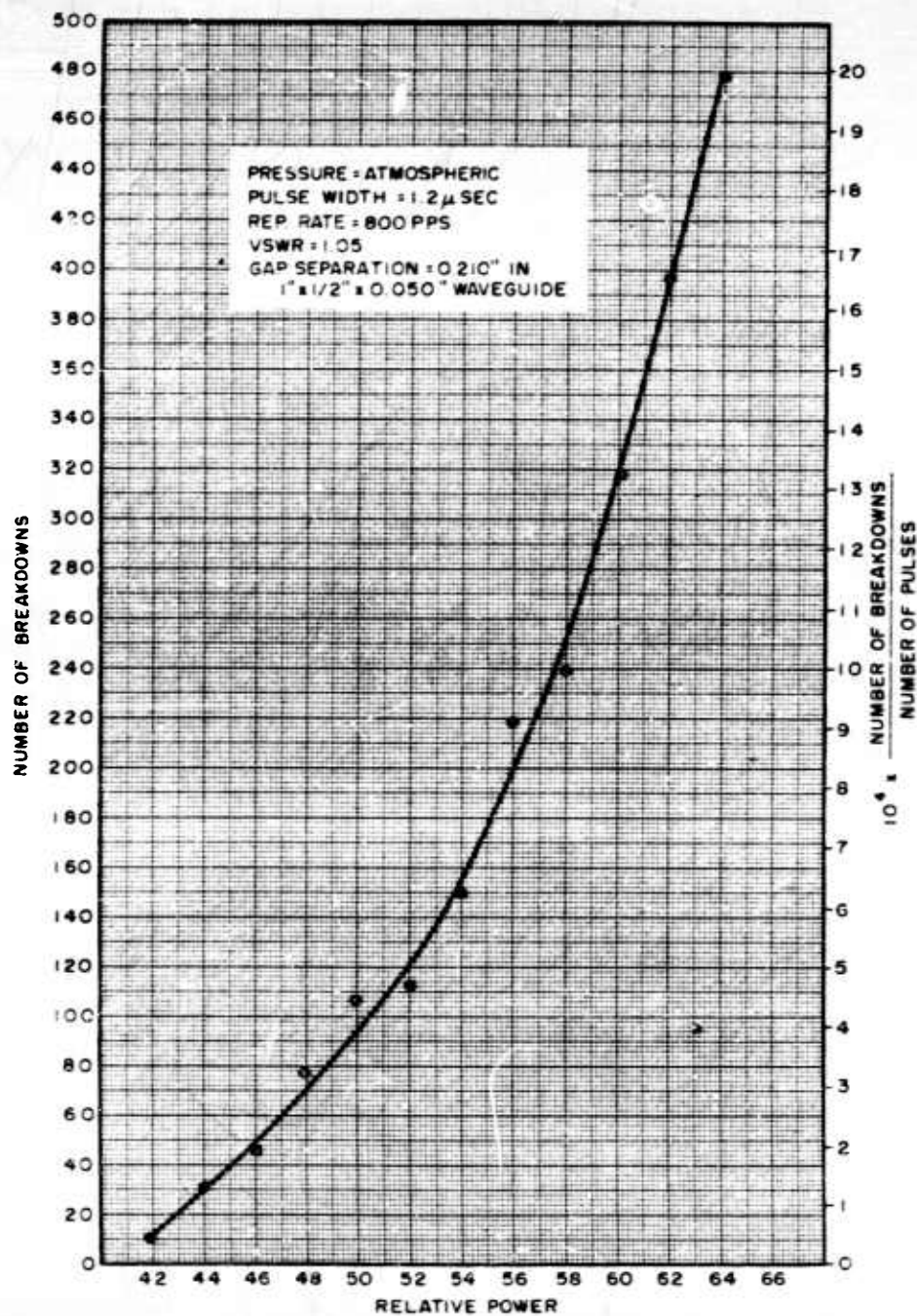


FIGURE 8  
BREAKDOWN PROBABILITY  
FOR SPARK GAP  
CONFIDENTIAL





CONFIDENTIAL

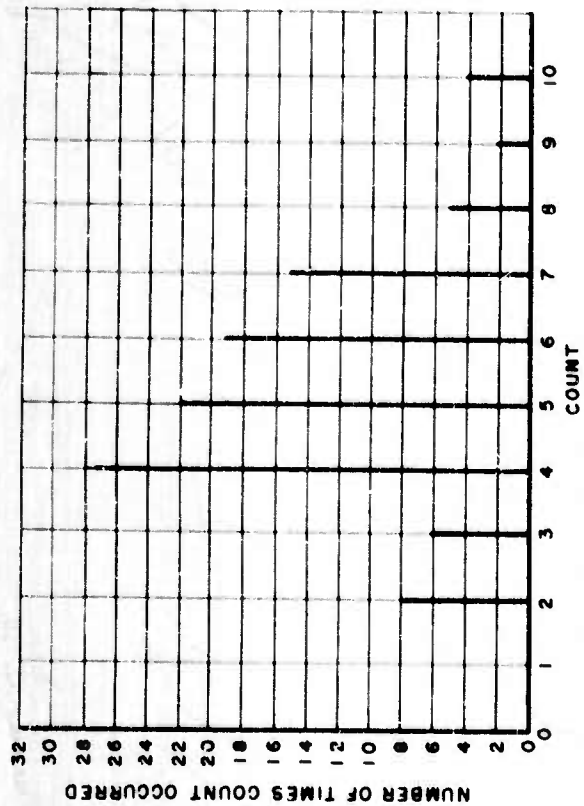


FIGURE 9

HISTOGRAM FOR HIGH-VOLTAGE BREAKDOWN  
(BRIDGE READING: 30 mw, TIME INTERVAL: 15 SEC)

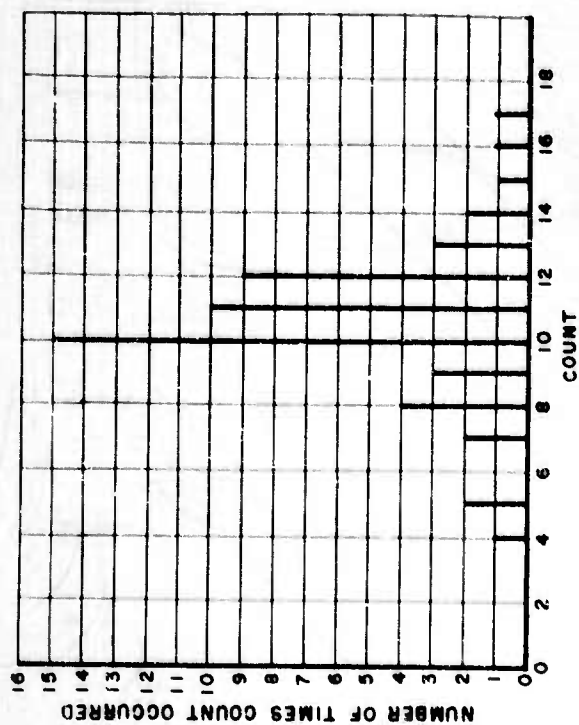


FIGURE 10

HISTOGRAM FOR HIGH-VOLTAGE BREAKDOWN  
(BRIDGE READING: 30 mw, TIME INTERVAL: 30 SEC)

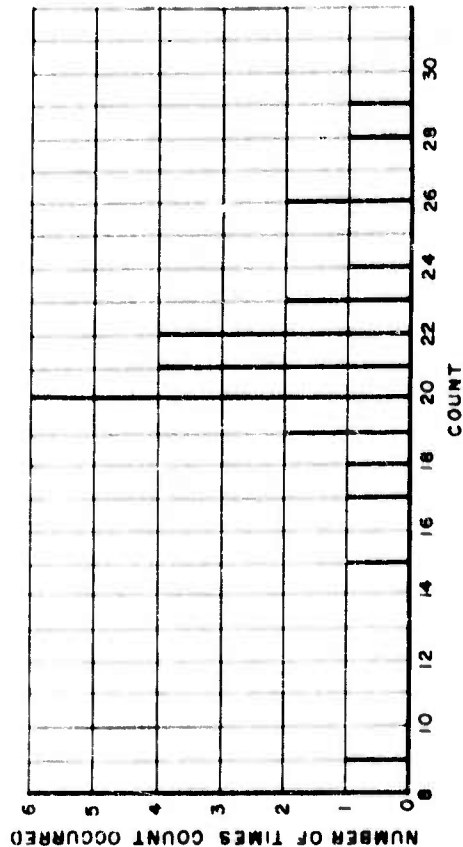


FIGURE 11

HISTOGRAM FOR HIGH-VOLTAGE BREAKDOWN  
(BRIDGE READING: 30 mw, TIME INTERVAL: 1 MIN)

CONFIDENTIAL



CONFIDENTIAL

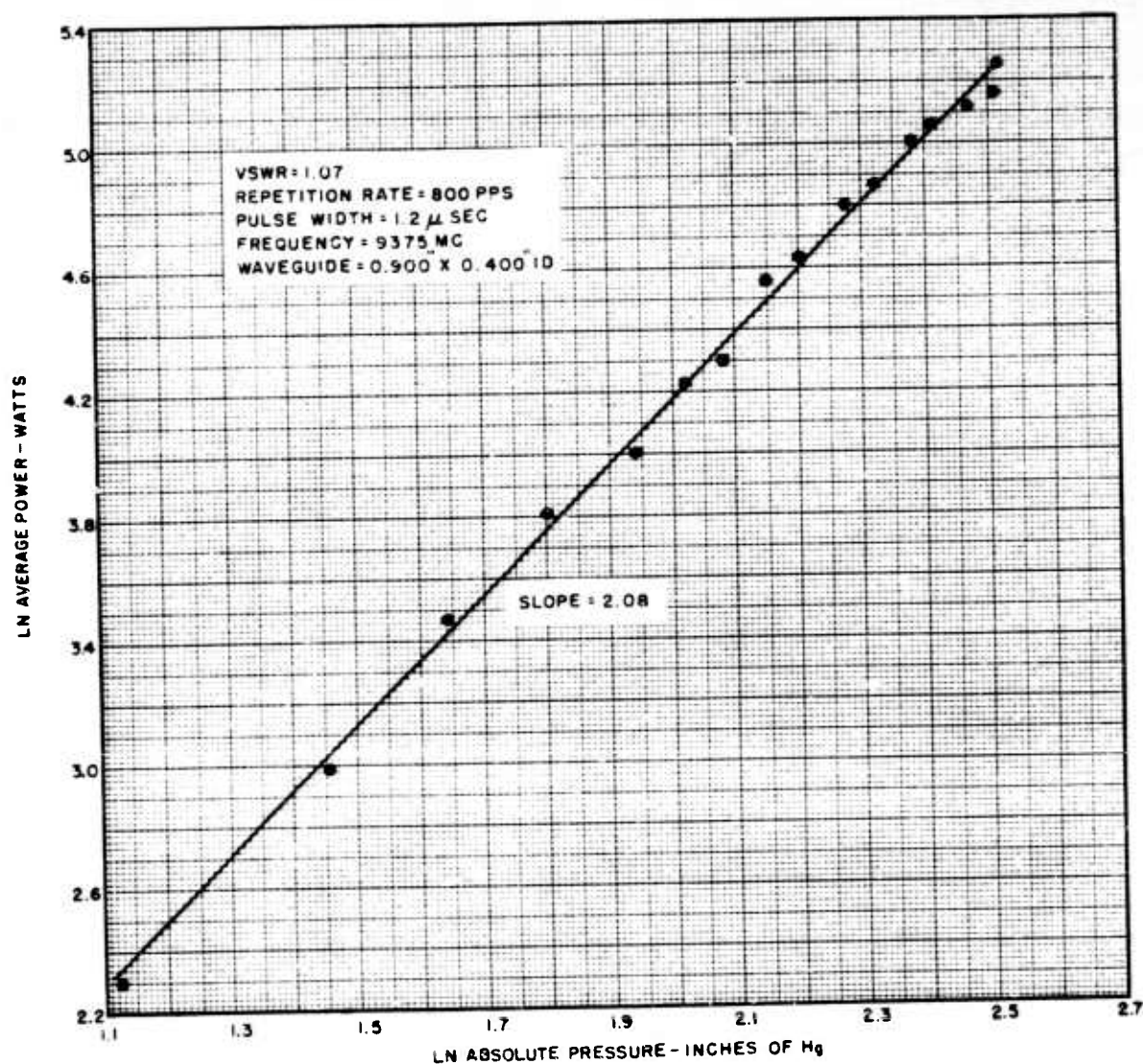


FIGURE 12  
BREAKDOWN POWER vs. PRESSURE  
WITH COBALT IN CONTACT WITH  
TAPERED-WAVEGUIDE BREAKDOWN GAP

CONFIDENTIAL



CONFIDENTIAL

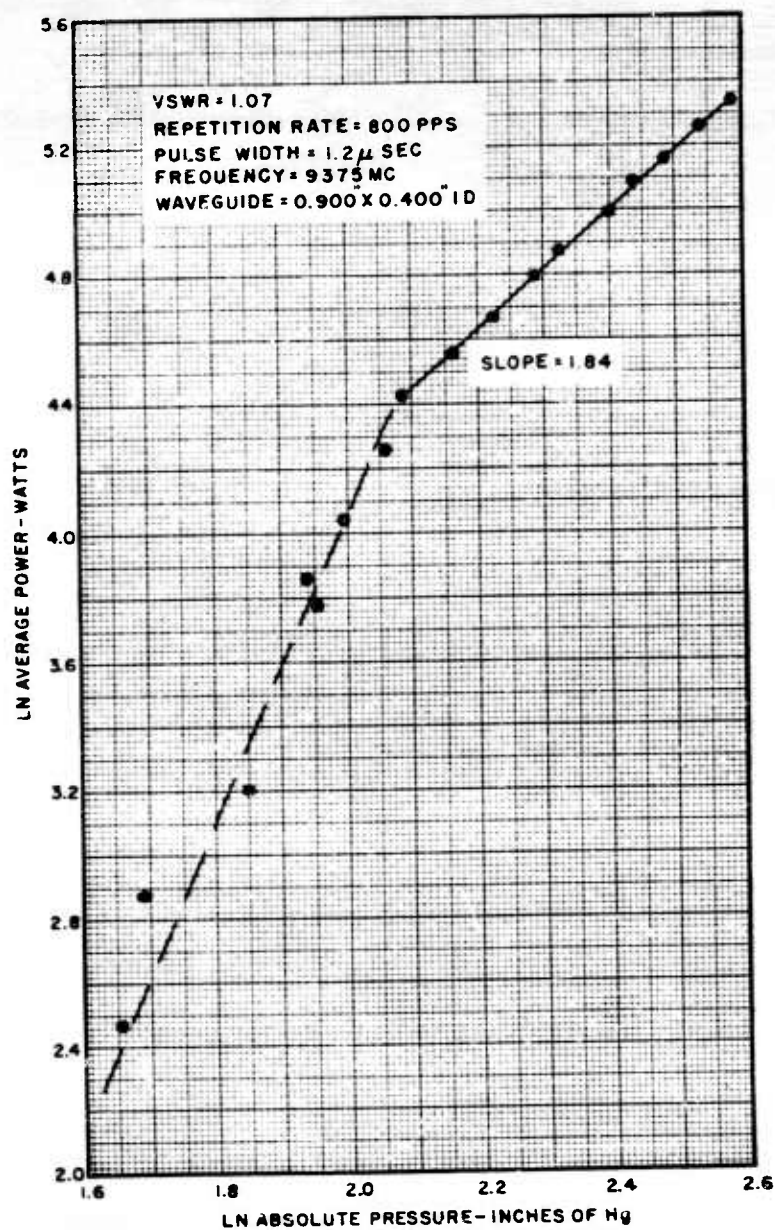


FIGURE 13  
BREAKDOWN POWER VS. PRESSURE WITH COBALT 1" ABOVE  
TAPERED-WAVEGUIDE BREAKDOWN GAP

CONFIDENTIAL



CONFIDENTIAL

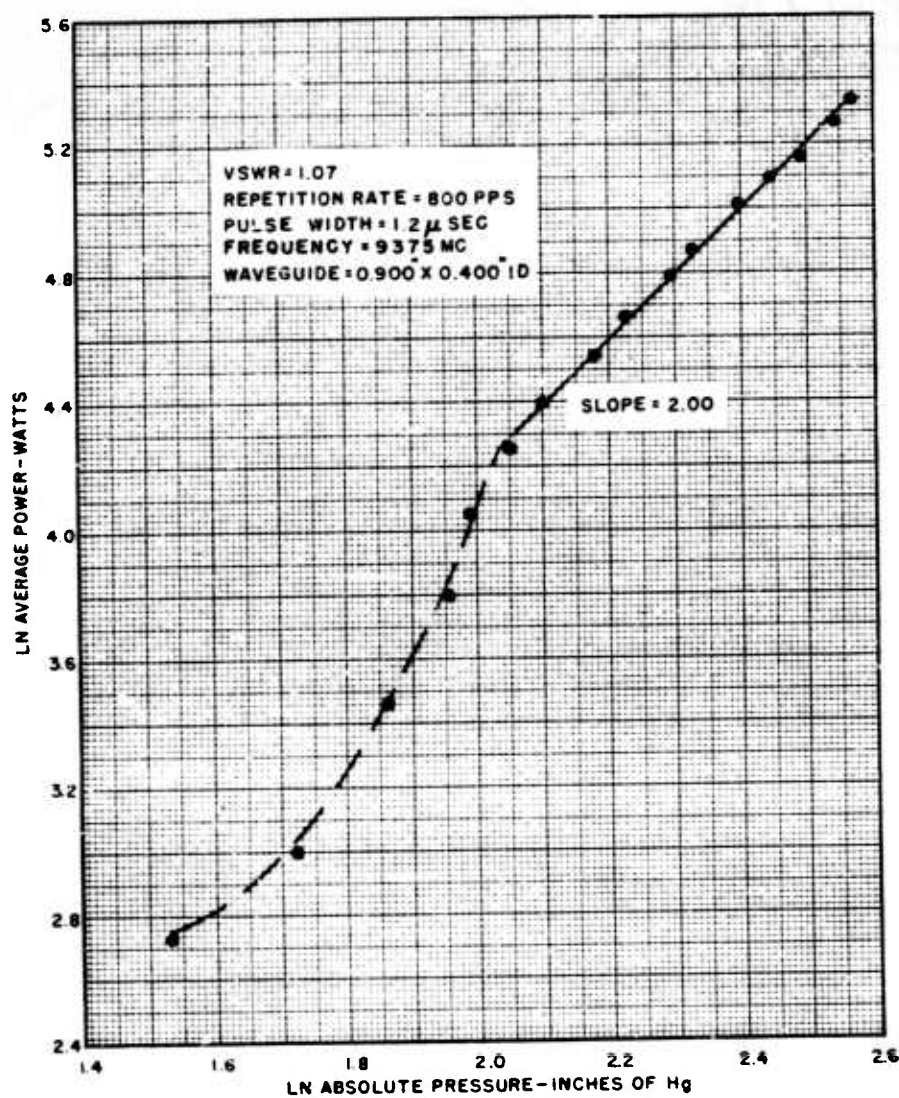


FIGURE 14  
BREAKDOWN POWER vs. PRESSURE WITH COBALT 2" ABOVE  
TAPERED-WAVEGUIDE BREAKDOWN GAP

CONFIDENTIAL





CONFIDENTIAL

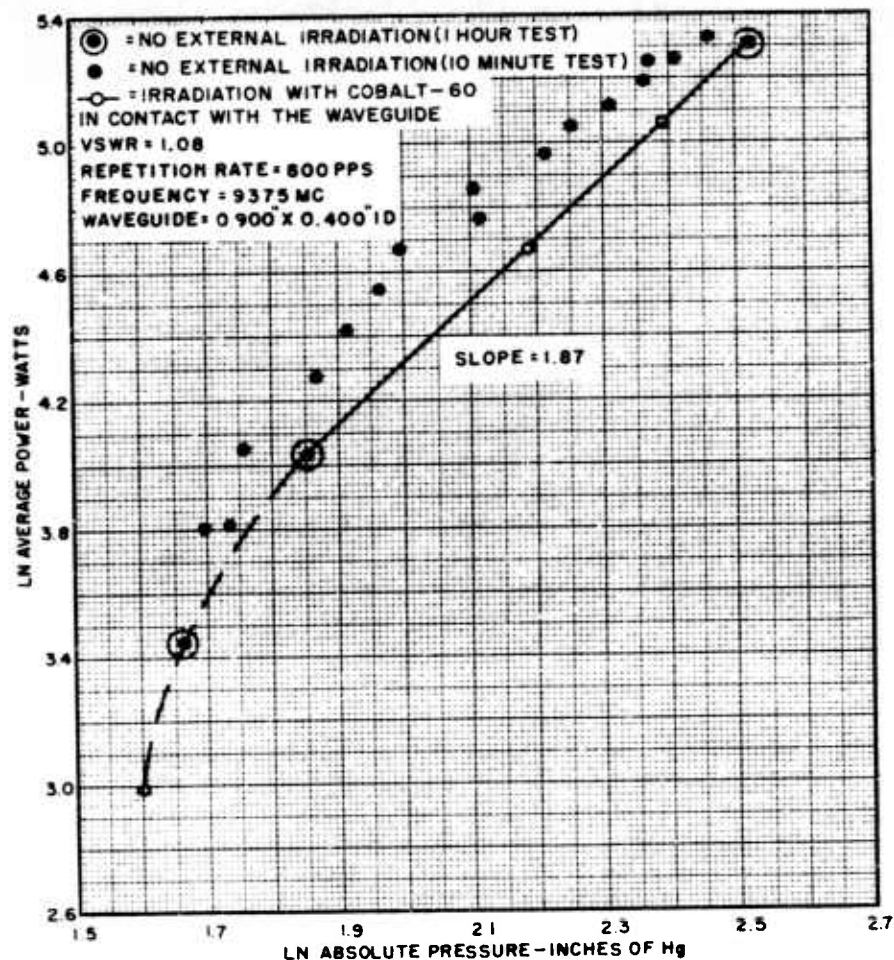


FIGURE 15  
BREAKDOWN POWER vs. PRESSURE  
FOR A PULSE WIDTH OF  $1.2\mu$  SEC

CONFIDENTIAL





CONFIDENTIAL

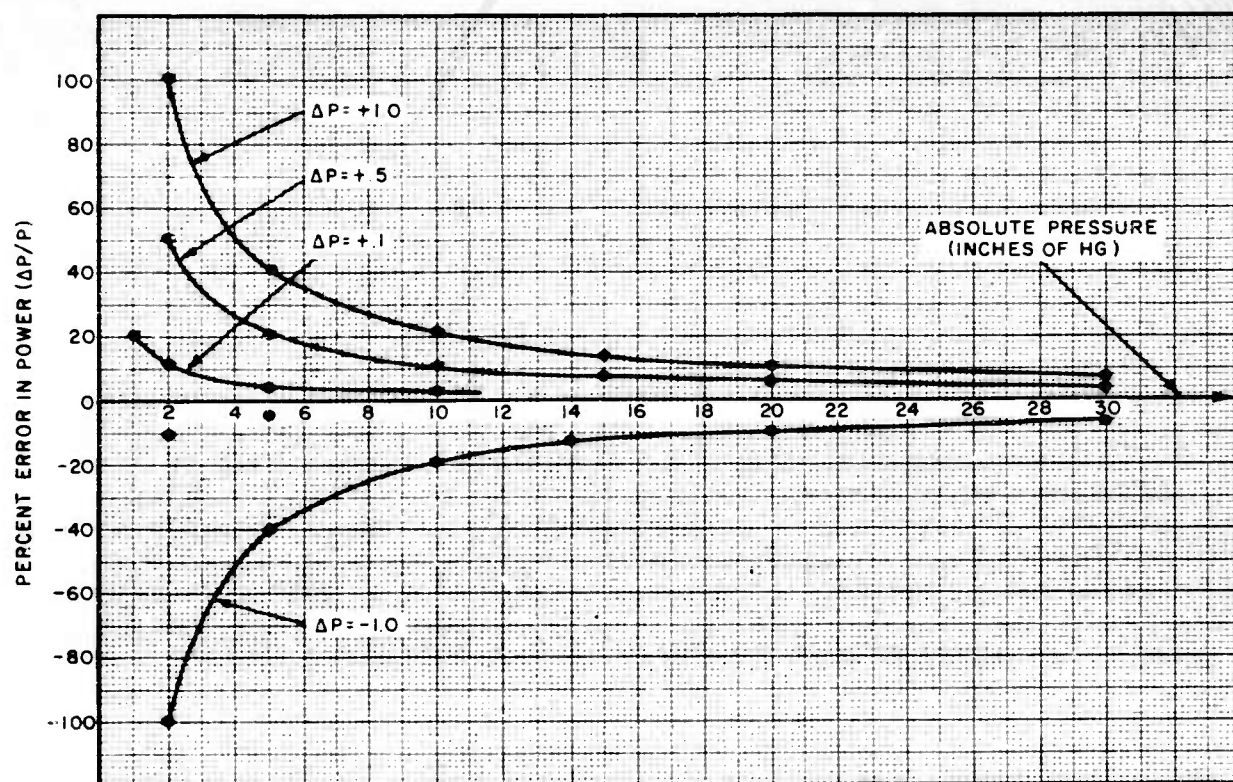


FIGURE 16  
ERROR IN BREAKDOWN POWER VS PRESSURE WITH  
THE ERROR IN PRESSURE AS A PARAMETER

CONFIDENTIAL



CONFIDENTIAL



TOP

SIDE

BOTTOM

SIDE

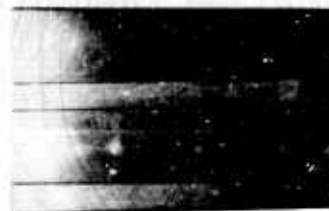


FIGURE 17  
PHOTOGRAPH OF BREAKDOWN SPOTS

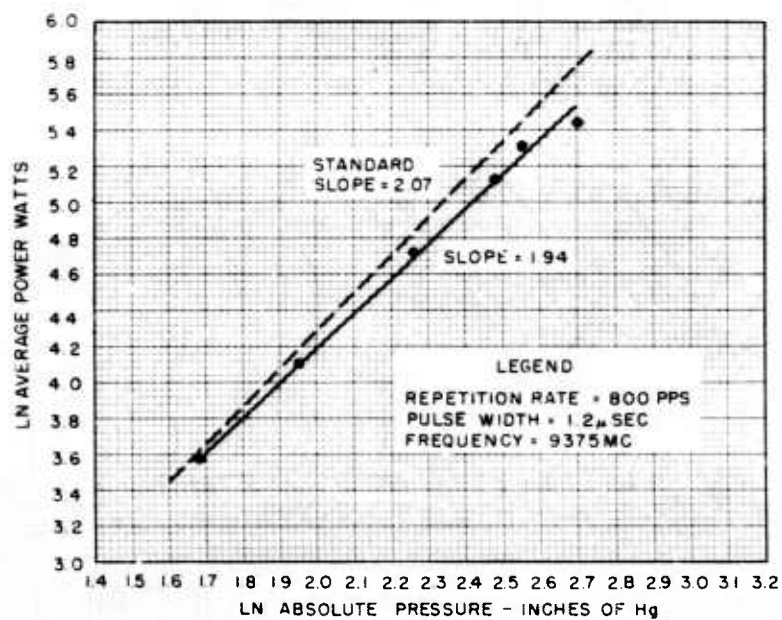


FIGURE 18  
POWER VS PRESSURE  
FOR 300-400 RMS FINISH  
(1"X 1/2"X C 050" WAVEGUIDE)

CONFIDENTIAL



CONFIDENTIAL

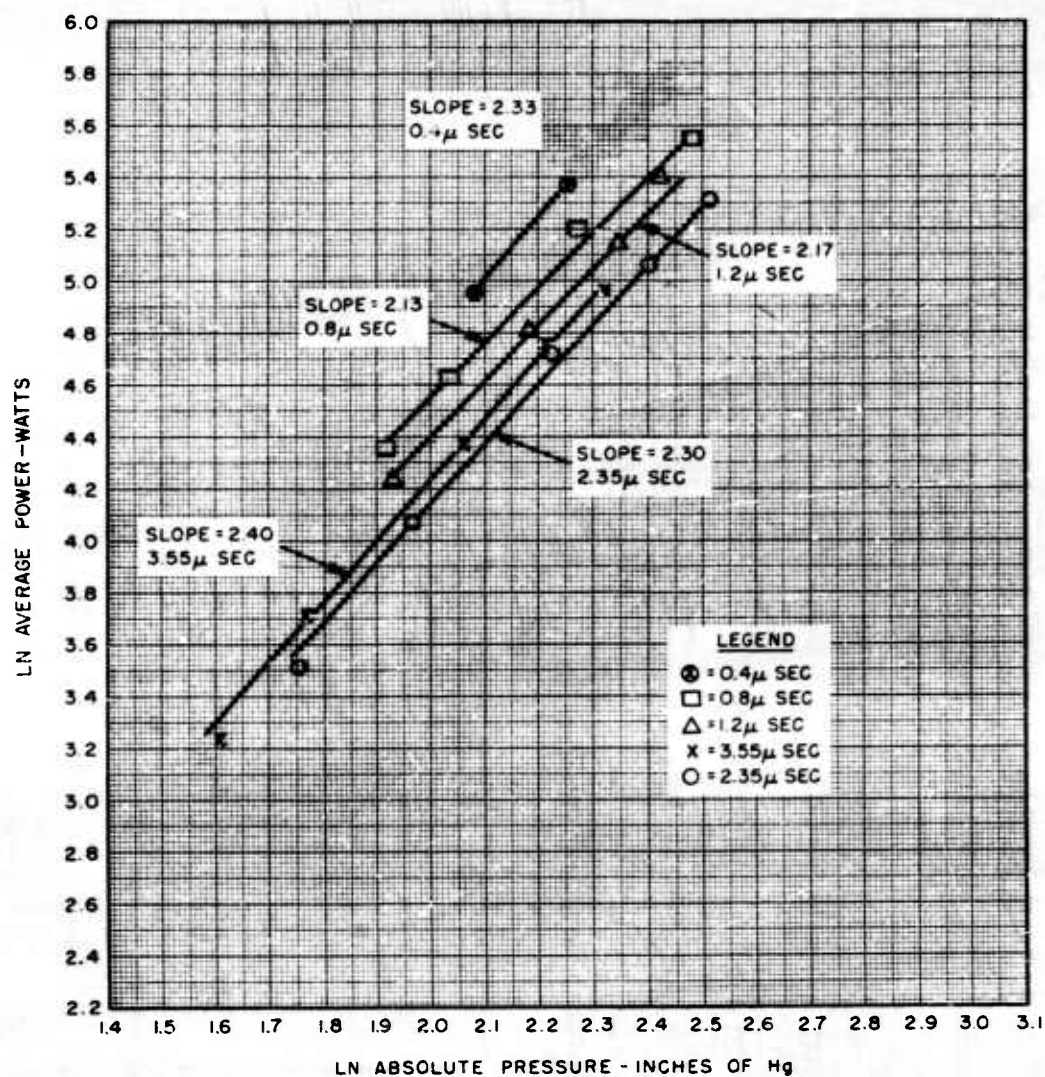


FIGURE 19  
VARIATION OF PULSE WIDTH AT CONSTANT 400-PPS  
REPETITION RATE OF 1" X 1/2" X 0.050" WAVEGUIDE TEST SECTION

CONFIDENTIAL





CONFIDENTIAL

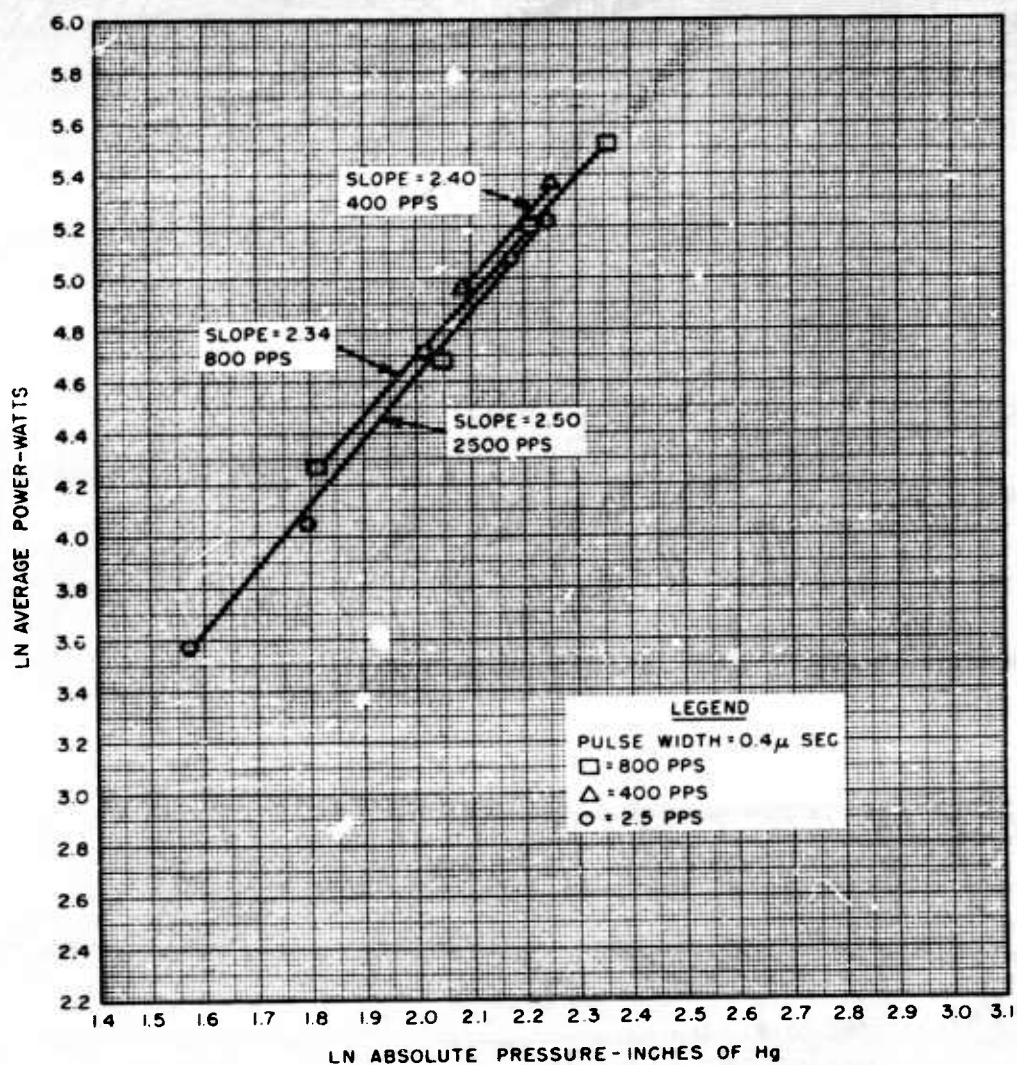


FIGURE 20  
VARIATION OF REPETITION RATE AT CONSTANT 0.4  $\mu$ -SEC  
PULSE WIDTH OF 1" X 1/2" X 0.050" WAVEGUIDE TEST SECTION

CONFIDENTIAL



CONFIDENTIAL

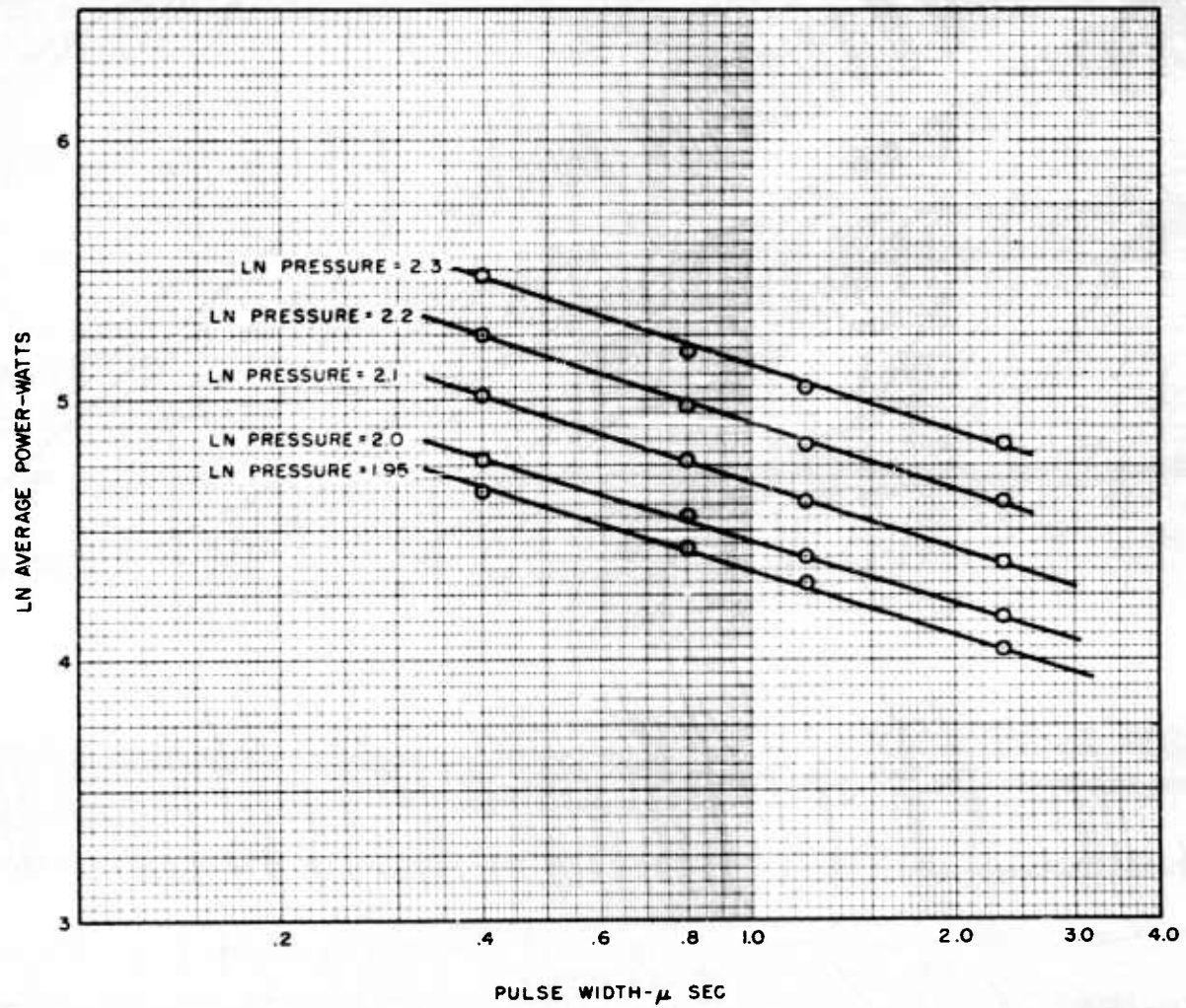


FIGURE 21  
POWER VS. PULSE WIDTH FOR  
CONSTANT REPETITION RATE OF 400 PPS

CONFIDENTIAL





CONFIDENTIAL

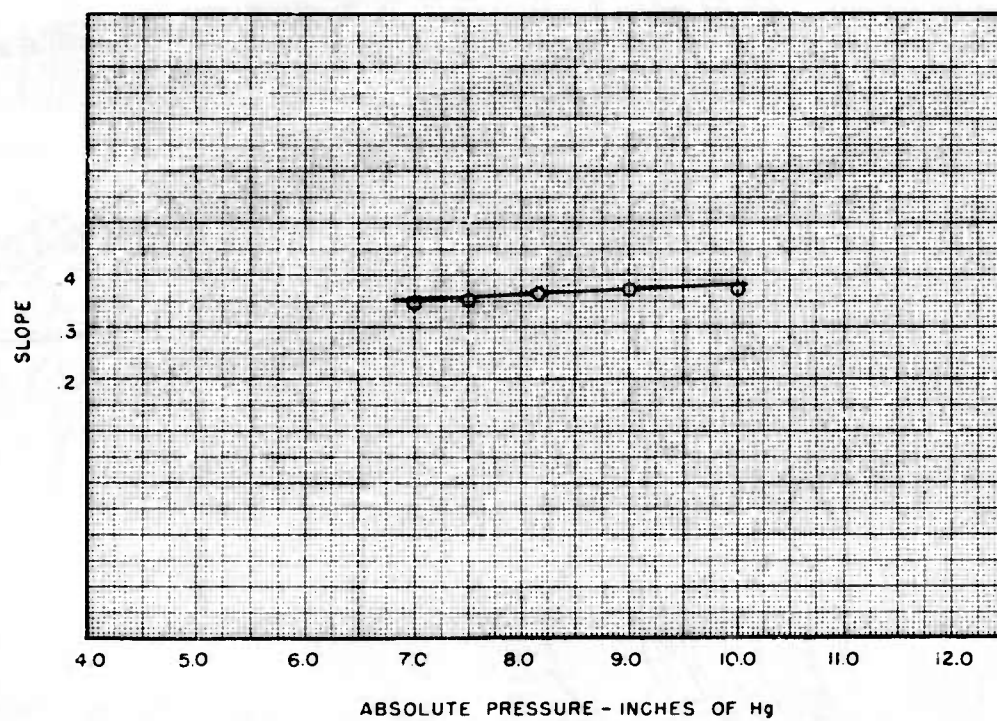


FIGURE 22  
PULSE-WIDTH EXPONENT VS. PRESSURE

CONFIDENTIAL



CONFIDENTIAL

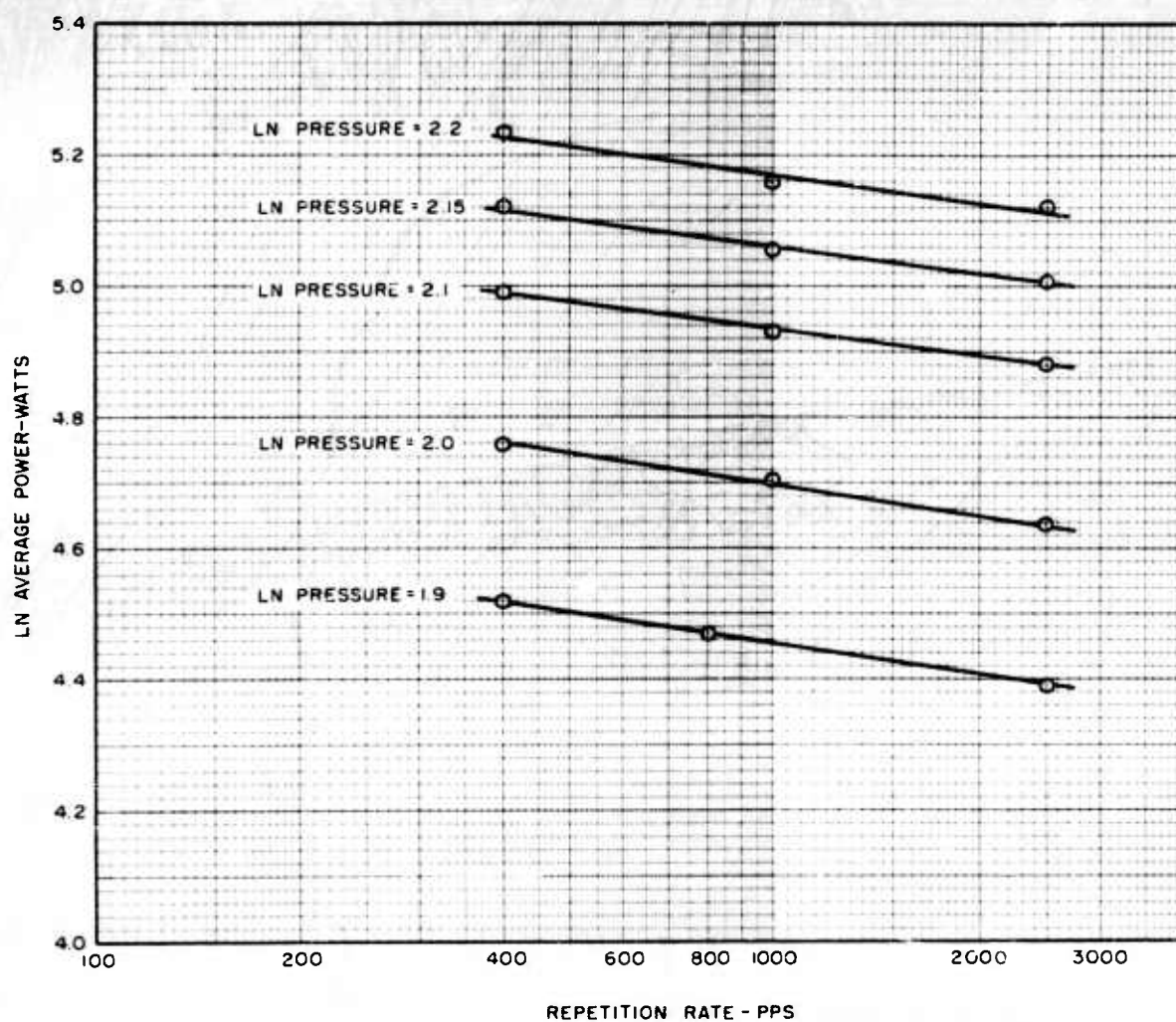


FIGURE 23  
POWER VS. REPETITION RATE  
FOR CONSTANT PULSE WIDTH OF  $0.4\mu$  SEC

CONFIDENTIAL



CONFIDENTIAL

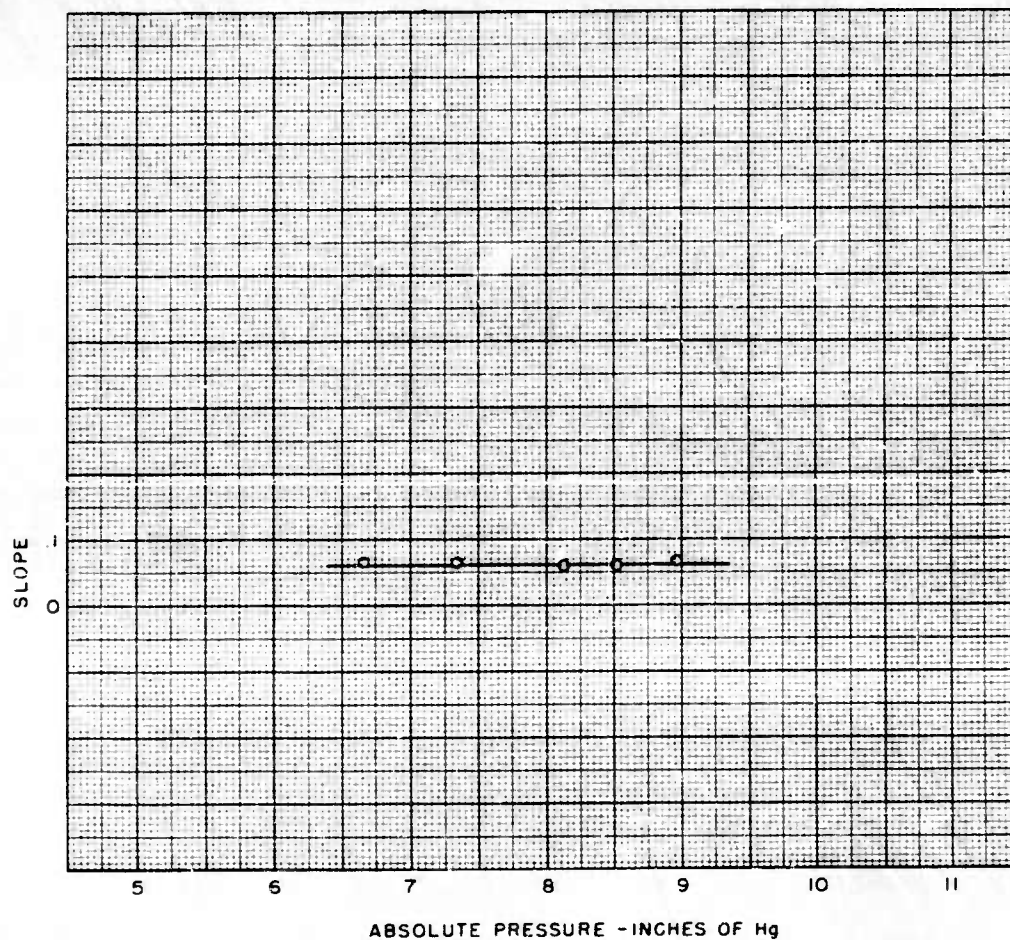


FIGURE 24  
REPETITION-RATE EXPONENT VS. PRESSURE

CONFIDENTIAL





CONFIDENTIAL

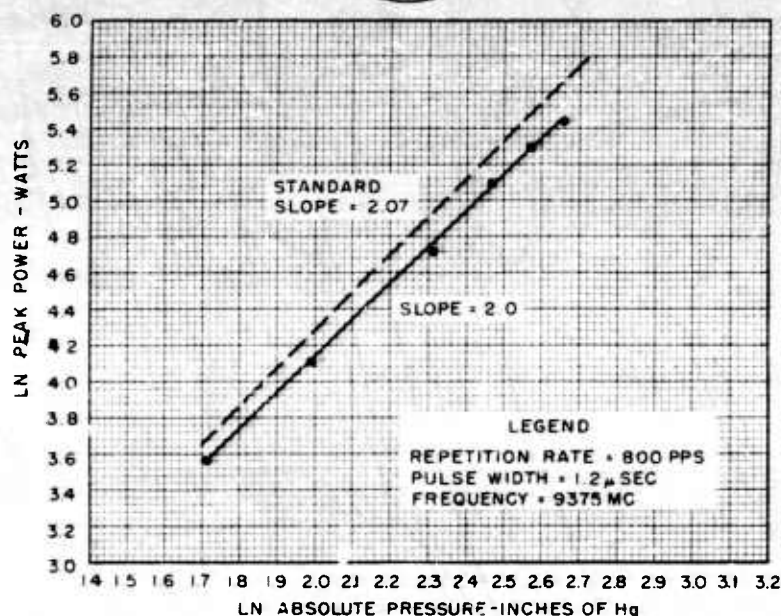


FIGURE 25  
POWER VS PRESSURE  
FOR 550-650 RMS FINISH  
(1" X 1/2" X 0.050" WAVEGUIDE)

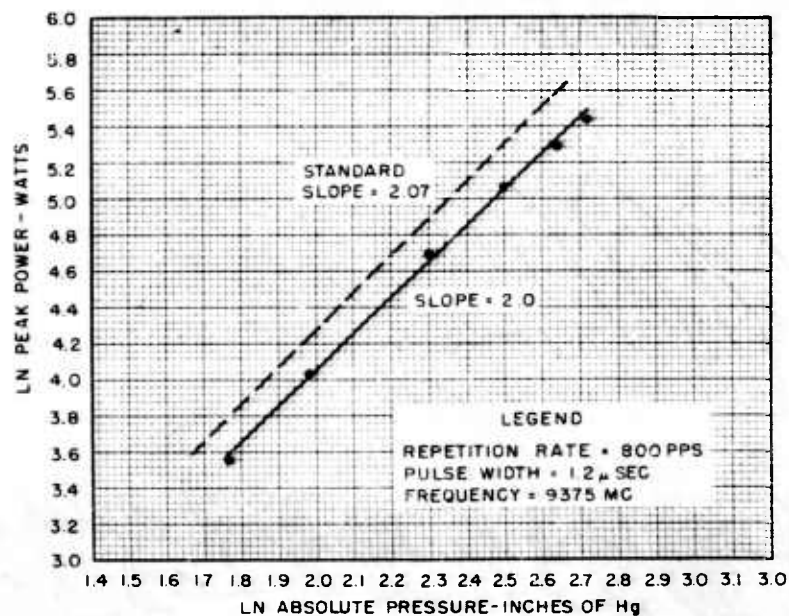


FIGURE 26  
POWER VS PRESSURE  
FOR 650-850 RMS FINISH  
(1" X 1/2" X 0.050" WAVEGUIDE)

CONFIDENTIAL



CONFIDENTIAL

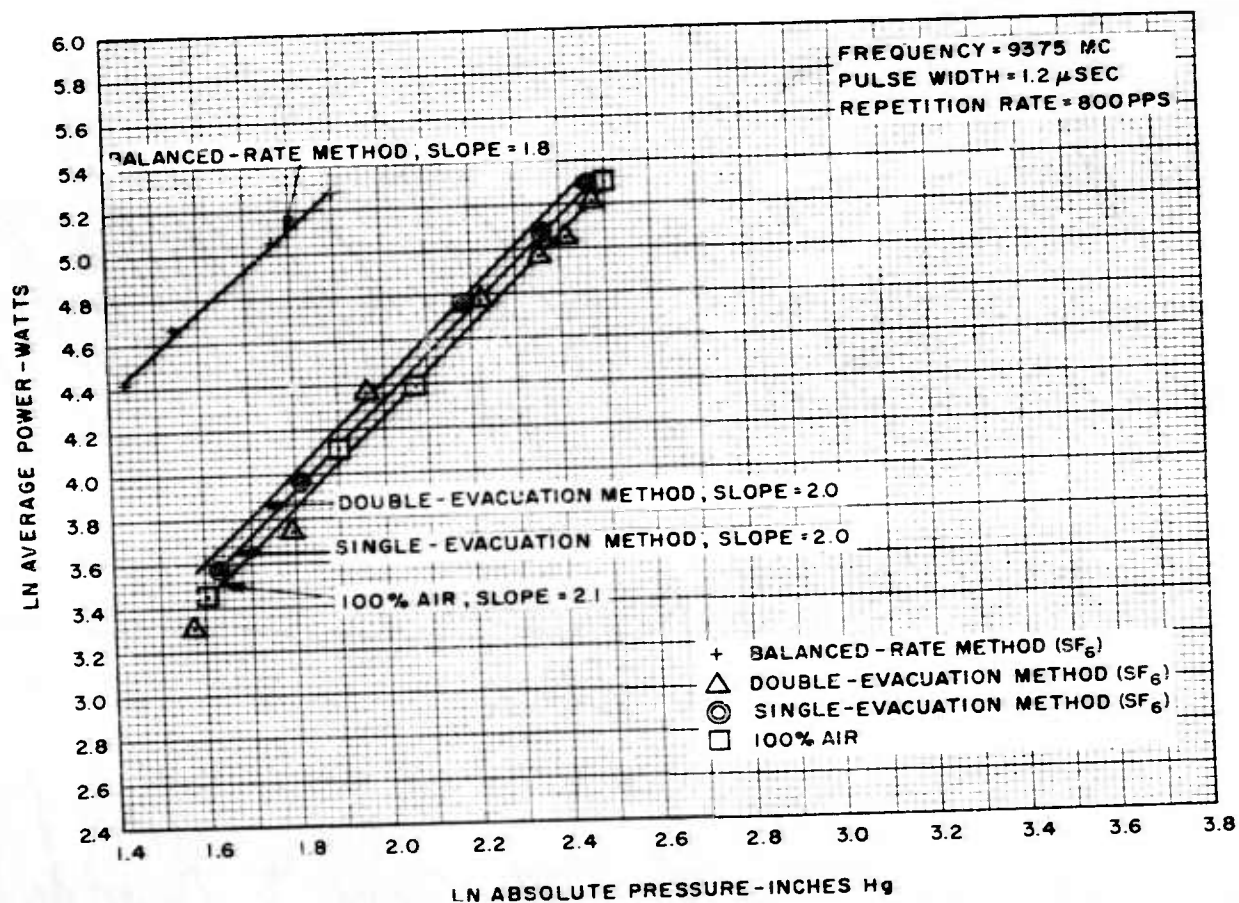
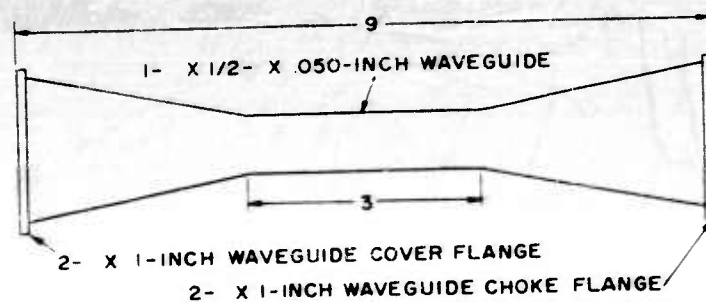


FIGURE 27  
LN POWER VS LN PRESSURE  
FOR STANDARD 1- X 1/2-INCH  
WAVEGUIDE

CONFIDENTIAL





CONFIDENTIAL

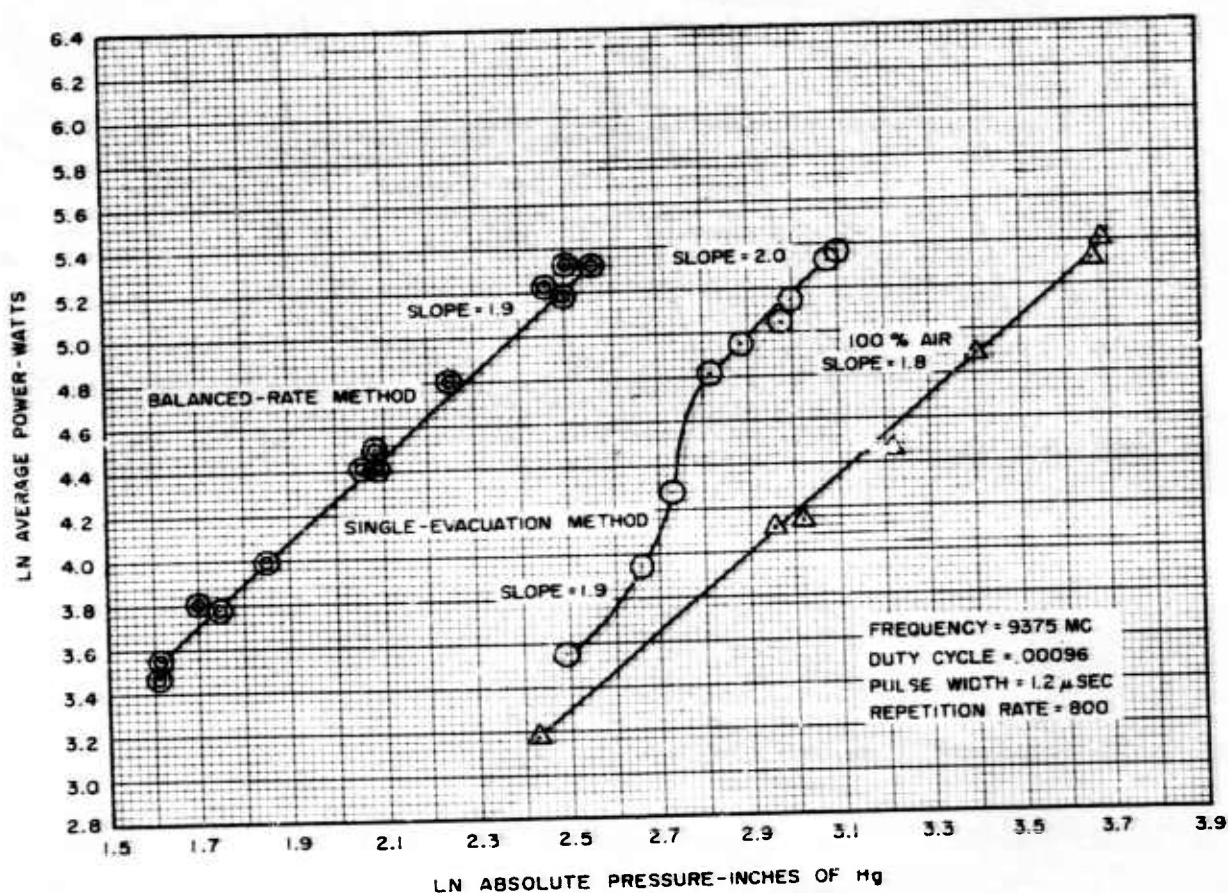
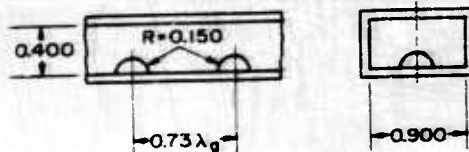


FIGURE 28  
LN POWER VS LN PRESSURE  
FOR 0.150-INCH RADIUS HEMISPHERICAL BUMP

CONFIDENTIAL



CONFIDENTIAL

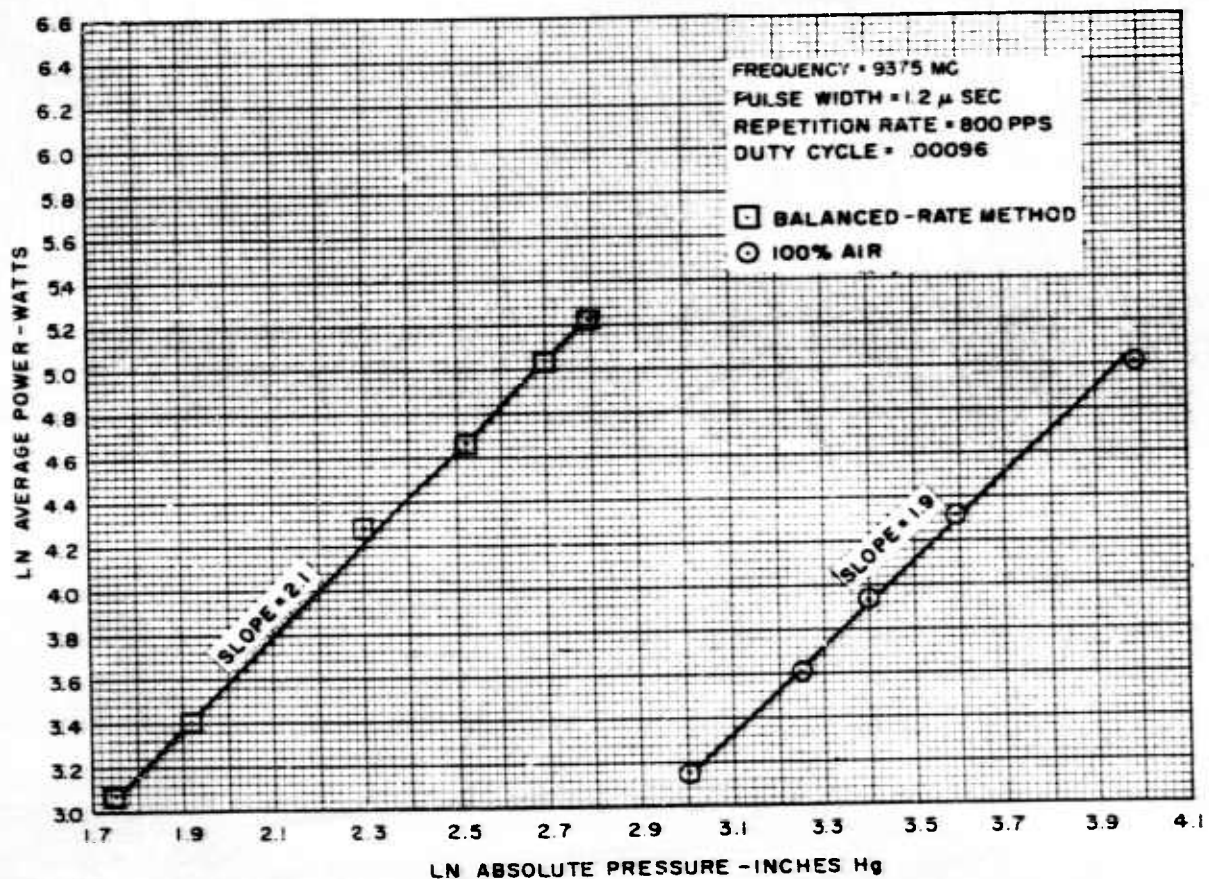
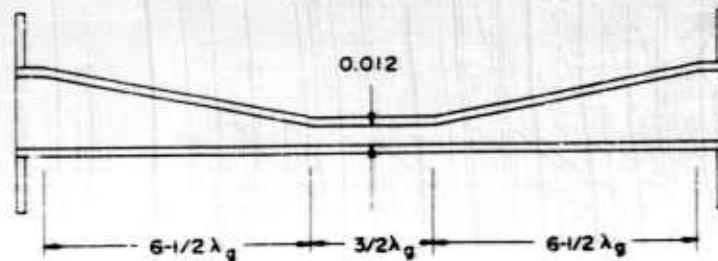


FIGURE 29

LN POWER VS LN PRESSURE  
FOR SWAYBACK TEST SECTION

CONFIDENTIAL



CONFIDENTIAL

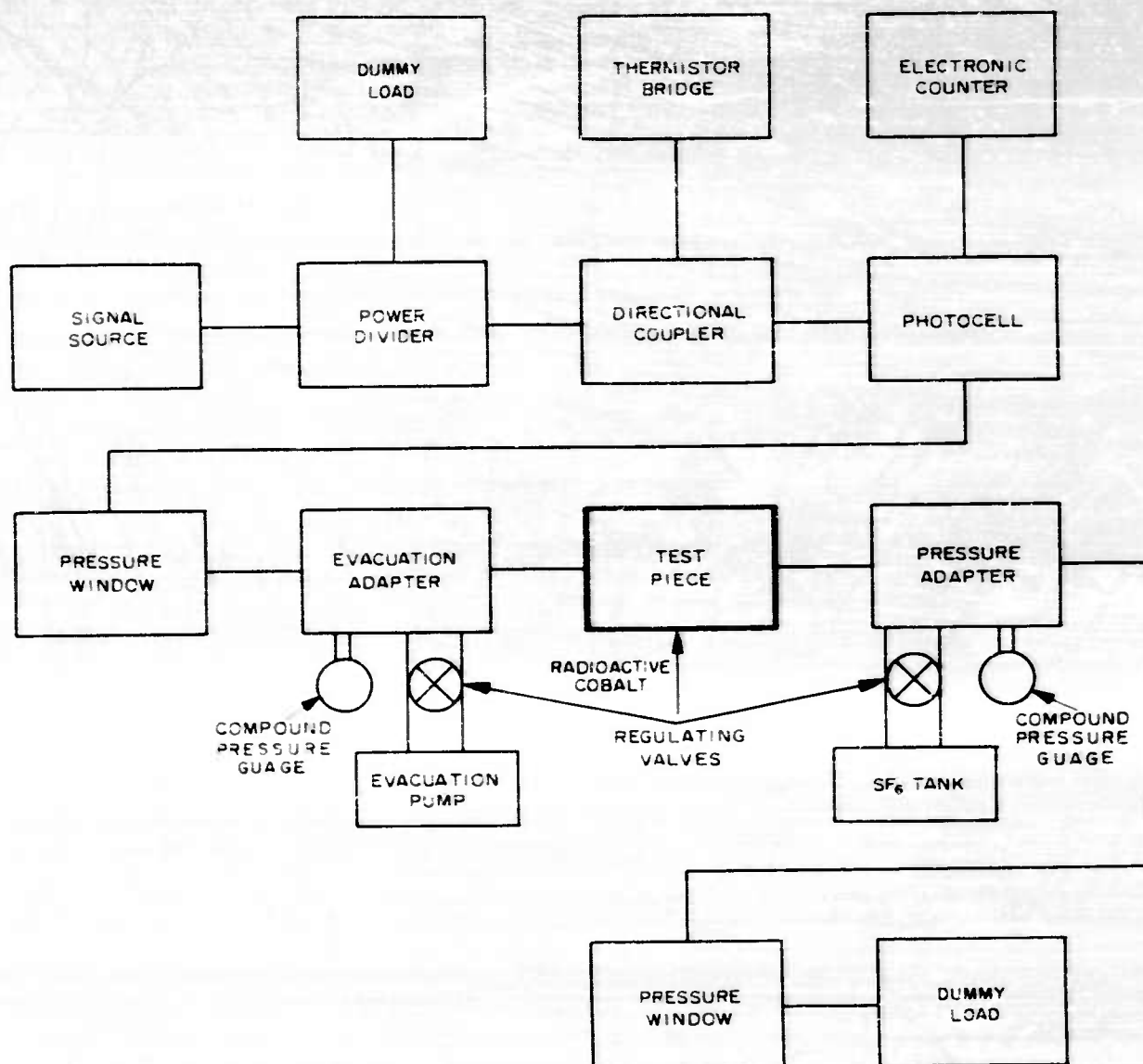


FIGURE 30  
BLOCK DIAGRAM OF CIRCUIT USED  
TO MEASURE EFFECT OF SF<sub>6</sub>  
UPON PEAK-POWER BREAKDOWN  
BY THE BALANCED-RATE METHOD

CONFIDENTIAL





CONFIDENTIAL

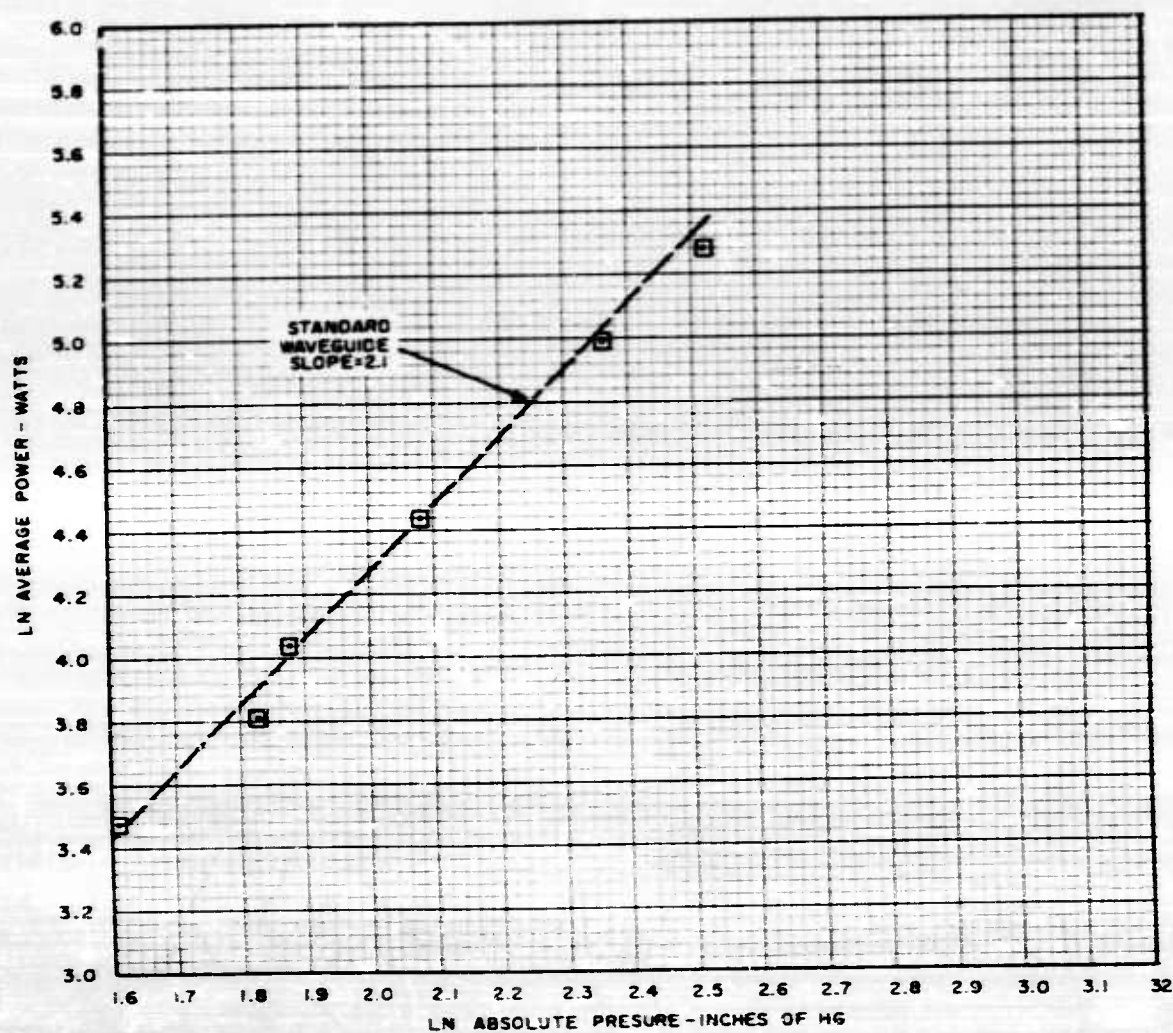
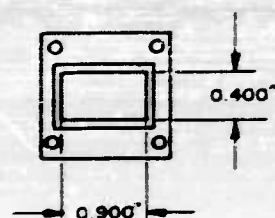
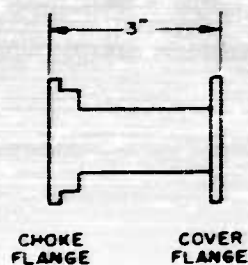


FIGURE 31

LN POWER VS LN PRESSURE  
FOR ANODIZED WAVEGUIDE

CONFIDENTIAL



CONFIDENTIAL

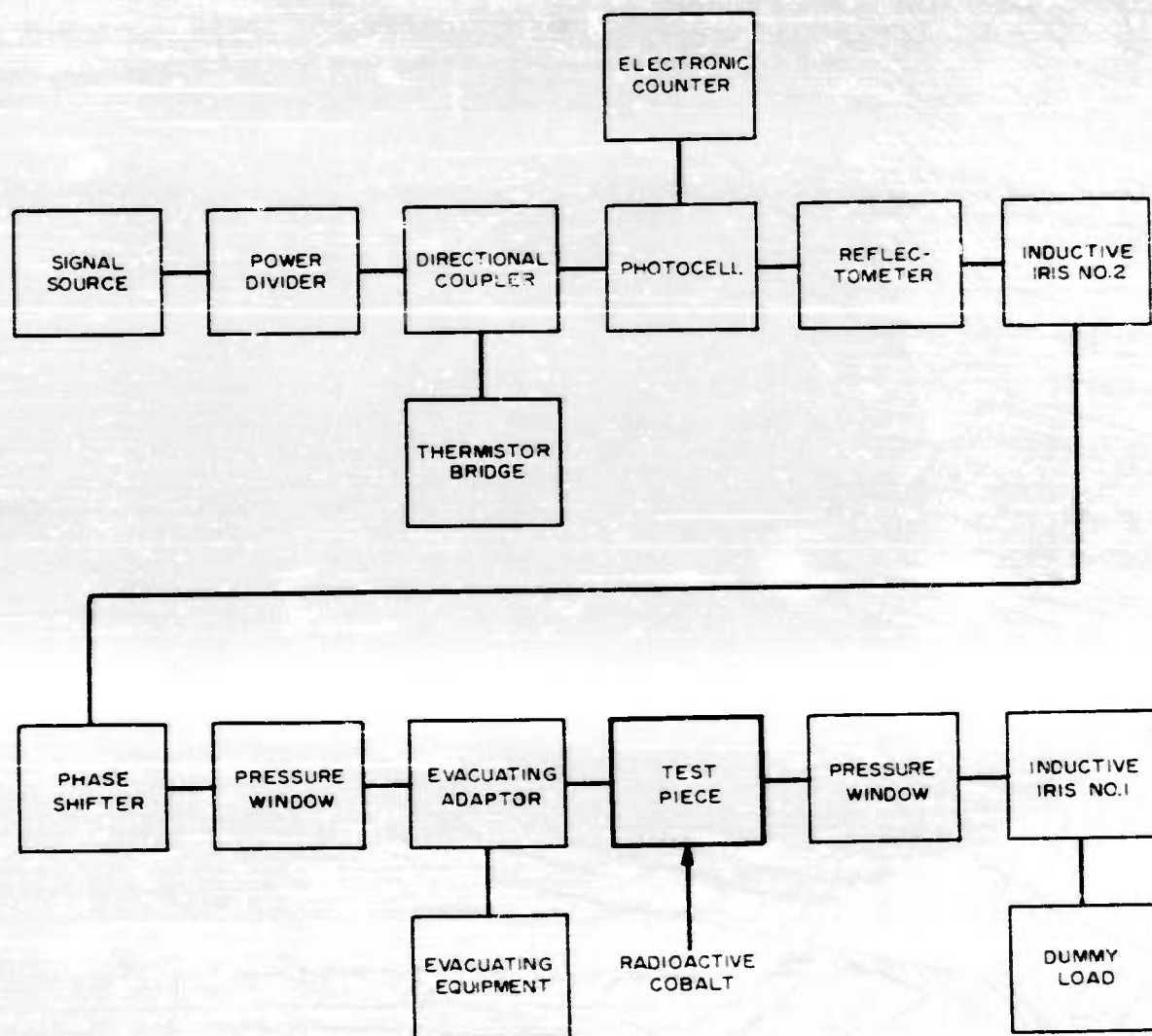


FIGURE 32  
BLOCK DIAGRAM OF CIRCUIT USED TO MEASURE  
EFFECT OF VSWR ON PEAK-POWER BREAKDOWN

CONFIDENTIAL





CONFIDENTIAL

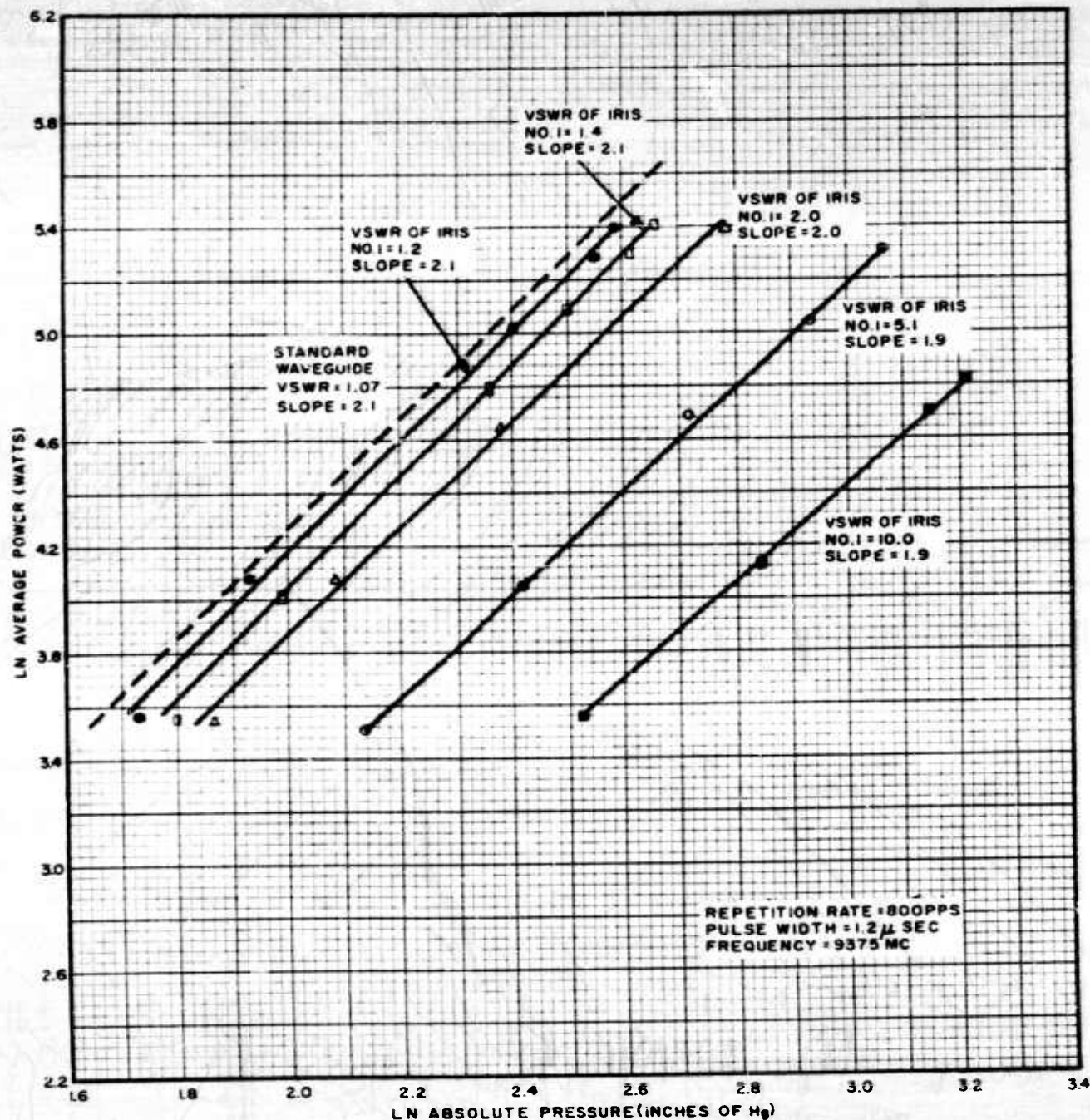


FIGURE 33  
POWER VS PRESSURE FOR  
DIFFERENT VALUES OF VSWR  
( $1 \times 1/2 \times .050$ " WAVEGUIDE)

CONFIDENTIAL



CONFIDENTIAL

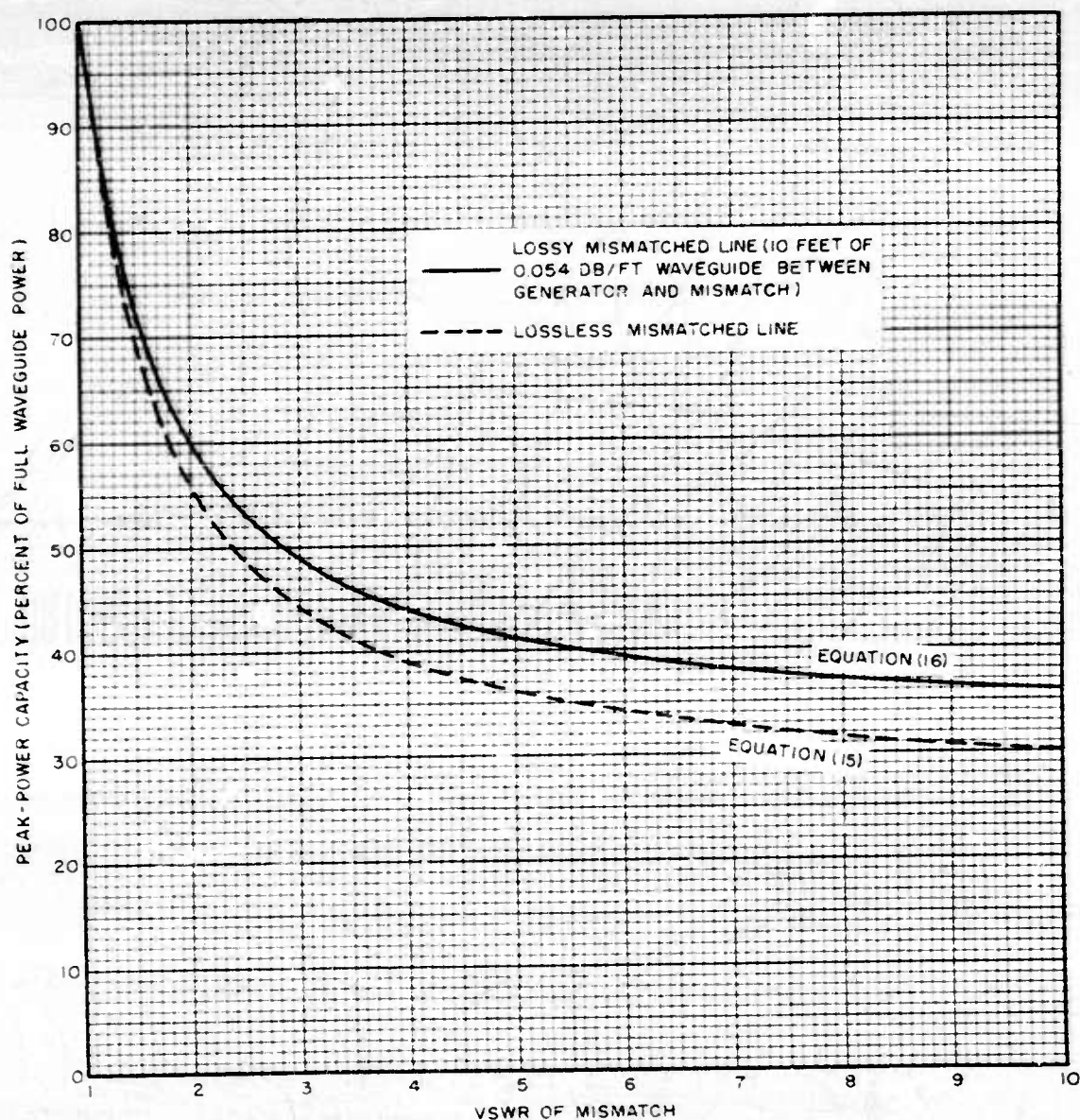


FIGURE 34  
CALCULATED PEAK-POWER CAPACITY  
VS VSWR FOR A SINGLE MISMATCH

CONFIDENTIAL



CONFIDENTIAL

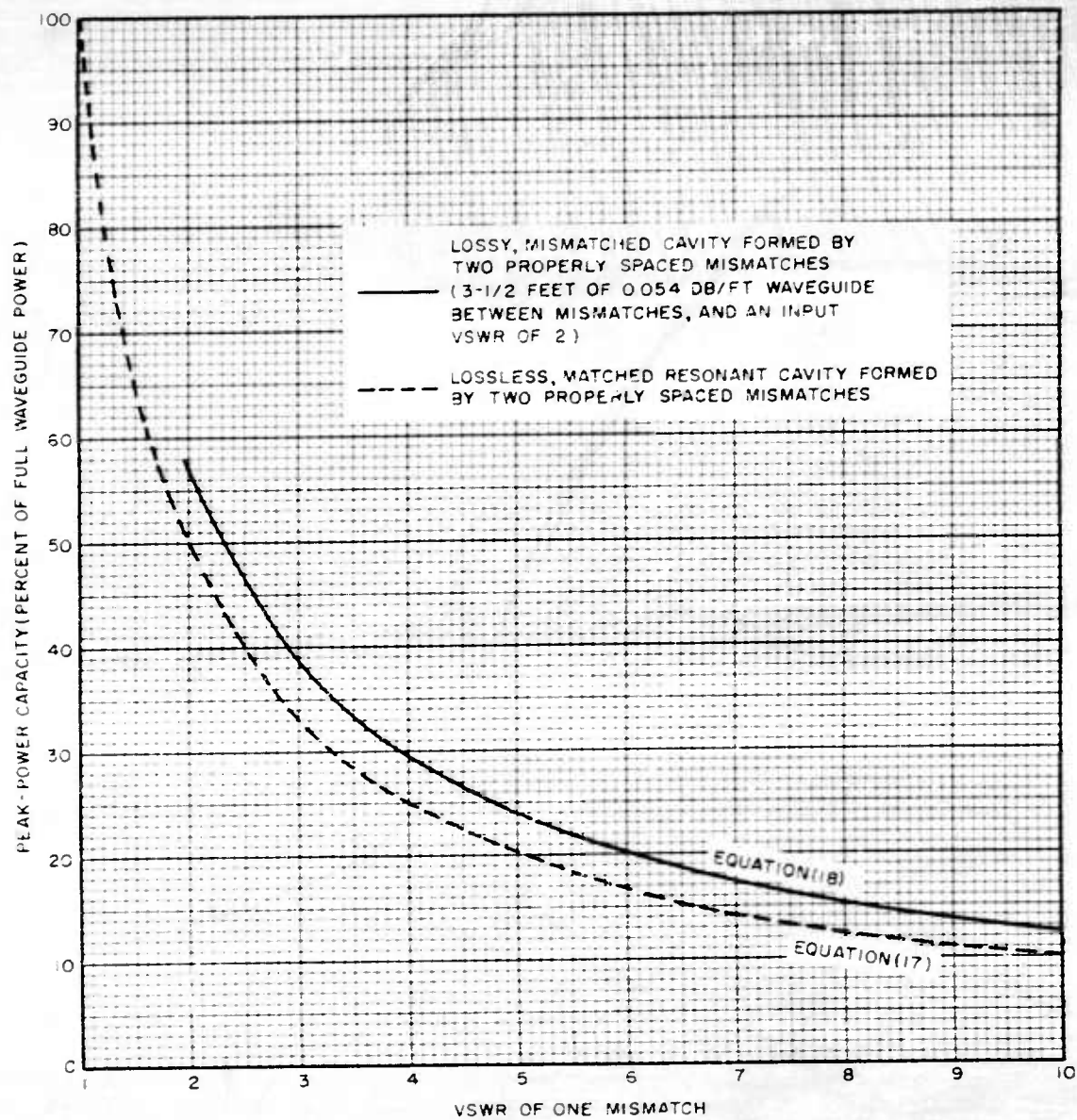


FIGURE 35  
CALCULATED PEAK-POWER CAPACITY  
VS VSWR FOR A RESONANT CAVITY  
FORMED BY TWO PROPERLY SPACED MISMATCHES

CONFIDENTIAL





CONFIDENTIAL

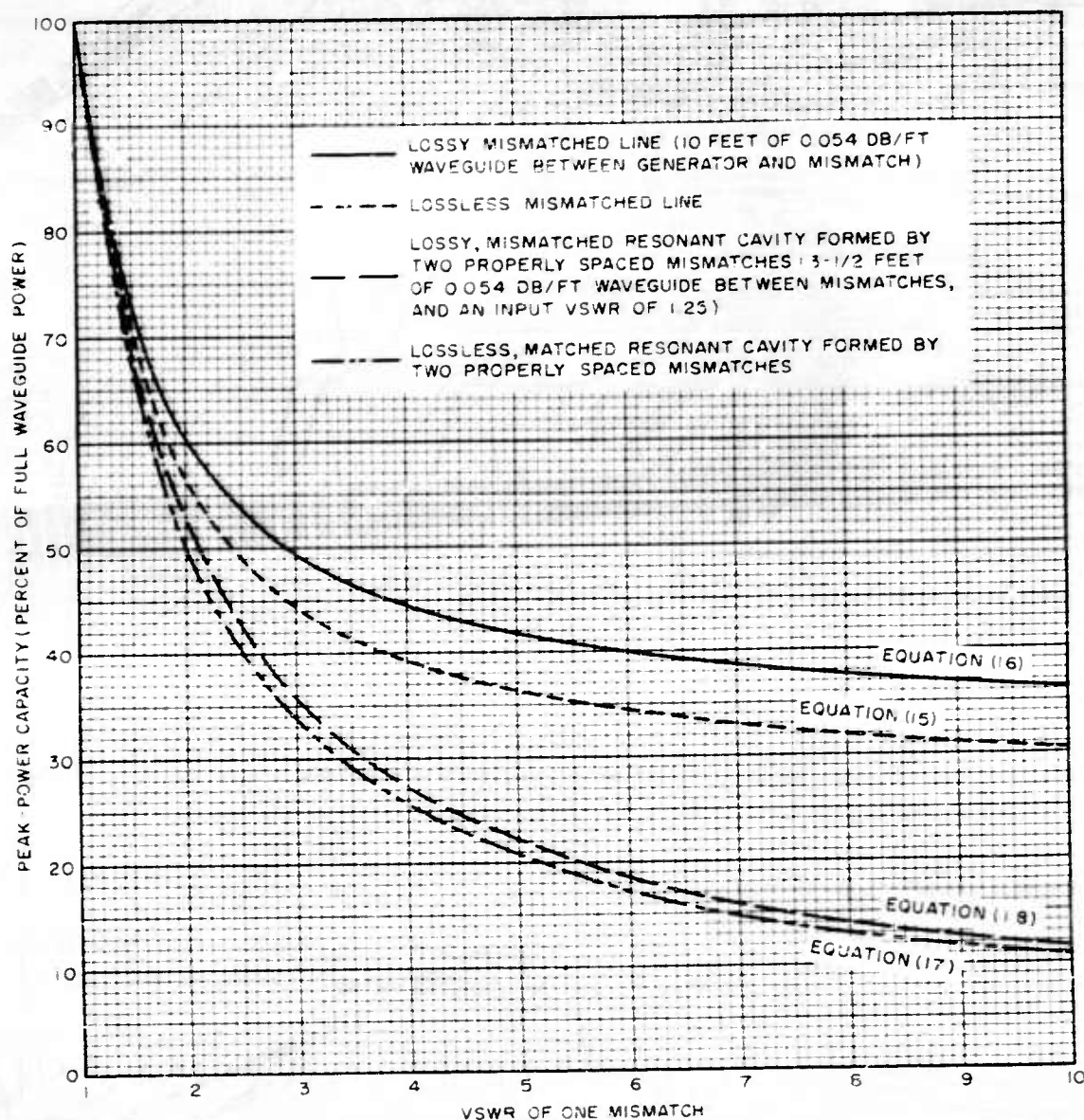


FIGURE 36  
COMPARISON OF CALCULATED PEAK-POWER  
CAPACITIES SHOWN IN FIGURES 34 AND 35

CONFIDENTIAL



CONFIDENTIAL

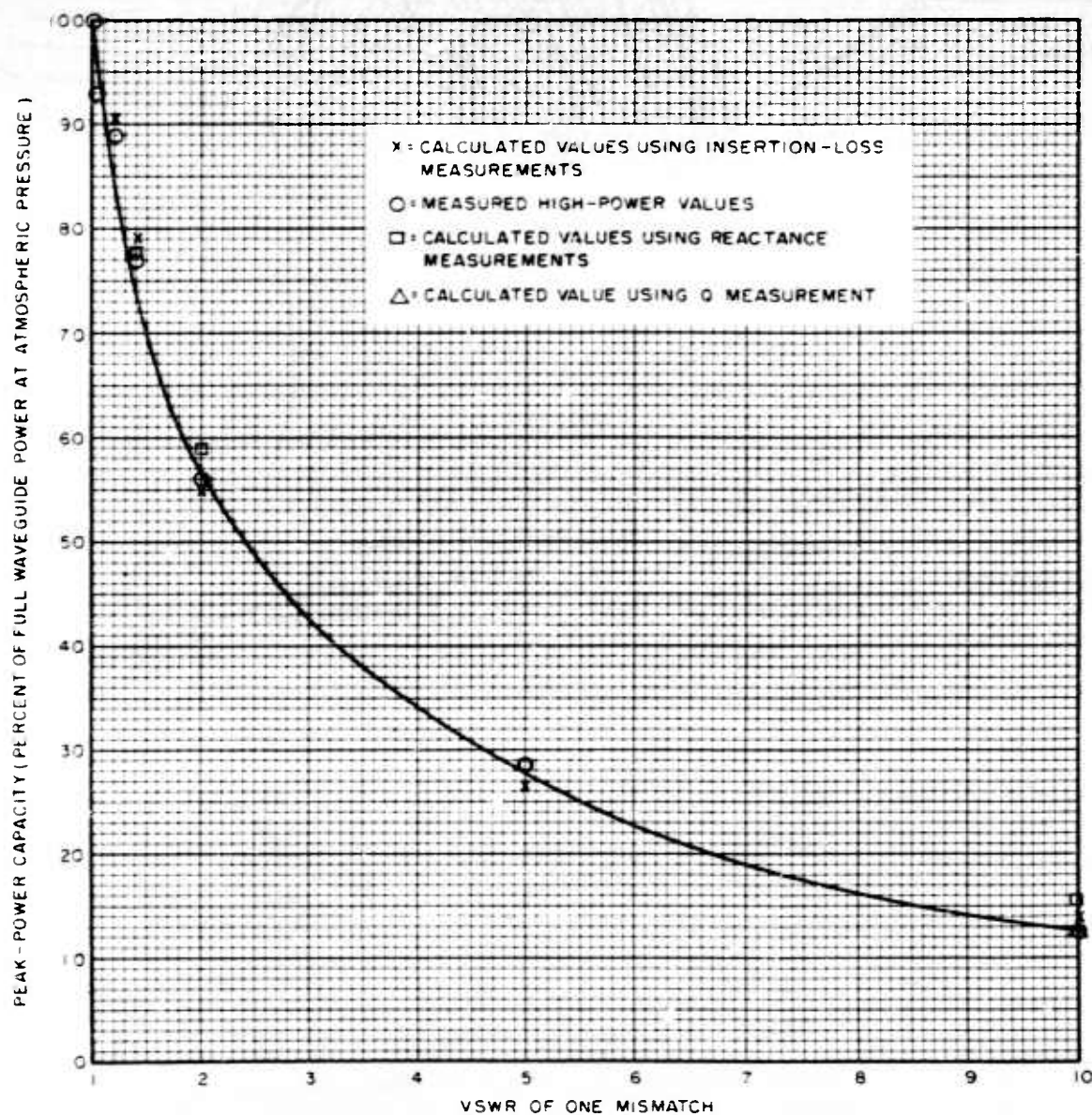


FIGURE 37  
MEASURED AND CALCULATED PEAK-POWER CAPACITIES  
VS VSWR FOR A RESONANT CAVITY FORMED  
BY TWO PROPERLY SPACED MISMATCHES

CONFIDENTIAL





CONFIDENTIAL

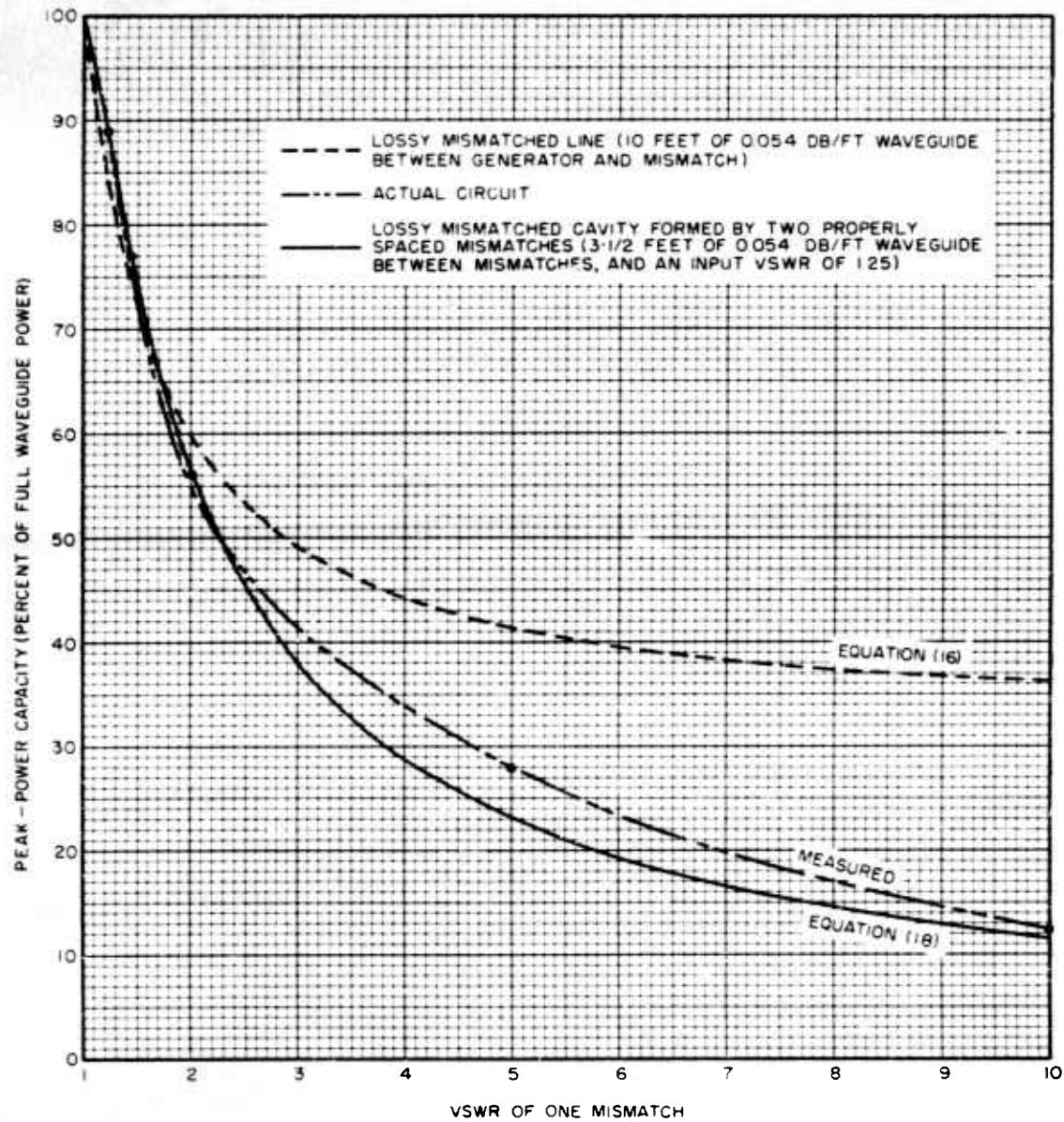


FIGURE 38  
MEASURED AND CALCULATED PEAK-POWER CAPACITIES  
VS VSWR FOR THREE MOST PERTINENT CONDITIONS

CONFIDENTIAL



CONFIDENTIAL

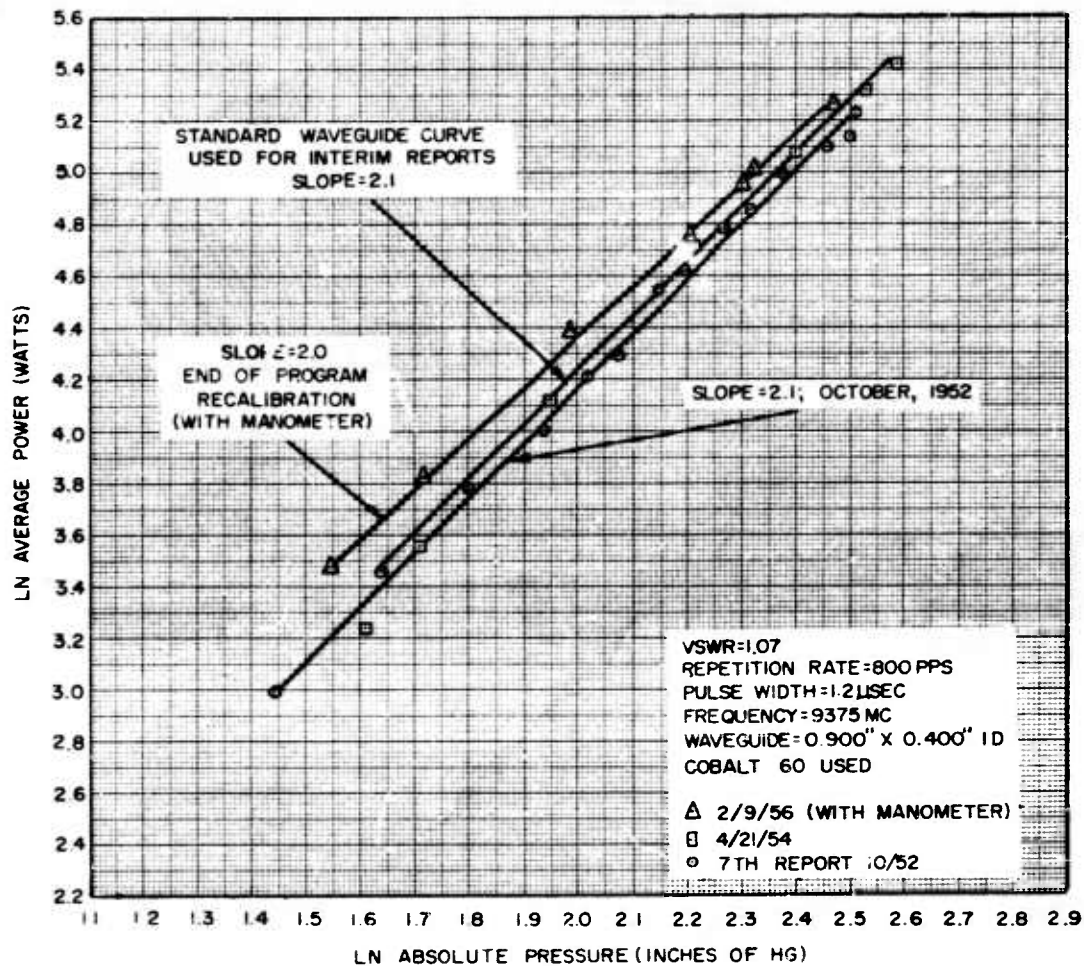


FIGURE 39  
BREAKDOWN POWER VS PRESSURE  
WITH TAPERED-WAVEGUIDE  
BREAK-DOWN GAP

CONFIDENTIAL



CONFIDENTIAL



SPECIALY ALIGNED COVER-TO-COVER  
FLANGE JUNCTION

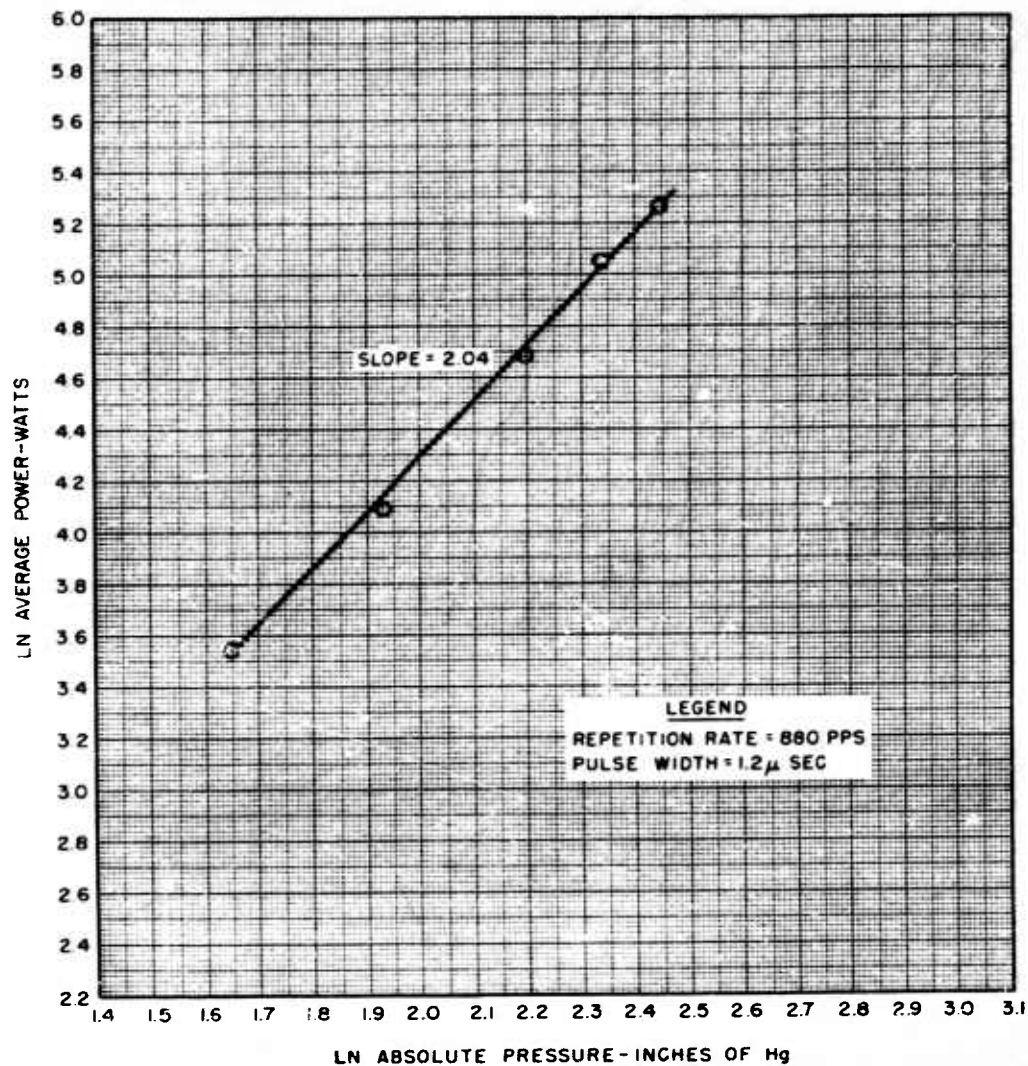


FIGURE 40

POWER VS. PRESSURE FOR SPECIALLY ALIGNED  
FLANGES IN 1" X 1/2" X 0.050" WAVEGUIDE TEST SECTION

CONFIDENTIAL





CONFIDENTIAL

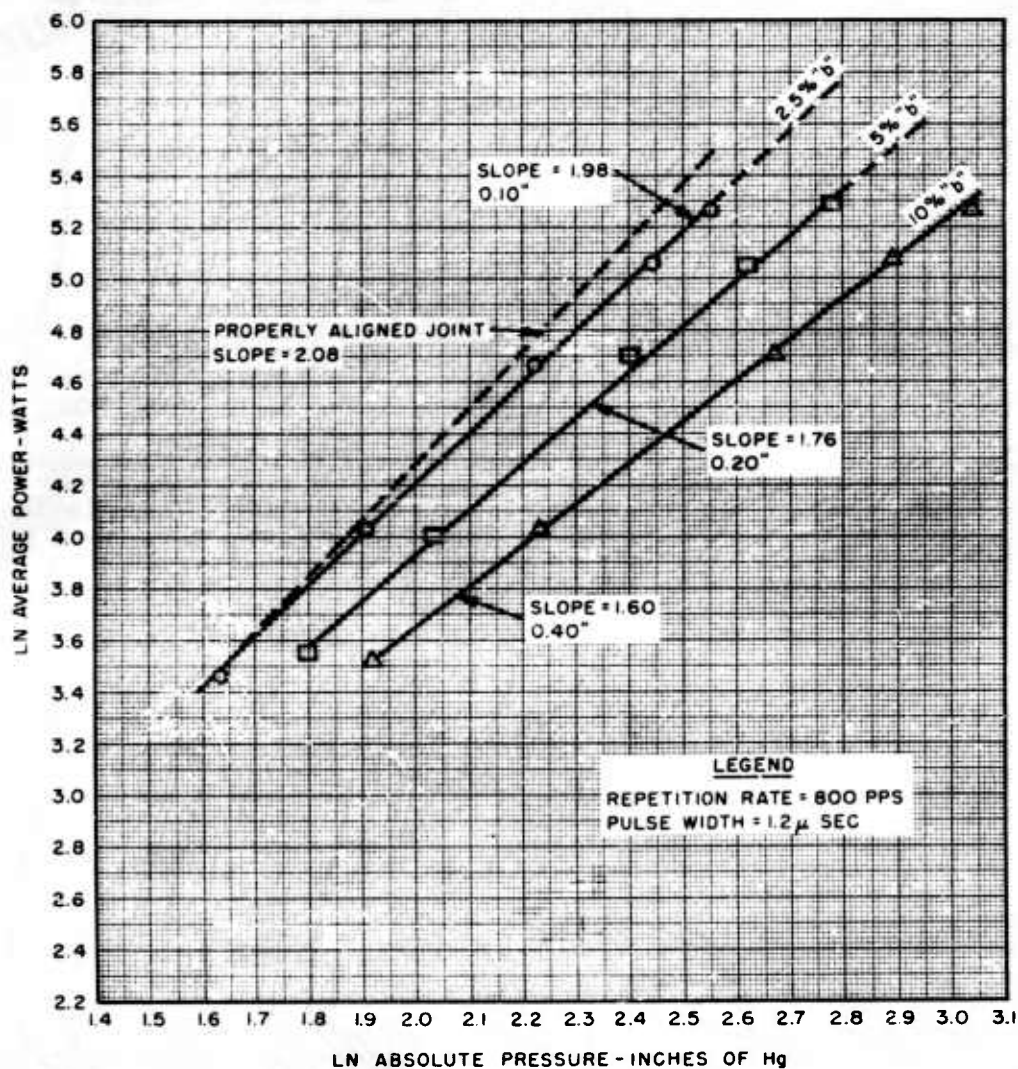
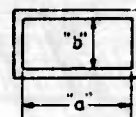
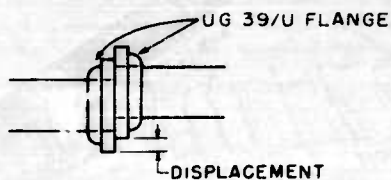


FIGURE 41  
POWER VS. PRESSURE FOR MISALIGNMENT  
BETWEEN COVER FLANGES IN VERTICAL PLANE  
FOR 1" X 1/2" X 0.050" WAVEGUIDE TEST SECTION

CONFIDENTIAL



CONFIDENTIAL

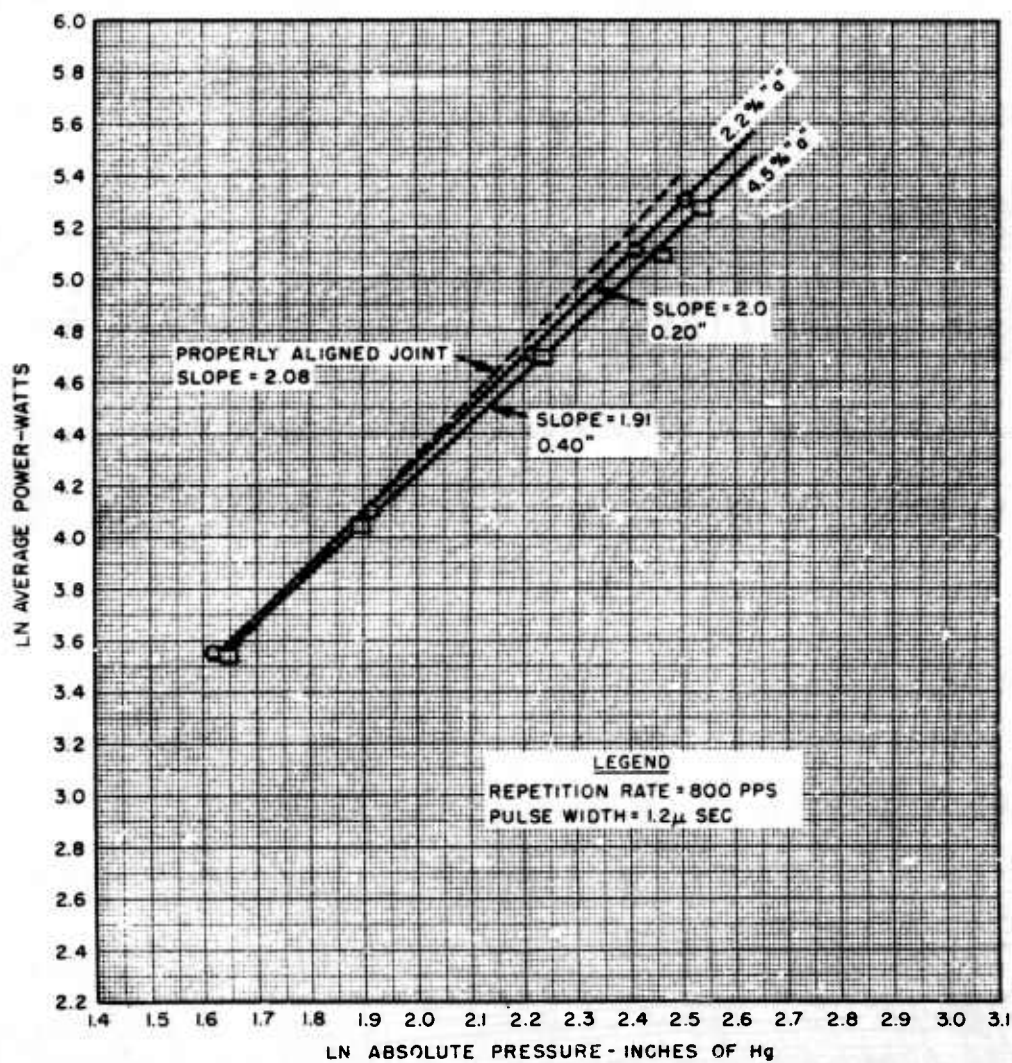
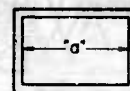
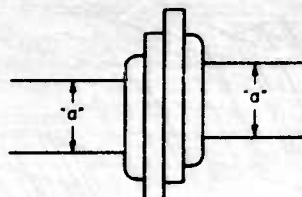


FIGURE 42  
POWER VS. PRESSURE FOR MISALIGNMENT  
FOR COVER FLANGES IN HORIZONTAL PLANE  
FOR 1" X 1/2" X 0.050" WAVEGUIDE TEST SECTION

CONFIDENTIAL





CONFIDENTIAL

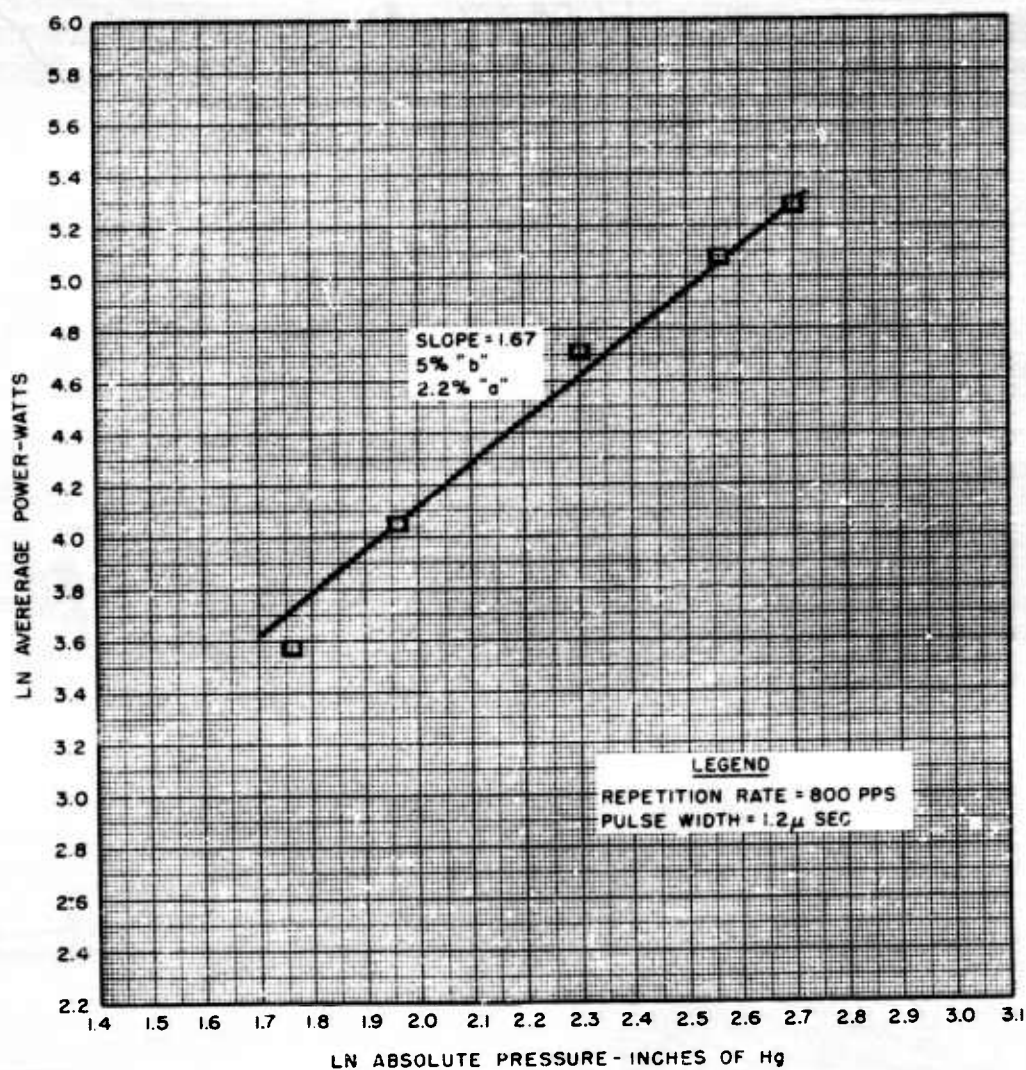


FIGURE 43

POWER VS. PRESSURE FOR COVER FLANGES MISALIGNED  
0.020" IN BOTH HORIZONTAL AND VERTICAL PLANES  
FOR 1" X 1/2" X 0.050" WAVEGUIDE TEST SECTION

CONFIDENTIAL



CONFIDENTIAL

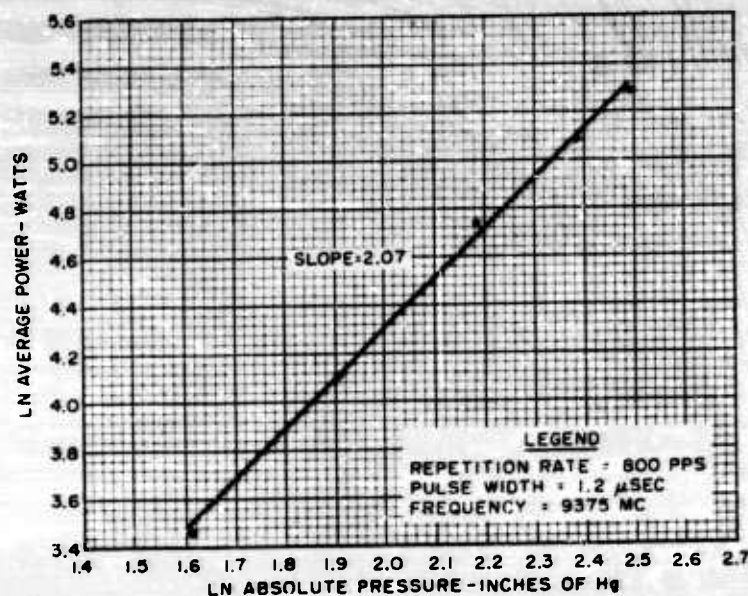


FIGURE 44  
 POWER VS PRESSURE FOR  
 CHOKE-TO-COVER FLANGE CONNECTION  
 (1" x 1/2" x 0.050" WAVEGUIDE)

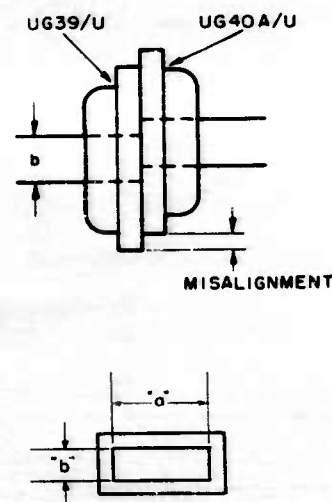
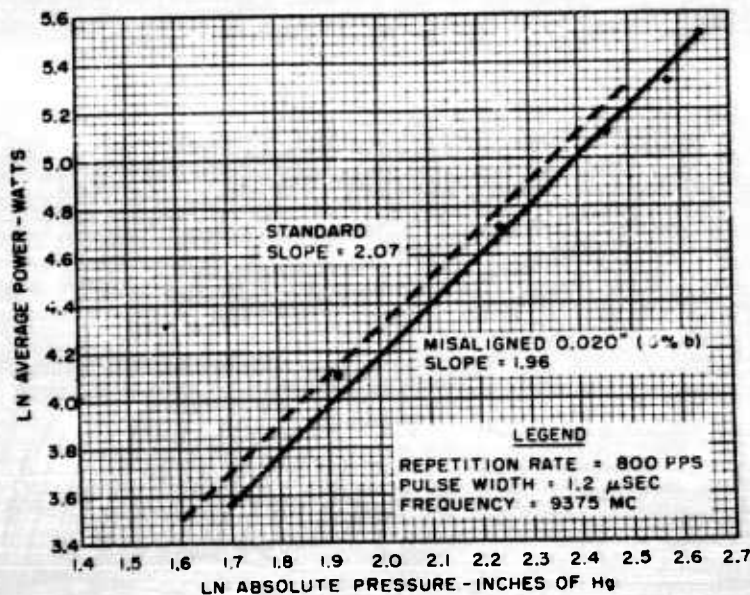


FIGURE 45  
 POWER VS PRESSURE FOR CHOKE-TO-COVER FLANGE CONNECTION  
 HAVING A 0.020" VERTICAL MISALIGNMENT  
 (1" x 1/2" x 0.050" WAVEGUIDE)

CONFIDENTIAL



CONFIDENTIAL

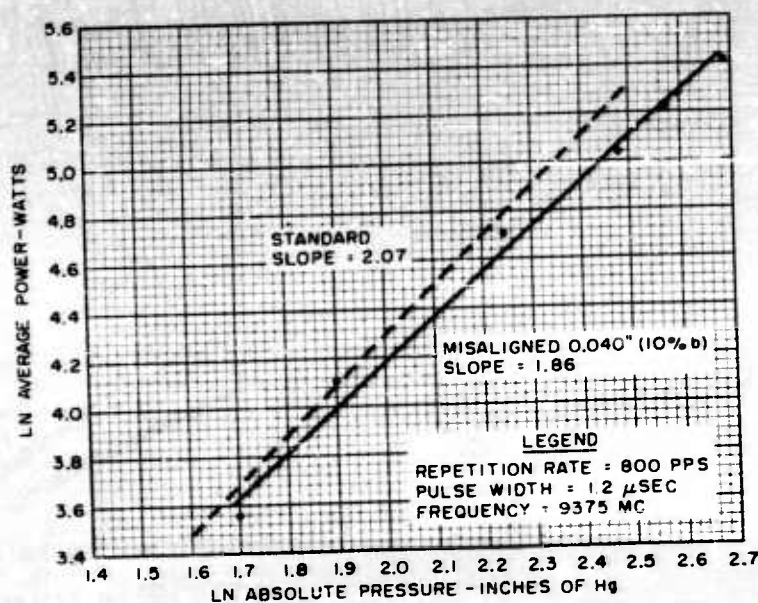


FIGURE 46

POWER VS PRESSURE FOR CHOKE-TO-COVER FLANGE CONNECTION  
HAVING A 0.040" VERTICAL MISALIGNMENT  
(1" x 1/2" x 0.050" WAVEGUIDE)

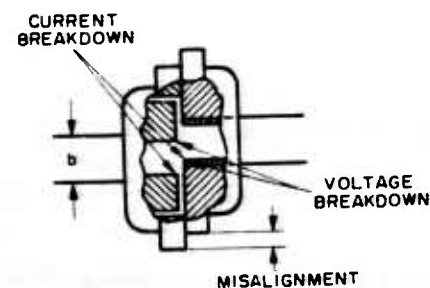
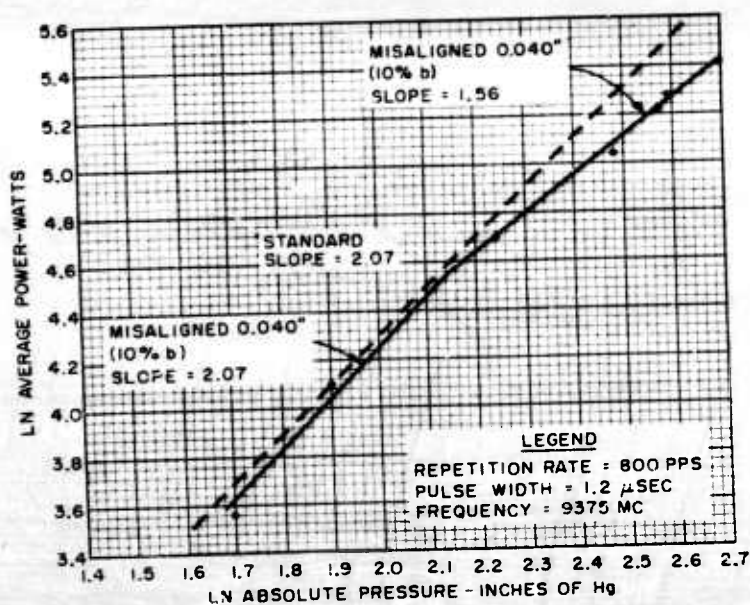


FIGURE 47

POWER VS PRESSURE FOR CHOKE-TO-COVER FLANGE CONNECTION  
HAVING A 0.040" VERTICAL MISALIGNMENT,  
SHOWING DUAL-SLOPE CURVE  
(1" x 1/2" x 0.050" WAVEGUIDE)

CONFIDENTIAL





CONFIDENTIAL

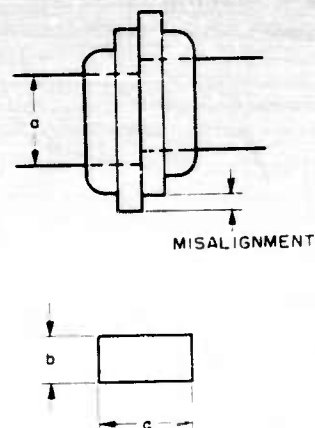
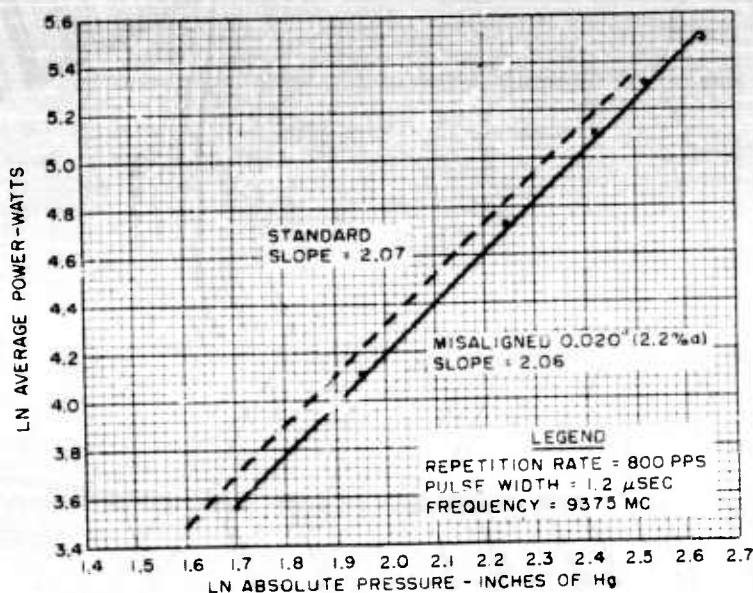


FIGURE 48

POWER VS PRESSURE FOR CHOKE-TO-COVER FLANGE CONNECTION  
HAVING A 0.020" HORIZONTAL MISALIGNMENT  
(1" x 1/2" x 0.050" WAVEGUIDE)

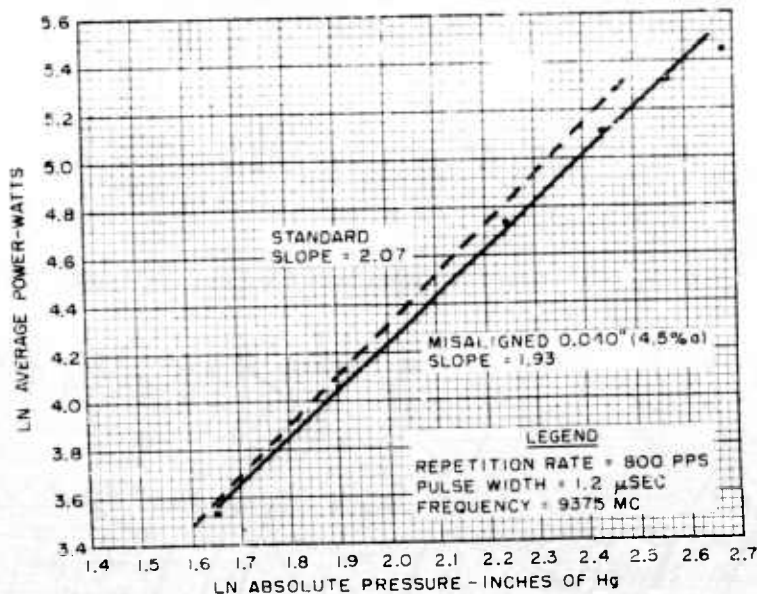


FIGURE 49

POWER VS PRESSURE FOR CHOKE-TO-COVER FLANGE CONNECTION  
HAVING A 0.040" HORIZONTAL MISALIGNMENT  
(1" x 1/2" x 0.050" WAVEGUIDE)

CONFIDENTIAL



CONFIDENTIAL

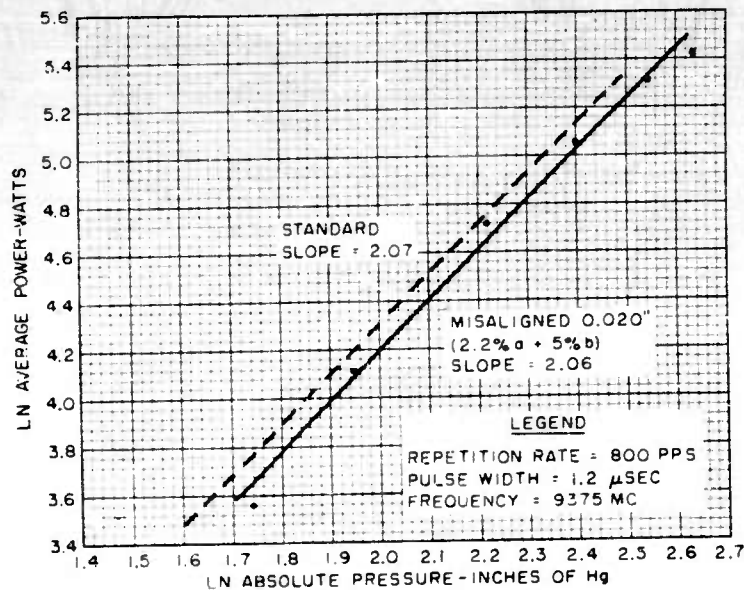


FIGURE 50

POWER VS PRESSURE FOR CHOKE-TO-COVER FLANGE CONNECTION  
HAVING A 0.020" HORIZONTAL AND VERTICAL MISALIGNMENT  
(1" x 1/2" x 0.050" WAVEGUIDE)

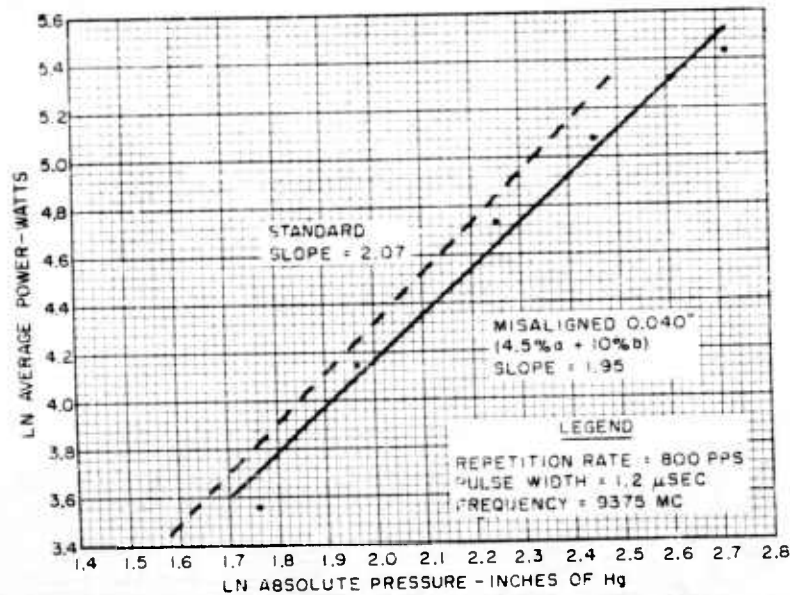


FIGURE 51

POWER VS PRESSURE FOR CHOKE-TO-COVER FLANGE CONNECTION  
HAVING A 0.040" HORIZONTAL AND VERTICAL MISALIGNMENT  
(1" x 1/2" x 0.050" WAVEGUIDE)

CONFIDENTIAL





CONFIDENTIAL

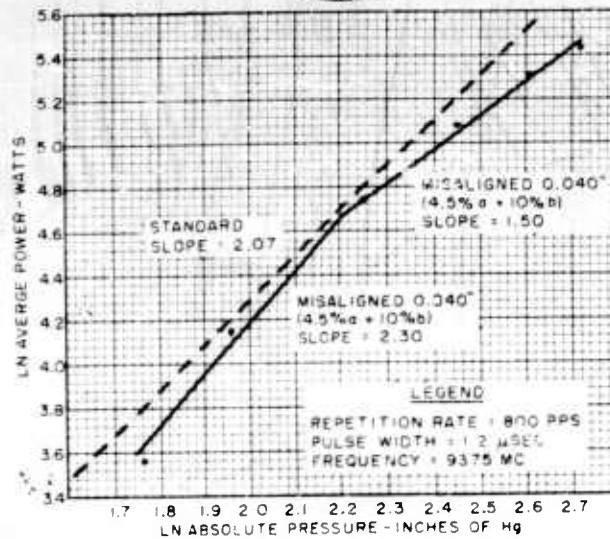


FIGURE 52

POWER VS PRESSURE FOR A CHOKE-TO-COVER FLANGE CONNECTION HAVING A .040" HORIZONTAL AND VERTICAL MISALIGNMENT, SHOWING DUAL-SLOPE CURVE (1"X1/2"X.050" WAVEGUIDE)

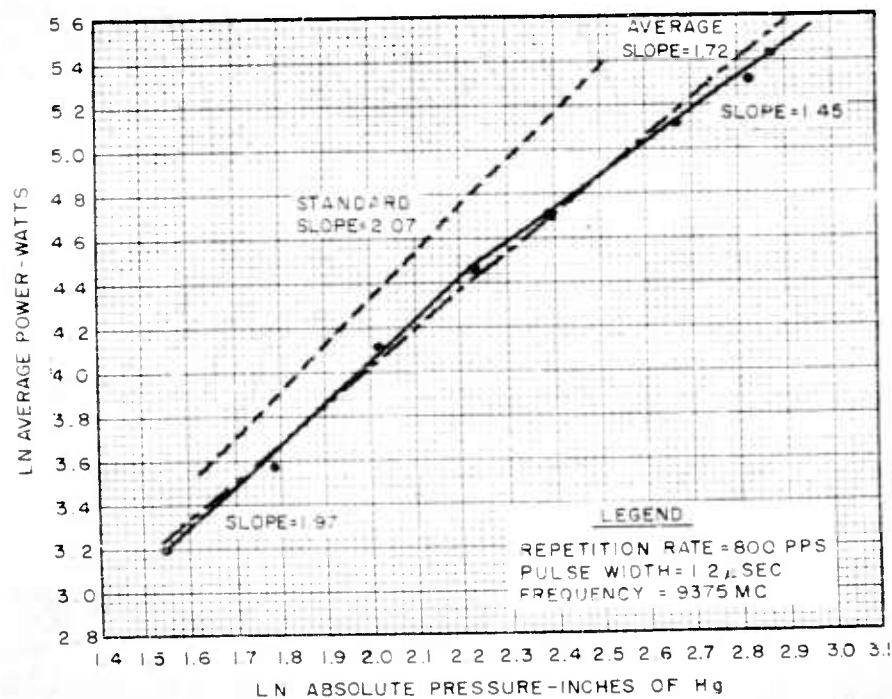


FIGURE 53

POWER VS PRESSURE FOR VERTEBRAE TYPE FLEXIBLE WAVEGUIDE (1"X1/2"X.050" WAVEGUIDE)

CONFIDENTIAL



CONFIDENTIAL

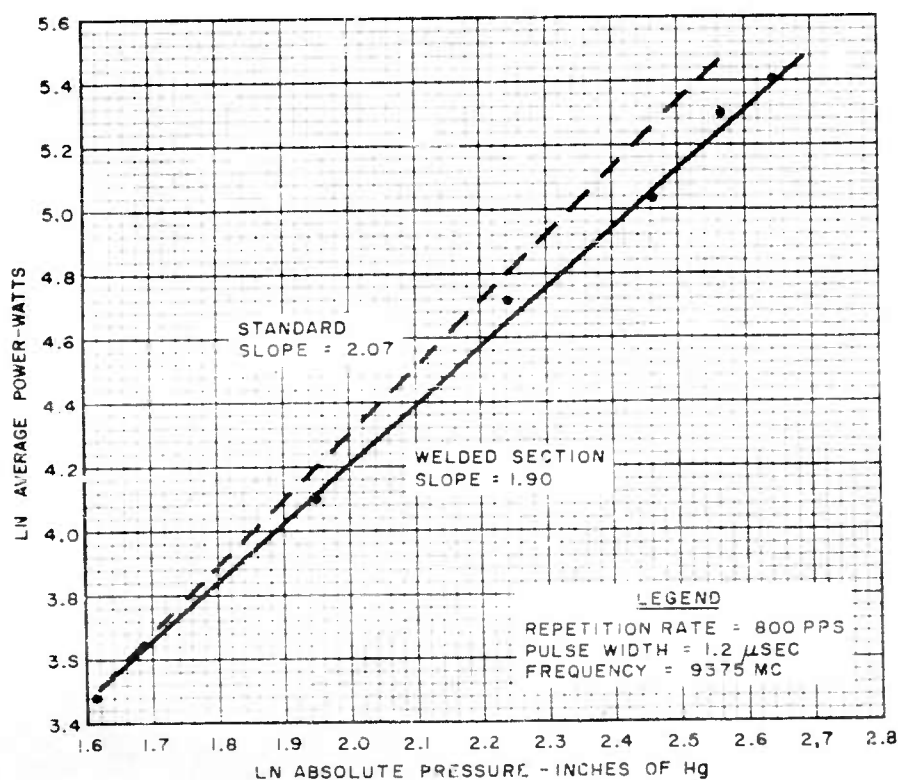
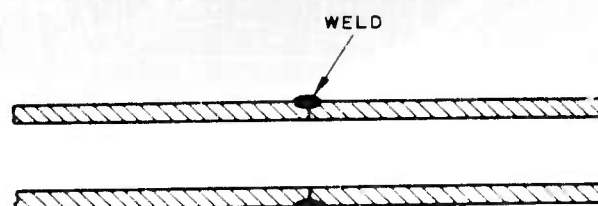


FIGURE 54  
POWER VS PRESSURE FOR  
TYPICAL WELDED BUTT JOINT  
(1"x1/2"x0.050" WAVEGUIDE)

CONFIDENTIAL



CONFIDENTIAL

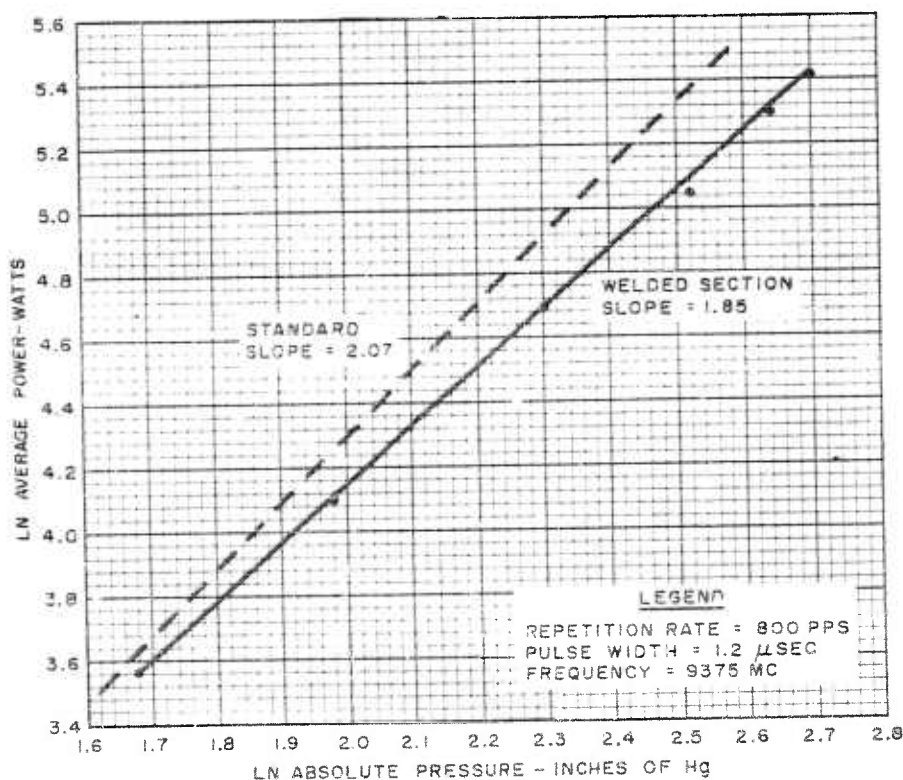
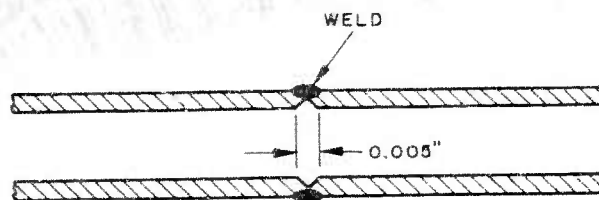


FIGURE 55  
POWER VS PRESSURE FOR WELDED  
BUTT JOINT HAVING A 0.005" GROOVE  
(1"x1/2"x0.050" WAVEGUIDE)

CONFIDENTIAL



CONFIDENTIAL

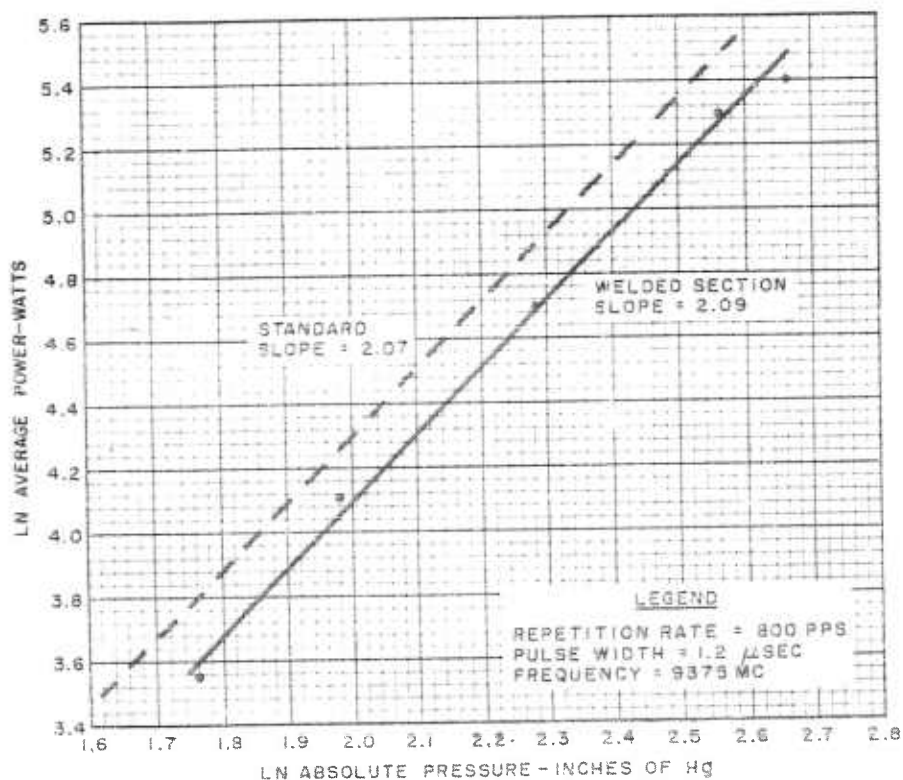
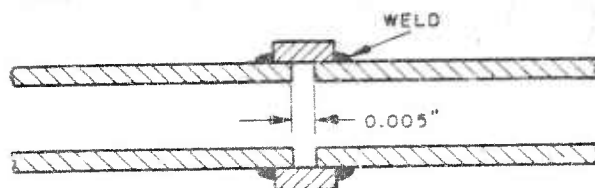


FIGURE 56  
POWER VS PRESSURE FOR  
WELDED BUTT JOINT HAVING 0.005" GAP  
(1" x 1/2" x 0.050" WAVEGUIDE)

CONFIDENTIAL





CONFIDENTIAL

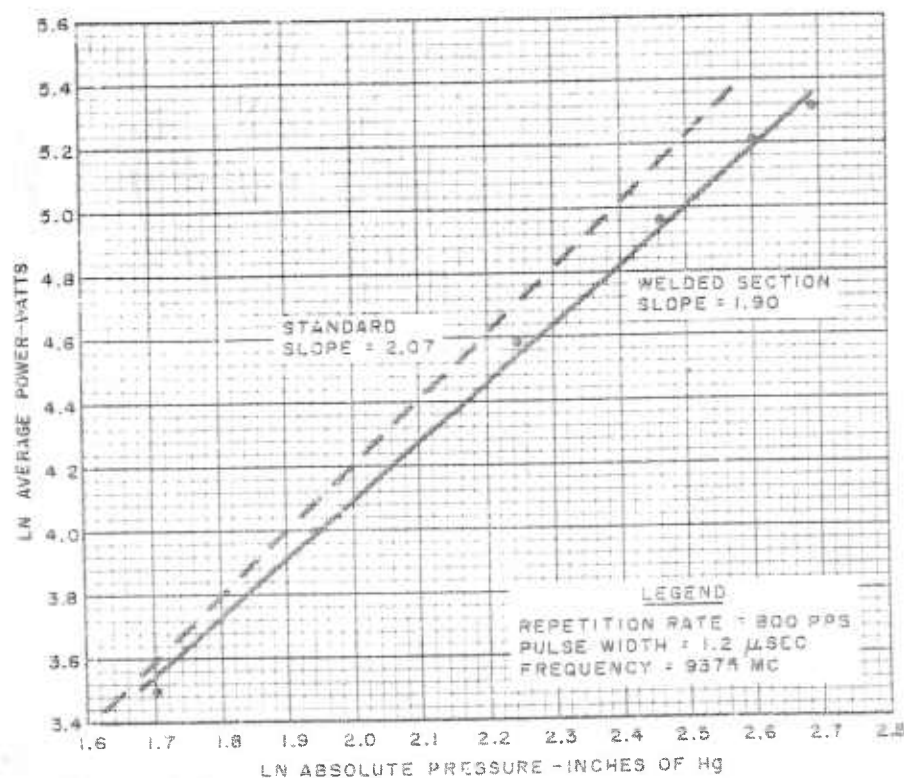
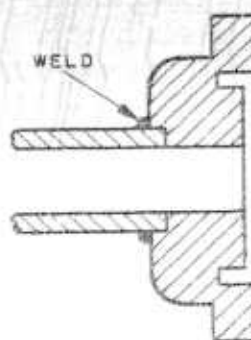


FIGURE 57  
POWER VS PRESSURE FOR  
TYPICAL WELDED CHOKE JOINT  
(1" x 1/2" x 0.050" WAVEGUIDE)

CONFIDENTIAL





CONFIDENTIAL

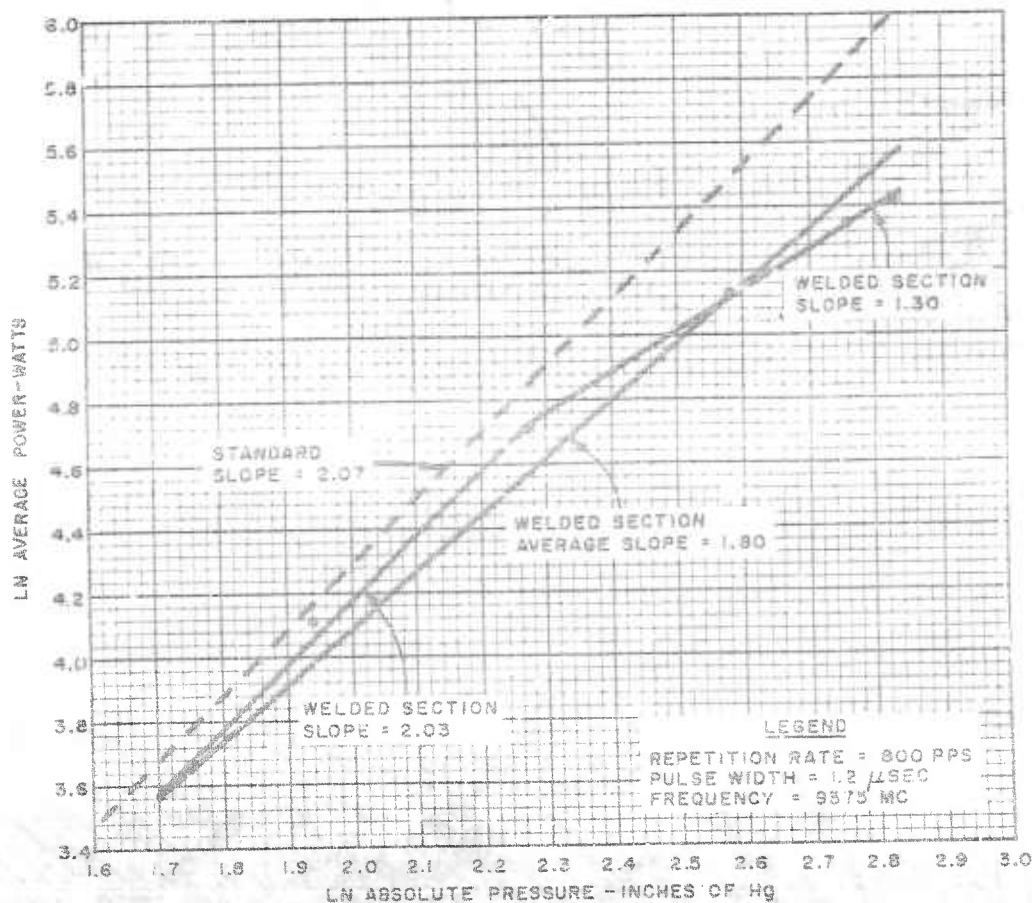
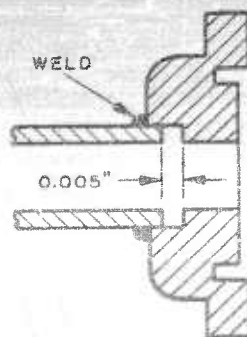


FIGURE 58  
POWER VS PRESSURE FOR  
WELDED CHOKE JOINT HAVING 0.005" GAP  
(1"x1/2"x0.050" WAVEGUIDE)

CONFIDENTIAL



CONFIDENTIAL

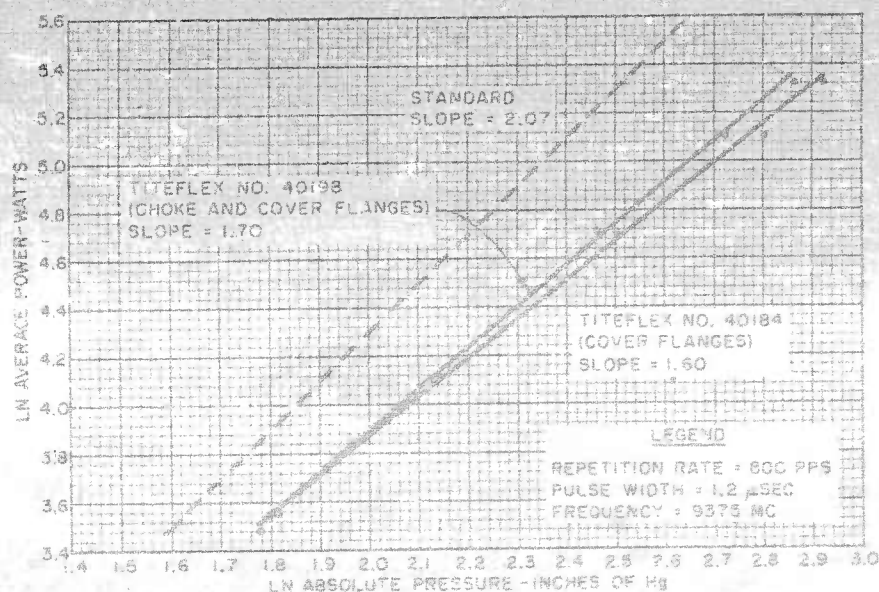


FIGURE 59  
POWER VS PRESSURE FOR  
TITEFLEX WAVEGUIDES NO. 40184 AND NO. 40198  
(1" x 1/2" x 0.050" WAVEGUIDE)

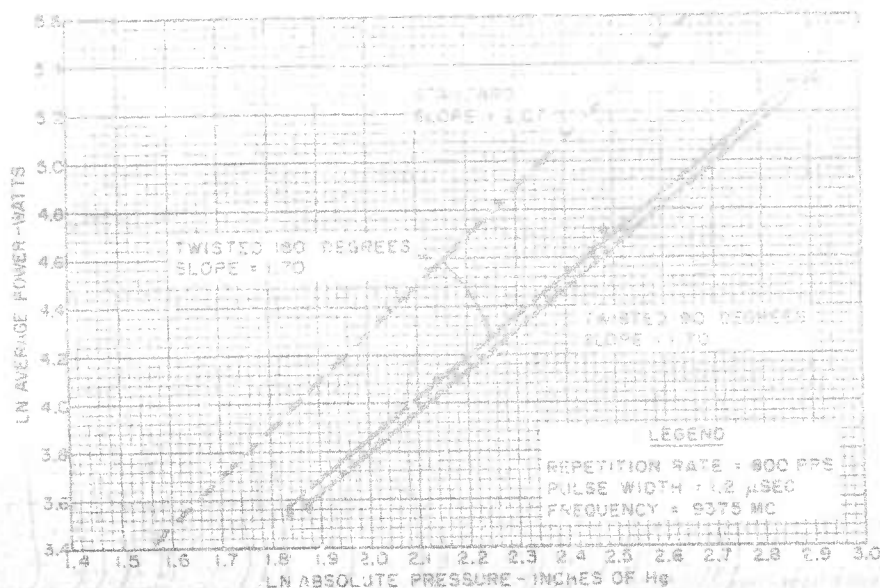


FIGURE 60  
POWER VS PRESSURE FOR  
TWISTED TITEFLEX WAVEGUIDE NO. 40198  
(1" x 1/2" x 0.050" WAVEGUIDE)

CONFIDENTIAL



CONFIDENTIAL

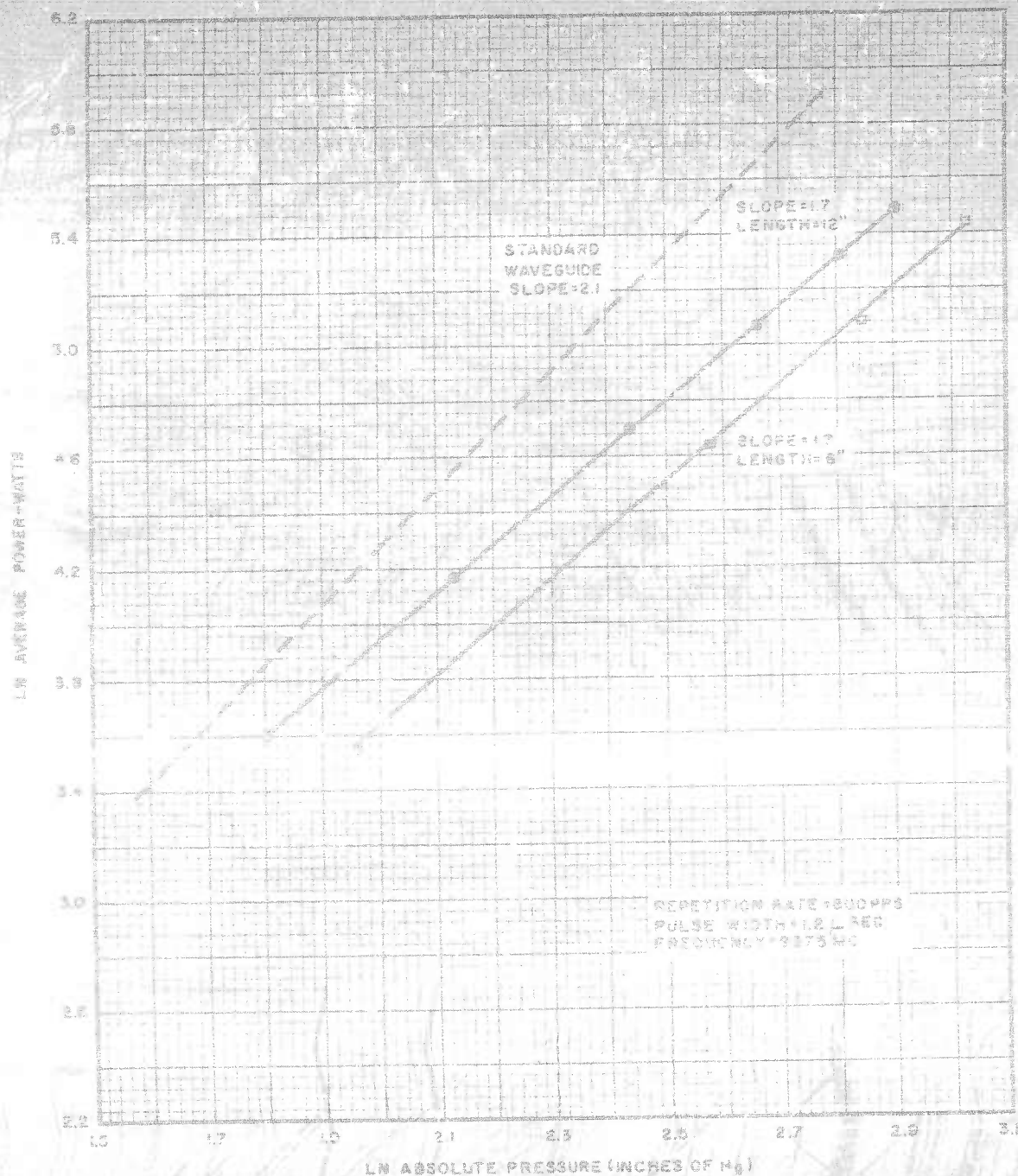


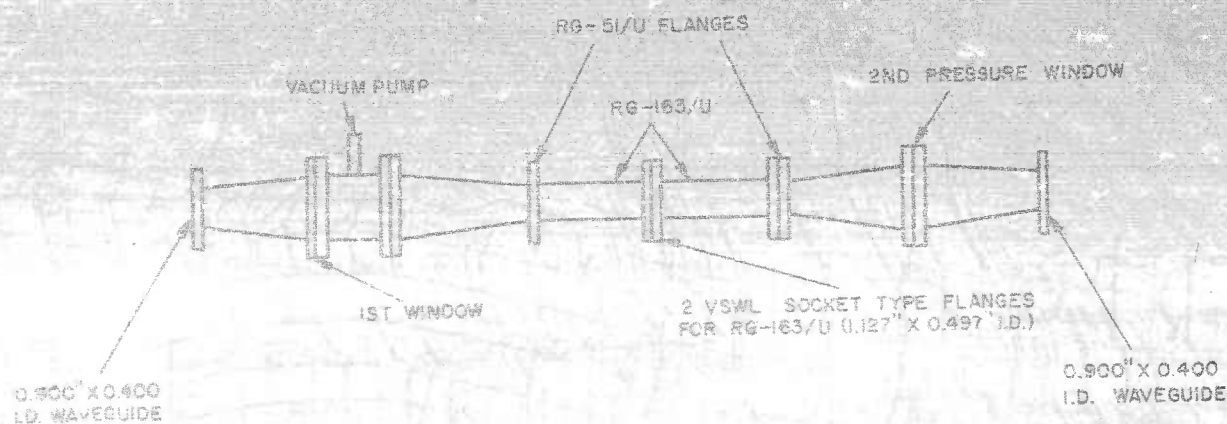
FIGURE 61  
POWER VS PRESSURE  
FOR FLEXIBLE WAVEGUIDE  
(1 1/2" x 0.050" WAVEGUIDE)

CONFIDENTIAL





CONFIDENTIAL



VSWR (OF 1ST WINDOW) = 1.18  
 VSWR (OF 2ND WINDOW AND HIGH POWER LOAD) = 1.3

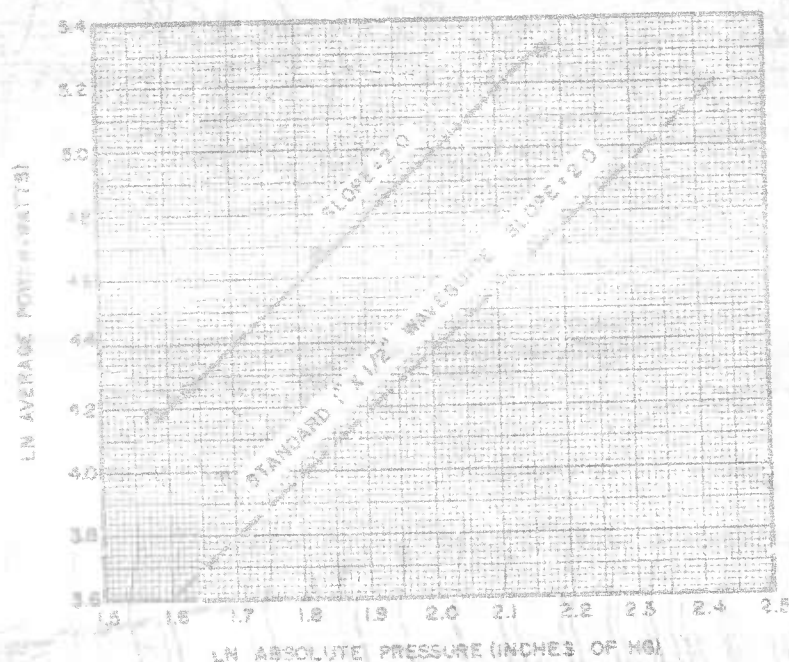


FIGURE 62  
 LN POWER VS LN PRESSURE  
 FOR USL CONTACT FLANGE

CONFIDENTIAL



CONFIDENTIAL

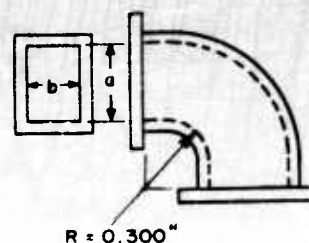
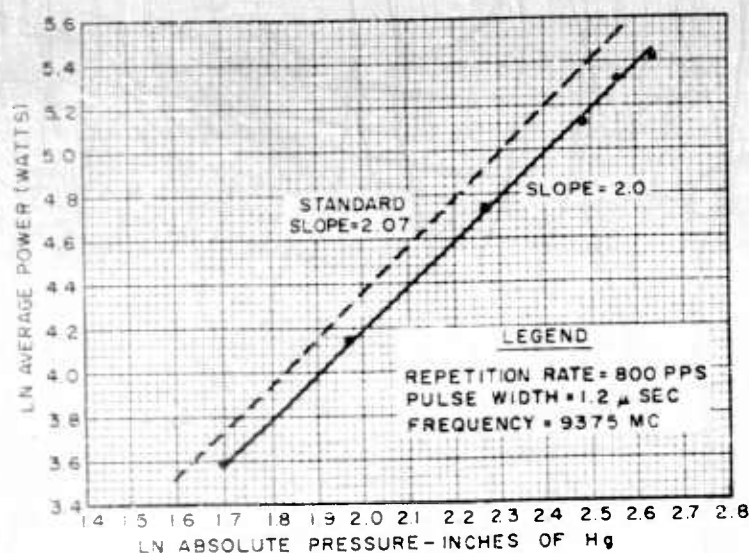


FIGURE 63  
POWER VS PRESSURE FOR 90-DEGREE  
H-PLANE BEND (1"X1/2" X .050" WAVEGUIDE)

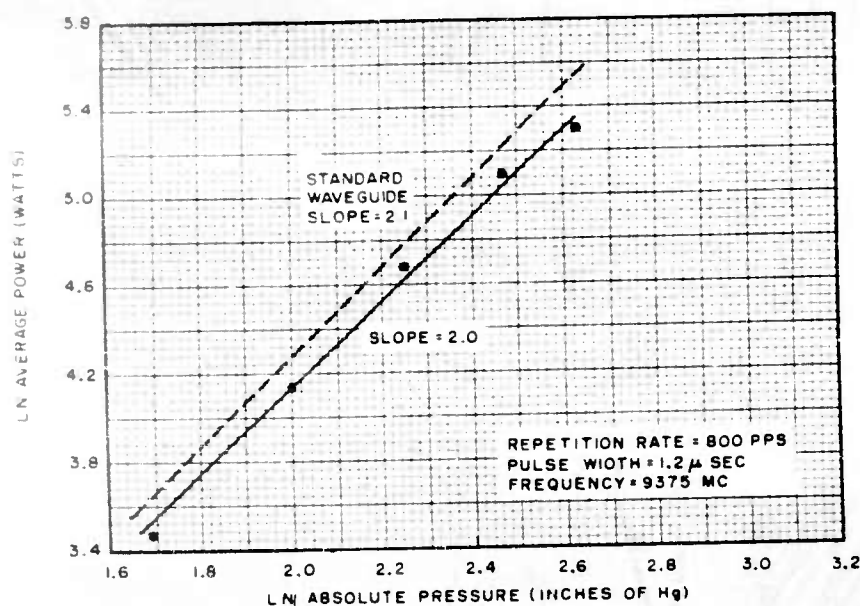
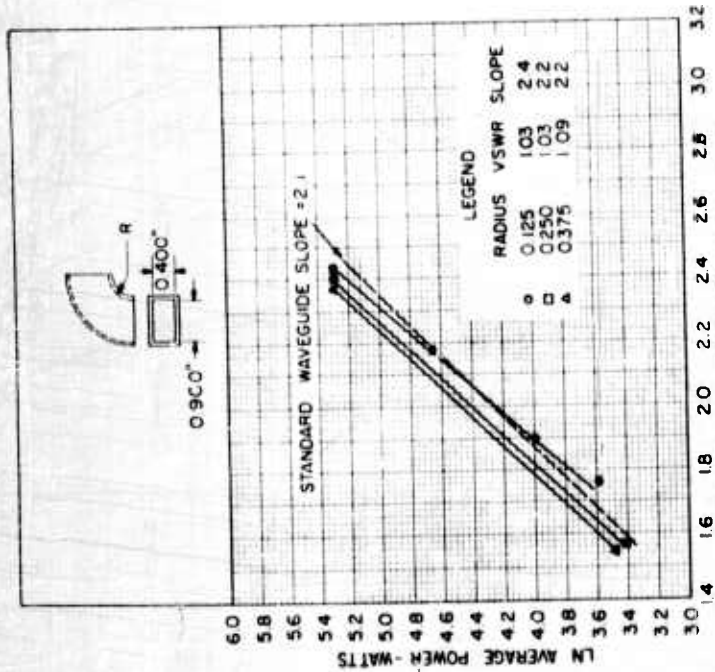


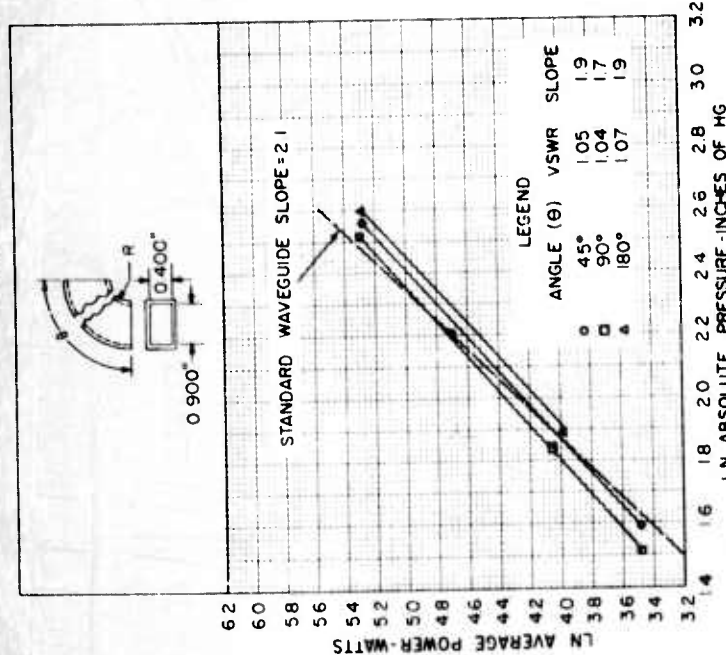
FIGURE 64  
POWER VS PRESSURE FOR 90-DEGREE  
H-PLANE BEND OF RADIUS 1 1/2 INCHES  
(1"X1/2" X .050" WAVEGUIDE)

CONFIDENTIAL

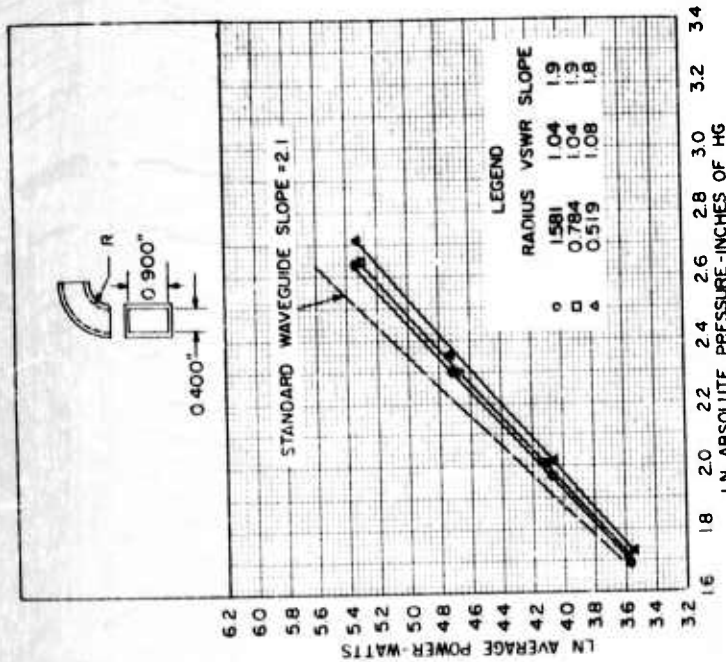




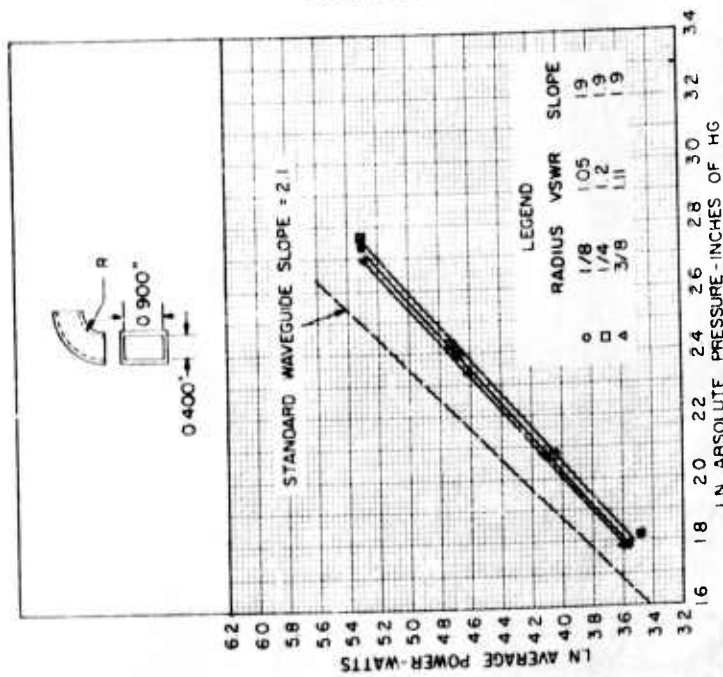
(a) MACHINED 90° H-PLANE BENDS  
(RADIUS VARIED)



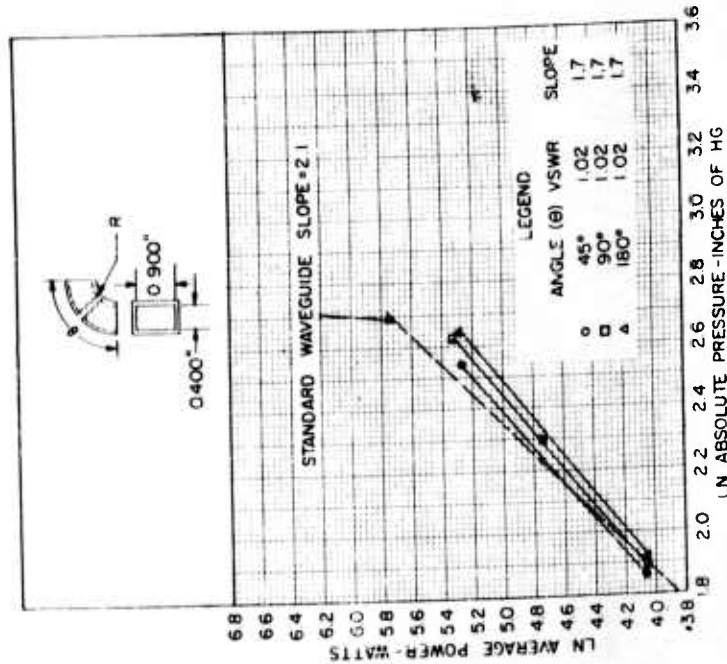
(b) 11/16-INCH RADIUS FABRICATED H-PLANE BENDS  
(ANGLE VARIED)



(c) FABRICATED 90° E-PLANE BEND  
(RADIUS VARIED)



(d) MACHINED 90° E-PLANE BENDS (RADIUS VARIED)



(e) 0.625-INCH RADIUS MACHINED E-PLANE BENDS  
(ANGLE VARIED)

FREQUENCY = 9375 MC  
PULSE WIDTH = 12 USEC  
REPETITION RATE = 800 PPS

FIGURE 65  
POWER-PRESSURE DATA FOR E- AND  
H-PLANE BENDS WITH VARYING RADIUS,  
BEND ANGLES, AND MANUFACTURES



CONFIDENTIAL

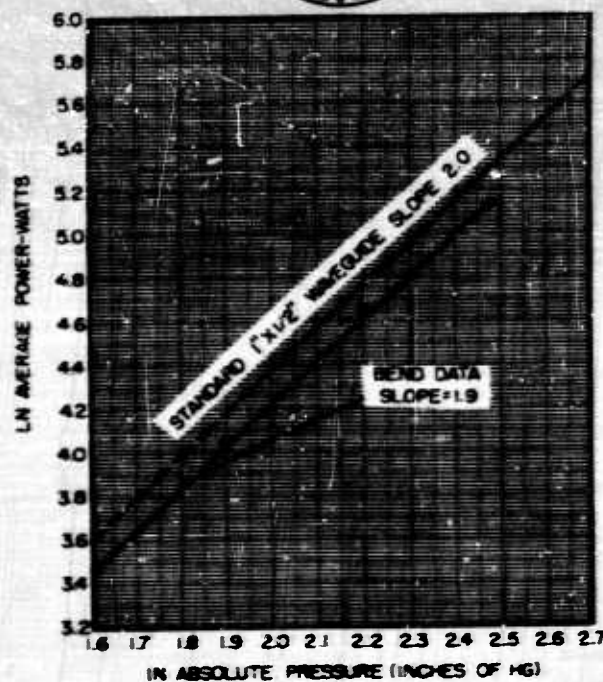


FIGURE 66

REPEAT TEST BREAKDOWN DATA  
FOR 90-DEGREE H-PLANE BEND  
(REF. TO BEND #3 TABLE 7)

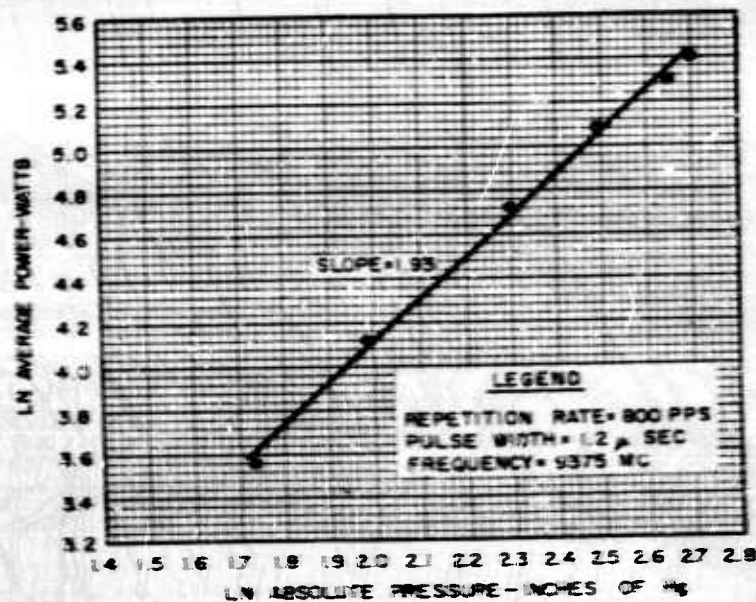


FIGURE 67

POWER VS PRESSURE FOR  
WAVEGUIDE SWITCH AND DUMMY LOAD  
(1-1/4" X 5/8" X .064" WAVEGUIDE)

CONFIDENTIAL



CONFIDENTIAL

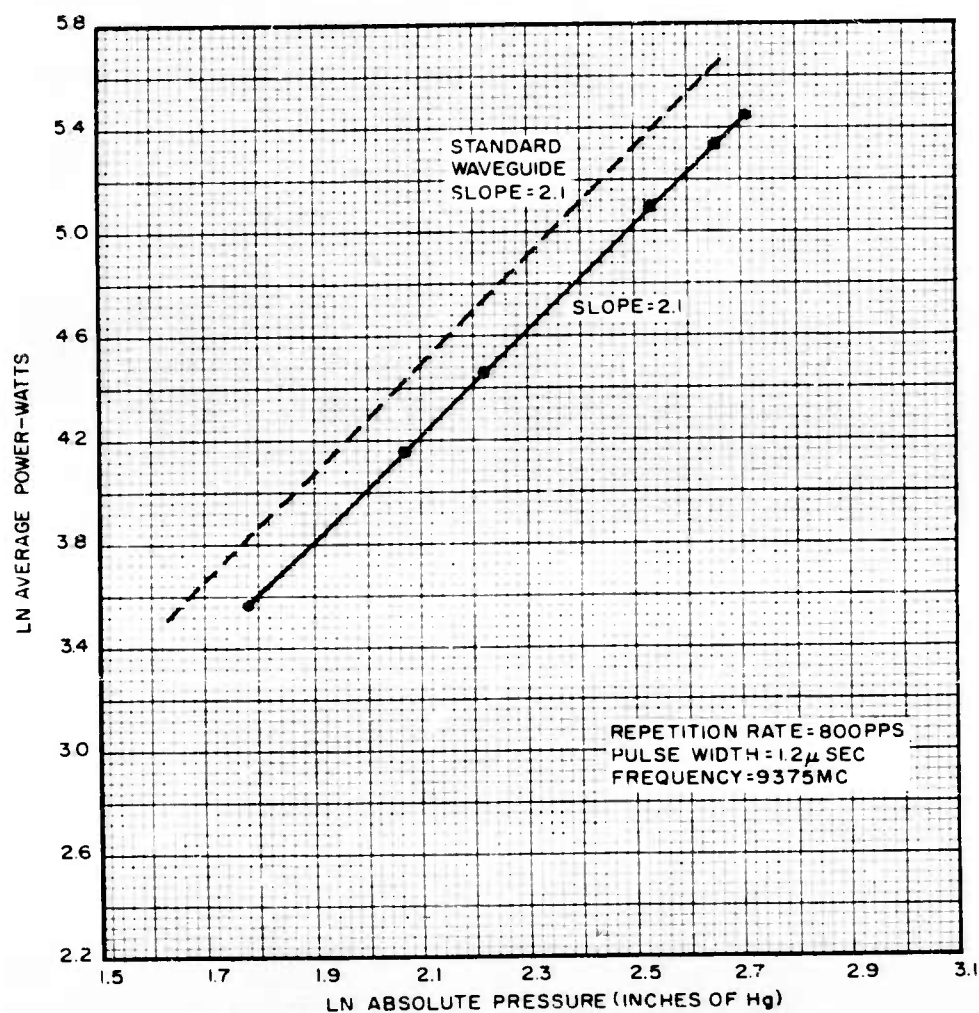
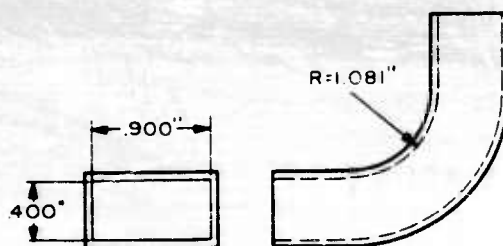


FIGURE 68  
POWER VS PRESSURE FOR 90-DEGREE  
E-PLANE BEND OF RADIUS 1.081 INCHES  
(1" x 1/2" x 0.050" WAVEGUIDE)

CONFIDENTIAL





CONFIDENTIAL

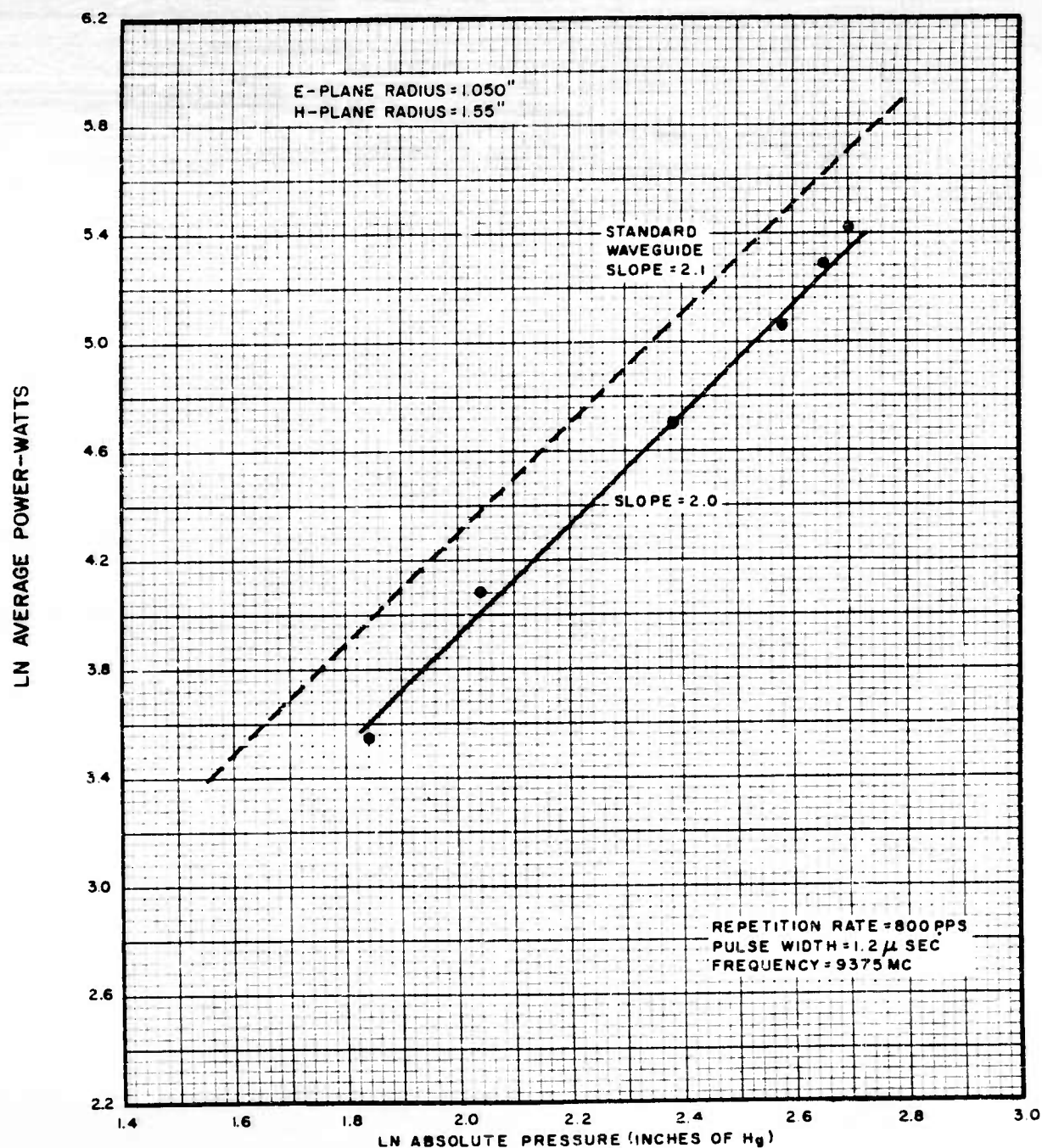


FIGURE 69

POWER VS PRESSURE FOR COMBINATION  
90-DEGREE E- AND H-PLANE BEND  
(1"X1/2"X0.050" WAVEGUIDE)

CONFIDENTIAL



CONFIDENTIAL

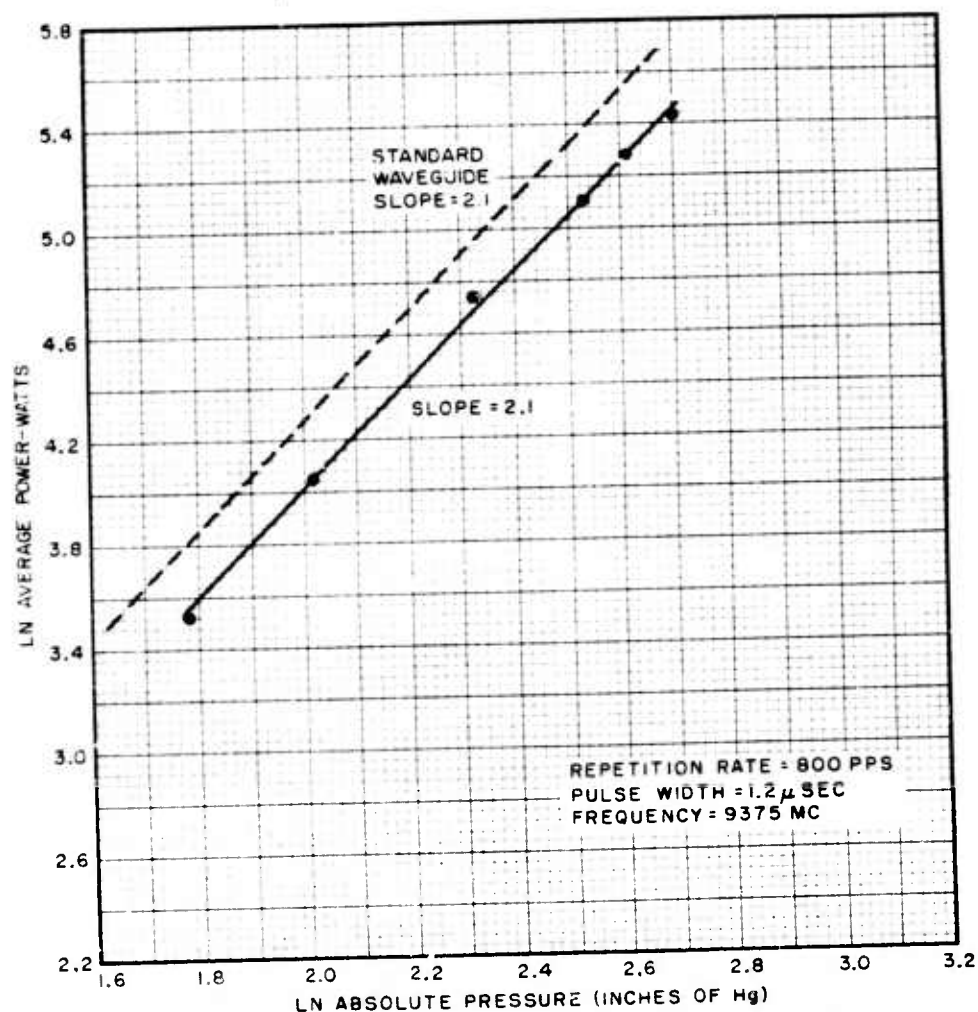
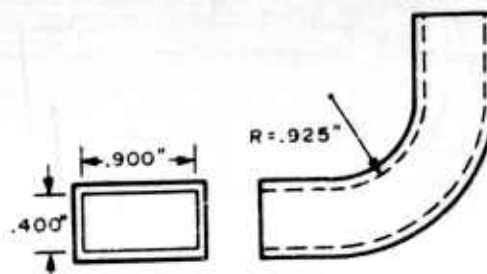


FIGURE 70  
POWER VS PRESSURE FOR 90-DEGREE  
E-PLANE BEND OF RADIUS 0.925 INCH  
(1" X 1/2" X 0.050" WAVEGUIDE)

CONFIDENTIAL





CONFIDENTIAL

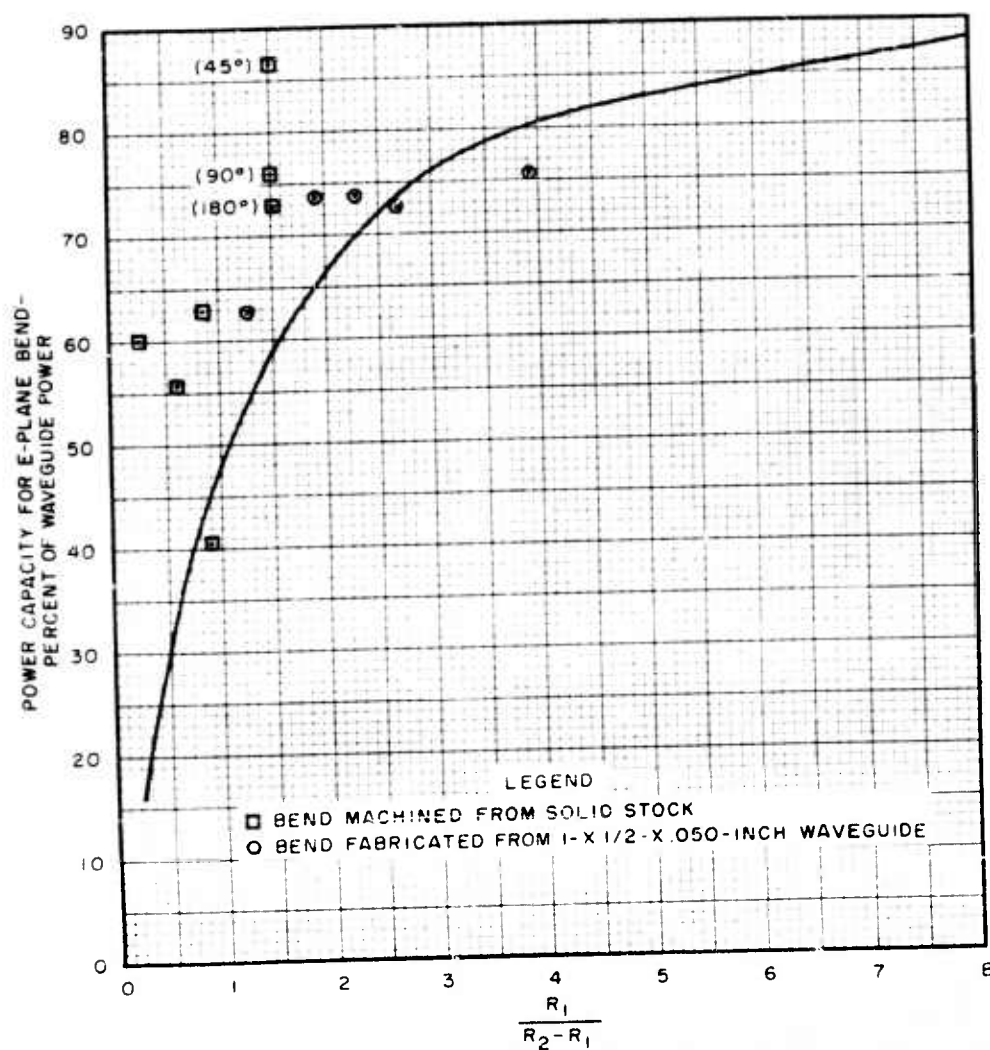
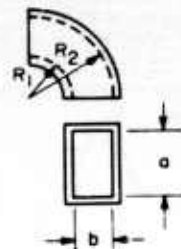


FIGURE 71  
POWER CAPACITY  
OF E-PLANE BEND VS RADIUS

CONFIDENTIAL

CONFIDENTIAL

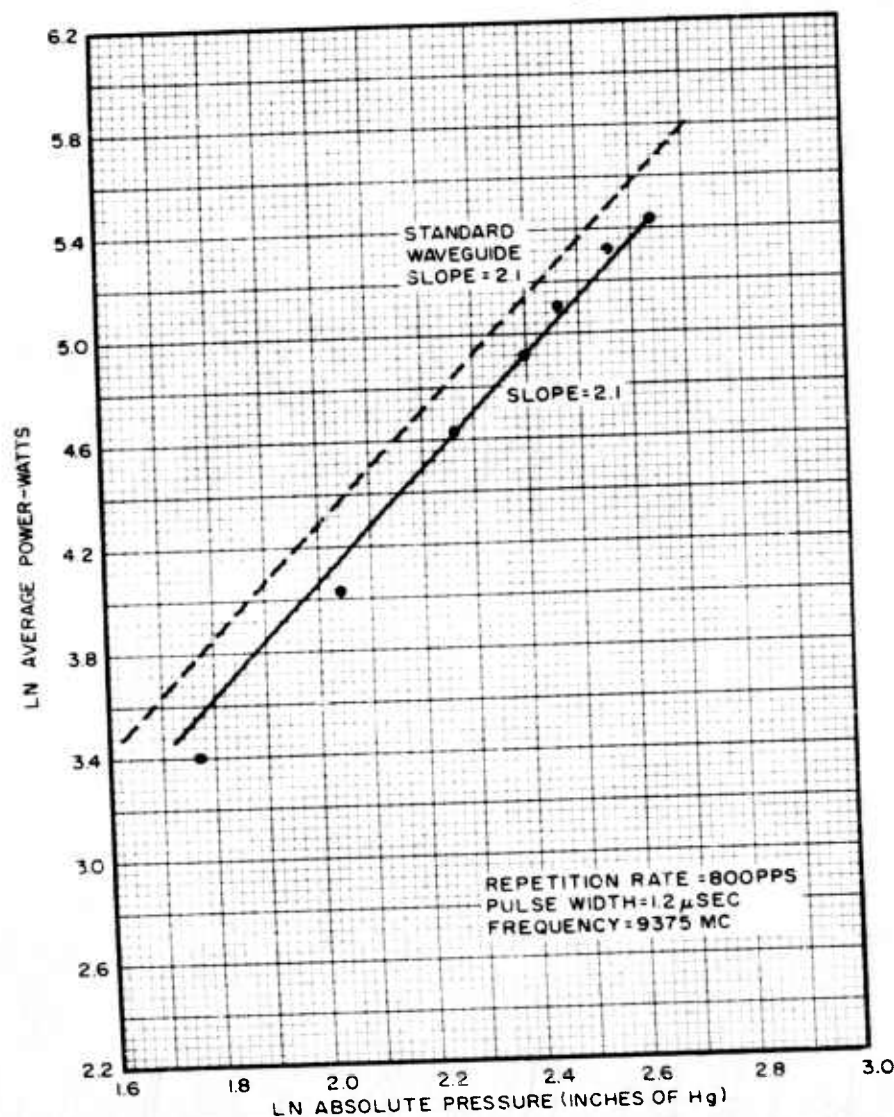
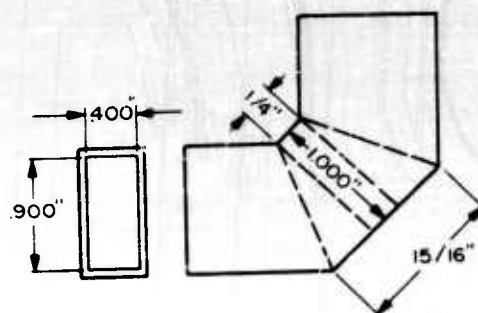


FIGURE 72  
POWER VS PRESSURE FOR 90-DEGREE  
H-PLANE MITERED CORNER  
(1" x 1/2" x 0.050" WAVEGUIDE)

CONFIDENTIAL

CONFIDENTIAL

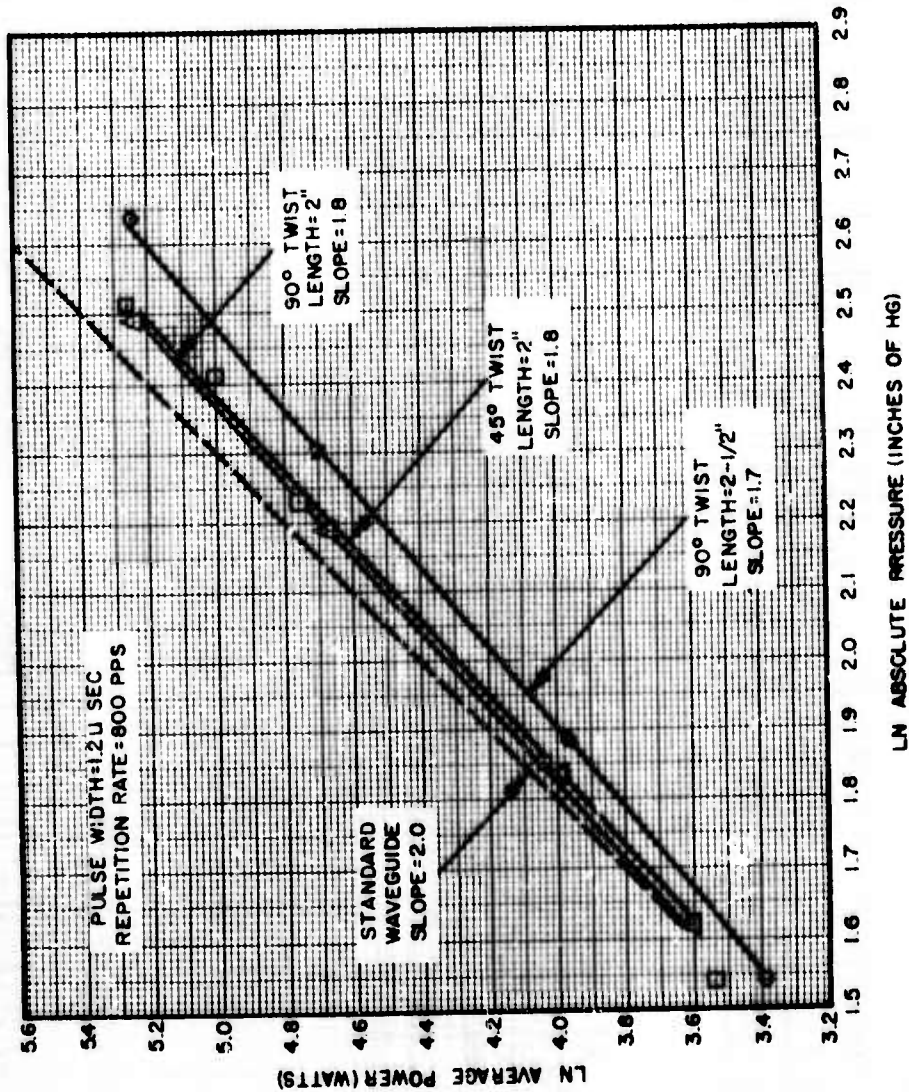


FIGURE 73b  
BREAKDOWN POWER VS PRESSURE  
FOR THREE-TWIST SECTIONS

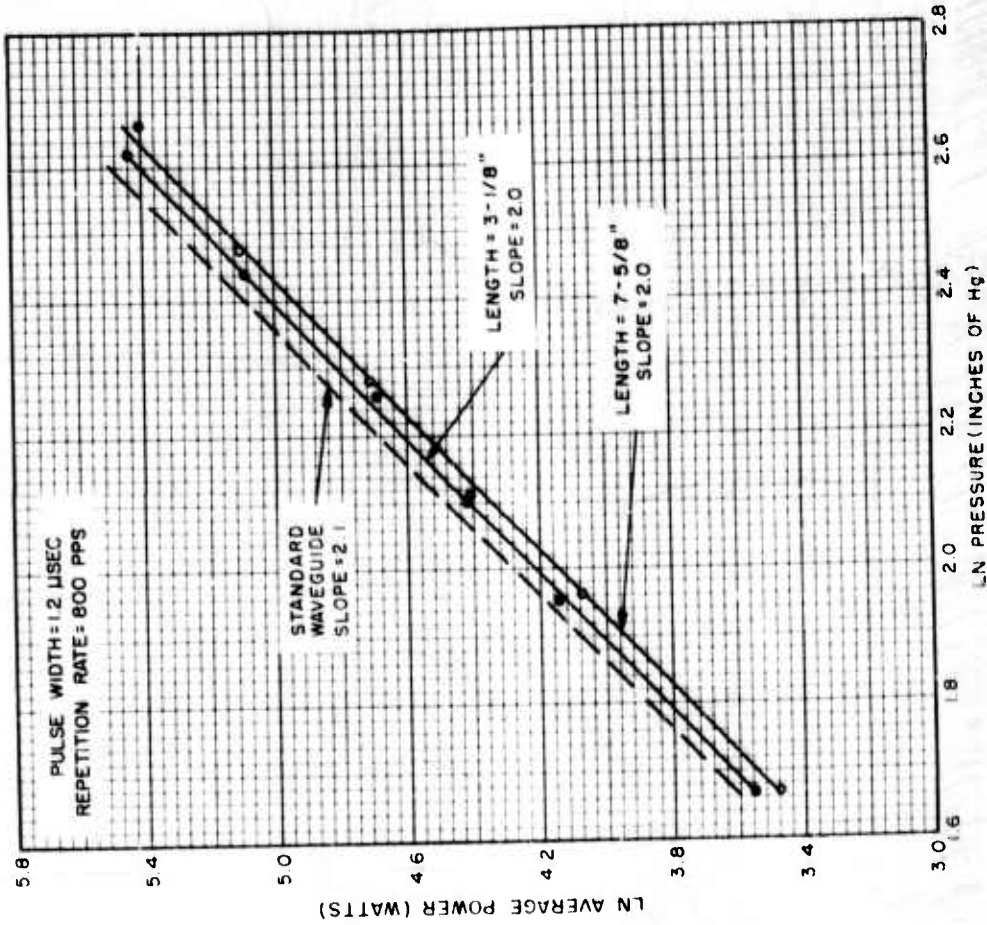


FIGURE 73a  
POWER VS PRESSURE FOR TWO 90-DEGREE  
TWIST SECTIONS (1" X 1/2" X 0.050" WAVEGUIDE)

CONFIDENTIAL





CONFIDENTIAL

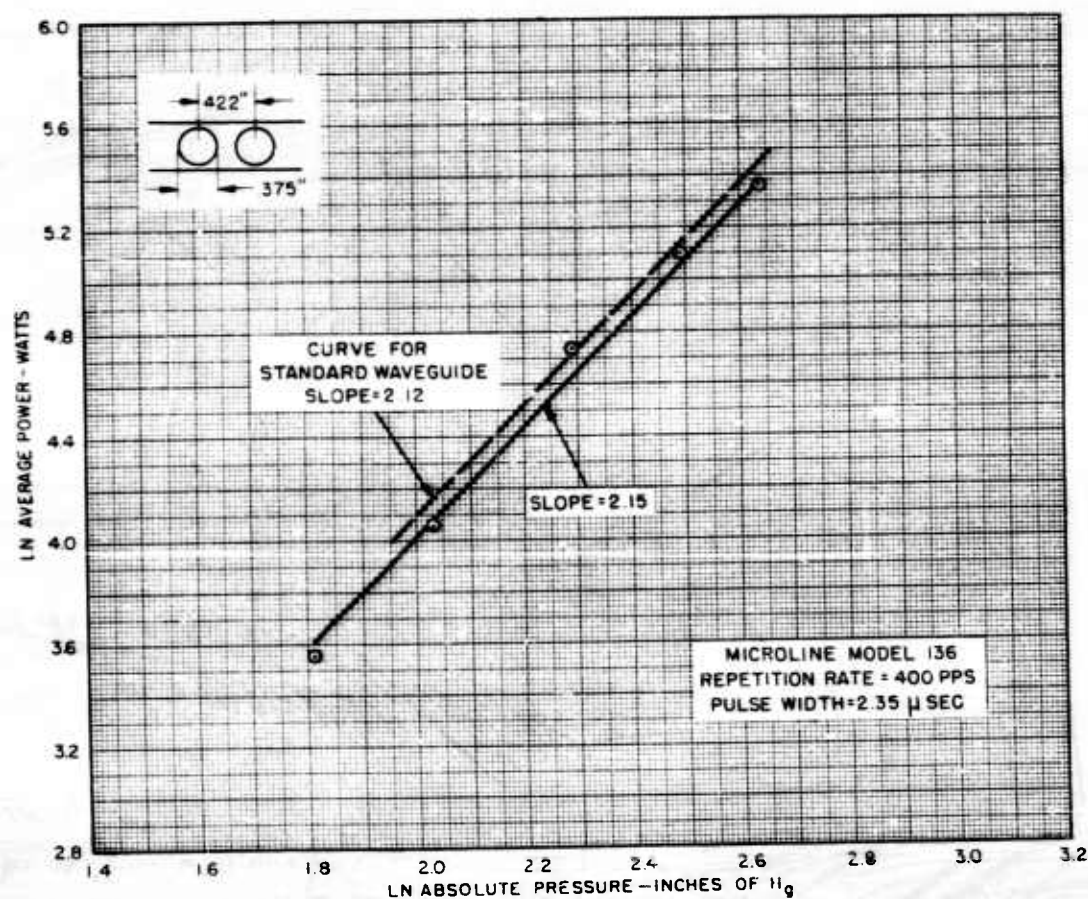
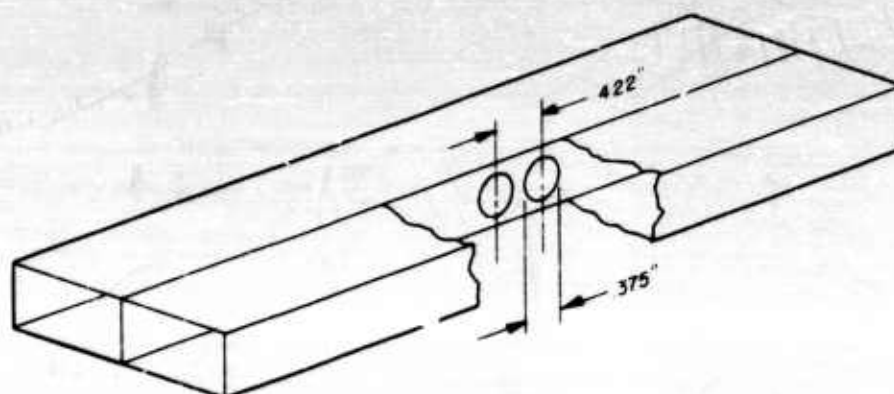


FIGURE 74  
BREAKDOWN POWER VS PRESSURE FOR  
THE TWO-HOLE DIRECTIONAL COUPLER

CONFIDENTIAL



CONFIDENTIAL

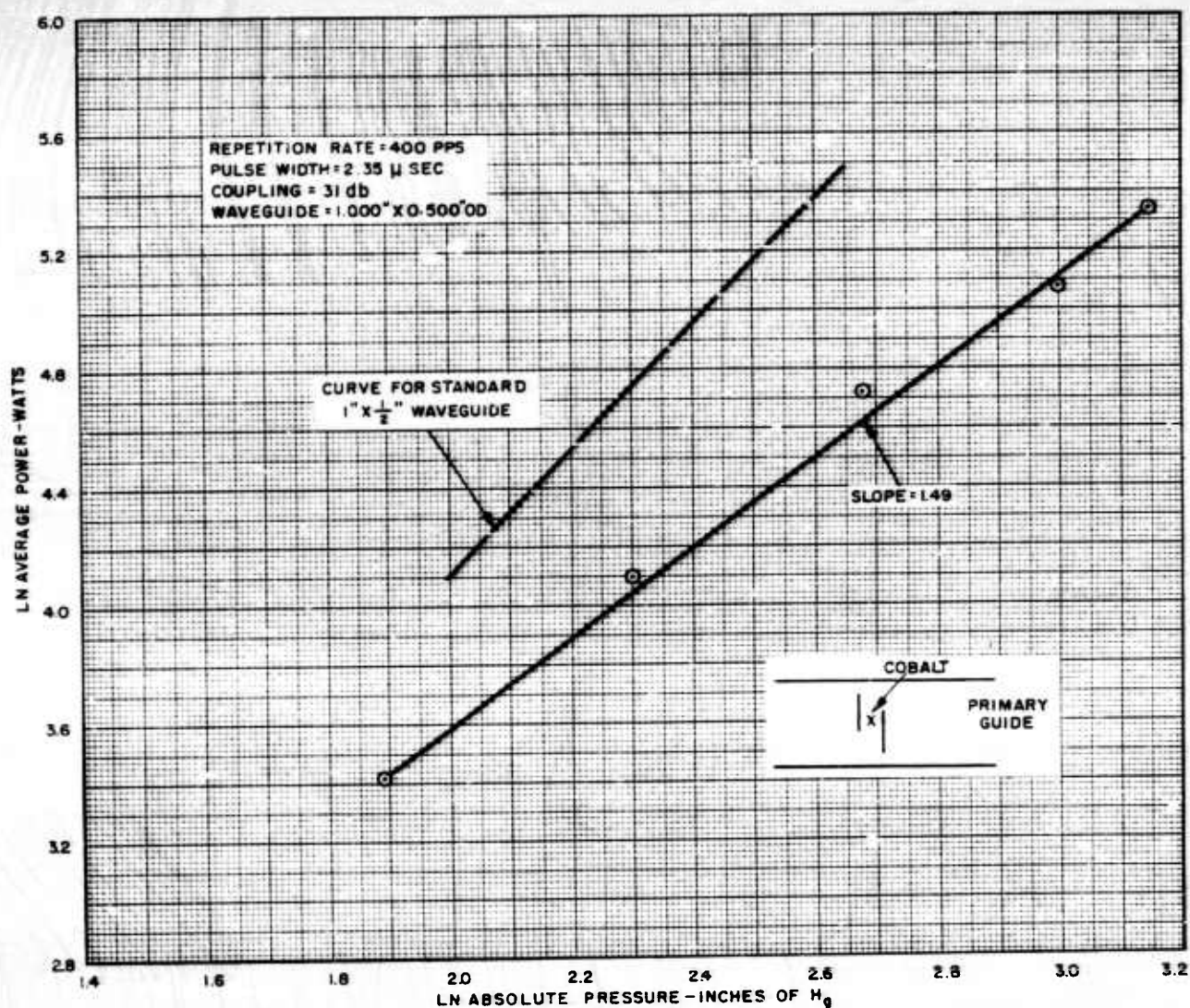


FIGURE 75  
BREAKDOWN POWER VS. PRESSURE  
FOR THE CROSS-GUIDE COUPLER WITH  
SLOTS TRANSVERSE TO PRIMARY WAVEGUIDE

CONFIDENTIAL





CONFIDENTIAL

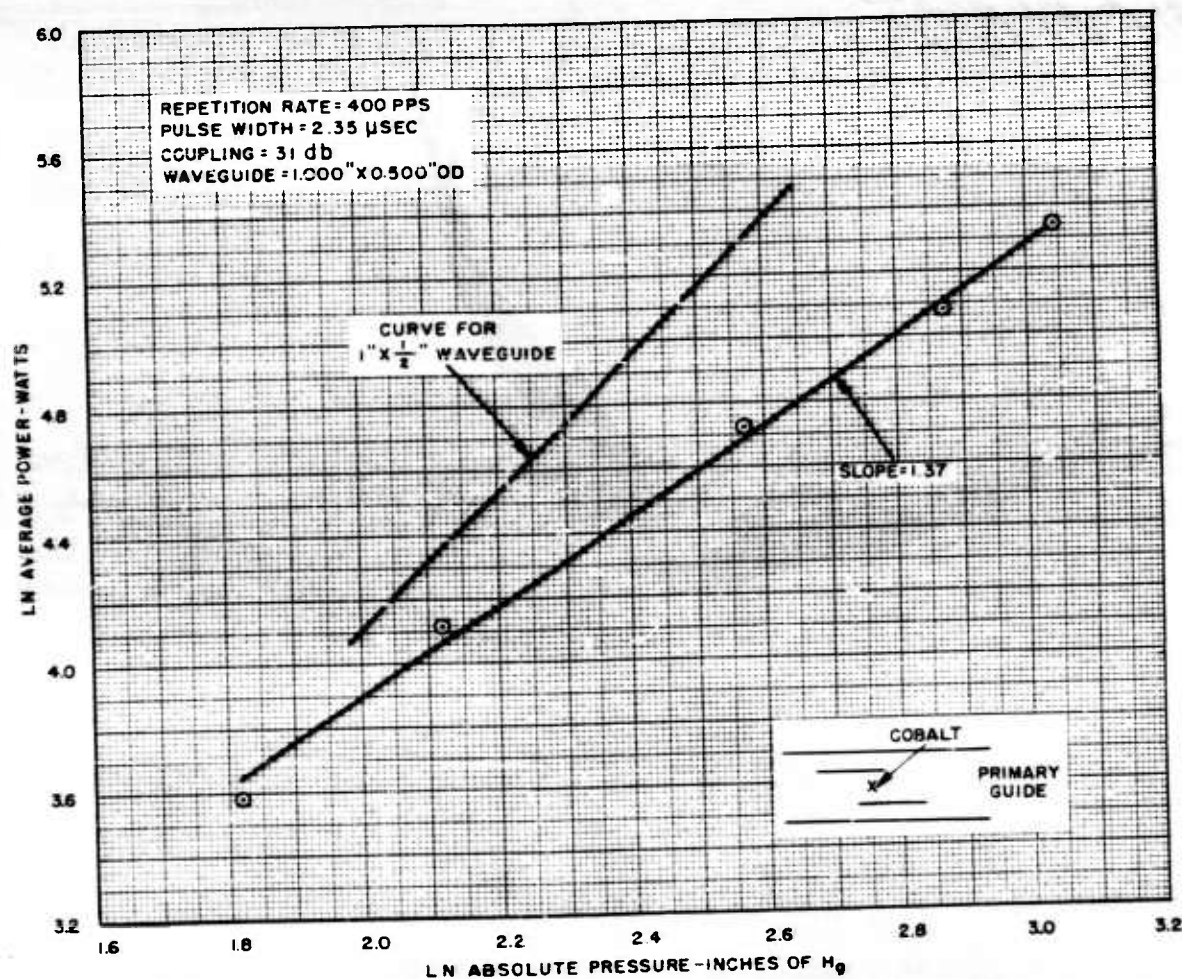


FIGURE 76  
BREAKDOWN POWER VS. PRESSURE  
FOR THE CROSS-GUIDE COUPLER WITH SLOTS  
PARALLEL TO PRIMARY WAVEGUIDE

CONFIDENTIAL



CONFIDENTIAL

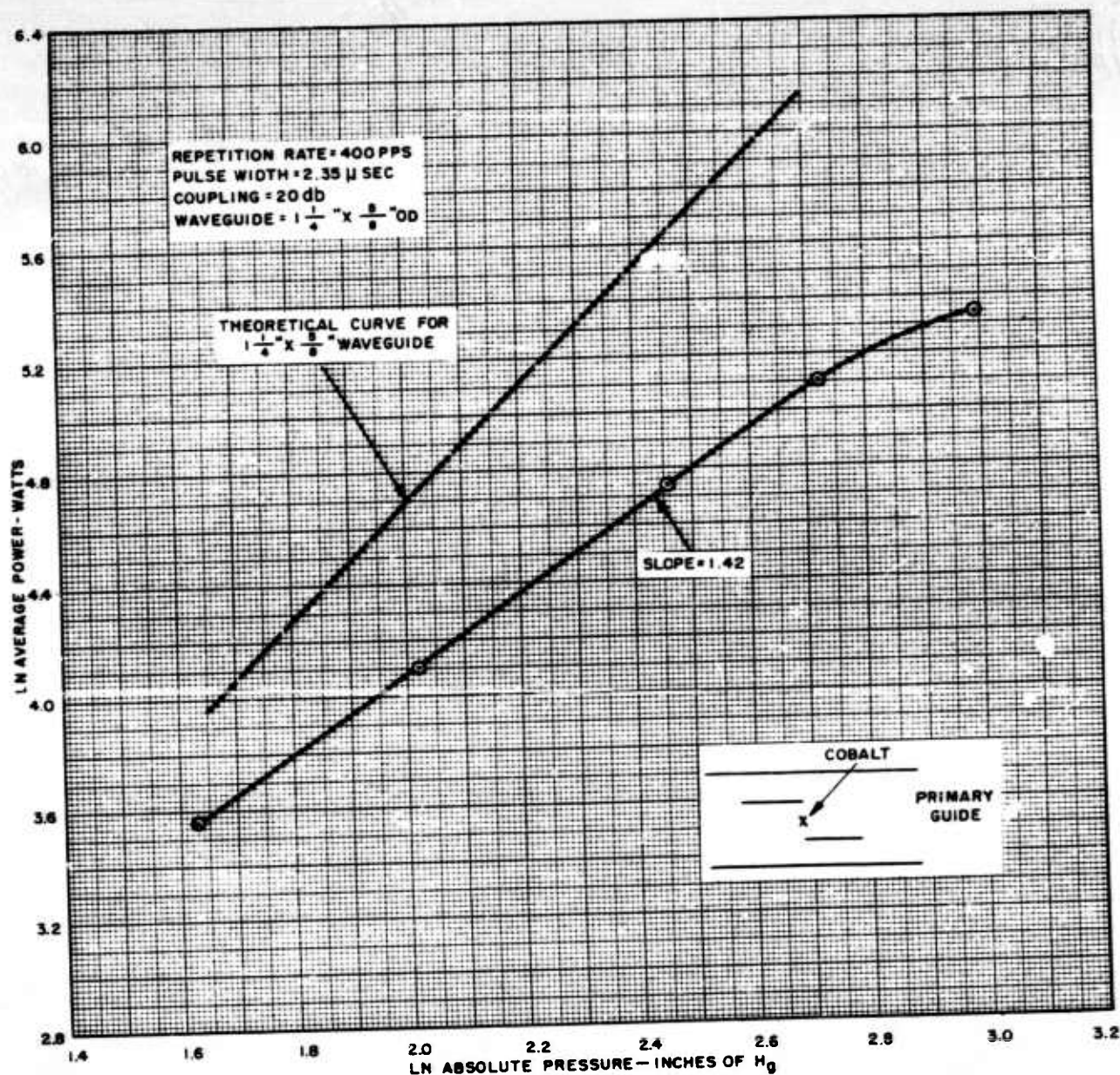


FIGURE 77  
BREAKDOWN POWER VS. PRESSURE  
FOR THE SCHWINGER COUPLER WITH  
SLOTS IN THE BROAD WALL OF PRIMARY GUIDE

CONFIDENTIAL



CONFIDENTIAL

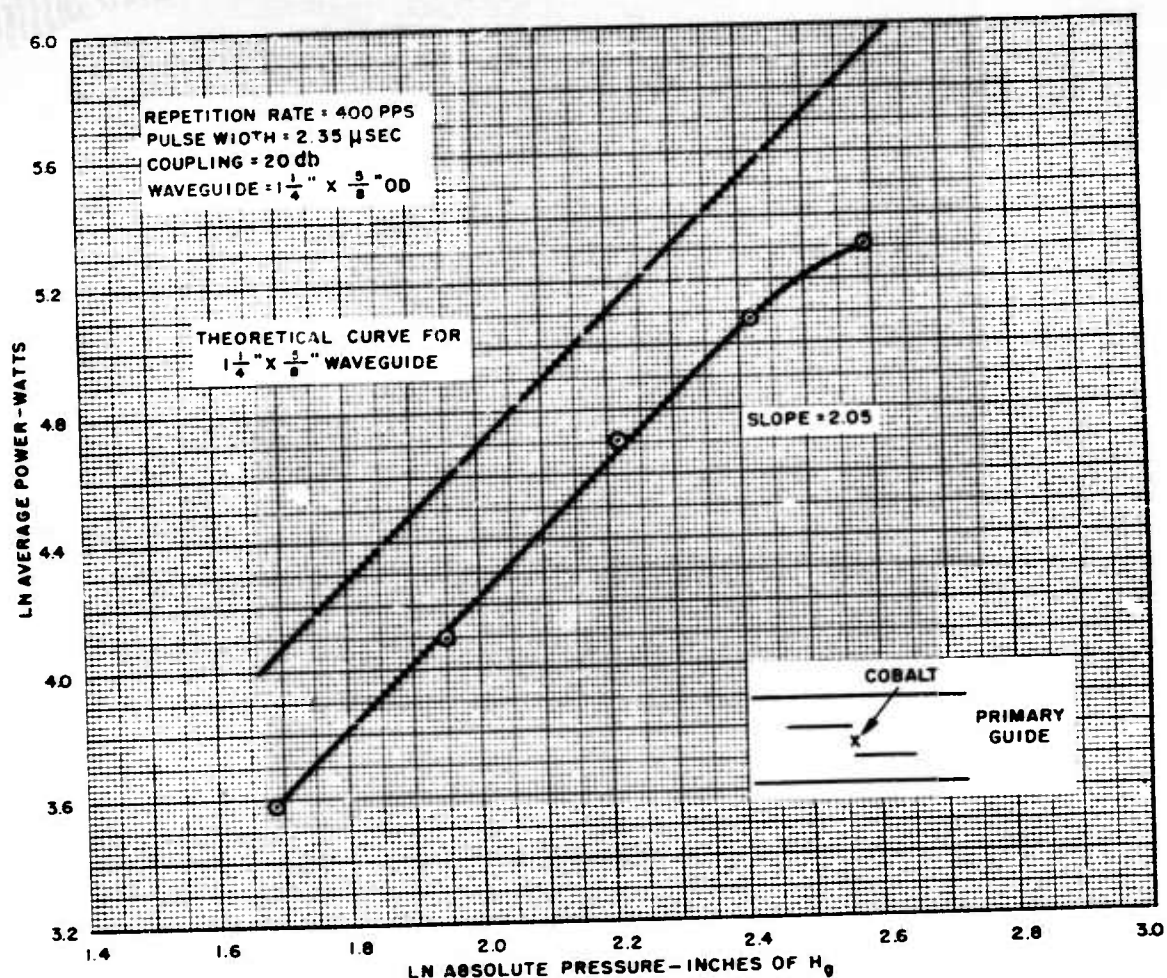


FIGURE 78  
BREAKDOWN POWER VS. PRESSURE FOR  
THE SCHWINGER COUPLER WITH SLOTS IN  
THE NARROW WALL OF PRIMARY WAVEGUIDE

CONFIDENTIAL





CONFIDENTIAL

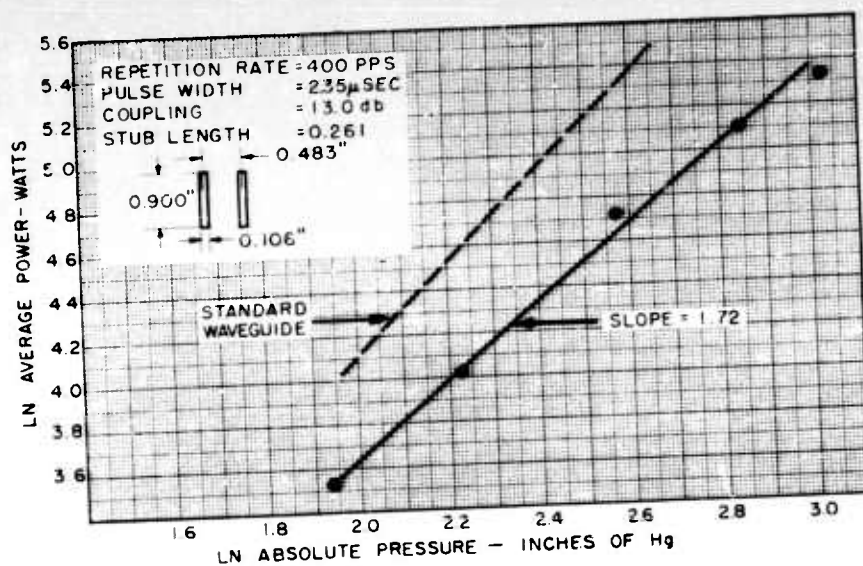


FIGURE 79  
BREAKDOWN POWER VS. PRESSURE FOR  
BRANCH-GUIDE DIRECTIONAL COUPLER

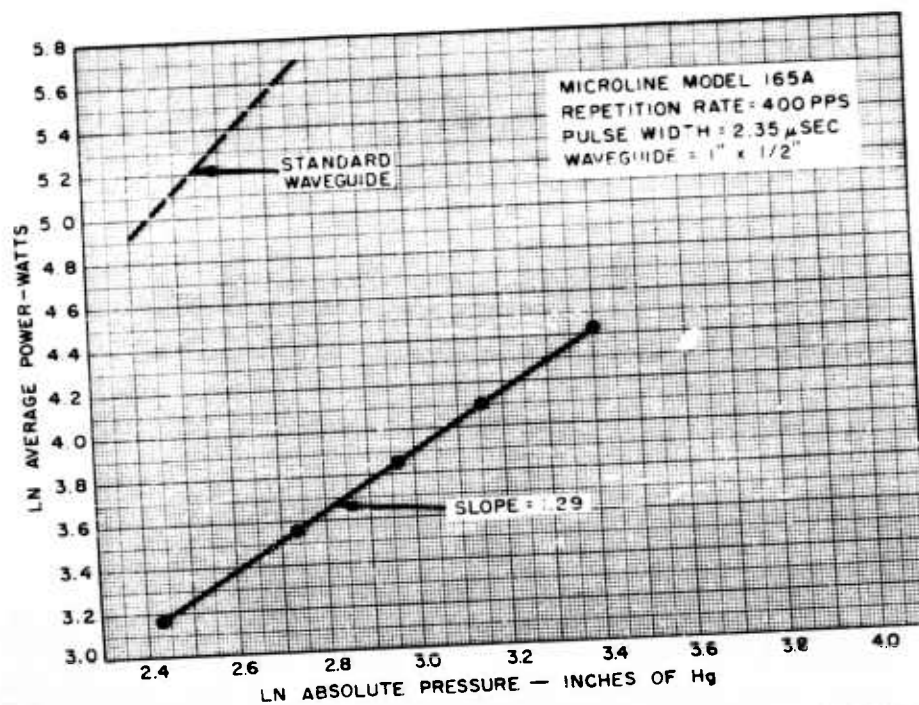


FIGURE 80  
BREAKDOWN POWER VS. PRESSURE  
FOR E-PLANE TEE

CONFIDENTIAL



CONFIDENTIAL

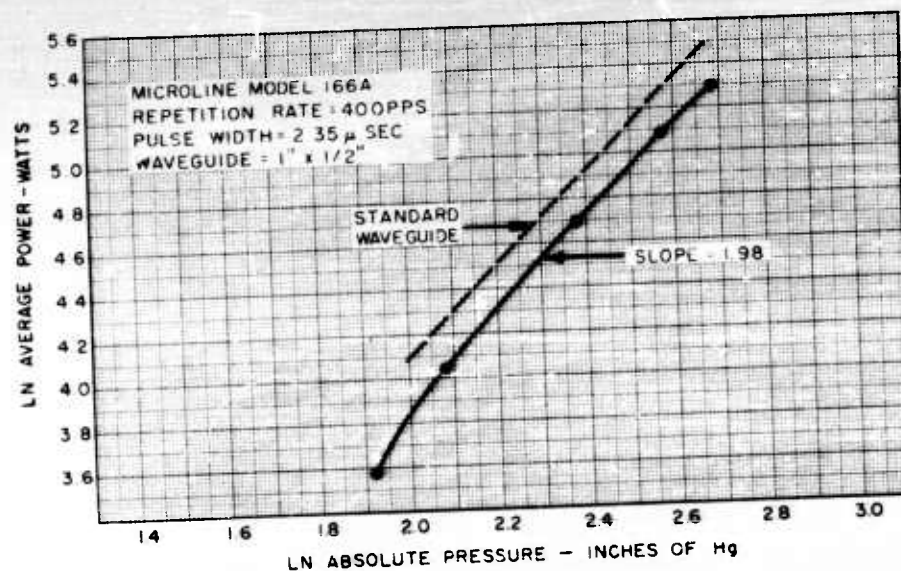


FIGURE 81  
BREAKDOWN POWER VS. PRESSURE  
FOR H-PLANE TEE

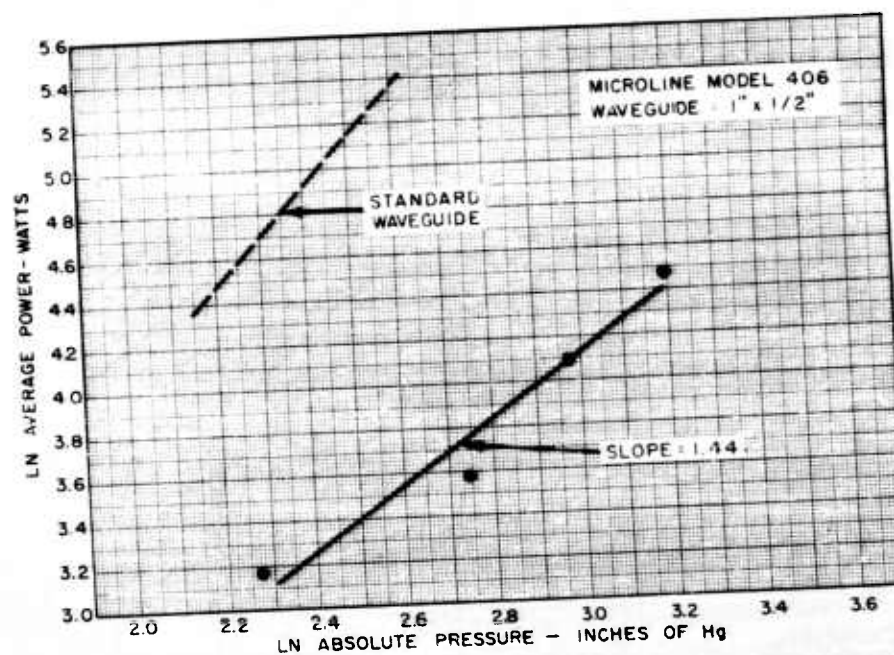


FIGURE 82  
BREAKDOWN POWER VS. PRESSURE  
FOR MAGIC TEE

CONFIDENTIAL





CONFIDENTIAL

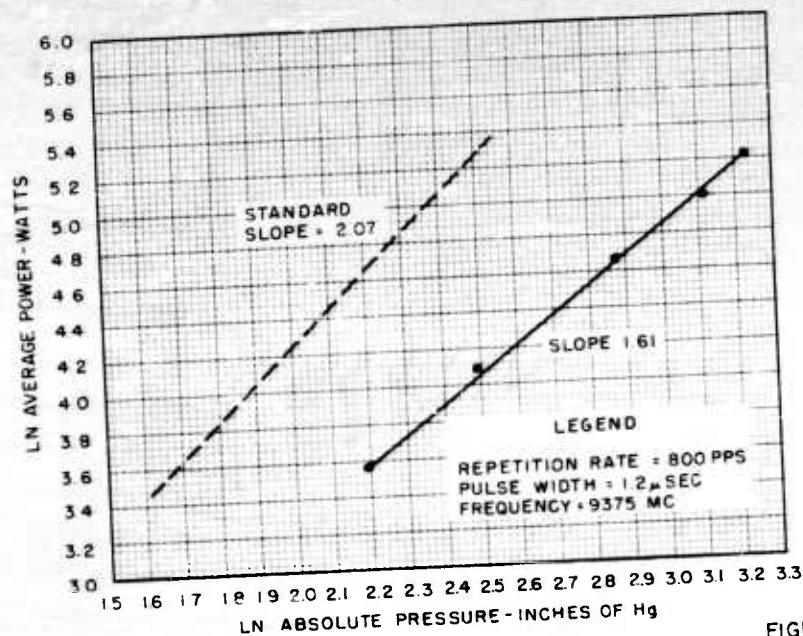


FIGURE 83  
POWER VS PRESSURE  
FOR HYBRID RING  
(1" X 1/2" X 0.050" WAVEGUIDE)

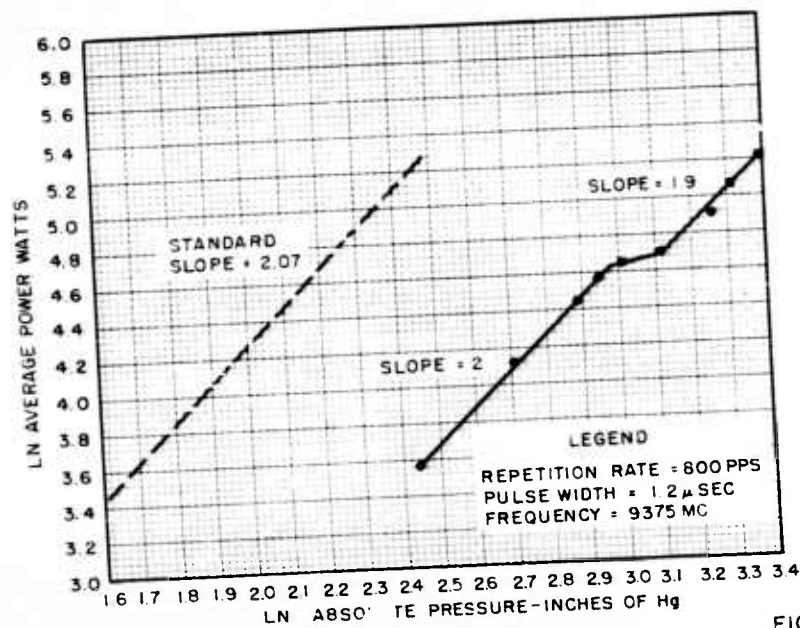


FIGURE 84  
POWER VS PRESSURE FOR  
RECTANGULAR-TO-CIRCULAR  
WAVEGUIDE ROTARY JOINT  
(1" X 1/2" X 0.050" WAVEGUIDE)

CONFIDENTIAL



CONFIDENTIAL

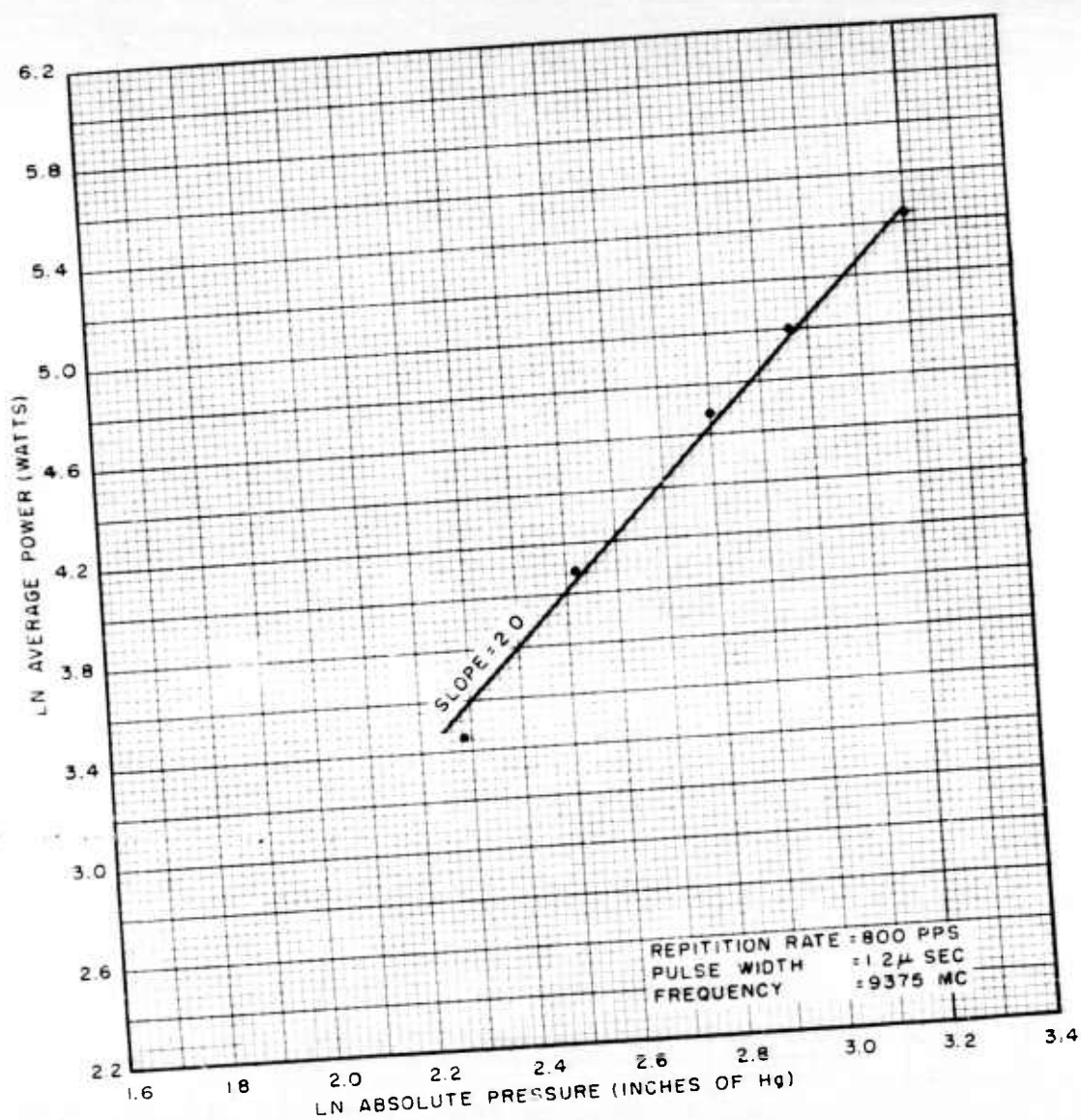


FIGURE 85  
POWER VS PRESSURE FOR  
ROTARY JOINT  
(1-1/4" X 5/8" X 0.064" WAVEGUIDE)

CONFIDENTIAL



CONFIDENTIAL

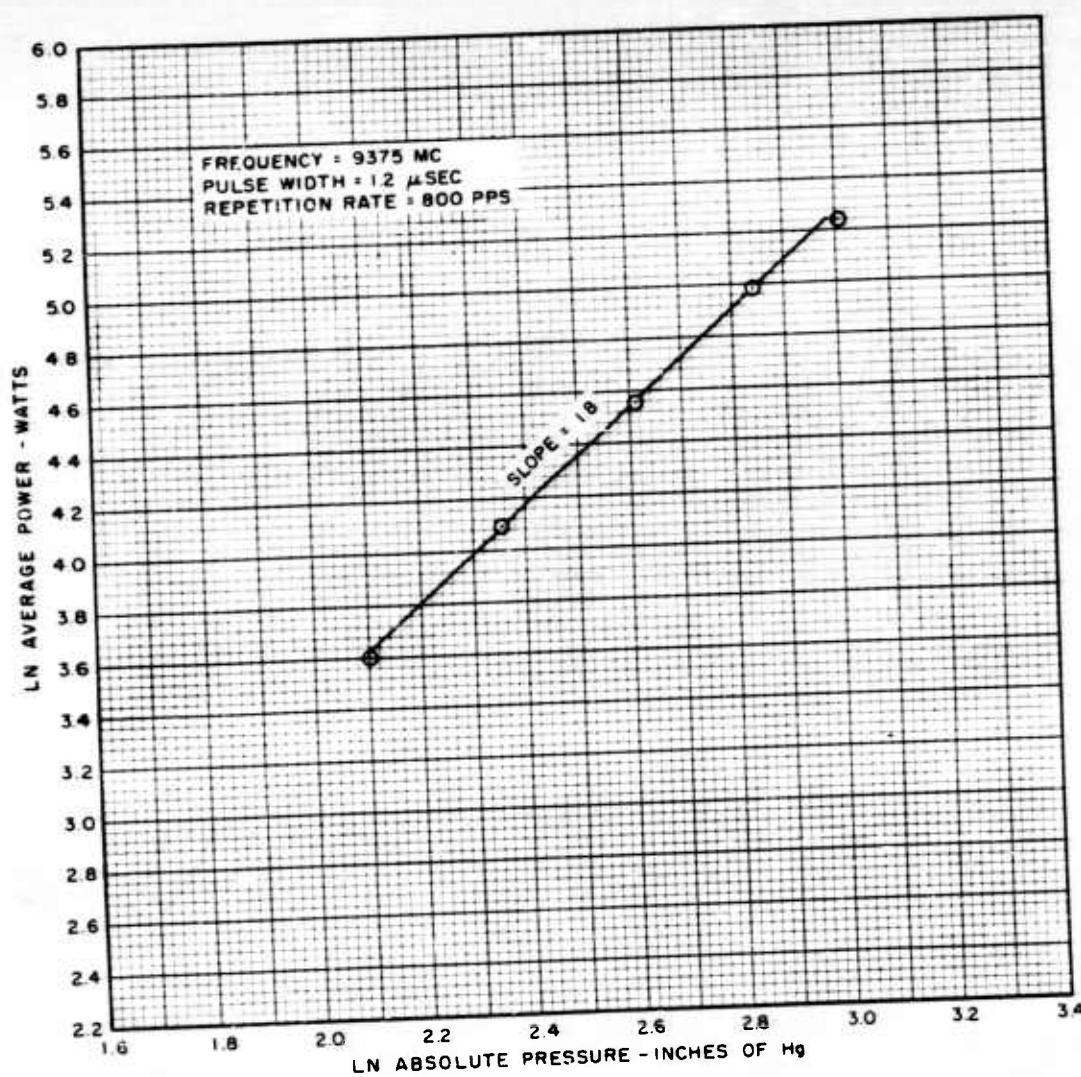


FIGURE 86

LN POWER VS LN PRESSURE  
FOR A DUAL-FEED COAXIAL-LINE  
ROTARY JOINT

CONFIDENTIAL



CONFIDENTIAL

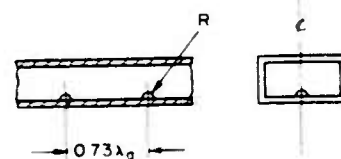
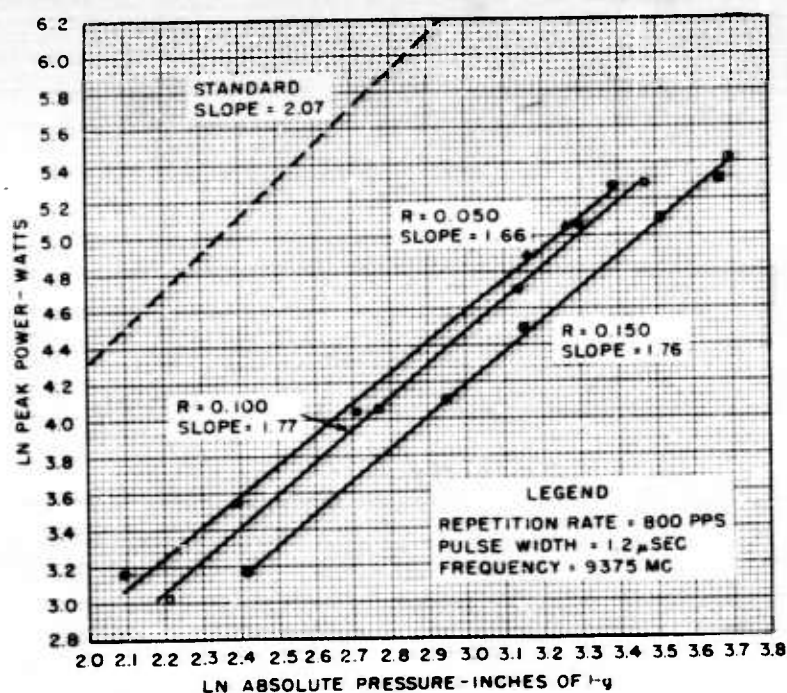


FIGURE 87  
POWER VS PRESSURE FOR SECTION  
CONTAINING HEMISPHERICAL BUMPS  
(1" X 1/2" X .050" WAVEGUIDE)

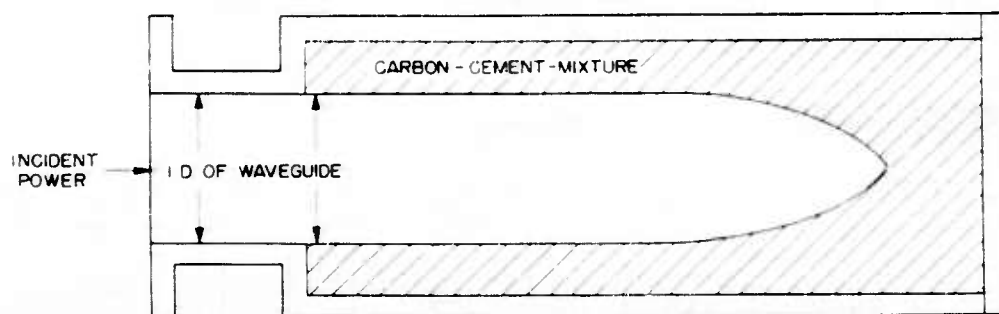


FIGURE 88  
LOSSY-WALL TYPE  
OF HIGH-POWER LOAD

CONFIDENTIAL





CONFIDENTIAL

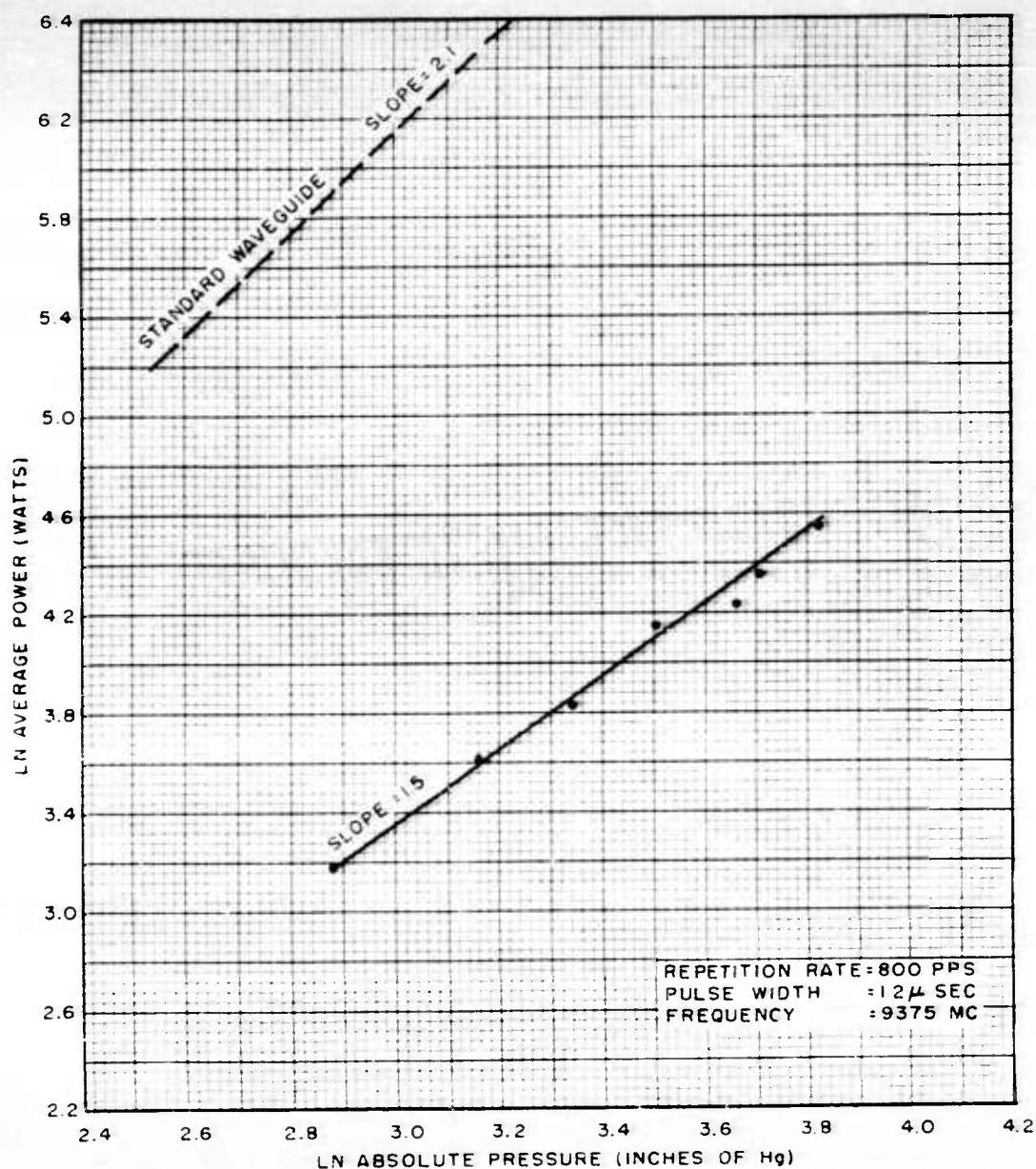


FIGURE 89  
POWER VS PRESSURE FOR  
COAXIAL-LINE-TO-WAVEGUIDE ADAPTER  
(1"X1/2"X 0.050" WAVEGUIDE)

CONFIDENTIAL





CONFIDENTIAL

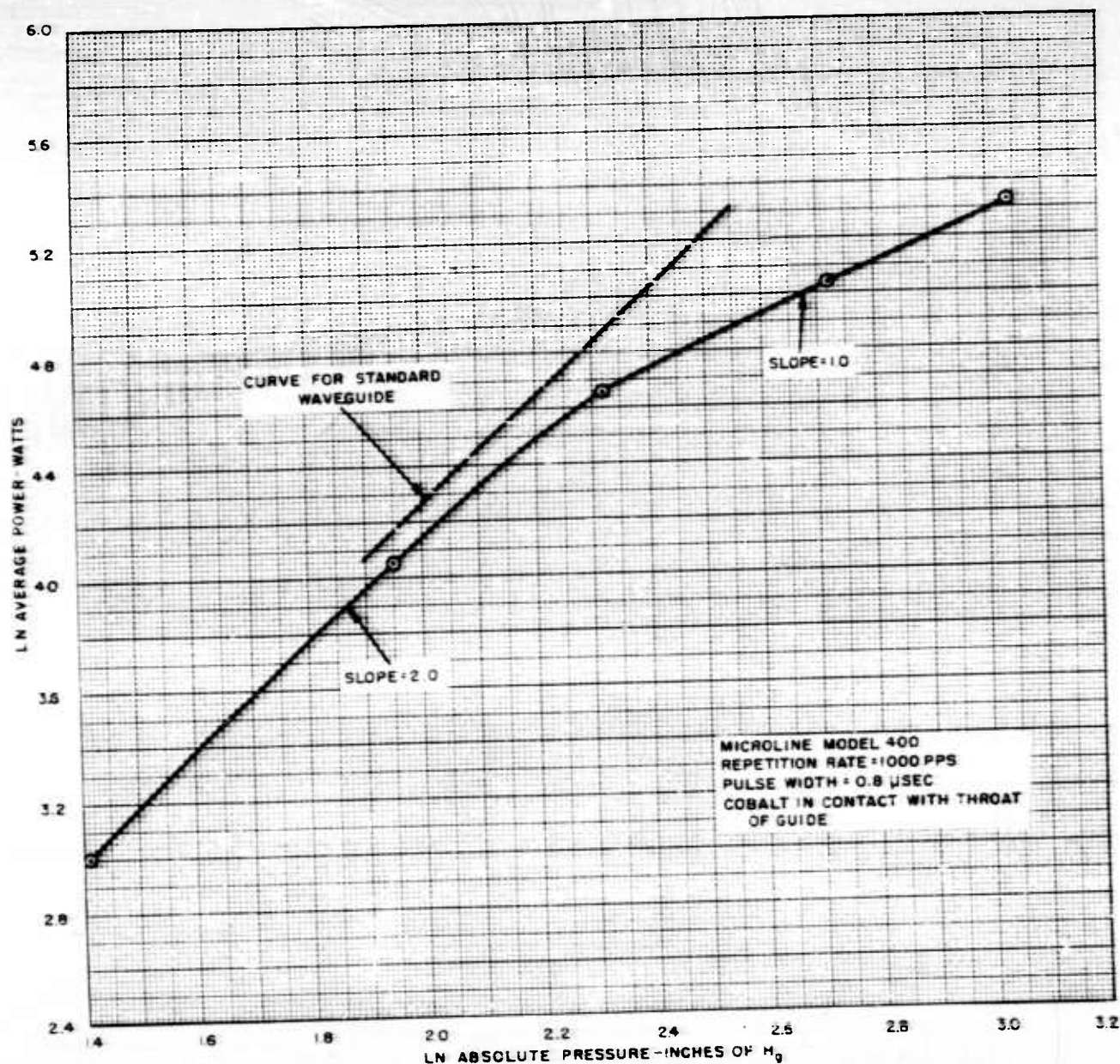


FIGURE 90  
BREAKDOWN POWER VS. PRESSURE  
FOR THE 1" X  $\frac{1}{2}$ " WAVEGUIDE DUMMY LOAD

CONFIDENTIAL



CONFIDENTIAL

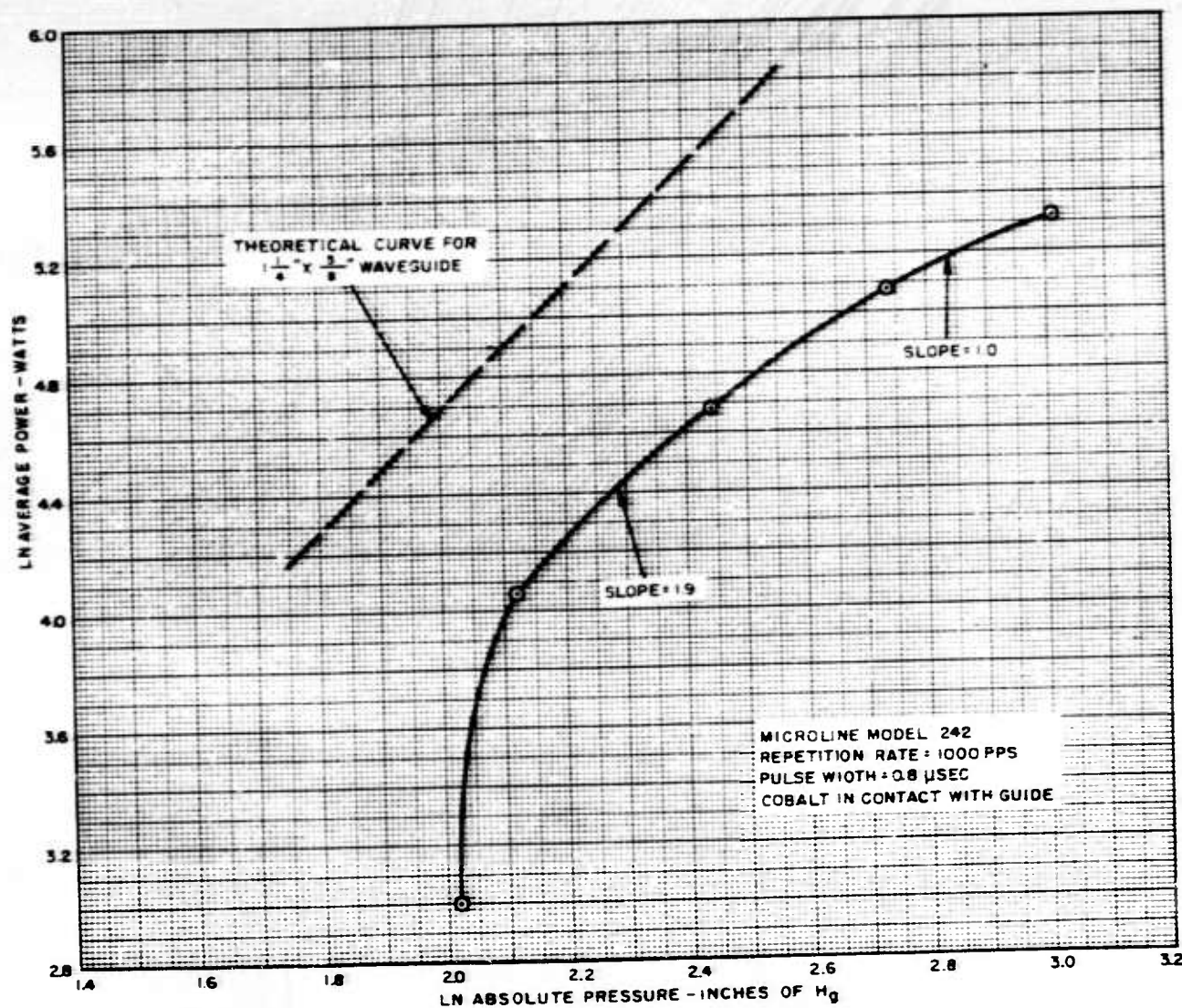


FIGURE 91  
BREAKDOWN POWER VS. PRESSURE FOR  
THE  $1\frac{1}{4} \times \frac{5}{8}$  WAVEGUIDE DUMMY LOAD

CONFIDENTIAL



CONFIDENTIAL

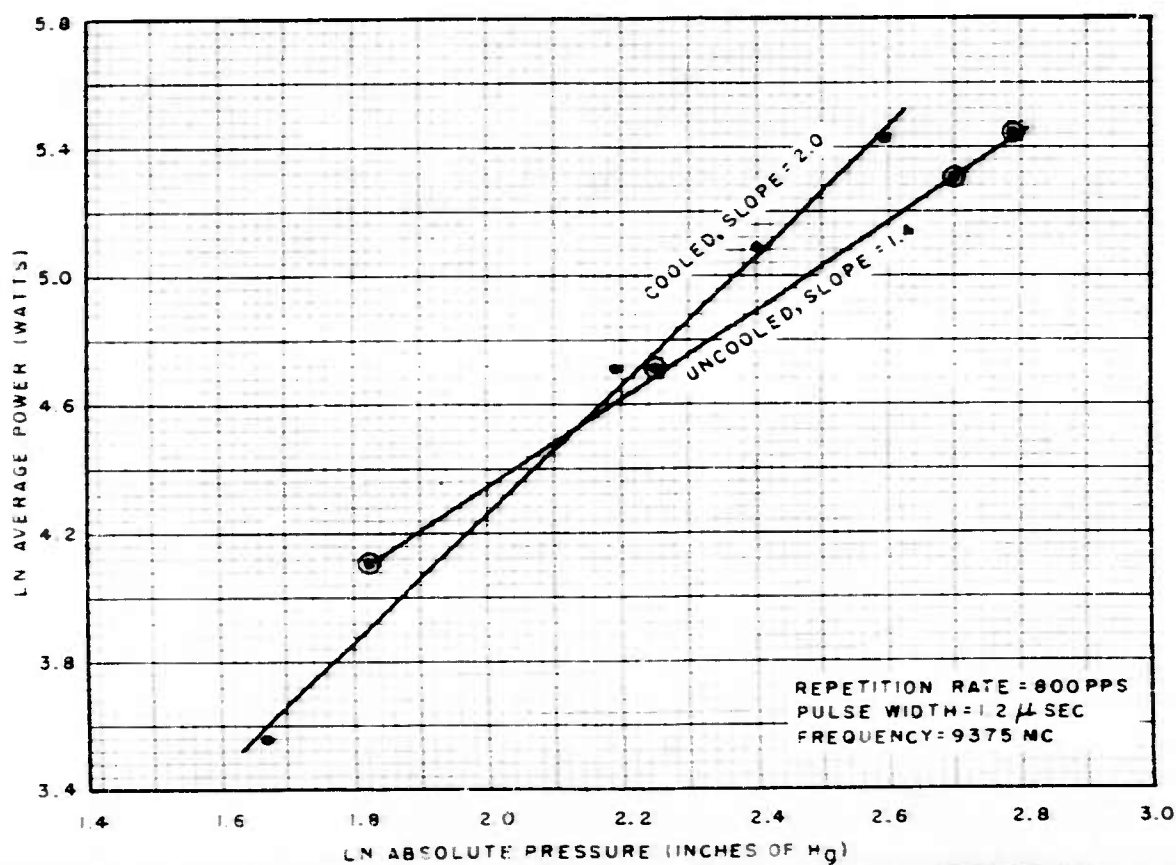
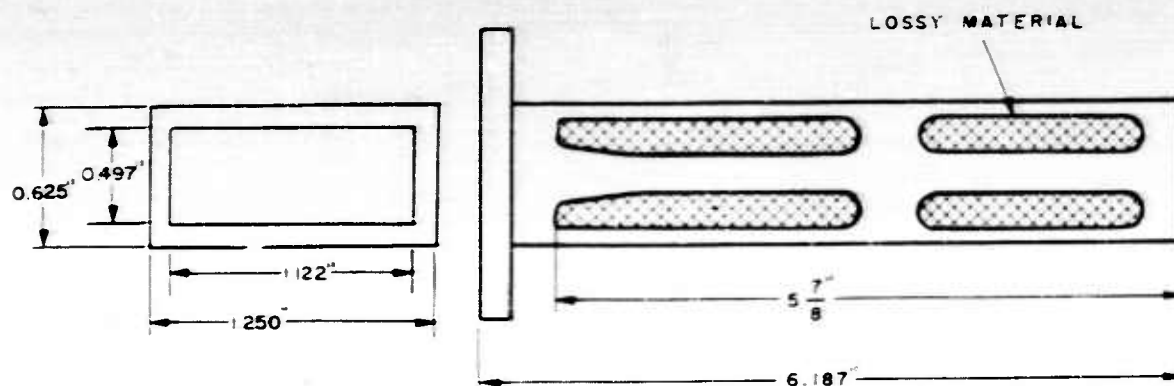


FIGURE 92  
POWER VS PRESSURE FOR  
WAVEGUIDE DUMMY LOAD  
(1-1/4" X 5/8" X 0.064" WAVEGUIDE)

CONFIDENTIAL



CONFIDENTIAL

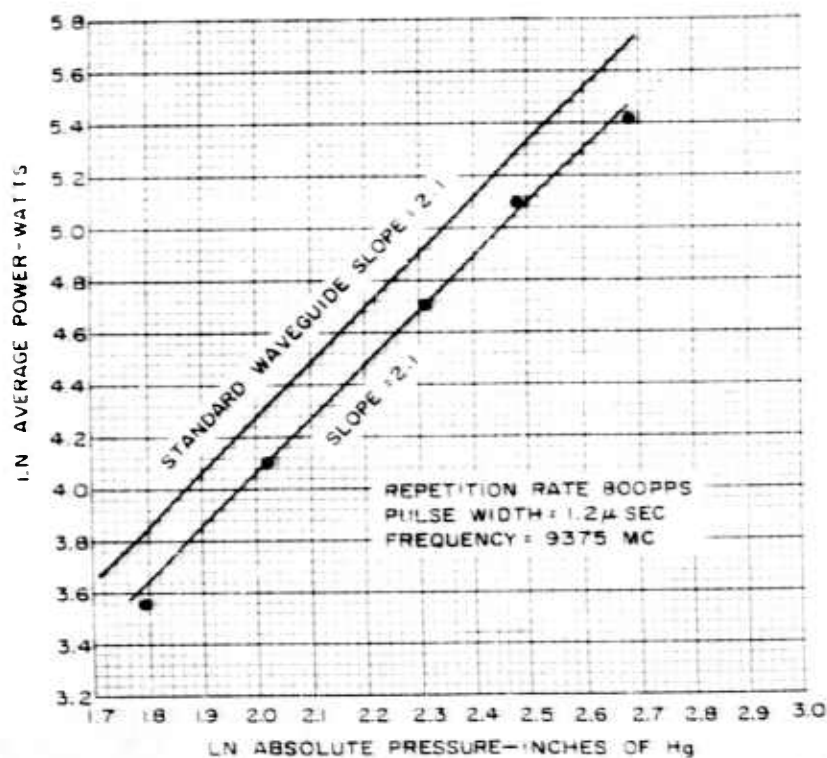
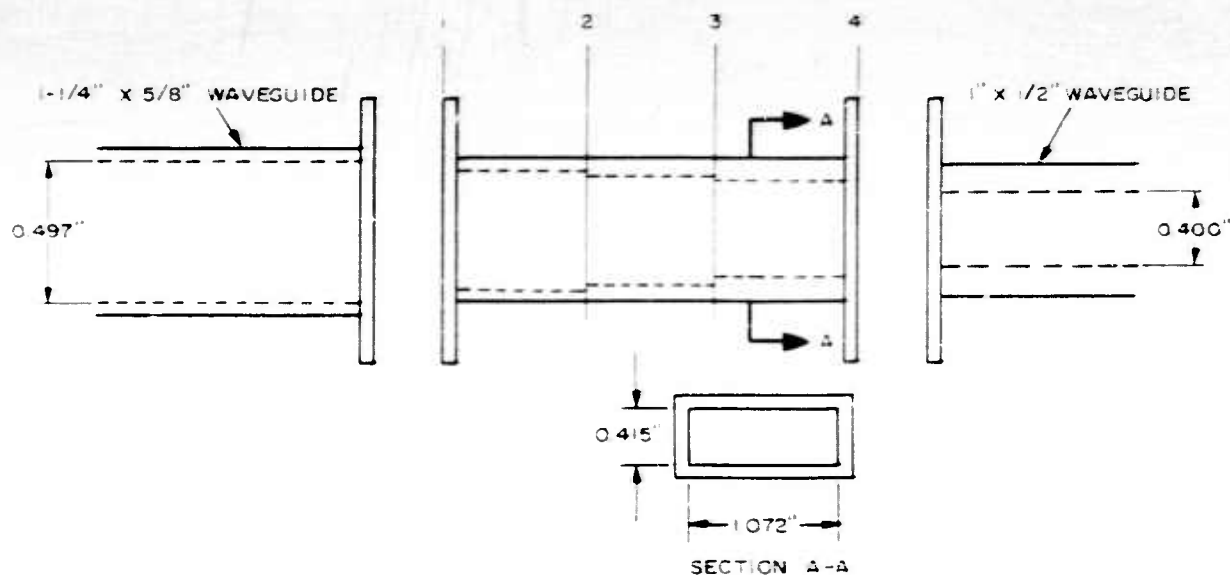


FIGURE 93  
POWER VS PRESSURE FOR  
STEP TRANSFORMER FROM  
1" X 1/2" TO 1-1/4" X 5/8" WAVEGUIDE

CONFIDENTIAL





CONFIDENTIAL

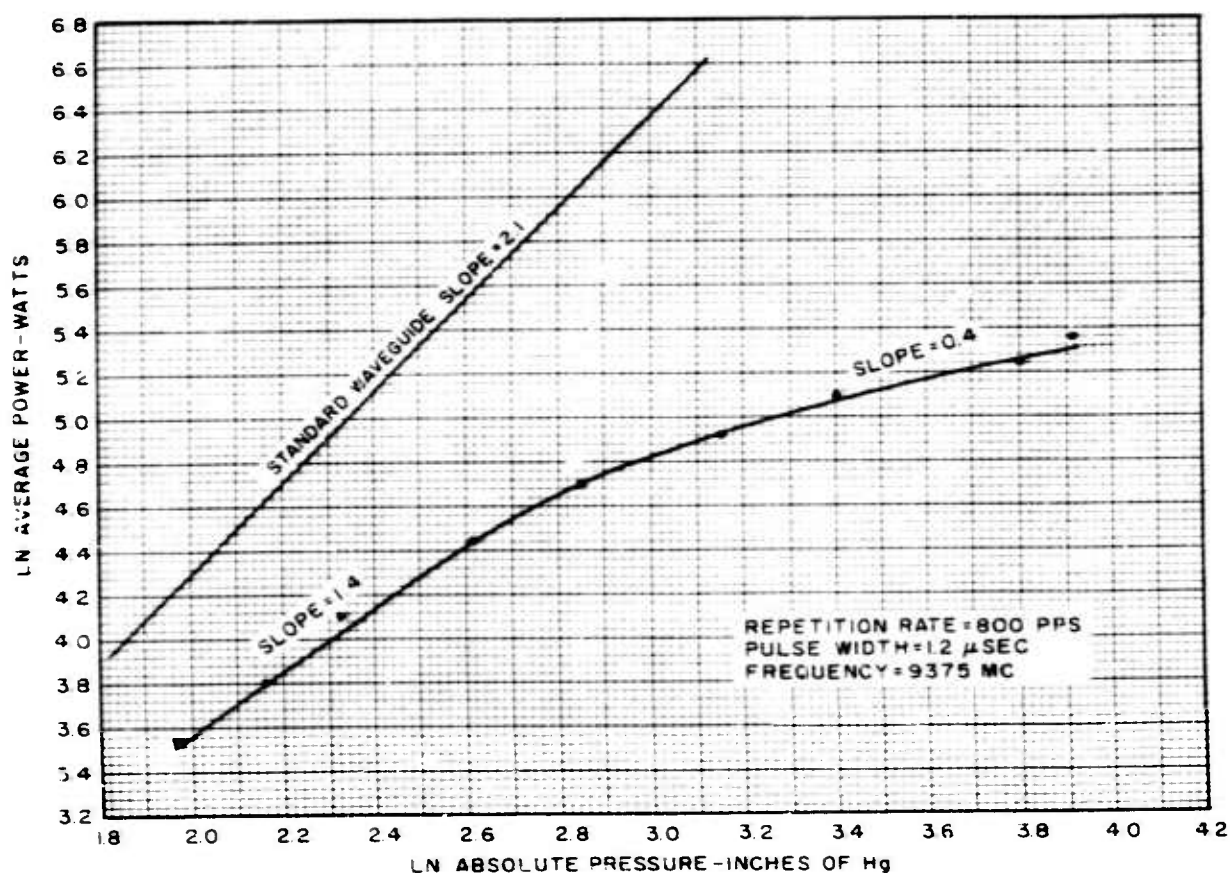
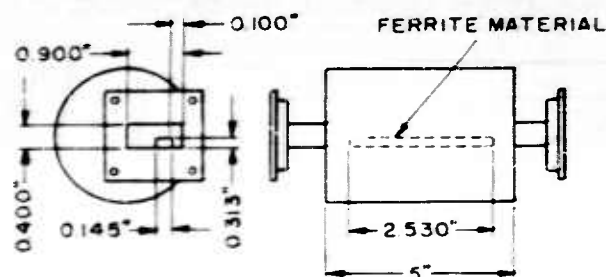


FIGURE 94  
POWER VS PRESSURE FOR  
MODEL X20L FERRITE ISOLATOR  
(1" x  $\frac{1}{2}$ " x 0.050" WAVEGUIDE)

CONFIDENTIAL



CONFIDENTIAL

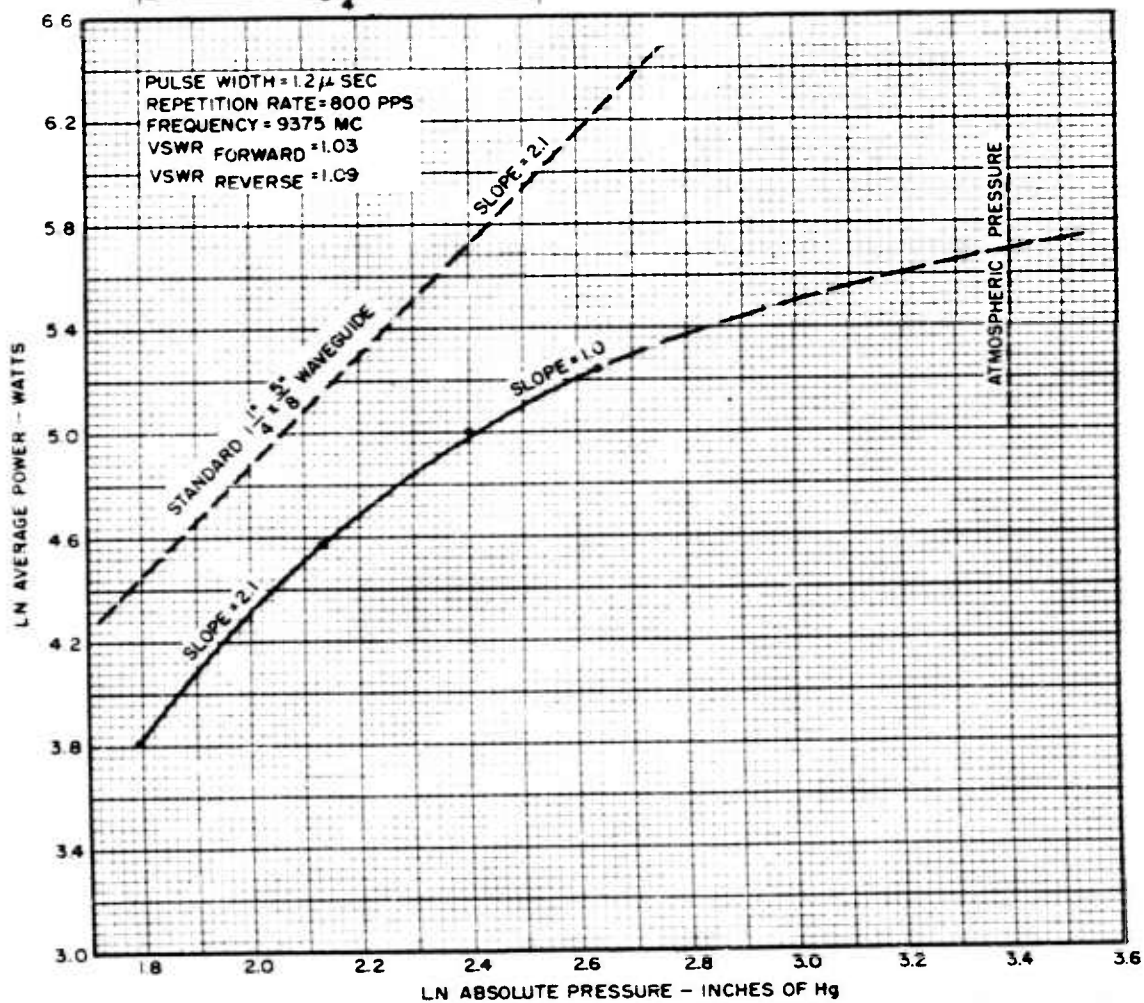
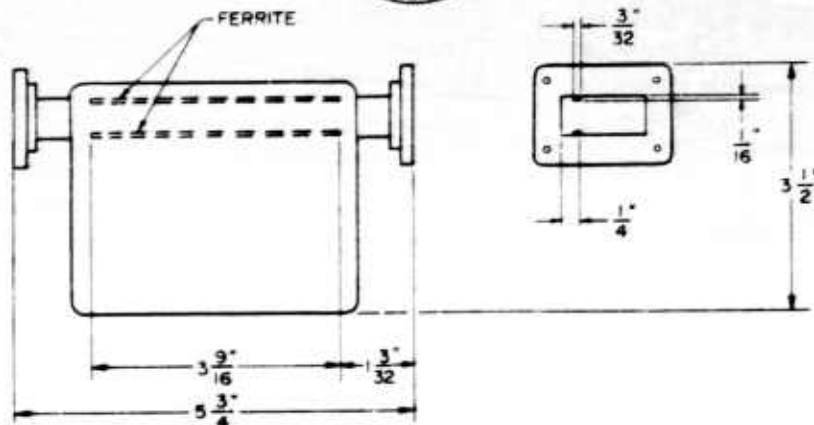


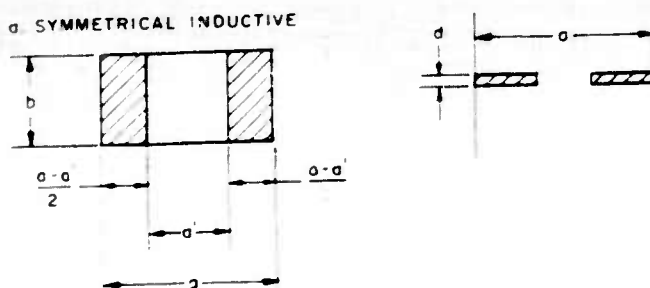
FIGURE 95  
 POWER VS PRESSURE FOR  
 MODEL HL86-96 UNILINE ISOLATOR  
 ( $\frac{1}{4} \times \frac{3}{8} \times .064$ -INCH WAVEGUIDE)

CONFIDENTIAL

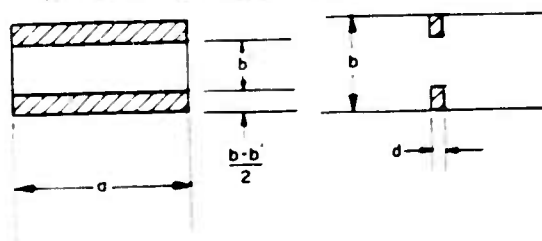


CONFIDENTIAL

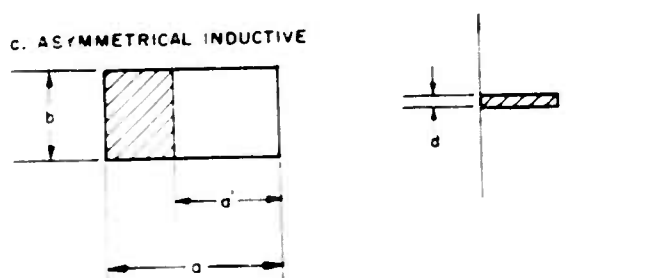
a SYMMETRICAL INDUCTIVE



b SYMMETRICAL CAPACITIVE



c. ASYMMETRICAL INDUCTIVE



d ASYMMETRICAL CAPACITIVE

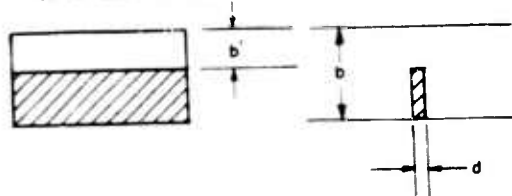


FIGURE 96  
VARIOUS TYPES OF  
WAVEGUIDE IRISES

CONFIDENTIAL



CONFIDENTIAL

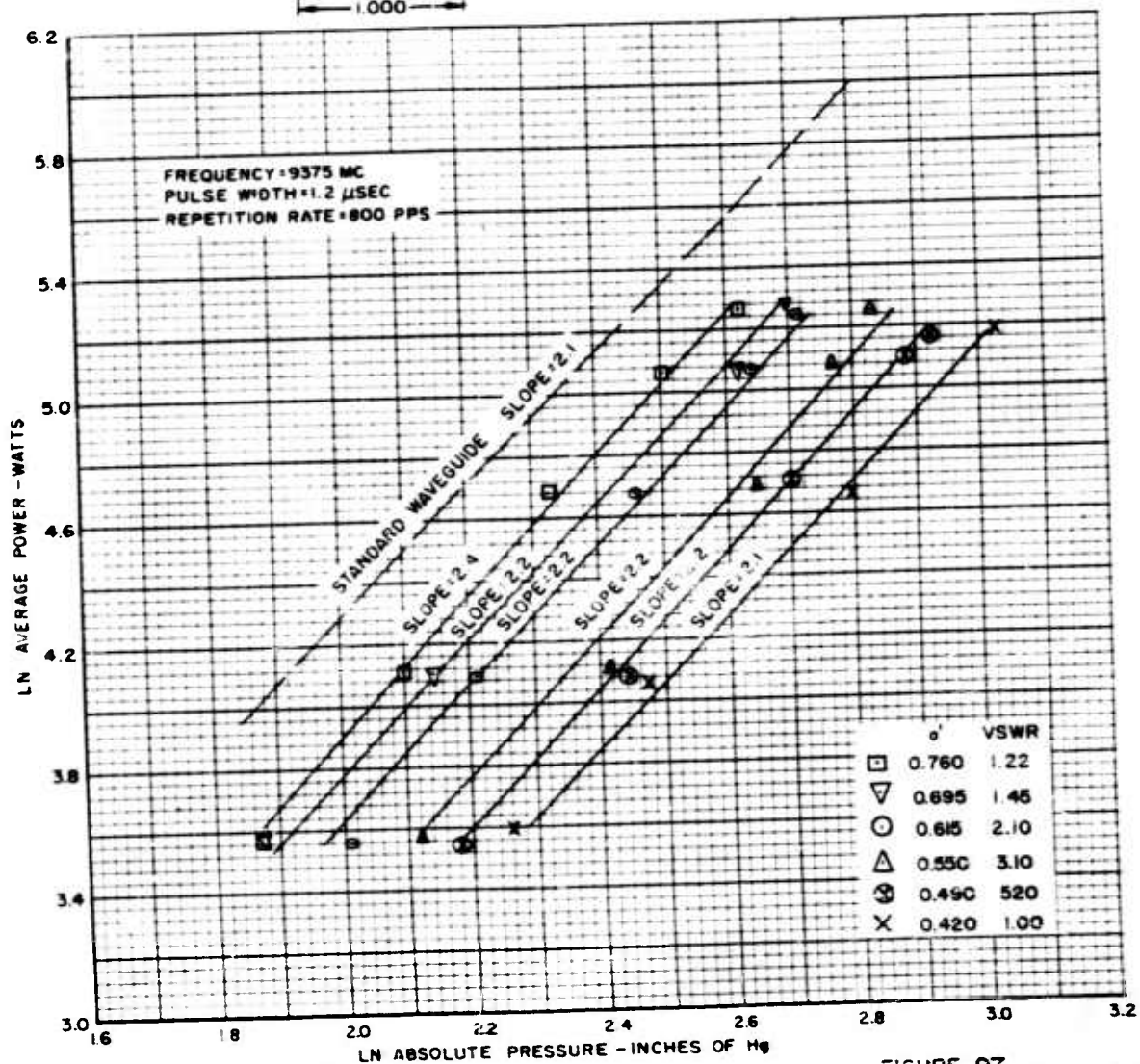
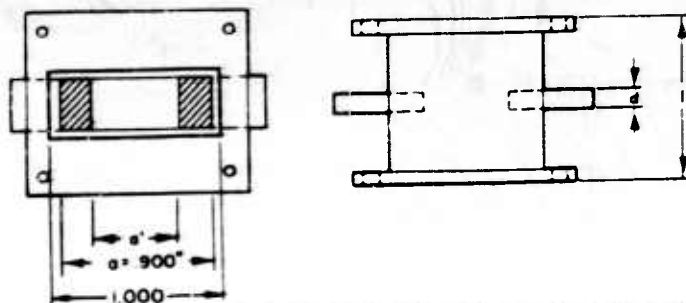


FIGURE 97

POWER VS PRESSURE FOR VARIOUS  
SYMMETRICAL INDUCTIVE IRISES  
( $d = 1/32$  INCH)

CONFIDENTIAL



CONFIDENTIAL

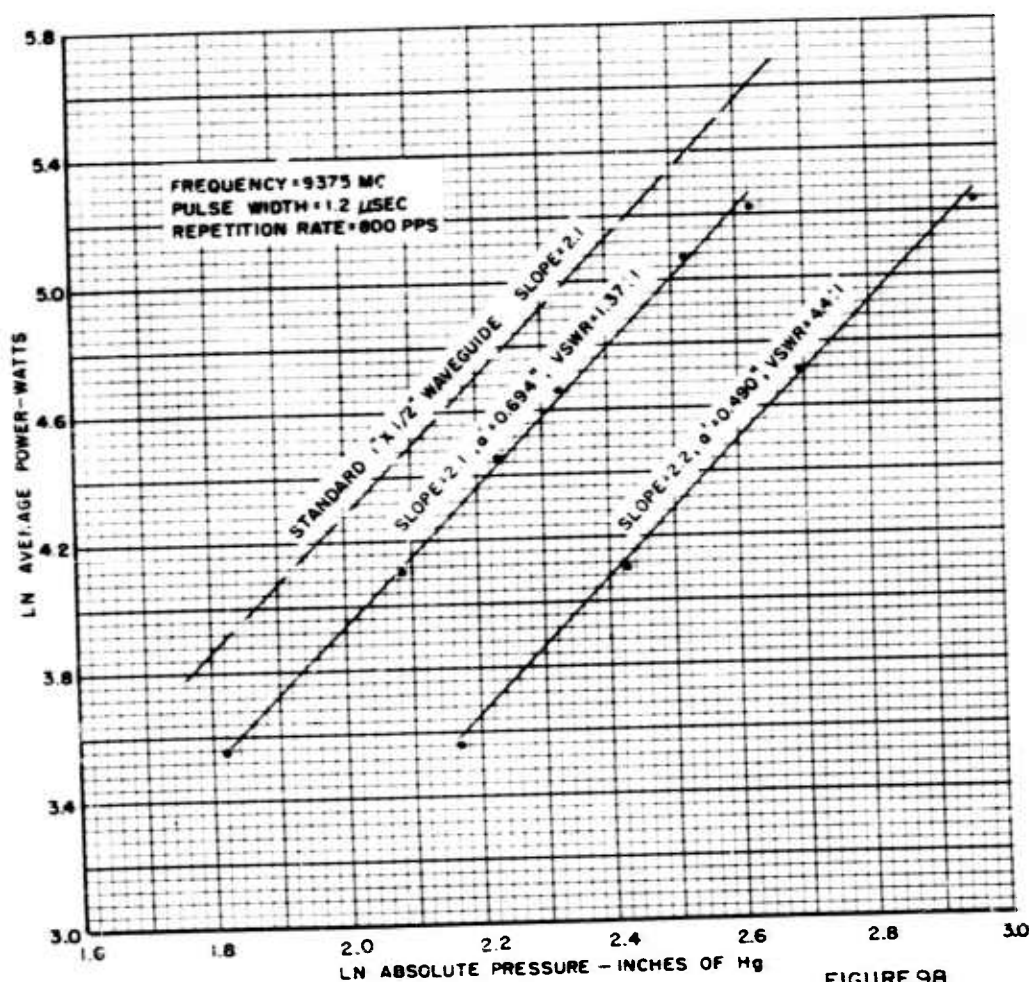
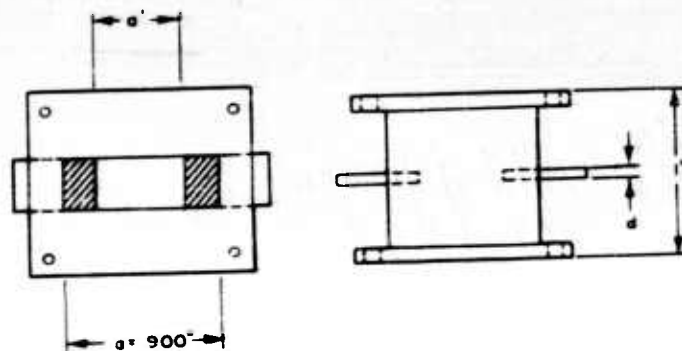


FIGURE 98

POWER VS PRESSURE FOR VARIOUS  
SYMMETRICAL INDUCTIVE IRISES  
( $d = 1/64$  INCH)

CONFIDENTIAL



CONFIDENTIAL

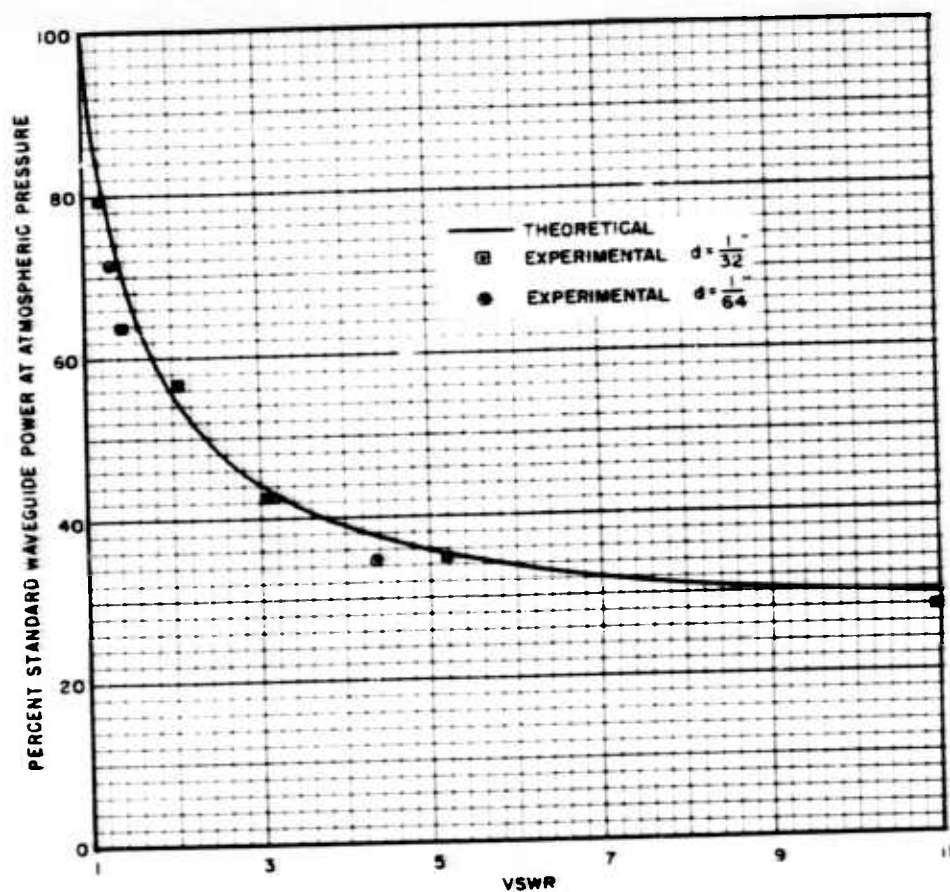


FIGURE 99  
PERCENTAGE WAVEGUIDE POWER  
VS VSWR FOR A SYMMETRICAL  
INDUCTIVE IRIS

CONFIDENTIAL





CONFIDENTIAL

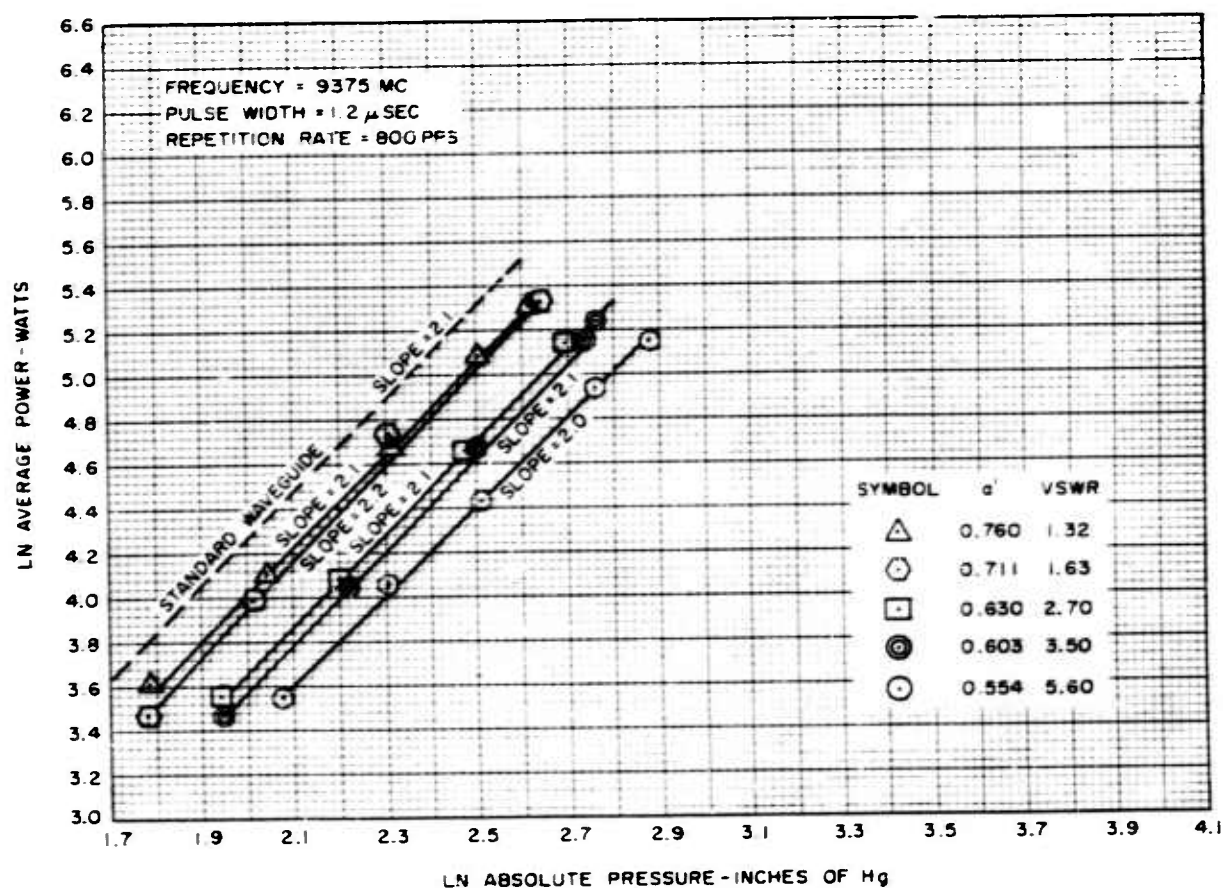
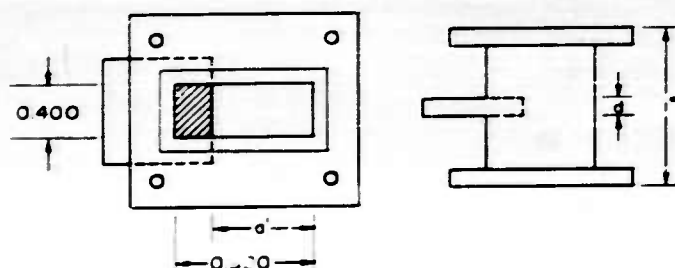


FIGURE 100  
LN POWER VS LN PRESSURE FOR VARIOUS  
ASYMMETRICAL INDUCTIVE IRISES  
( $d = 1/32"$ )

CONFIDENTIAL



CONFIDENTIAL

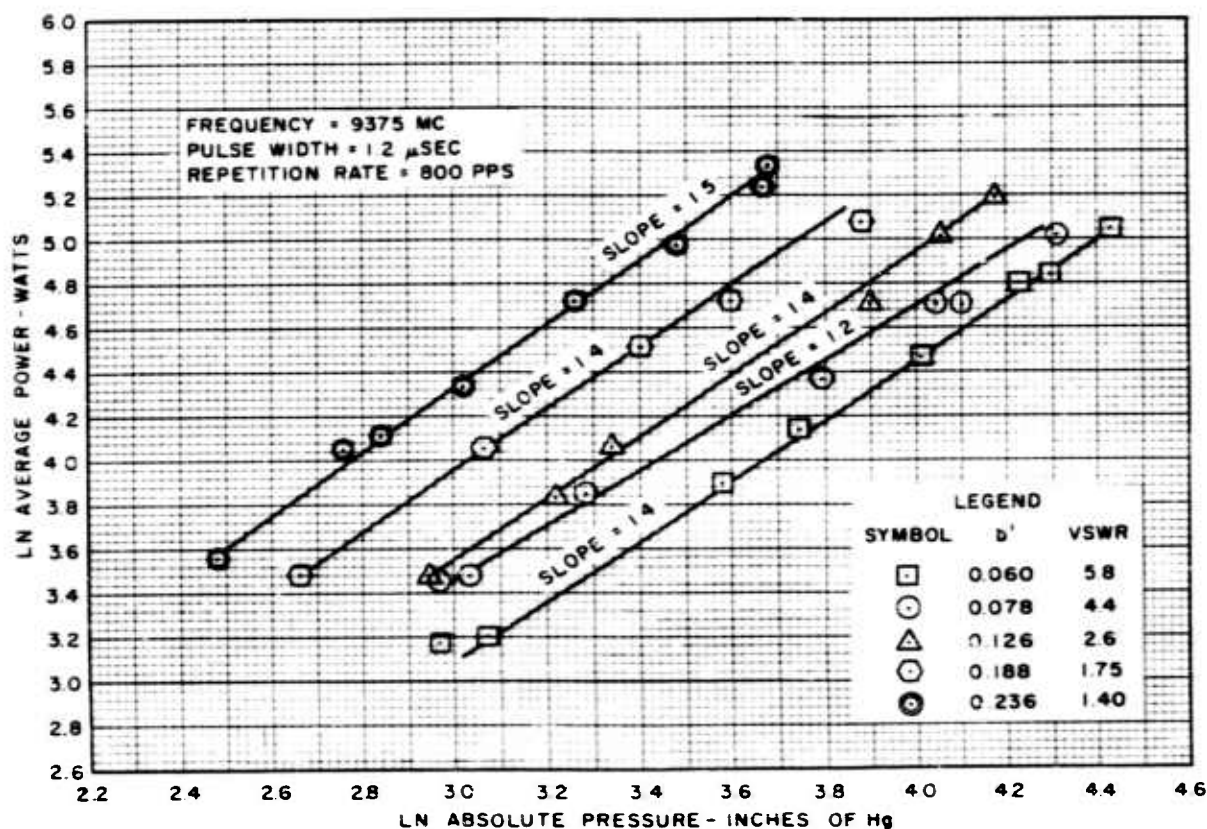
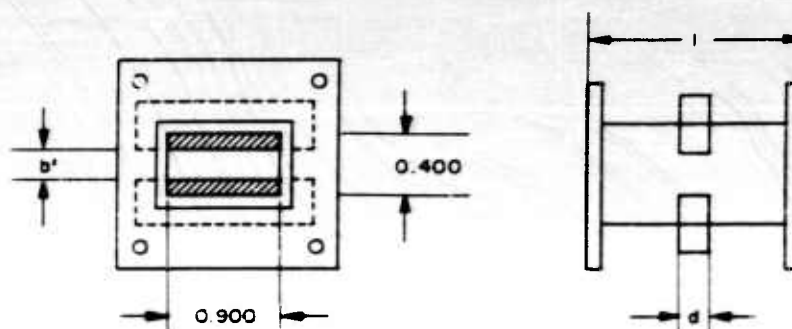


FIGURE 101

LN POWER VS LN PRESSURE FOR VARIOUS  
 SYMMETRICAL CAPACITIVE IRISES  
 ( $d = 1/32"$ )

CONFIDENTIAL



CONFIDENTIAL

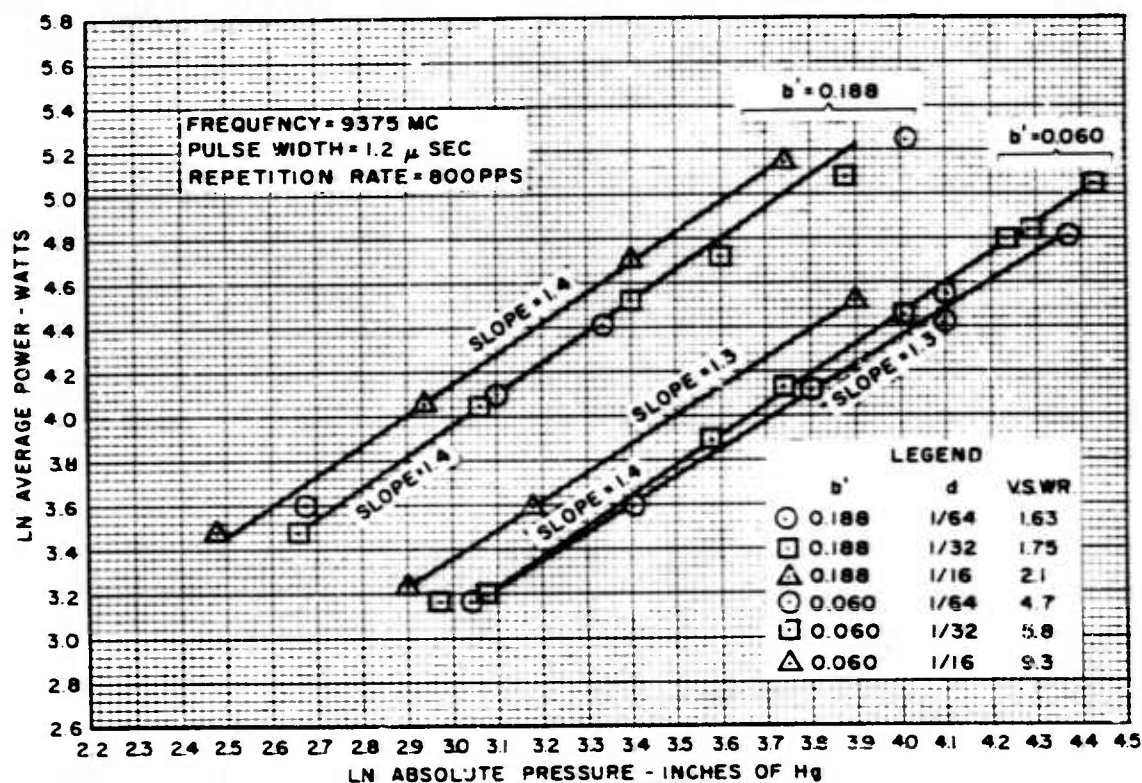
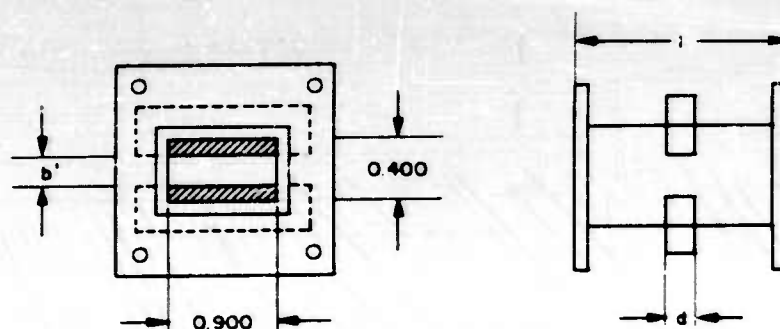


FIGURE 102

LN POWER VS LN PRESSURE  
FOR SYMMETRICAL CAPACITIVE  
IRISES WITH VARIOUS THICKNESS ( $d$ )

CONFIDENTIAL



CONFIDENTIAL

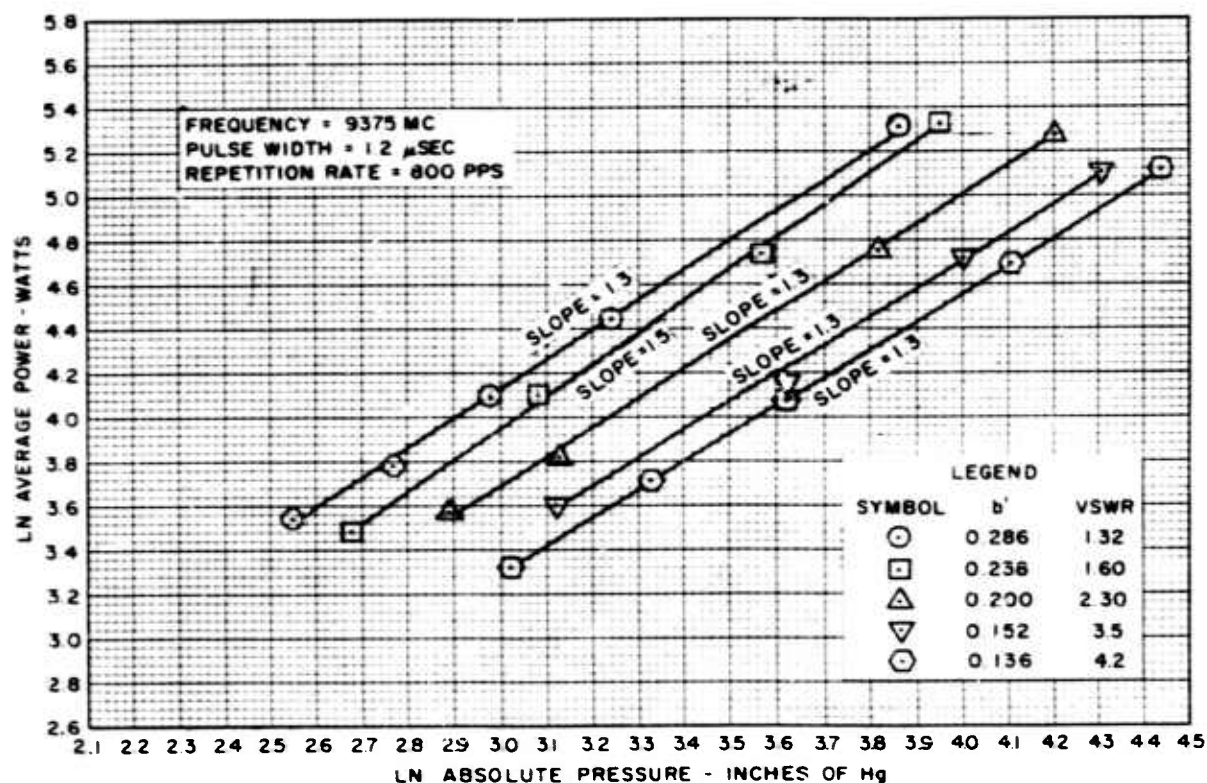
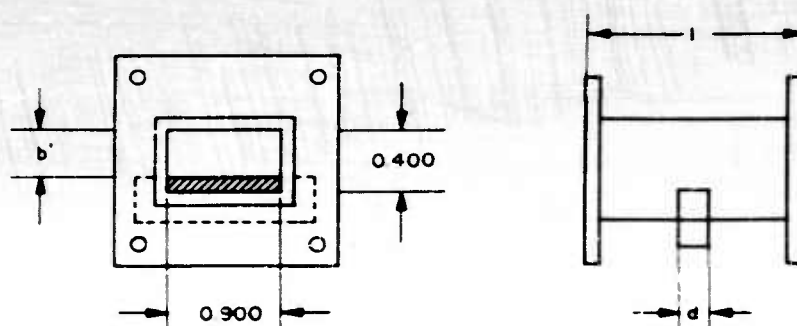


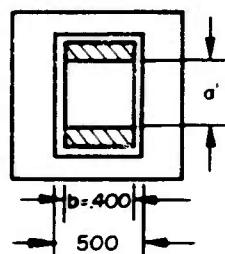
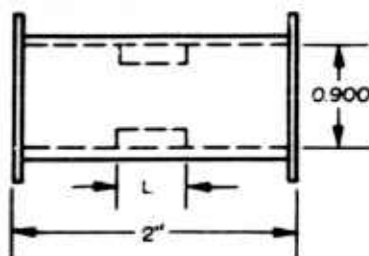
FIGURE 103  
LN POWER VS LN PRESSURE FOR VARIOUS  
ASYMMETRICAL CAPACITIVE IRISES  
( $d = 1/32"$ )

CONFIDENTIAL





CONFIDENTIAL



FREQUENCY=9375MC  
PULSE WIDTH=1.2 $\mu$ SEC  
REPETITION RATE=800PPS  
 $a=0.440=\lambda_g/4$

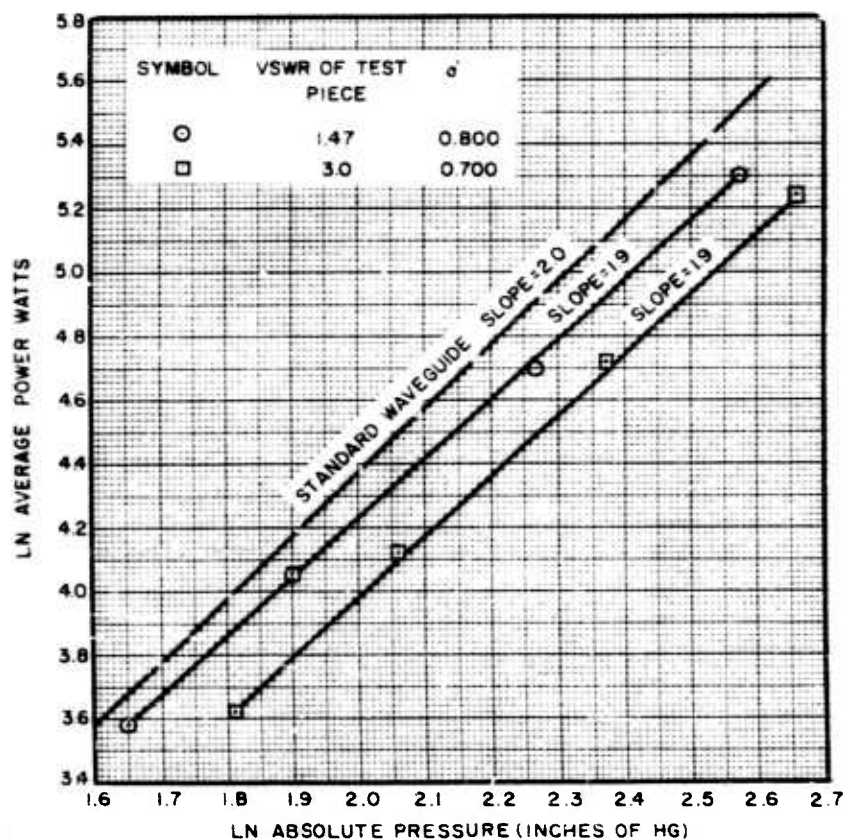


FIGURE 104

LN POWER VS LN PRESSURE  
FOR SYMMETRICAL INDUCTIVE STEP

CONFIDENTIAL





CONFIDENTIAL

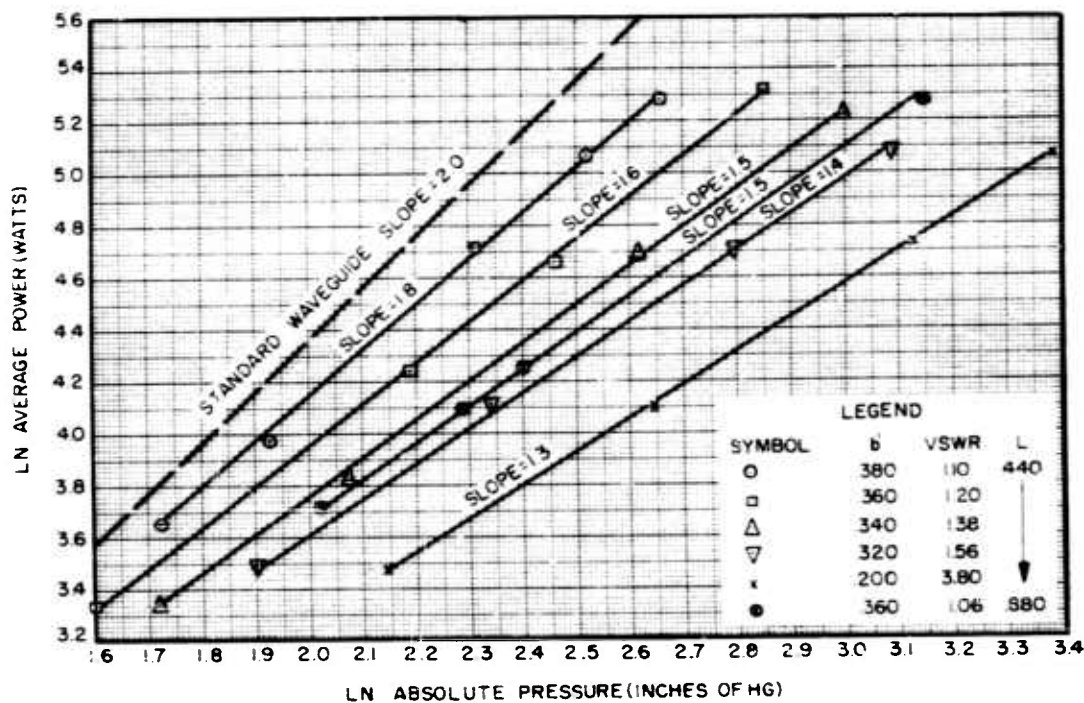
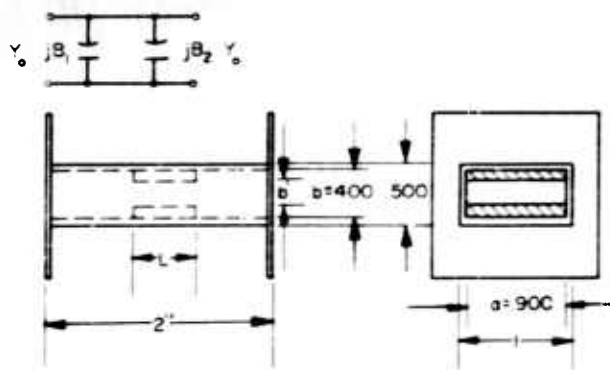


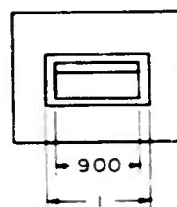
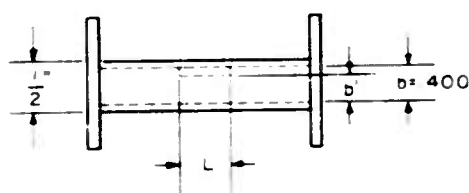
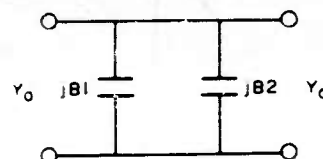
FIGURE 105

LN POWER VS LN PRESSURE FOR  
SYMMETRICAL CAPACITIVE STEP

CONFIDENTIAL



CONFIDENTIAL



FREQUENCY = 9375 MC  
PULSE WIDTH = 1.2  $\mu$  SEC  
REPETITION RATE = 800 PPS  
 $L = 4.40$  INCH =  $\lambda_g/4$

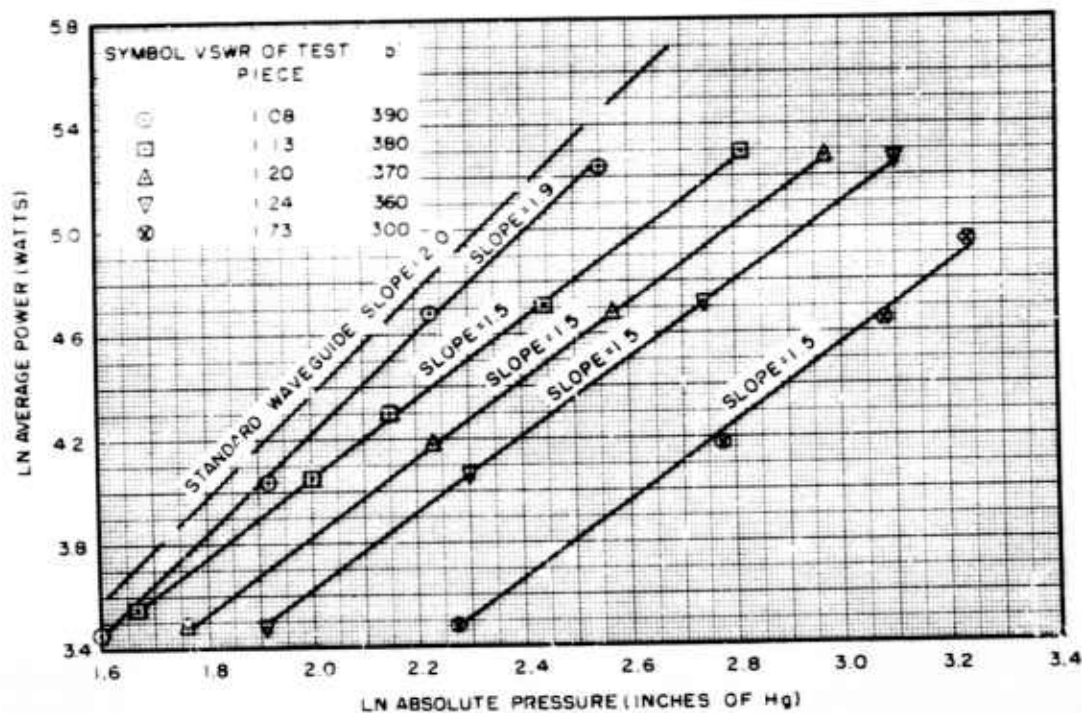


FIGURE 106  
LN POWER VS LN PRESSURE  
FOR ASYMMETRICAL  
CAPACITIVE STEP

CONFIDENTIAL



CONFIDENTIAL

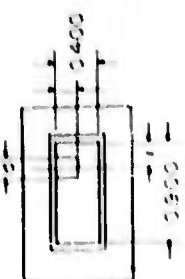
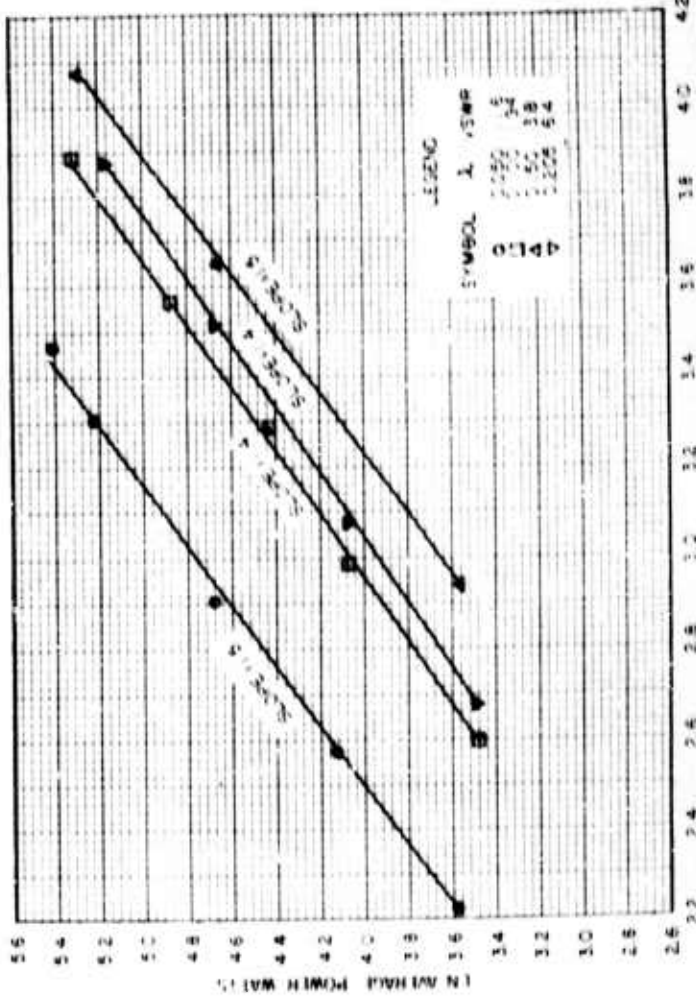
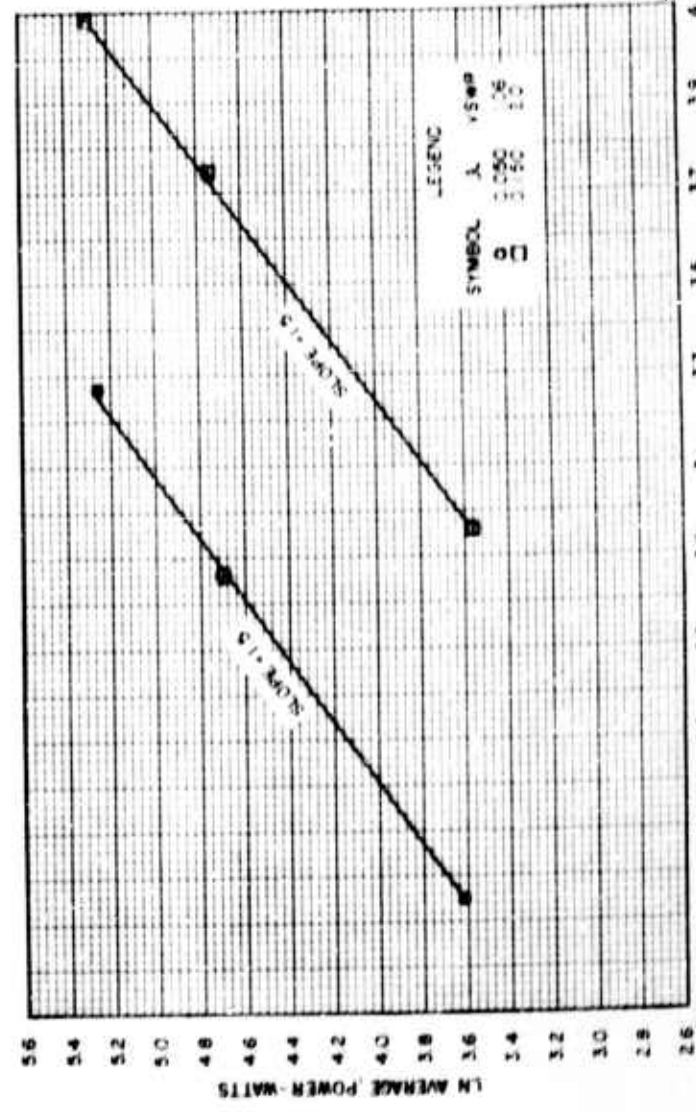
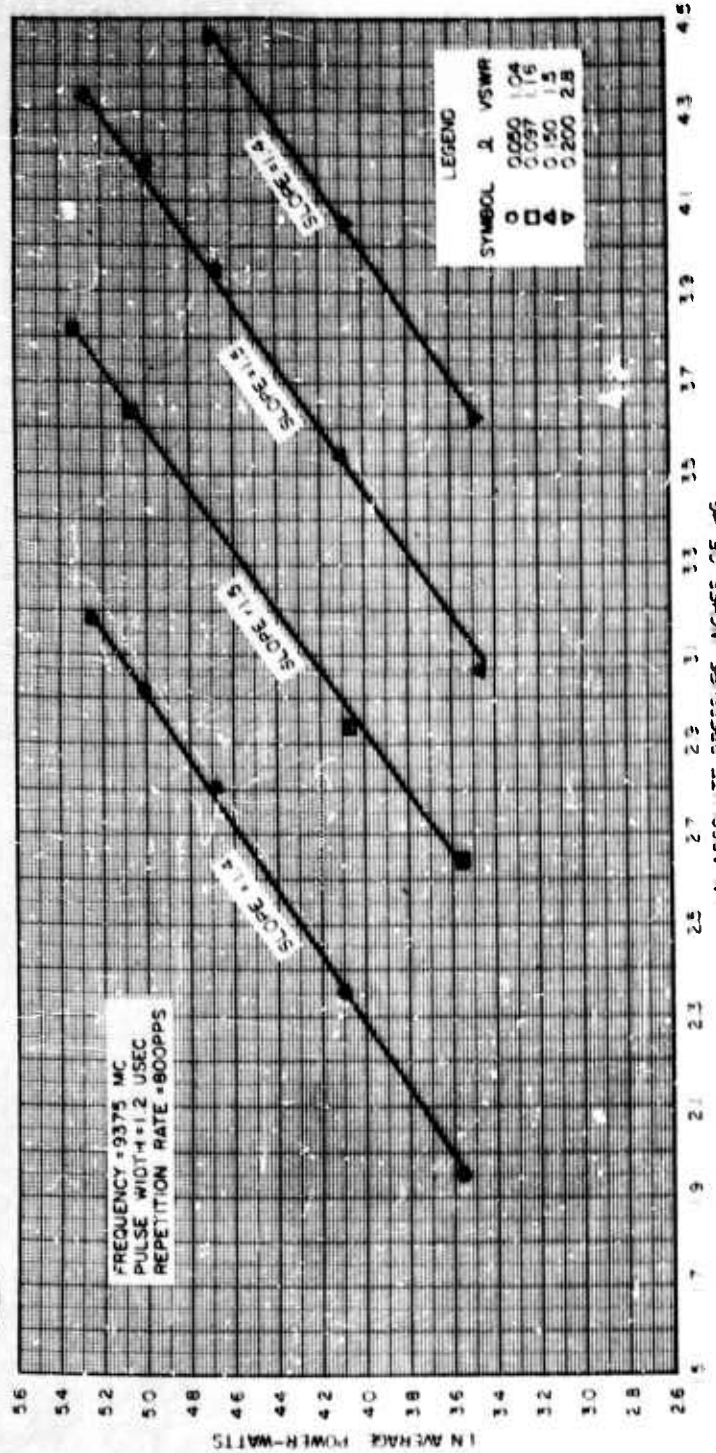
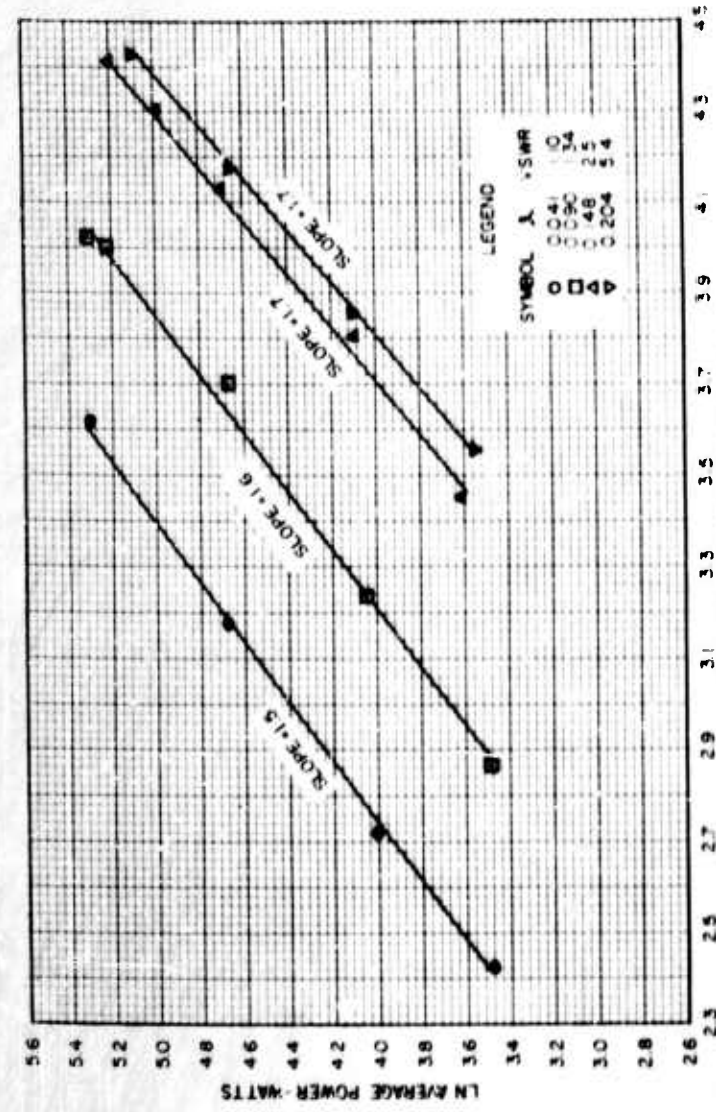
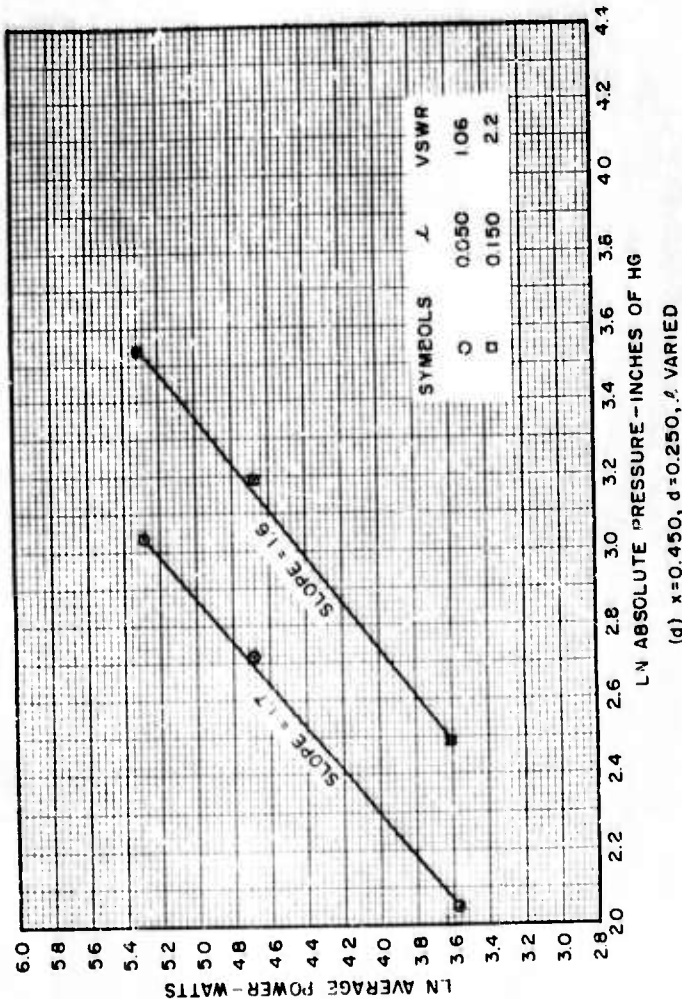
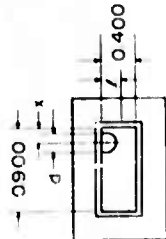
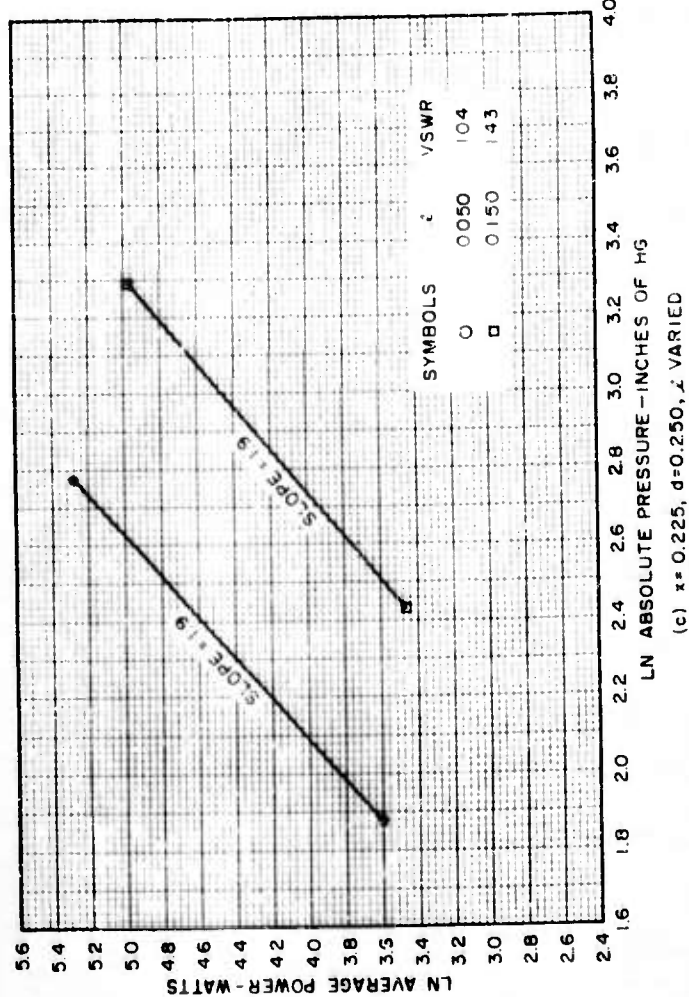
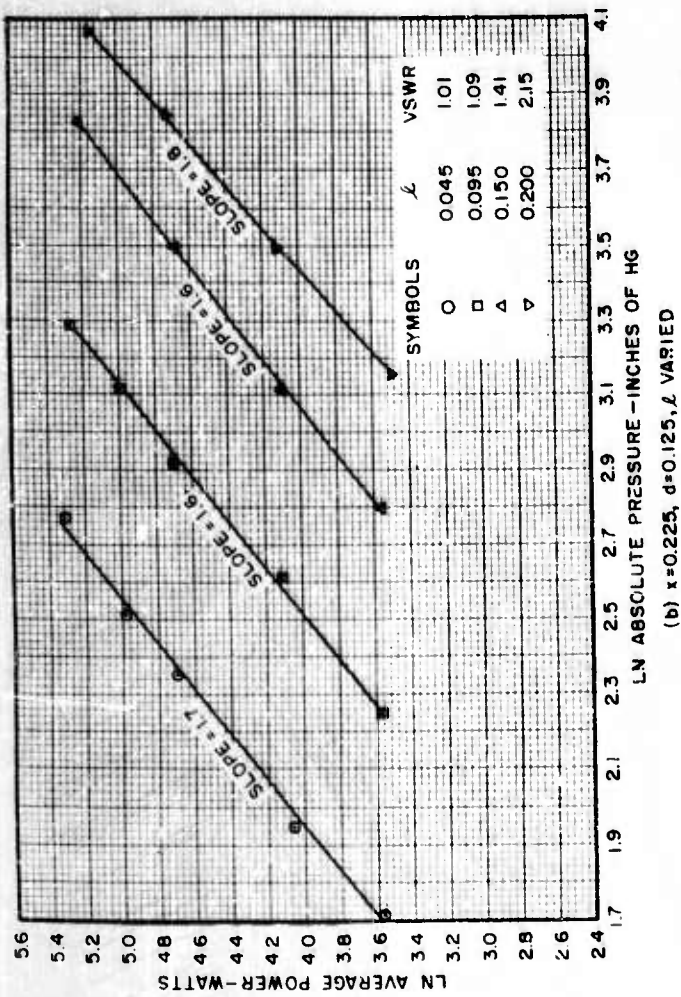
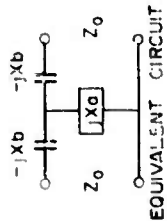
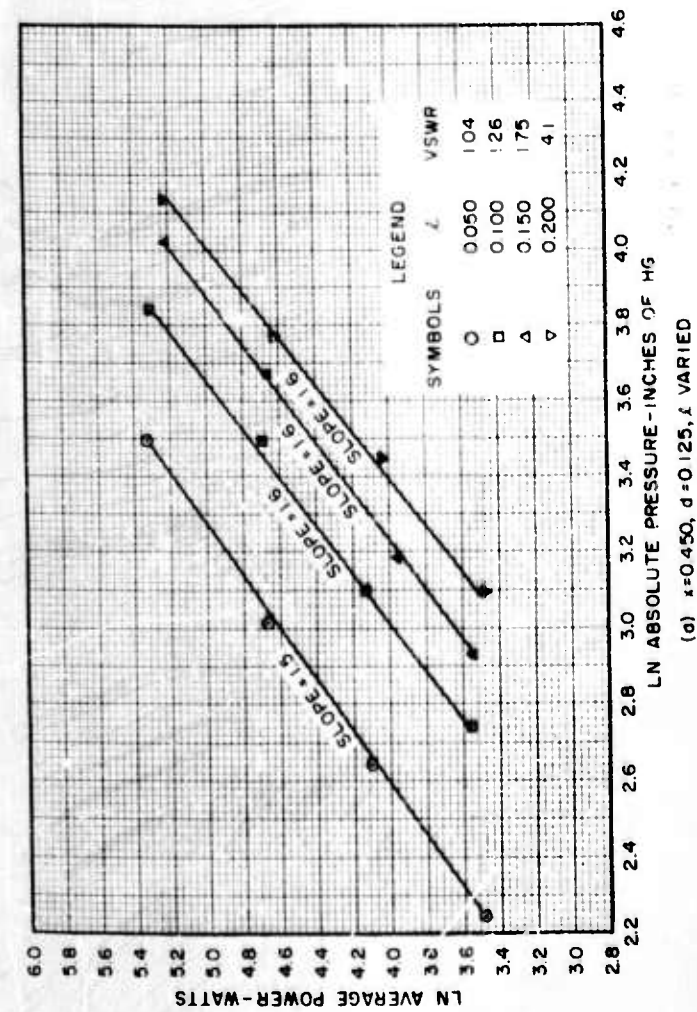


FIGURE 107  
POWER-PRESSURE DATA FOR  
FLAT-ENDED CYLINDRICAL POSTS

CONFIDENTIAL



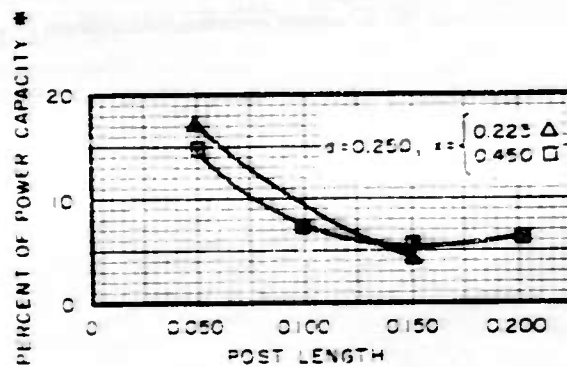
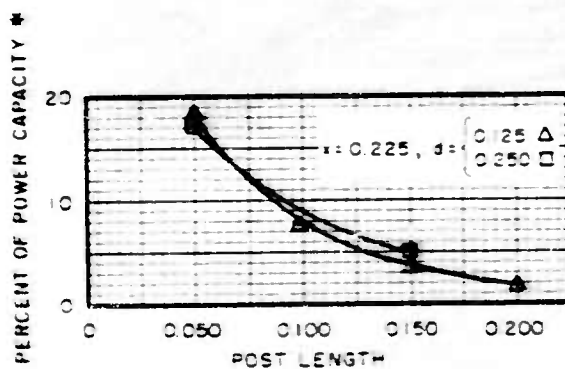
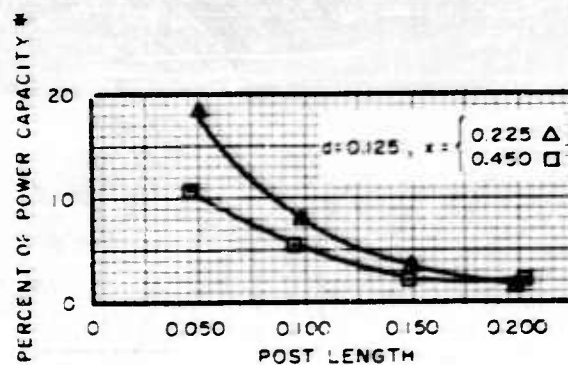
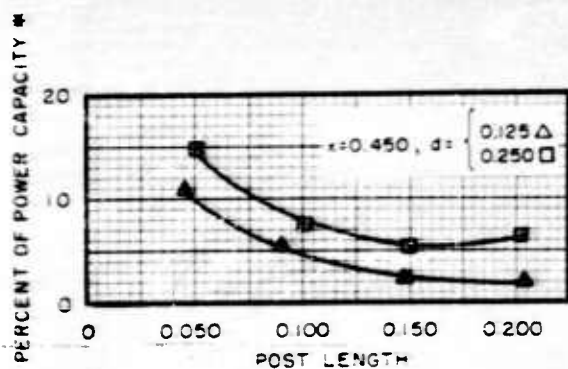


FREQUENCY = 9375 MC  
PULSE WIDTH = 1.2 USEC  
REPETITION RATE = 800 PPS

FIGURE 10B  
POWER-PRESSURE DATA FOR HEMISPHERICAL-  
ENDED CYLINDRICAL POSTS



CONFIDENTIAL



\* OF STANDARD WAVEGUIDE

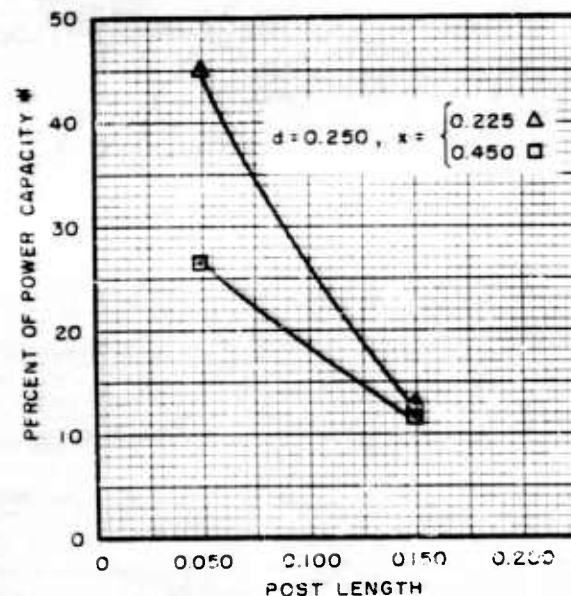
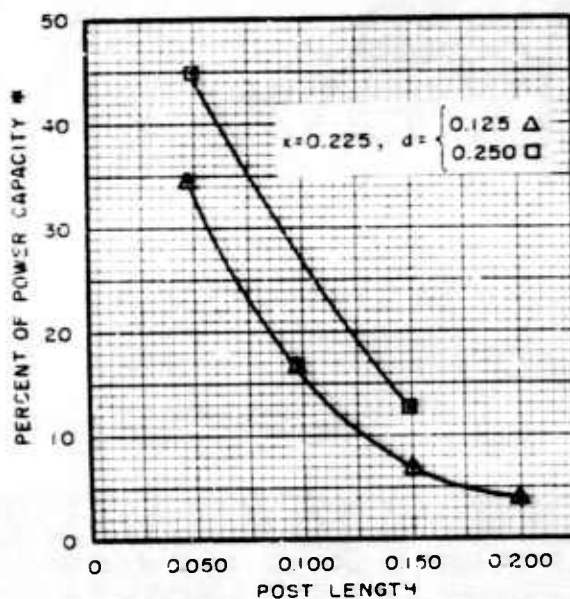
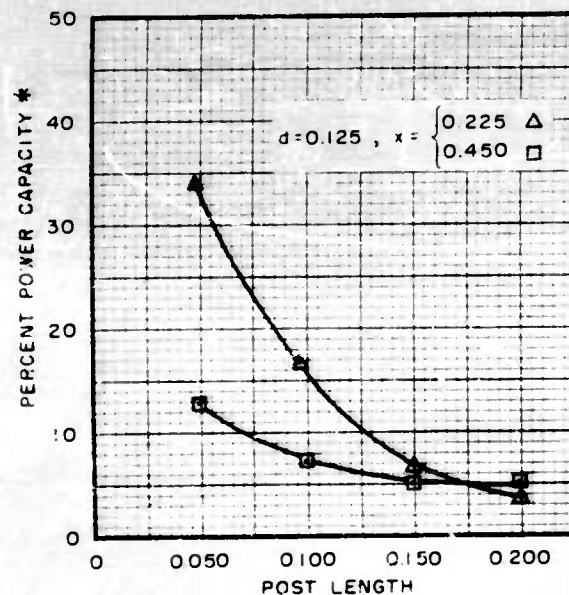
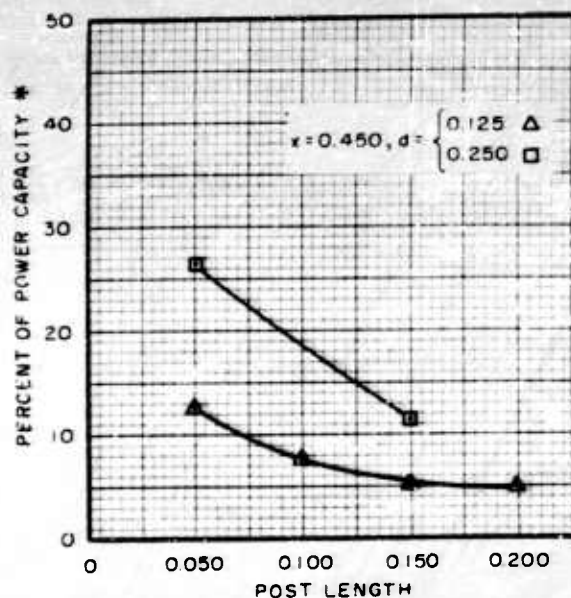
FIGURE 109  
RELATIVE POWER CAPACITY VS POST LENGTH  
FOR FLAT-ENDED CAPACITIVE WAVEGUIDE POST  
(REFER TO TABLE 15)

CONFIDENTIAL





CONFIDENTIAL



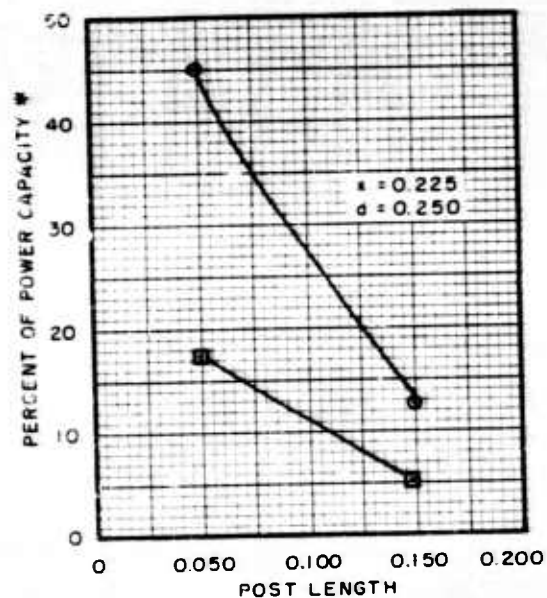
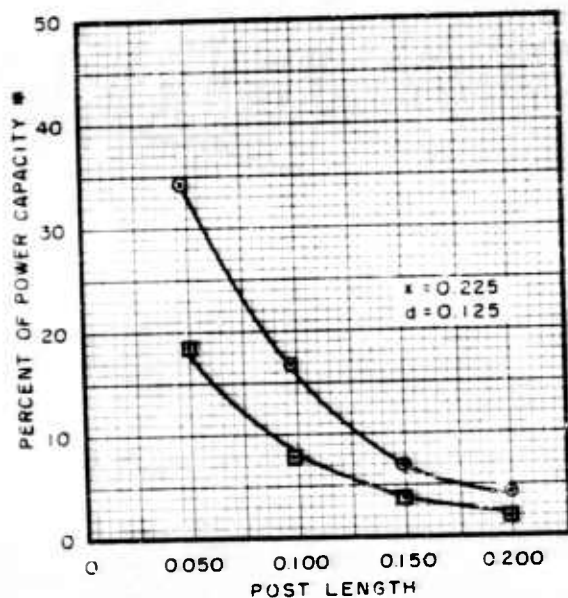
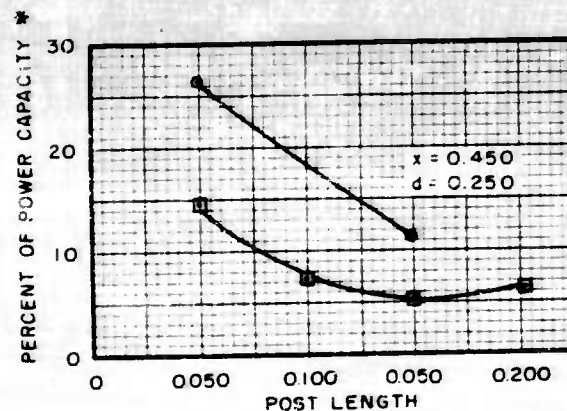
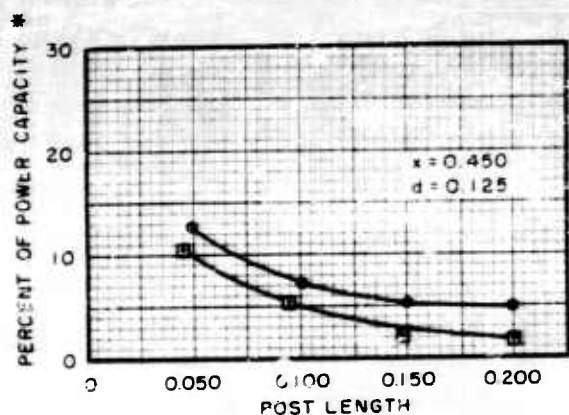
\* OF STANDARD WAVEGUIDE

FIGURE 110  
RELATIVE POWER CAPACITY VS POST LENGTH  
FOR SPHERICAL-ENDED CAPACITIVE WAVEGUIDE POST  
(REFER TO TABLE 16)

CONFIDENTIAL



CONFIDENTIAL



LEGEND

- SPHERICAL END
- FLAT END

\* OF STANDARD WAVEGUIDE

FIGURE III  
RELATIVE POWER CAPACITY VS POST LENGTH  
FOR FLAT-AND SPHERICAL-ENDED CAPACITIVE  
WAVEGUIDE POSTS (REFER TO TABLES 15 AND 16)

CONFIDENTIAL



CONFIDENTIAL

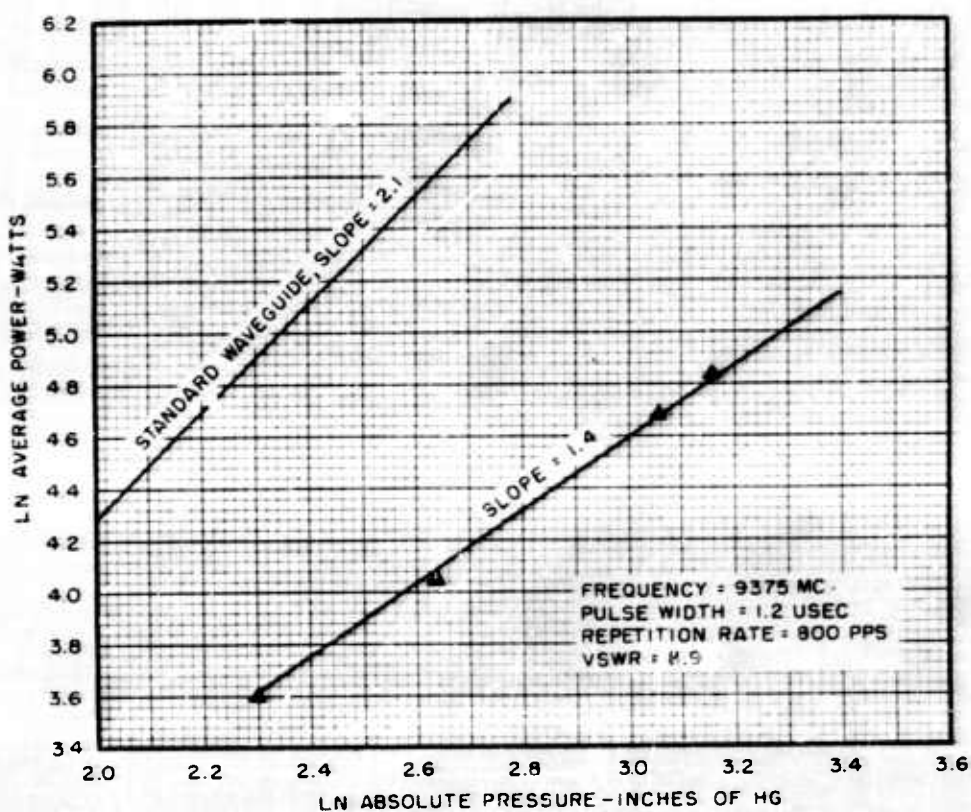
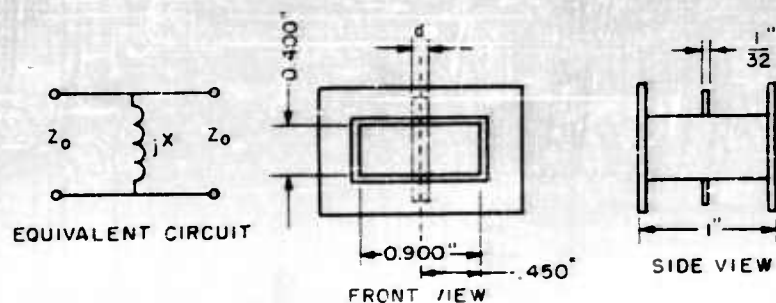


FIGURE 112  
LN POWER VS LN PRESSURE  
FOR THIN INDUCTIVE STRIP  
( $d=0.250$ )

CONFIDENTIAL





CONFIDENTIAL

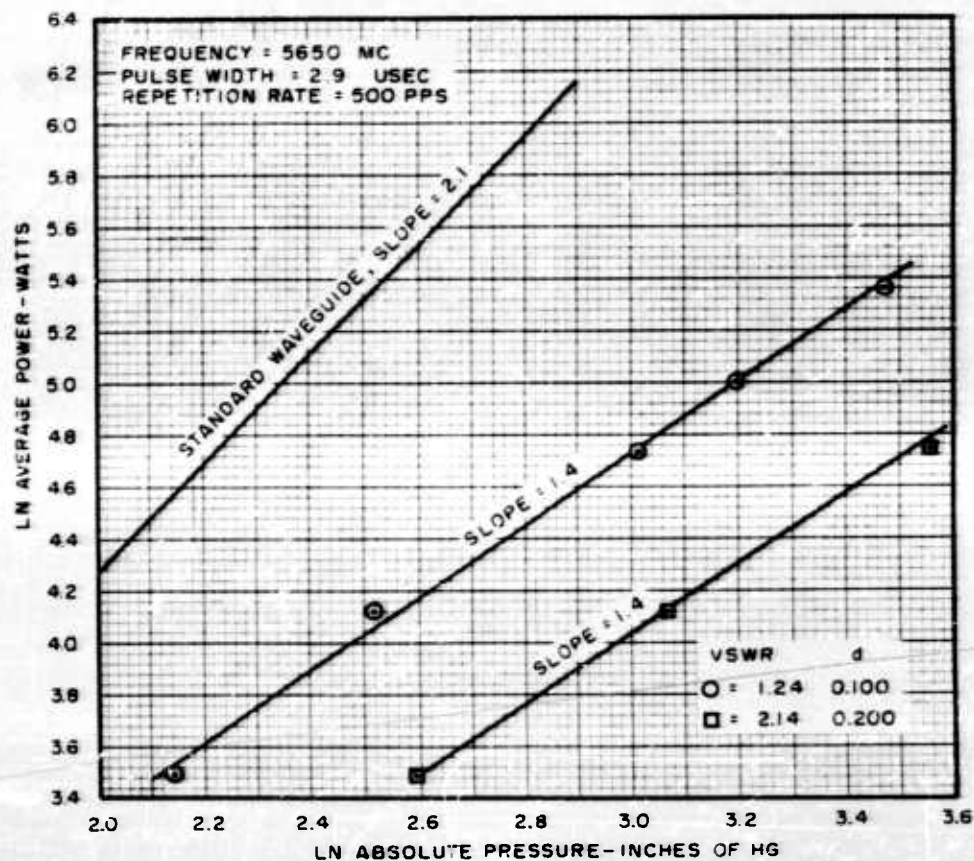
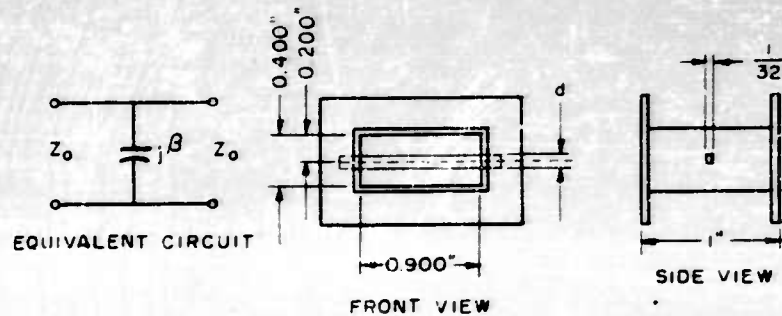


FIGURE 113  
LN POWER VS LN PRESSURE  
FOR THIN CAPACITIVE STRIP  
(d VARIED)

CONFIDENTIAL



CONFIDENTIAL

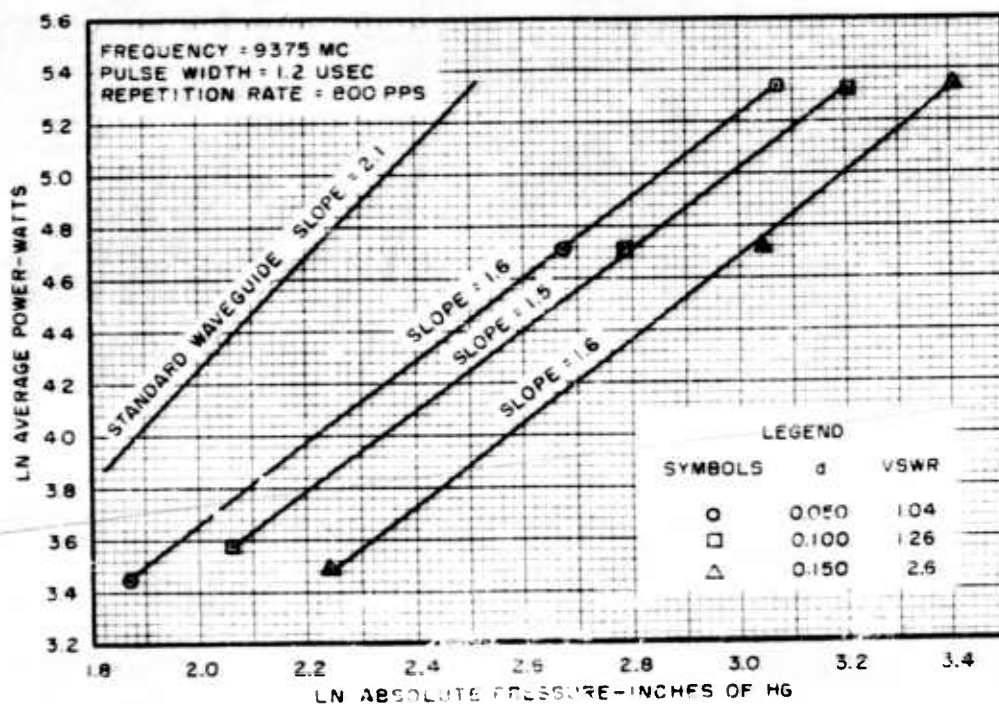
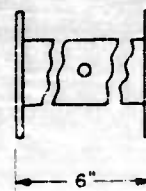
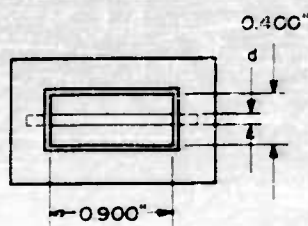
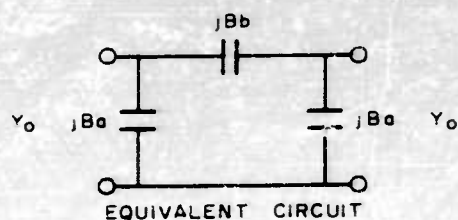


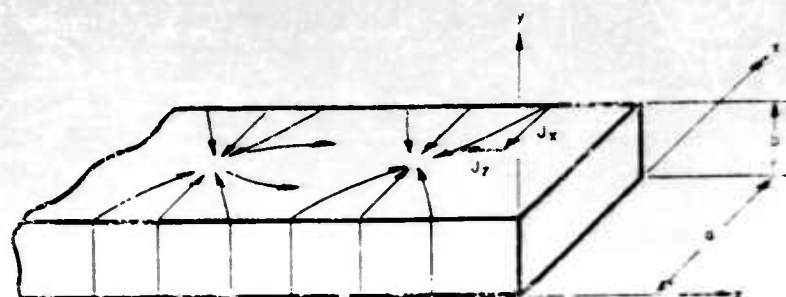
FIGURE 114  
LN POWER VS LN PRESSURE  
FOR CYLINDRICAL CAPACITIVE ROD  
(d VARIED)

CONFIDENTIAL





CONFIDENTIAL



$$J_x \sim \sin \frac{\pi x}{a}$$
$$J_y \sim \cos \frac{\pi x}{a}$$

CURRENT DENSITY

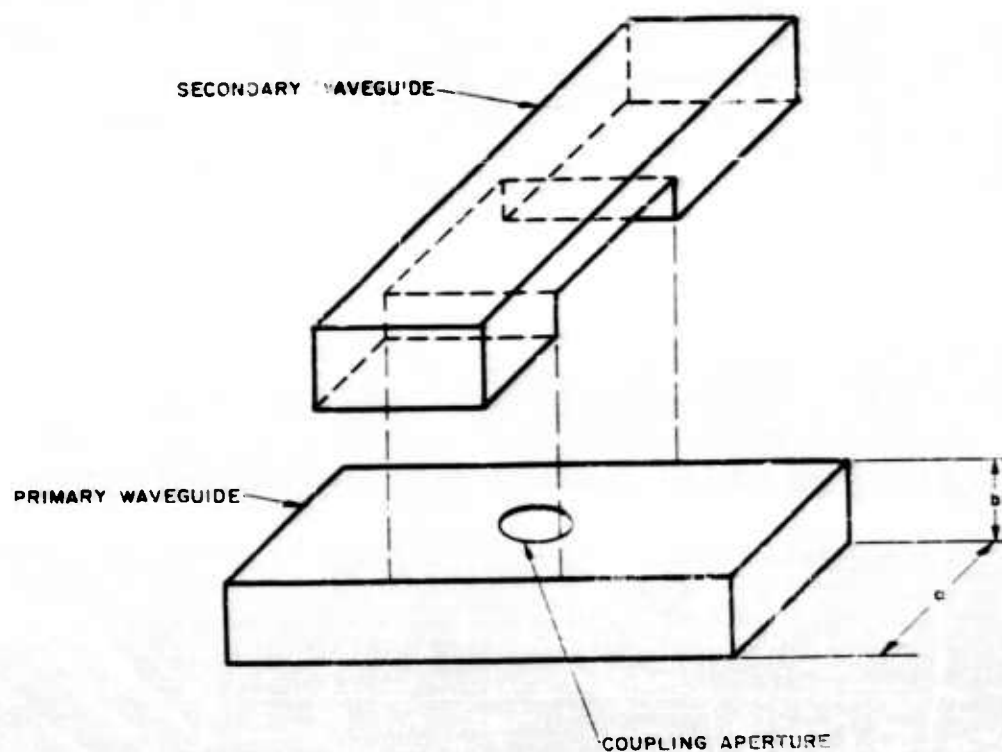


FIGURE 115  
WAVEGUIDE APERTURES

CONFIDENTIAL



CONFIDENTIAL

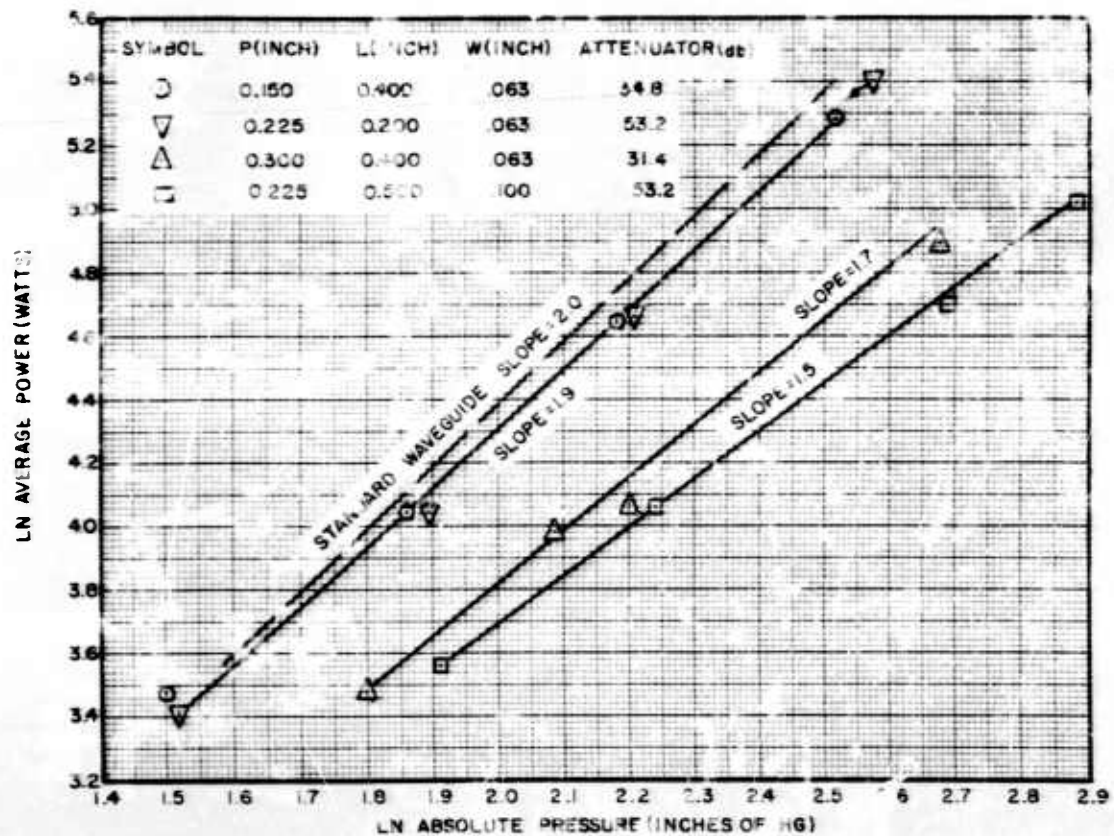
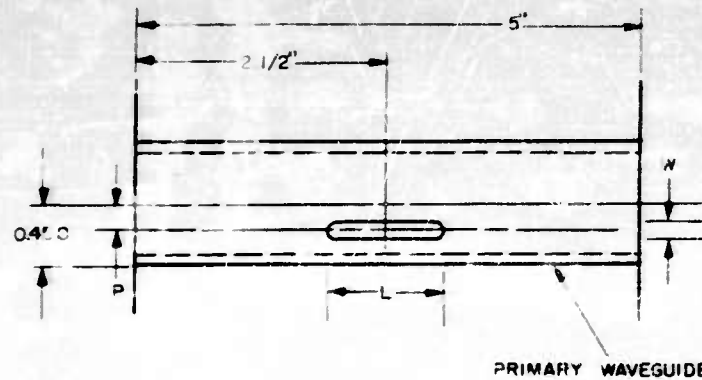


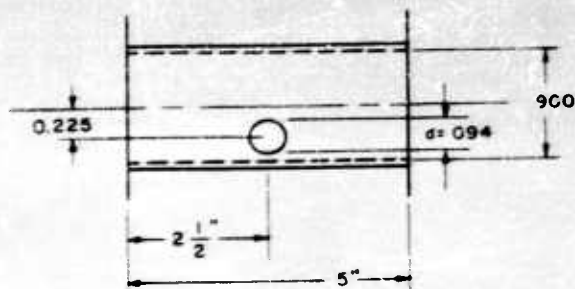
FIGURE 116

LN POWER VS LN PRESSURE  
FOR LONGITUDINAL APERTURE  
IN BROAD WALL

CONFIDENTIAL



CONFIDENTIAL



FREQUENCY : 9375 MC  
PULSE WIDTH : 1.2  $\mu$  SEC  
REPETITION RATE : 800 PPS  
ATTENUATION THROUGH HOLE > 40 DB

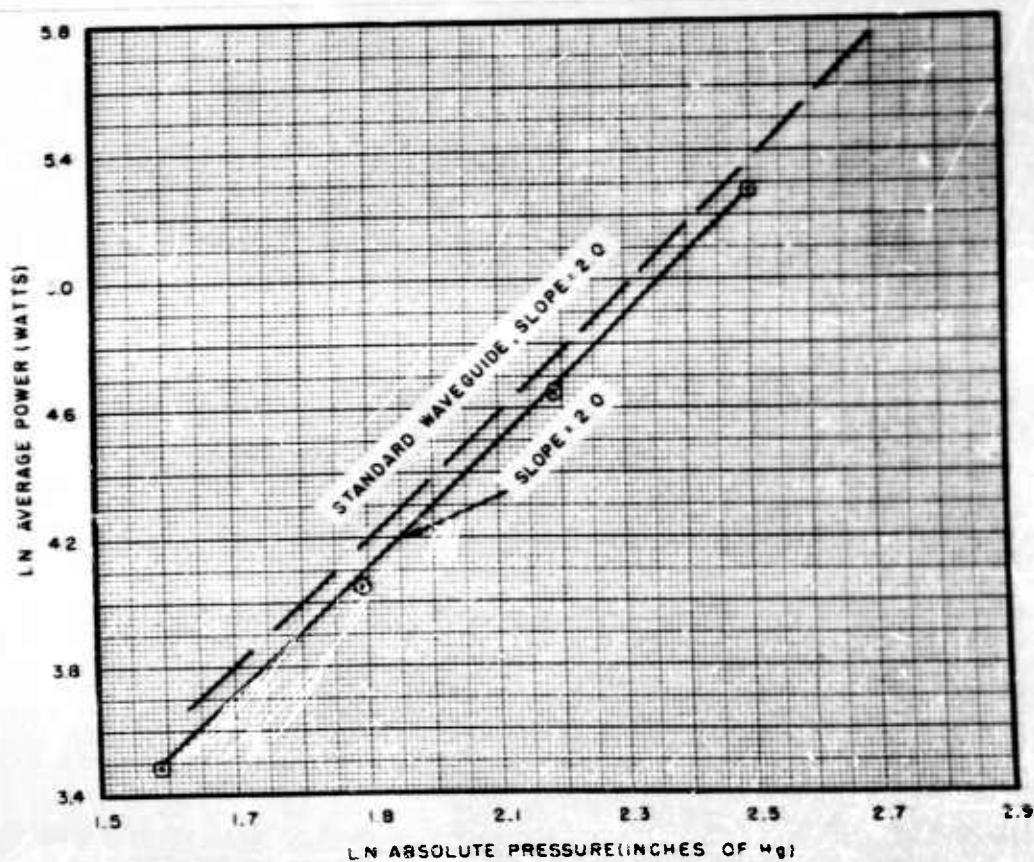


FIGURE 117  
LN POWER VS PRESSURE FOR  
ROUND APERTURE IN BROAD WALL

CONFIDENTIAL





CONFIDENTIAL

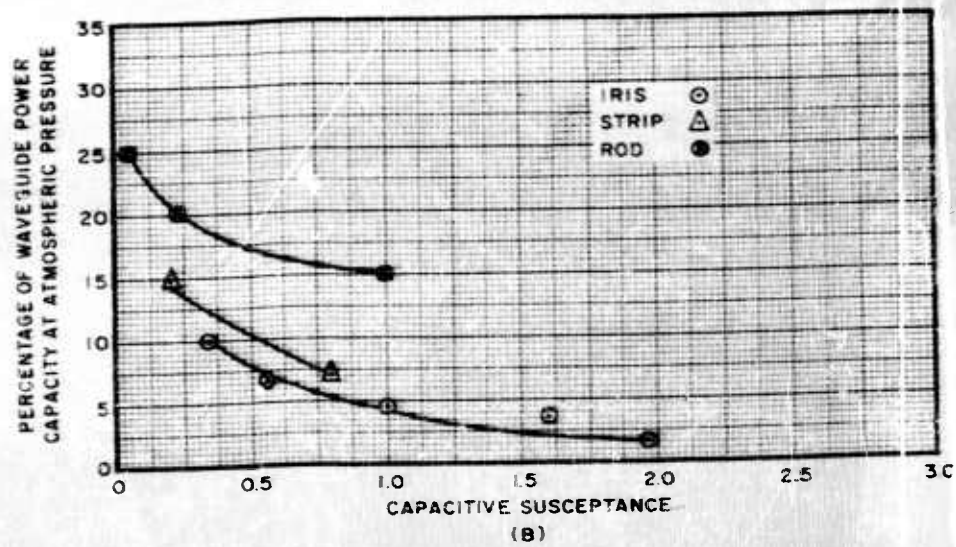
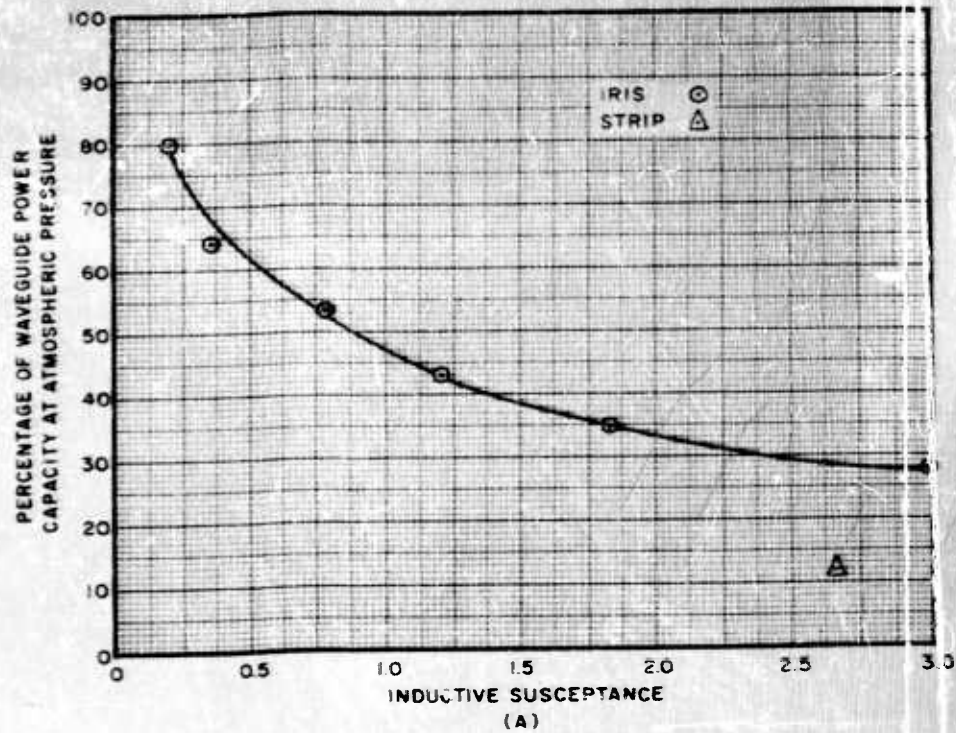


FIGURE 118  
POWER CAPACITY VS  
SUSCEPTANCE

CONFIDENTIAL